Graft-versus-Leukaemia Antigen Discovery Utilising the Bone Marrow T Cell Repertoire in Patients with Acute Myeloid Leukaemia

Bing Shian Tseu

Green Templeton College
University of Oxford

A thesis submitted for the degree of Doctor of Philosophy

Trinity 2025

Abstract

Acute myeloid leukaemia (AML) is a highly aggressive haematological malignancy for which allogeneic stem cell transplantation (alloSCT) remains the most effective curative therapy. Durable disease control relies on the graft-versus-leukaemia (GvL) effect, where donor-derived T cells eradicate residual leukaemia. Despite over 60 years of clinical use, the identity and dynamics of GvL-specific T cells remain poorly defined, with limited investigation into the early post-alloSCT bone marrow, at a time when relapse risk is greatest.

Using a high-risk, GvL-enriched patient cohort, novel methodological platforms were developed to overcome the limited viability and proliferative capacity of early post-alloSCT bone marrow, enabling the detection and characterisation of rare T cells specific to minor histocompatibility antigens (miHAs). Across complementary approaches, multiple GvL clonotypes recognising miHAs were detected at frequencies as low as 0.01% and shown to persist for years across marrow and blood compartments. Importantly, four clonotypes were identified from bone marrow directly *ex vivo*, providing unambiguous evidence for their presence *in vivo*. Phenotypic profiling showed that T cells expressing a TCR previously found to be enriched in GSTZ1-responsive T cells had a Th1-polarised central memory phenotype consistent with long-term surveillance. Functional testing also validated a TCR clonotype enriched in METTL22-responsive CD4+ T cells as mediating selective HLA-DR-restricted recognition of the patient-derived variant.

These findings establish that GvL immunity can be detected in the marrow within the first year post-alloSCT, persists long-term despite extreme rarity and includes $CD4^+$ T cell subsets with durable effector potential. By expanding the catalogue of validated GvL responses and providing a framework for their detection in the bone marrow, this work advances the understanding of the cellular basis of GvL to inform future developments within the field of transplant immunology.

Word Count: 39191

Graft-versus-Leukaemia Antigen Discovery Utilising the Bone Marrow T Cell Repertoire in Patients with Acute Myeloid Leukaemia

Bing Shian Tseu

Green Templeton College

University of Oxford

A thesis submitted for the degree of

Doctor of Philosophy

Trinity 2025

Abstract

Acute myeloid leukaemia (AML) is a highly aggressive haematological malignancy for which allogeneic stem cell transplantation (alloSCT) remains the most effective curative therapy. Durable disease control relies on the graft-versus-leukaemia (GvL) effect, where donor-derived T cells eradicate residual leukaemia. Despite over 60 years of clinical use, the identity and dynamics of GvL-specific T cells remain poorly defined, with limited investigation into the early post-alloSCT bone marrow, at a time when relapse risk is greatest.

Using a high-risk, GvL-enriched patient cohort, novel methodological platforms were developed to overcome the limited viability and proliferative capacity of early post-alloSCT bone marrow, enabling the detection and characterisation of rare T cells specific to minor histocompatibility antigens (miHAs). Across complementary approaches, multiple GvL clonotypes recognising miHAs were detected at frequencies as low as 0.01% and shown to persist for years across marrow and blood compartments. Importantly, four clonotypes were identified from bone marrow directly *ex vivo*, providing unambiguous evidence for their presence *in vivo*. Phenotypic profiling showed that T cells expressing a TCR previously found to be enriched in GSTZ1-responsive T cells had a Th1-polarised central memory phenotype consistent with long-term surveillance. Functional testing also validated a TCR clonotype enriched in METTL22-responsive CD4+ T cells as mediating selective HLA-DR-restricted recognition of the patient-derived variant.

These findings establish that GvL immunity can be detected in the marrow within the first year post-alloSCT, persists long-term despite extreme rarity and includes $CD4^+$ T cell subsets with durable effector potential. By expanding the catalogue of validated GvL responses and providing a framework for their detection in the bone marrow, this work advances the understanding of the cellular basis of GvL to inform future developments within the field of transplant immunology.

Word Count: 39191

Acknowledgements

I would like to thank my supervisor, Paresh Vyas, for giving me this opportunity in the world of academia. He has taught me so much about how I can best impact on patient care and has forever changed what I value most in the field of medicine.

I would like to thank my co-supervisor, Persephone Borrow, for her incisive and thoughtful guidance. Her care, dedication and unwavering support for her students have been invaluable, and I truly appreciate all her efforts.

Special thanks to my partner-in-crime, Maria Barbanti, who has made the DPhil experience much more enjoyable. Much of the work in this thesis was conducted in unison with her and I could not have asked for a better companion.

To the other members of the T cell team, I am grateful for all your contributions. Connor Sweeney, whose foundational work built these projects; Gerda Mickute, who helped me find my footing and remains hilarious to this day; and Abhi, who cloned what I could not.

To the other members of the Vyas lab, thank you for putting up with my inane questions, with a special mention to Angus Groom, Asger Jakobsen, Batchimeg Usukhbayar, David Cruz-Hernandez, Felix Radtke, and Sven Turkalj.

Special thanks to Andy Peniket, my clinical idol and the reason I even applied for this DPhil in the first place.

I gratefully acknowledge the Medical Research Council for funding this project, and above all, the patients who have kindly donated samples, without whom this work would not have been possible.

Finally, to my family, my friends, and my other half: thank you for constant love, patience and support through this journey. You are, and will always be, the most important part of it all.

Contents

Abbreviations

5'-RACE	5'-rapid amplification of cDNA ends
7+3	Seven days of cytarabine and three days of anthracycline
7BS	7-β-strand
AEC	3-amino-9-ethylcarbazole
AIM	Activation-induced marker
ALL	Acute lymphoblastic leukaemia
AlloSCT	Allogeneic haematopoietic stem cell transplantation
APC	Antigen-presenting cell
APL	Acute promyelocytic leukaemia
ATG	Antithymocyte globulin
β**2M**	β-2 microglobulin
BM	Bone marrow
BMMNC	Bone marrow mononuclear cell
bp	Base pair
BSA	Bovine serum albumin
Bu	Busulfan
cDNA	Complementary DNA
CEF	CMV/EBV/Flu peptide pool
CEFTA	CMV/EBV/Flu/Tetanus/Adenovirus peptide pool
CH	Cieri-Herda culture method
CML	Chronic myeloid leukaemia
CMP	Common myeloid progenitor
CMV	Cytomegalovirus
CR	Complete remission
CR1/2	First/second complete remission
CS	Connor Sweeney culture method
DA	Daunorubicin + cytarabine regimen
DAPI	4',6-diamidino-2-phenylindole

DFS	Disease-free survival
DLI	Donor lymphocyte infusion
DMEM	Dulbecco's Modified Eagle Medium
DMF	Dimethylformamide
DMSO	Dimethyl sulfoxide
DNA	Deoxyribonucleic acid
dsDNA	Double-stranded DNA
EBMT	European Society for Blood and Marrow Transplantation
EBV	Epstein-Barr virus
EDTA	Ethylenediaminetetraacetic acid
ELISpot	Enzyme-linked immunospot
ELN	European LeukemiaNet
ER	Endoplasmic reticulum
ESC	Embryonic stem cell
FAB	French-American-British
FACS	Fluorescence-activated cell sorting
FDR	False discovery rate
FLAG-Ida	Fludarabine, cytarabine, G-CSF, idarubicin
FLT3L	FMS-like tyrosine kinase 3 ligand
Flu	Influenza virus
FMO	Fluorescence minus one
G-CSF	Granulocyte colony-stimulating factor
GEM	Gel bead-in-emulsion
GM-CSF	Granulocyte-macrophage colony-stimulating factor
GMP	Granulocyte-monocyte progenitor
GO	Gemtuzumab ozogamicin
GRCh38	Genome Reference Consortium Human Build 38
GvHD	Graft-versus-host disease
GvL	Graft-versus-leukaemia

HCT-CI	Haematopoietic Cell Transplantation-Comorbidity Index
HD	Healthy donor
HEPES	4-(2-hydroxyethyl)-1-piperazineethanesulfonic acid
HiDAC	High-dose cytarabine
HI-FBS	Heat-inactivated foetal bovine serum
HLA	Human leukocyte antigen
HMA	Hypomethylating agent
HPA	Human Protein Atlas
HSC	Haematopoietic stem cell
ICC	International Consensus Criteria
Ii	Invariant chain
IL-1β,2,4,5,7,15,22	Interleukin 1β, 2, 4, 5, 7, 15, 22
IMDM	Iscove's Modified Dulbecco's Medium
iNKT	Invariant natural killer T cell
LAIP	Leukaemia-associated immunophenotype
LB	Luria-Bertani medium
LPS	Lipopolysaccharide
M	Mean
MAC	Myeloablative conditioning
MDS	Myelodysplastic syndromes
Mel	Melphalan
MEP	Megakaryocyte-erythroid progenitor
MHC	Major histocompatibility complex
miHA	Minor histocompatibility antigen
MNC	Mononuclear cell
MPN	Myeloproliferative neoplasm
MRD	Measurable residual disease
mRNA	Messenger RNA
MSD	Matched sibling donor

mTCRβ	Murine TCRβ
MUD	Matched unrelated donor
NGS	Next-generation sequencing
NK	Natural killer cell
NRM	Non-relapse mortality
nTPM	Normalised transcripts per million
OS	Overall survival
PB	Peripheral blood
PBMC	Peripheral blood mononuclear cell
PCR	Polymerase chain reaction
PHA	Phytohaemagglutinin
PLC	Phospholipase C
PT-MTX	Post-transplant methotrexate
PTCy	Post-transplant cyclophosphamide
PVDF	Polyvinylidene fluoride
Q30	Quality score 30
R848	Resiquimod
RIC	Reduced intensity conditioning
RNA	Ribonucleic acid
RPMI-1640	Roswell Park Memorial Institute Medium 1640
RT	Reverse transcription
RT-PCR	Reverse transcription polymerase chain reaction
SD	Standard deviation
SNP	Single nucleotide polymorphism
$\mathbf{T_{CM}}$	Central memory T cell
$\mathbf{T_{EM}}$	Effector memory T cell
$\mathbf{T_{EMRA}}$	Effector memory T cells re-expressing CD45RA

$T_{Naïve}$	Naïve T cell
TAA	Tumour-associated antigen
TAP	Transporter associated with antigen processing
TBI	Total body irradiation
TCD	T cell depletion/depleted
TCE	T cell epitope
TCR	T cell receptor
TCRα	T cell receptor α chain
TCRβ	T cell receptor β chain
TFH	Follicular helper T
Th1	Type 1 T helper
Th17	Type 17 T helper
Th2	Type 2 T helper
Th22	Type 22 T helper
Th9	Type 9 T helper
TL	Transduction-like culture method
TNFα	Tumour necrosis factor α
TPM	Transcripts per million
Treg	Regulatory T cell
TRM	Tissue-resident memory T cell
UCB	Umbilical cord blood
UMAP	Uniform manifold approximation and projection
UMI	Unique molecular identifier
WHO	World Health Organisation

1 Introduction

Contents

1.1 Acute Myeloid Leukaemia

Acute Myeloid Leukaemia (AML) is an aggressive haematological malignancy characterised by the uncontrolled clonal proliferation of poorly differentiated myeloid precursors within the bone marrow. The disruption of normal haematopoiesis by AML leads to bone marrow failure, manifesting clinically as fatigue, shortness of breath, easy bruising and recurrent infections. AML most commonly arises *de novo* but can also evolve from a pre-existing haematological disorder or as a consequence of prior exposure to chemoradiotherapy. The clinical course of AML is rapidly progressive, and without treatment, universally fatal [1, 2].

Accounting for the majority of adult acute leukaemia cases, AML has an estimated incidence of 3-5 cases per 100,000 individuals annually worldwide. The incidence of AML rises markedly with age, with the median age at diagnosis being reported as >65 years. Globally, the annual burden of AML has been rising due to both increased population age and the rise of secondary leukaemias as a consequence of the use of cytotoxic chemotherapy in the treatment of other malignancies [3, 4].

The classification of AML has undergone significant refinement over the last few decades, transitioning from the morphology-based systems with set thresholds for the presence of myeloid blasts, such as the historical French-American-British (FAB) approach, to molecularly-informed frameworks that reflect advances in genomics and disease biology [5–7]. This shift reflects a change in the paradigm, in that AML is understood not as a single disease entity but instead represents a biologically diverse group of clonal myeloid neoplasms with diverse genetic drivers and clinical trajectories.

Two principal classification systems are currently widely used in both research and clinical settings, the International Consensus Criteria (ICC) and the fifth edition of the World Health Organisation (WHO) classification (Figure 1.1) [6, 7]. While they differ in specific criteria and nomenclature, they share several key principles and provide a structured framework for the categorisation and description of AML.

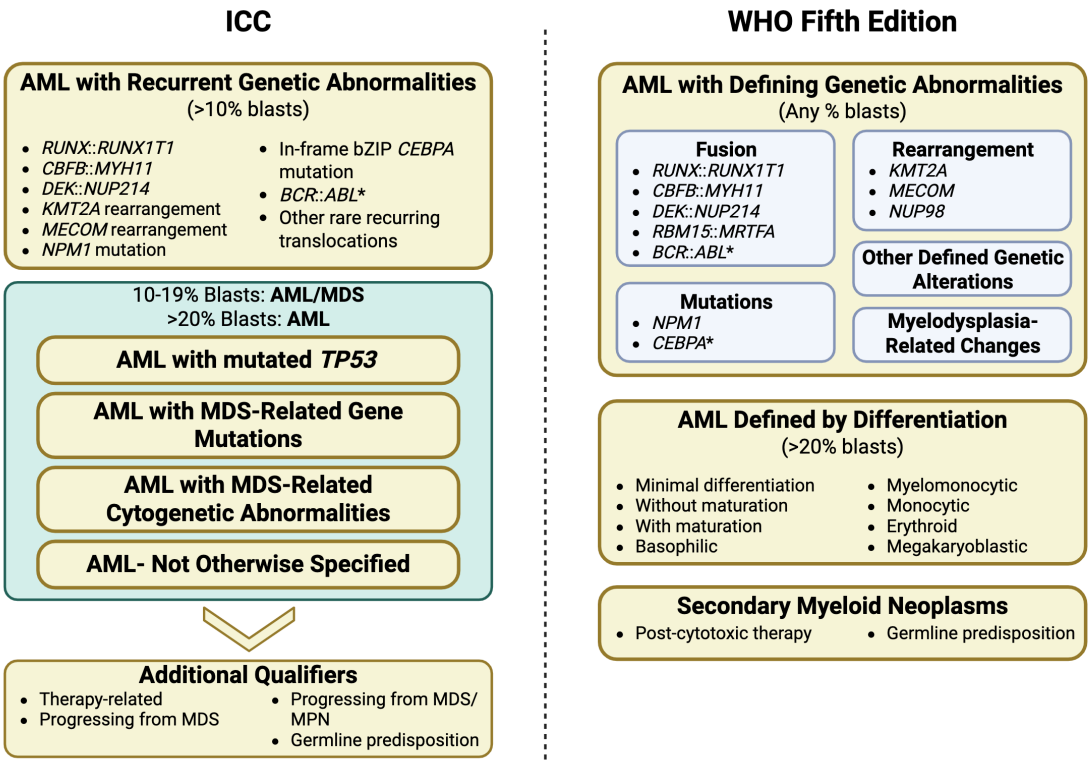

Figure 1.1: Summary of ICC and WHO Fifth Edition classifications of AML. Subtypes marked with "*" require ≥20% blasts to be defined as AML. MDS = Myelodysplastic Syndrome. MPN = Myeloproliferative Neoplasm.

A central feature of both systems is the prioritisation of recurrent genetic abnormalities as primary diagnostic criteria. These include gene fusions such as *RUNX1*::*RUNX1T1*, rearrangements in genes such as *KMT2A*, and mutations in *NPM1* or *TP53*. In cases where these defining molecular lesions are present, the traditional blast threshold for AML diagnosis, typically ≥ 20% blasts, may be lowered or waived entirely. For cases which lack defining genetic features, classification is instead based on morphological and lineage-specific characteristics.

Both systems also incorporate the clinical context in which AML arises, as it has prognostic relevance and is considered in conjunction with genetic features in forming a final diagnostic classification. In addition to *de novo* AML, further subcategories are defined for therapy-related AML (t-AML) and AML evolving from an antecedent myeloid neoplasm, such as myelodysplastic syndromes (MDS) or myeloproliferative neoplasms (MPN). These latter categories are frequently grouped

under the umbrella term of secondary AML and are associated with adverse risk and inferior clinical outcomes.

One AML subtype of particular note is acute promyelocytic leukaemia (APL), which is classically defined by the *PML*::*RARA* fusion gene arising from t(15;17). Due to its unique molecular pathogenesis, presentation and curability with targeted therapy, APL is classified separately from other AML subtypes and is therefore typically excluded from general discussions of AML [8].

1.2 Prognostic Stratification in AML

In parallel to diagnostic classification, AML is also stratified by risk of relapse and overall survival. The most widely used prognostic framework in adult AML is the European LeukemiaNet (ELN) categorisation, recently revised in 2022 [9]. This divides patients into three risk groups (favourable, intermediate and adverse) based on the presence of specific gene mutations, chromosomal rearrangements and karyotypic abnormalities at time of diagnosis (Figure 1.2).

These genetic risk groups are associated with distinct differences in treatment outcomes. In a large prospective cohort of 1,637 adults with *de novo* AML, the complete remission (CR) rate was 84% in the favourable group, compared to 68% in the intermediate and 44% in the adverse groups. Corresponding disease-free survival (DFS) rates at 5 years were 44%, 21% and 6%, with overall survival (OS) rates of 48%, 22% and 7% respectively (Figure 1.3) [10]. Notably, patients with secondary AML are frequently assigned to the adverse-risk category under ELN criteria, owing to the high prevalence of adverse cytogenetic features such as complex or monosomal karyotypes and recurrent mutations in genes including *TP53*, *ASXL1* and *RUNX1*.

Risk Category	Genetic Abnormality
Favourable	t(8;21)/*RUNX1*::*RUNX1T1*
	inv(16) or t(16;16);*CBFB*::*MYH11*
	NPM1 mutation without *FLT3*-ITD
	In-frame bZIP *CEBPA* mutation
Intermediate	*FLT3*-ITD
	t(9;11)/*MLLT3*::*KMT2A*
	Other cytogenetic or molecular abnormalities not classified as favourable or adverse
Adverse	t(6;9)/*DEK*::*NUP214*
	Other KMT2A rearrangements
	t(9;22)/*BCR*::*ABL1*
	t(8;16)*KAT6A*::*CREBBP*
	inv(3) or t(3;3)/*GATA2*,*MECOM*
	MECOM rearrangement
	-5, del(5q), -7, -17, abn(17p)
	Complex or monosomal karyotype
	ASXL1, *BCOR*, *EZH2*, *RUNX1*, *SF3B1*, *SRSF2*, *STAG2*, *U2AF1* or *ZRSR2* mutations
	TP53 mutations (variant allele frequency ≥10%)

Figure 1.2: 2022 European LeukemiaNet risk classification by genetics at initial diagnosis. Complex karyotype = ≥ 3 unrelated chromosomal abnormalities. Monosomal karyotype = two or more distinct monosomies, including loss of X or Y.

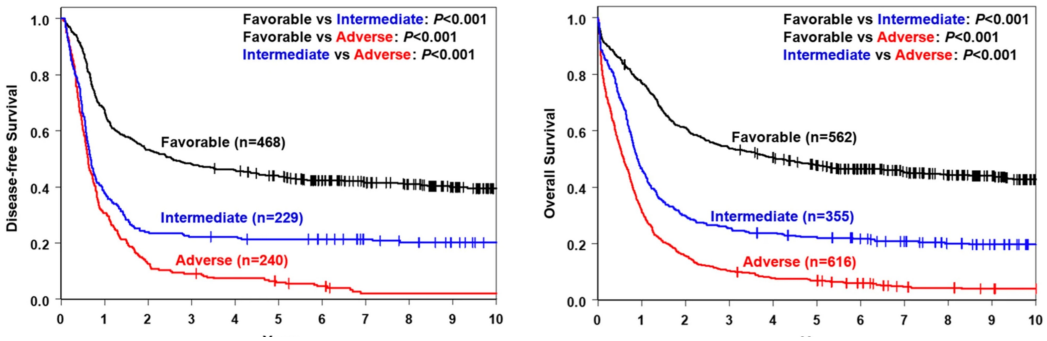

Figure 1.3: Disease-free and overall survival of patients classified by ELN 2022 criteria. *Adapted from Mrózek et al., Leukemia (2023)* [10]

In addition to these static diagnostic features, measurable residual disease (MRD) has emerged as a dynamic and independent predictor of relapse and long-term outcome.

MRD can be assessed through multiple methodologies, including multiparameter flow cytometry to detect leukaemia-associated immunophenotypes (LAIPs), quantitative PCR (qPCR) for fusion transcripts or mutant alleles, or increasingly, next-generation sequencing-based methods. Common targets for MRD monitoring

include *NPM1* mutations and fusion transcripts such as *RUNX1*::*RUNX1T1* [11–13].

Persistent MRD following induction or consolidation therapy is associated with a significantly increased risk of relapse, even among patients with otherwise favourable-risk genetics. As a result, MRD status is increasingly used alongside ELN-defined genetic risk to dynamically guide and refine treatment decisions for patients with AML.

Together, the integration of ELN-defined genetic risk and MRD assessment forms the basis of contemporary AML prognostication. These tools underpin current risk-adapted treatment strategies and are widely employed in both routine practice and in clinical trial design.

1.3 Treatment Strategies in AML

The treatment landscape for AML has undergone significant evolution, driven by advances in molecular profiling, prognostic classification and drug development. Current treatment approaches are increasingly tailored not only to disease characteristics, but also to patient-specific factors including age, performance status and the presence of comorbidities. This balance of risk is of critical importance in the choice of therapy, where the benefits of treatment must be carefully balanced against its toxicities.

The therapeutic approach to AML is typically divided into two phases. The first of these is induction, which aims to achieve complete disease remission, and the second is consolidation, intended to eradicate residual disease and prevent relapse.

For fit patients considered eligible for intensive therapy, the standard induction regimen remains “7+3”, which combines seven days of cytarabine with three days of anthracycline, most commonly daunorubicin. Despite being introduced in the 1970s, this regimen serves as the benchmark against which novel approaches are evaluated [14, 15]. Alternative regimens include FLAG-Ida (fludarabine, cytarabine,

granulocyte-colony stimulating factor (G-CSF), and idarubicin), which is used in select high-risk or refractory settings, and CPX-351 (liposomal daunorubicin and cytarabine) [16]. The latter is approved for secondary AML, where it shows improved outcomes compared to conventional 7+3 [17]. Nonetheless, no single regimen has replaced 7+3 as a standard first-line approach for younger patients with *de novo* AML.

In addition to conventional chemotherapy, targeted therapies are increasingly being incorporated into frontline AML induction for patients with certain genetically defined subtypes. For example, the addition of FLT3 inhibitors, such as midostaurin and quizartinib, has been shown to improve outcomes in patients harbouring FLT3 mutations, and is now standard of care in this setting [18, 19].

Another agent used in combination with induction chemotherapy is gemtuzumab ozogamicin (GO), an anti-CD33 antibody-drug conjugate. GO has demonstrated survival benefits when added to chemotherapy in a number of patient populations, particularly those with favourable or intermediate-risk genetics. Its benefit is most pronounced in core-binding factor positive AML, which is characterised by the presence of t(8;21) or inv(16) [20].

For patients deemed unfit for intensive chemotherapy, commonly due to advanced age or comorbidity, lower-intensity regimens are preferred. The most widely used approach is the combination of venetoclax, a BCL-2 inhibitor, with a hypomethylating agent (HMA), such as azacitidine or decitabine. This regimen has demonstrated superior outcomes compared to HMA monotherapy and is now standard of care in this setting [21–23]. In frailer individuals who cannot tolerate combination therapy, HMA monotherapy or alternative low-dose chemotherapy regimens remain an option, often delivered with palliative intent.

The expanding breadth of AML therapy includes several novel targeted agents beyond FLT3 and CD33-directed therapies. IDH1 and IDH2 inhibitors, ivosidenib

and enasidenib, are approved for patients with the respective mutations and are being explored in combination with chemotherapy, HMAs and venetoclax-based regimens [24–28]. Menin inhibitors, targeting leukaemias with *KMT2A* rearrangements or *NPM1* mutations, are currently under active clinical evaluation, alongside many other novel therapies [29, 30]. These developments are continually reshaping treatment algorithms and expanding options for patients who relapse or are ineligible for intensive standard-of-care treatment with conventional chemotherapy.

Following successful induction, patients proceed to consolidation therapy, which is necessary to achieve a reasonable chance of a durable remission or cure. The choice of consolidation therapy is guided primarily by the genetic risk of the AML and its response to induction.

For patients with favourable-risk disease, chemotherapy-based consolidation remains standard. This typically consists of intermediate- or high-dose cytarabine administered over up to four cycles [31].

For patients at a higher risk of relapse, allogeneic haematopoietic stem cell transplantation (alloSCT) offers the most effective long-term disease control. The indications, mechanisms and clinical outcomes of alloSCT are discussed in the following sections.

1.4 Core Principles of Immunology in Allogeneic Haematopoietic Stem Cell Transplantation (alloSCT)

Immunology is an immensely broad and complex field, encompassing diverse innate and adaptive mechanisms of host defence. A comprehensive overview is far beyond the scope of this work, but as alloSCT relies fundamentally on the recognition of peptide-HLA complexes by donor T cells, a concise outline of antigen presentation and T cell biology is warranted (Figure 1.4).

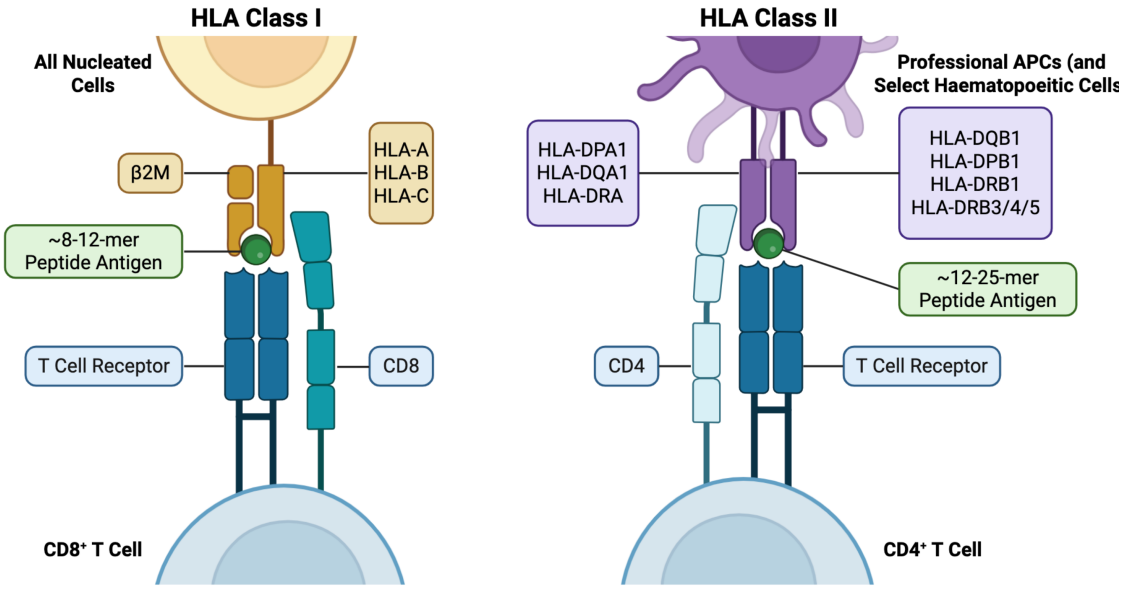

Figure 1.4: HLA class I and class II presentation to T cells. Simplified schematic demonstrating mechanistic differences between HLA class I and class II presentation. APC = Antigen-Presenting Cell. β2M = β-2 Microglobulin.

1.4.1 The Major Histocompatibility Complex

The major histocompatibility complex (MHC) encodes the human leucocyte antigens (HLA) on chromosome 6. HLA molecules are highly polymorphic glycoproteins that are inherited *en bloc* as haplotypes from each parent. Their primary function is the presentation of peptides to T cells, allowing for immune surveillance.

HLA molecules are broadly classified into two groups. Class I molecules, which comprise HLA-A, -B and -C, are expressed on nearly all nucleated cells and present to $CD8^+$ T cells. Structurally, class I HLA is composed of a heavy α chain and an invariant light chain of β-2 microglobulin (β2M) which stabilises the class I molecule. Class I HLA molecules possess a closed-ended peptide-binding groove that accommodates short peptides of around 8-12 amino acids [32].

HLA class II molecules, comprising HLA-DP, -DQ and -DR, are structurally distinct, consisting of two chains, α and β, which present antigen to $CD4^+$ T cells. The expression of class II HLA is more restricted, being limited at steady

state to professional antigen-presenting cells (APCs) and haematopoietic cells, including leukaemic blasts.

The α chains exhibit limited polymorphism, whereas β chains are highly polymorphic and dictate the majority of peptide-binding diversity. The peptide-binding groove of class II is open at both ends, allowing for the binding of longer peptides, typically 12-25 amino acids in length, with flanking residues that extend beyond the groove. This open architecture allows considerable flexibility in the repertoire of presented peptides and facilitates more complex interactions between peptide-HLA and the T cell receptor (TCR) [33, 34].

1.4.2 Antigen Processing and Presentation

The processing pathways that generate peptides for HLA binding and presentation also differ between class I and II.

HLA class I molecules primarily sample the intracellular proteome. Class I peptides are derived from endogenous proteins, degraded by the proteasome into short fragments. These fragments are then transported into the endoplasmic reticulum (ER) by the transporter associated with antigen processing (TAP), trimmed by ER aminopeptidases such as ERAP1/2 and stabilised within a peptide-loading complex that includes tapasin, calreticulin and Erp57. Only high-affinity peptides form stable complexes with the class I HLA, which are then trafficked to the cell surface as peptide-HLA [35].

Class II HLA molecules are canonically associated with the presentation of exogenous antigens. This occurs through the capture of extracellular material through a number of mechanisms that include macropinocytosis, receptor-mediated endocytosis and phagocytosis, delivering proteins to endosomal and lysosomal compartments for degradation into shorter peptide fragments.

The formation of class II peptide-HLA occurs through a different process. Class II αβ heterodimers are assembled with the invariant chain (Ii), which occupies

the peptide-binding groove and traffics the complex into the endocytic pathway. Degradation of Ii leaves the class II invariant peptide (CLIP) fragment in the groove, which is subsequently exchanged for higher-affinity peptides through the action of HLA-DM. Although this exogenous pathway represents the classical paradigm, it is clear that a substantial fraction of class II-bound peptides derive from endogenous sources. Cytosolic proteins can access class II loading compartments through mechanisms such as autophagy or recycling. This flexibility enables APCs or leukaemic blasts to present both self and exogenous peptides, expanding the range of $CD4^+$ T cell surveillance [36, 37].

1.4.3 T Cell Effector Function

The biological consequences of antigen presentation occur as a result of the effector activities of $CD8^+$ and $CD4^+$ T cells. In both lineages, recognition is mediated by the TCR, with the assistance of co-receptors. The most important of these co-receptors are the eponymous CD8, which binds HLA class I, and CD4, which binds HLA class II. These co-receptors stabilise the TCR-peptide-HLA interaction at the immunological synapse and also recruit the tyrosine kinase Lck, mediating downstream activation [38].

$CD8^+$ T cells recognise class I peptide-HLA complexes and act as cytotoxic effectors. Their effector mechanisms include perforin-granzyme release, Fas-FasL interactions, as well as the secretion of pro-inflammatory cytokines such as interferon gamma (IFNγ) and tumour necrosis factor alpha (TNFα). In addition, $CD8^+$ T cells can also induce alternative forms of target cell death, including ferroptosis and pyroptosis. Though historically understood as exclusively cytotoxic, increasing evidence suggests greater effector heterogeneity, with subsets displaying distinct cytokine profiles. In alloSCT, the classical cytotoxic programme remains the dominant and most studied effector mechanism [39, 40].

$CD4^+$ T cells recognise class II peptide-HLA complexes and whilst they have traditionally been viewed as "helper T cells," their roles are considerably broader. Upon activation, naïve $CD4^+$ T cells differentiate into specialised subsets according to the environmental context.

The type 1 helper (Th1) lineage, induced by interleukin-12 (IL-12) and governed by the transcription factor T-bet, produces IFNγ, interleukin-2 (IL-2) and TNFα. These cytokines activate innate immune effectors, upregulate antigen presentation and provide support for $CD8^+$ T cell-mediated cytotoxicity. Th1 immunity is consistently associated with effective control in the malignant setting, although its role in alloSCT is not well defined [41].

Type 2 helper (Th2) responses are dependent on GATA3, and result in the production of interleukin-4 (IL-4), interleukin-5 (IL-5) and interleukin-13 (IL-13). These cytokines promote humoral B cell responses and eosinophil recruitment. Their functions are overall less relevant to GvL, although in some contexts their action has been associated with AML control [42, 43].

Type 17 helper (Th17) cells are dependent on RORγt and STAT3. They secrete interleukin-17 (IL-17) and interleukin-22 (IL-22) and are instead associated with neutrophil recruitment and tissue inflammation. Though well recognised as key mediators of graft-versus-host disease (GvHD), their precise contribution in leukaemia control is uncertain [44].

Regulatory T cells (Tregs) are marked by FoxP3 and high CD25 and unlike the above subsets act to limit immune activation through mechanisms including suppressive cytokines and CTLA-4-mediated modulation of co-stimulation.

Other lineages, such as T follicular helper (TFH), type 9 helper (Th9) and type 22 helper (Th22) further illustrate the diversity of $CD4^+$ T cell differentiation [45].

Finally, $CD4^+$ T cells are not confined to helper or regulatory functions. They are capable of acquiring cytotoxic potential, expressing perforin and granzyme and directly killing HLA class II-positive targets. Though once considered atypical, they are now increasingly recognised in cancer responses [46, 47].

1.5 AlloSCT as a Therapeutic Strategy in AML

AlloSCT is a key consolidation strategy and represents the most effective curative option for many patients, particularly those at increased risk of relapse. Although alloSCT is used in the treatment of a number of malignant and non-malignant haematological conditions, AML remains the most common indication for alloSCT, accounting for approximately 40% of all adult transplants performed in Europe and North America [48, 49].

Early clinical attempts at transplantation in the mid-20th century demonstrated the potential of donor-derived marrow to reconstitute haematopoiesis following the use of myeloablative chemoradiotherapy. These initial trials were limited by high rates of treatment-related mortality, due to graft rejection, infection and the toxic effects of GvHD [50, 51]. Though it was initially viewed as a method to restore healthy haematopoiesis following the ablative effects of cytotoxic therapies, over time, growing clinical and experimental evidence led to the recognition of the immunological contribution of the graft itself. This is known as the graft-versus-leukaemia (GvL) effect, where donor immune cells mediate anti-leukaemic activity [52].

Despite ongoing advances in transplant and supportive care, alloSCT remains a complex and high-risk intervention. Its success depends on achieving a delicate balance between disease eradication and immune tolerance, or the competing effects of GvL and GvHD. Understanding how this balance is shaped, through transplant strategy and the biology of the immune response, is essential to optimising the outcomes of patients undergoing alloSCT for AML.

1.5.1 Clinical Indications and Patient Selection

AlloSCT remains the most effective post-remission therapy for patients with AML. However, as it is associated with significant toxicities, the decision to proceed to

transplantation hinges on the careful evaluation of both disease- and patient-specific factors, as the potential benefits of relapse prevention must be balanced against the risks of transplant-related morbidity and mortality.

AlloSCT is therefore generally reserved for fit patients who would be considered unlikely to achieve a durable remission or cure with chemotherapy alone.

The ELN recommends consideration of an alloSCT in the first complete remission (CR1) when the estimated relapse risk without transplantation exceeds 35-40% [9]. This threshold is typically met in patients with intermediate- or adverse-risk AML, though risk estimation can be further refined with the incorporation of additional biomarkers and early treatment response dynamics. In these higher-risk groups, transplantation in CR1 has consistently been associated with reduced relapse incidence and improved relapse-free survival in both prospective and registry-based studies [49, 53–55].

In contrast, the ELN does not routinely recommend alloSCT in CR1 for patients with favourable-risk disease. Treatment response, and in particular, the presence of MRD does however, play an important role in transplant selection. The detection of MRD following induction or consolidation is a powerful independent predictor of relapse across all risk groups and would strengthen the case to proceed to alloSCT to reduce relapse risk [11, 12, 56]. Conversely, patients who achieve sustained MRD negativity may be appropriate candidates for chemotherapy-based consolidation, even in the context of higher baseline genetic risk [57].

Importantly, the risk of relapse alone does not determine transplant eligibility. AlloSCT carries a substantial risk of non-relapse mortality (NRM), which may offset its curative potential, particularly in patients with lower-risk disease or limited physiological reserve. Even in otherwise fit individuals, NRM rates may reach 10-20%. Tools such as the Haematopoietic Cell Transplantation-Comorbidity Index (HCT-CI) are routinely used to estimate this risk and guide clinical decision-making

[58, 59].

The option of alloSCT can also be deferred in select patients, particularly those with lower estimated relapse risk or those who are likely to respond to salvage chemotherapy. In such cases, a delayed transplant at first relapse or in second remission remains a viable strategy [60].

Ultimately, the selection of patients to undergo alloSCT reflects a personalised synthesis of diagnostic risk, treatment response, fitness for transplant and patient preference. This integrated approach aims to identify those most likely to derive long-term benefit from alloSCT whilst avoiding unnecessary toxicities in those who are unlikely to benefit.

1.5.2 Donor Selection and HLA Matching

The selection of a suitable donor represents a fundamental determinant of outcome in alloSCT, with direct implications for engraftment, immune reconstitution, GvHD risk and overall survival. Historically, only a minority of patients had access to a suitable donor, but this landscape has evolved substantially due to global donor registries, the refinement of HLA typing technologies and the use of alternative donor platforms. As a result, nearly all patients now have access to a graft source [61].

At the heart of donor selection lies HLA compatibility, which serves as the primary immunological barrier to transplantation. Donor T cell recognition of mismatched recipient HLA can elicit potent alloreactive responses, manifesting clinically as GvHD, with primary graft failure occurring when the response is in the reverse direction.

To minimise these immunological complications, allele-level HLA matching at five loci (HLA-A, -B, -C, -DQB1 and DRB1) is now standard for donor selection. Transplants using fully matched, 10/10 donors are consistently associated with the lowest rates of GvHD, superior engraftment and improved long-term survival [62, 63].

However, not all HLA mismatches confer equal clinical risk. Certain HLA mismatches, depending on the alleles involved and their immunogenicity, may be considered "permissive". These permissive mismatches are associated with relatively low immunogenicity, a reduced likelihood of triggering harmful alloreactive responses and in some cases can confer transplant outcomes approaching those of fully matched pairs. A well-characterised example of this is the HLA-DPB1 locus, which is not routinely included in standard 10/10 matching. Mismatches within the same T cell epitope (TCE) group are considered permissive given their immunologic similarity, and are associated with improved outcomes when compared to non-permissive mismatches that span different TCE groups [64, 65].

In clinical practice, the choice of donor source is shaped not only by immunological compatibility but by logistical considerations such as donor availability and the urgency of transplant. Where feasible, there is a clear hierarchy of preference for donor source. The optimal donor source remains an HLA-identical sibling, or matched sibling donor (MSD). Siblings offer the highest probability of 10/10 HLA matching due to shared parental haplotypes. Transplants from MSDs are associated with superior outcomes across patient populations. However, only a minority of patients, around 25-30%, will have a suitably matched sibling [66].

For the remainder, international donor registries are used to identify a matched unrelated donor (MUD). When a 10/10 HLA match is achieved, a MUD transplant provides outcomes comparable to those of MSDs, albeit with a modest increase in GvHD risk [67]. Donor identification through these registries may be time-consuming, and is particularly limited for individuals from ethnically diverse backgrounds, where underrepresentation remains a significant barrier [68].

For patients lacking a matched sibling or unrelated donor, haploidentical transplantation has become an increasingly viable option. Haploidentical donors, typically parents, children or half-matched siblings, share only one HLA haplotype with the recipient. These transplants were historically associated with high rates of graft

failure and severe GvHD, but the incorporation of post-transplant cyclophosphamide (PTCy) has revolutionised the safety of these transplants, making this approach widely adopted across transplant centres [69].

Finally, where haploidentical donors are unavailable or unsuitable, umbilical cord blood (UCB) offers a further graft source. UCB is immunologically naïve and more tolerant of HLA mismatching without the same degree of GvHD risk. However, this advantage is offset by low cell doses, delayed engraftment and a higher risk of early infectious complications [70].

Where multiple potential donors are available, additional biological and clinical factors are considered to refine donor selection. Donor age is a key consideration, with younger donors being associated with lower rates of chronic GvHD and improved overall survival. Donor-recipient sex mismatching, particularly when female multiparous donors are used for male recipients, has been associated with increased chronic GvHD risk [71]. Cytomegalovirus (CMV) serostatus mismatch, especially where a CMV-negative donor is used for a CMV-positive recipient, confers a heightened risk of viral reactivation and therefore adverse outcomes. This risk has been partially mitigated with the introduction of CMV-targeted prophylactic agents such as letermovir [72]. Finally, while ABO incompatibility does not preclude transplantation, major mismatches can lead to delayed erythroid engraftment or haemolytic complications [73].

1.5.3 Transplant Conditioning

Prior to the infusion of haematopoietic stem and progenitor cells, patients first undergo conditioning with chemotherapy, with or without radiotherapy. This serves a dual purpose in both eliminating residual leukaemia and providing sufficient immunosuppression to enable donor engraftment. Commonly used conditioning agents include alkylating agents such as busulfan, cyclophosphamide and melphalan, as well as fludarabine, a purine analogue with potent lymphodepleting properties.

Total body irradiation (TBI) remains part of some regimens, particularly in cases with extramedullary disease [74].

In some settings, *in vivo* depletion of donor T cells is also incorporated into conditioning. This includes antithymocyte globulin (ATG), a polyclonal infusion of T cell-depleting antibodies, and alemtuzumab, a monoclonal anti-CD52 antibody [75]. These agents contribute to GvHD prevention but may delay post-alloSCT immune reconstitution.

Conditioning regimens are broadly divided into myeloablative (MAC) and reduced intensity (RIC) approaches, reflecting their degree of marrow ablation and reliance on GvL for disease control.

MAC regimens induce irreversible pancytopenia requiring stem cell rescue. They offer maximal cytoreduction that directly contributes to disease control, but at the cost of a higher NRM. MAC regimens are generally favoured in younger, fit patients with high-risk AML, particularly those with active disease at time of alloSCT. In contrast, RIC regimens deliver less intensive cytotoxic therapy with a lower NRM but are more reliant on GvL, allowing alloSCT to be extended to patients who would not tolerate MAC protocols [76, 77]. The optimal balance between the relapse risk and toxicity for these two approaches remains the subject of ongoing clinical investigation.

1.5.4 Immunosuppression and Graft-versus-Host Disease (GvHD)

The success of alloSCT hinges not only on achieving durable donor engraftment, but on the controlled modulation of immune responses in the post-transplant period. Central to this is the prevention and management of GvHD, a major immunological complication arising from donor T cell recognition of recipient tissues as foreign. GvHD remains a leading cause of NRM following alloSCT and imposes a significant burden on long-term morbidity. It is expected that 30-50%

of patients will experience acute GvHD with around 40% of long-term survivors being affected by chronic GvHD [78, 79].

Acute GvHD is defined as occurring within the first 100 days post-alloSCT and primarily affects the skin, liver and gastrointestinal tract, whereas chronic GvHD occurs after this timeframe and can involve any organ system, often mimicking autoimmune or fibrosing disorders. Known risk factors for the development of GvHD include HLA mismatch, increased age, gender or ABO mismatches, and the use of peripheral blood stem cell grafts [80].

Following engraftment, a further phase of pharmacological immunosuppression is required to prevent GvHD. Standard prophylactic regimens involve a calcineurin inhibitor (such as cyclosporine or tacrolimus), in combination with methotrexate or mycophenolate mofetil [81].

In haploidentical and MUD transplants, PTCy has become a widely adopted strategy. PTCy selectively depletes proliferating alloreactive T cells whilst sparing tolerogenic regulatory populations, and has been shown to reduce the incidence of GvHD without adversely affecting relapse risk [69, 82].

Tapering of immunosuppression typically begins between 60 and 100 days post-transplant in the absence of active GvHD. When GvHD occurs despite prophylaxis, the first-line therapy for both acute and chronic GvHD remains systemic corticosteroids. However, steroid-refractory GvHD is common and associated with poor outcomes. Second-line therapies include ruxolitinib, a JAK2 inhibitor, or extracorporeal photopheresis [83, 84].

The depth and duration of immunosuppression must be carefully balanced. Excessive immunosuppression increases susceptibility to infection and relapse, whereas insufficient suppression heightens GvHD risk. Modern strategies have substantially reduced the incidence and severity of GvHD but must be carefully tailored to support timely immune recovery.

1.6 Immune Reconstitution Following AlloSCT

The recovery of immune competence following alloSCT is a prolonged, multi-phased process that determines susceptibility to infection, the balance between GvL and GvHD and ultimately long-term survival. Compared to innate myeloid compartments, which usually normalise within weeks, adaptive immune recovery is slower and more variable. In particular, T cells show the most delayed reconstitution, both in number and function and their recovery trajectory is a major determinant of post-transplant outcome [85].

T cell reconstitution occurs through two overlapping but biologically distinct pathways. In the early weeks following transplantation, peripheral homeostatic expansion predominates, driven by passenger mature donor-derived T cells transferred in the graft. These cells undergo cytokine- and antigen-driven proliferation in a profoundly lymphopenic, post-conditioning environment, generating an oligoclonal repertoire [86, 87]. This thymus-independent mechanism is predominant during the first 6 months, given the delay to thymopoiesis. Thymic-dependent lymphopoiesis then progressively contributes to the T cell pool, producing novel and phenotypically naïve T cells with a diverse TCR repertoire. This process is essential for long-term immune competence but is highly sensitive to multiple factors, including age, cell source, conditioning and concurrent immunosuppression [87–89].

T cell subsets reconstitute in distinct patterns post-alloSCT. $CD4^+$ T cells reconstitute more slowly than $CD8^+$ T cells, and delayed $CD4^+$ recovery is a consistent predictor of opportunistic infection, viral reactivation, relapse and inferior survival [90].

In T cell-replete grafts, numbers of conventional $CD4^+$ T cells may begin to rise within one to two months, but normalisation often takes up to a year. There are major differences in $CD4^+$ T cell reconstitution based on the cell source of the donor graft. Peripheral blood stem cell grafts generally result in faster $CD4^+$ reconstitution than bone marrow grafts [88, 90]. Early $CD4^+$ reconstitution is also

highly affected by the choice of conditioning. As an example, T cell-depleted grafts, such as those which use *in vivo* depletion with ATG, result in extreme delays of reconstitution, where patients can take up to 2 years to fully recover [91, 92].

Tregs, which maintain immune homeostasis and promote self-tolerance typically comprise 4-10% of the circulating $CD4^+$ population in healthy adults. The proportion of Tregs returns to normal within 6 weeks post-alloSCT, and it has been suggested that Treg reconstitution is primarily achieved by homeostatic peripheral expansion [93, 94]. High numbers of Tregs in the graft and early post-alloSCT period are negatively correlated with GvHD [95, 96]. Over the following months, Treg populations vary between individuals, reflecting differences in clinical context. As an example, the use of sirolimus, common in haploidentical transplantation, promotes Treg expansion [97].

The recovery of $CD8^+$ T cells begins earlier than that of $CD4^+$ T cells, with an inverted CD4:CD8 ratio being a common feature of the early post-alloSCT period. $CD8^+$ T cell reconstitution is detectable within the first month and most patients reach normal circulating $CD8^+$ levels by approximately 10 months [89, 98]. This fast $CD8^+$ reconstitution is a result of efficient peripheral expansion of effector memory cells. Unlike $CD4^+$ T cells, $CD8^+$ counts are more variable, fluctuating in response to microbial events and viral reactivation [99]. CMV plays an important role, with a substantial portion of the post-alloSCT $CD8^+$ repertoire dedicated to CMV control, and a markedly faster reconstitution in patients receiving grafts from CMV^+ donors [100–102].

Several non-classical T cell lineages display distinct reconstitution kinetics and clinical associations. γδ T cells, which express the γδ TCR instead of the conventional αβ TCR, comprise around 5% of the T cell population in healthy individuals. γδ T cells lack CD4 and CD8 co-receptors and mediate HLA-independent innate immunity through recognition of phosphoantigens, lipids and stress-induced ligands [103]. Although their precise role in GvL and GvHD has not been fully elucidated,

high levels of γδ T cells post-alloSCT are associated with improved leukaemia-free survival, reduced rates of infection, and reduced relapse rates in the absence of GvHD [104, 105]. γδ T cells typically recover early, within 1-2 months post-alloSCT, with similar dynamic changes in response to the clinical context [106].

Invariant NKT (iNKT) cells are another rare, innate-like subset with potent immunomodulatory properties. They express a semi-invariant αβ TCR that recognises lipid antigens presented by CD1d. iNKT cells also reconstitute rapidly, reaching normal values within 1 month post-alloSCT [107]. High numbers of iNKT cells have been associated with protection against GvHD and relapse [108–110].

An important parallel measure of immune reconstitution is donor chimerism, which refers to the proportion of haematopoietic and immune cells in the recipient that are derived from donor cells. Full donor chimerism denotes 95-100% donor-derived cells, whereas mixed chimerism indicates the persistence of a measurable recipient-derived population [111]. Mixed chimerism can be stable or progressive, with falling levels of donor chimerism often heralding impending graft rejection or relapse. In the T cell compartment, persistent mixed chimerism in the early post-alloSCT period may reflect delayed immune reconstitution and is variably associated with increased rates of relapse [112, 113].

1.7 Evidence for the Graft-versus-Leukaemia (GvL) Effect

The long-term efficacy of alloSCT in AML is fundamentally dependent on the GvL effect. Rather than serving solely as a means for haematopoietic rescue following conditioning, the donor graft acts as a potent immunological agent capable of recognising and eradicating leukaemic cells.

A substantial body of clinical and experimental evidence has established GvL as the principal mediator of durable remission post-transplant. This section examines the origins of this concept and the major strands of evidence that continue to define

its biological and therapeutic significance.

1.7.1 The Link Between GvL and GvHD

The earliest evidence for the GvL effect in humans emerged from clinical observations in the 1970s, where investigators noted a striking inverse correlation between the occurrence of GvHD and relapse following alloSCT. In a series of landmark studies, patients with acute leukaemia who developed chronic GvHD were found to relapse less frequently than those who did not, despite experiencing higher non-relapse mortality due to GvHD itself [114, 115]. These findings suggested that donor-derived alloimmunity, while deleterious in the form of GvHD, might simultaneously mediate beneficial anti-leukaemic activity.

Over the following decades, this relationship has been repeatedly recapitulated in large observational analyses. Both acute and chronic GvHD have been associated with lower relapse rates in a range of haematological malignancies [116, 117]. The strength of the GvHD-GvL association does appear to vary by clinical context and disease. In patients with chronic myeloid leukaemia (CML) and acute lymphoblastic leukaemia (ALL), this correlation is particularly pronounced, with the presence of chronic GvHD conferring a marked reduction in relapse risk. In AML, this relationship is somewhat less robust but remains both statistically and clinically significant [118]. Notably, these associations are more consistently observed in patients transplanted in complete remission, suggesting that GvL may be most effective in settings of low disease burden.

Further indirect evidence for the GvL effect comes from comparisons between syngeneic and allogeneic transplantation. Patients receiving syngeneic grafts from identical twins (in whom donor T cells are immunologically tolerant and incapable of enacting GvHD) experience consistently higher relapse rates than those receiving matched sibling allografts, despite comparable disease risk and pre-transplant

conditioning [52]. This supports the concept that alloreactivity is a key determinant of sustained disease control.

Although GvHD and GvL frequently co-occur, they are not inextricably linked. There are many documented instances of patients achieving a durable remission in the absence of clinically apparent GvHD, particularly in the context of donor lymphocyte infusions (DLI) administered for post-transplant relapse [119, 120]. These cases provide proof of principle that selective GvL is possible, even if it currently is not reliably achieved.

1.7.2 T Cell Depletion (TCD)

Efforts to reduce the incidence of GvHD through T cell depletion (TCD) have inadvertently provided some of the strongest evidence for the existence of GvL. Across both *ex vivo* and *in vivo* approaches, the consistent consequence of TCD in the alloSCT setting for AML has been a substantial increase in relapse risk, underscoring the indispensable role of donor T cells in post-transplant disease control.

The increased incidence of leukaemia relapse associated with TCD alloSCT was first noted in a prospective clinical trial in the 1980s involving 40 patients with leukaemia. This study utilised *ex vivo* antibody-mediated depletion of donor T cells from the graft prior to infusion. Although the difference did not reach statistical significance, relapse was more than three times as frequent in the TCD group compared to the control arm [121]. Subsequent larger retrospective analyses demonstrated a consistent two- to threefold increase in relapse among patients receiving TCD grafts, compared to those receiving unmodified transplants [52, 122].

A similar pattern has been observed in patients receiving *in vivo* T cell depletion, using serotherapeutic agents such as ATG or alemtuzumab. While these agents

effectively reduce the incidence of chronic GvHD, they have also been associated with impaired GvL and higher rates of relapse. Retrospective analyses have reported a relapse rate of 35% in patients receiving alemtuzumab compared with 19% of those receiving standard GvHD prophylaxis [123].

1.7.3 Reduced Intensity Conditioning (RIC)

The clinical success of RIC regimens offers further evidence for the capacity of the GvL effect to mediate durable disease control in AML. By design, unlike MAC, RIC delivers cytotoxic chemotherapy at doses that are insufficient to reliably eradicate leukaemia. The achievement of long-term remission in this setting therefore provides direct evidence for the therapeutic potency of GvL [124].

This principle was first demonstrated in early studies of transplantation in older or comorbid patients, where durable remissions were observed despite substantial dose reductions in conditioning. Initial concerns that reducing conditioning would lead to unacceptably high relapse rates were assuaged following early studies demonstrating that long-term survival was still achievable, even in this frailer cohort [125].

Subsequent comparative analyses between RIC and MAC have consistently shown that while relapse rates are higher after RIC, there was no overall survival difference between the two groups. This was due to the increased relapse rate of RIC being compensated by a reduced treatment-related mortality (TRM). In fact, when patients were transplanted in complete remission, the outcomes for RIC were superior, with comparable relapse rates but lower TRM, indicating that in the context of low disease burden, GvL can compensate for reduced cytoreduction [126, 127].

1.7.4 Donor Lymphocyte Infusions (DLI)

The clinical activity of DLI provides some of the most direct evidence for GvL in AML. DLI involves the infusion of lymphocytes from the original stem cell donor into the recipient after alloSCT, most commonly for treatment of overt or molecular relapse. As no cytotoxic agents are administered at the time of infusion, any anti-leukaemic effect can be attributed to the immunological activity of the donor lymphocytes.

The ability of DLI to induce durable remissions was first demonstrated in the 1990s for the treatment of CML, with subsequent extension of its use to acute leukaemias [128]. In larger analyses of patients with AML relapsing after alloSCT, DLI achieved sustained remission in a subset of patients, with outcomes most favourable when given for molecular or early relapse. In a cohort of 399 patients taken from the European Society for Blood and Marrow Transplantation (EBMT), the estimated survival at 2 years was 9% for patients who did not receive DLI, and 56% for those receiving DLI in the context of low-burden disease [129, 130].

In addition to its role as salvage therapy, DLI has also been employed in prophylactic (administered in remission, when MRD-negative) and pre-emptive (administered when MRD-positive) strategies to augment GvL activity in AML. Both strategies have shown improved survival when compared to DLI given at overt relapse, attributed to intervention at a stage of low disease burden, where GvL is most effective [131–133].

Beyond demonstrating the existence of GvL, DLI highlights the potential to uncouple its beneficial effects from GvHD. While GvHD is a frequent complication, its incidence can be mitigated through the use of escalating-dose schedules, and durable molecular remissions have been achieved without clinically significant GvHD, providing proof-of-principle that selective GvL is achievable [129, 134, 135].

1.7.5 Post-AlloSCT Immune Evasion

Many cases of post-alloSCT relapse occur as the AML acquires the capacity to evade immune recognition and destruction. The mechanisms by which AML is able to achieve this immune escape are now increasingly well-defined and their very existence supports the powerful selective pressure exerted by GvL from donor-derived immunity [136].

The most clearly characterised mechanism of post-transplant immune escape is genomic loss of the mismatched HLA haplotype after haploidentical transplantation. This phenomenon occurs in around 30% of patients relapsing after haploidentical alloSCT and is mediated by acquired uniparental disomy of chromosome 6p [137]. Although first described in haploidentical transplants, similar losses of mismatched HLA are reported in MUD transplants, where focal deletions or mutations in both class I and class II HLA genes have been identified at relapse [138, 139].

In other patients, the evasion of GvL through loss of HLA-mediated antigen presentation can occur through transcriptional silencing rather than structural loss. Post-alloSCT relapsed AML samples have demonstrated marked downregulation of HLA class II genes and their transcriptional regulators, with expression of class II HLA at relapse being up to 12 times lower than paired samples at diagnosis [140, 141]. Notably, given selective pressure on both class I and class II pathways, this supports roles for both $CD8^+$ and $CD4^+$ T cell-mediated responses in GvL.

AML relapse is frequently accompanied by upregulation of inhibitory ligands on AML blasts, including PD-L1 and B7-H3, alongside the downregulation of co-stimulatory ligands such as CD80 and CD86. This phenotype was associated with functional T cell exhaustion and diminished cytotoxicity [141]. Finally, AML is also able to remodel its metabolic environment to suppress T cell-mediated surveillance. Examples of this include the expression of arginase II, which impairs T cell proliferation, and indoleamine 2,3-dioxygenase 1, which suppresses effector T

cells and promotes immunosuppressive Treg differentiation [142, 143].

1.8 Identification of GvL Responses

An ongoing question in the field of alloSCT is the nature of GvL antigens. Identifying these targets is not only essential for understanding the biology of GvL, but also for developing strategies to separate its beneficial effects from the morbidity of GvHD. Knowledge of the precise antigens involved could inform donor selection, allow real-time tracking of anti-leukaemic immunity and facilitate the development of targeted cellular therapies [144, 145].

1.8.1 Methods for GvL Antigen Discovery

The earliest insights into GvL-specific immunity in humans came in the early 1990s, when donor-derived cytotoxic T cells were cloned from the peripheral blood of post-alloSCT patients and tested for reactivity against recipient-derived target cells [146, 147]. Although much of this work took place in the context of GvHD or shared GvL/GvHD responses, it revealed that certain antigens, such as HA-1 and HA-2, were also expressed on AML blasts and could mediate clinically significant anti-leukaemic effects [148].

Approaches that proceed in this manner, starting with a functionally relevant GvL effector T cell population and working backwards to identify the cognate peptide-HLA, are referred to as forward immunology.

Forward immunological approaches face several challenges. The first is isolating a meaningful T cell population, which is to say one that is clonally expanded, functionally relevant and leukaemia-reactive. Once such a population is identified, the next task is to define the peptide-HLA complex it recognises. Historically, this has been achieved through cDNA library screening of recipient-derived cell lines, linkage analysis or genome-wide association studies of single nucleotide

polymorphism (SNP) variation. More recently, combinatorial pipelines have begun to streamline antigen discovery, exemplified by approaches such as CANTiGEN, which integrates positional scanning peptide library data with cancer proteomic databases to predict peptide–HLA ligands for orphan TCRs [149].

Regardless of approach, mapping the peptide-HLA in this manner is technically challenging and labour-intensive [150]. Full characterisation also requires identification of the cognate TCR, which can be achieved by a number of sequencing approaches [151].

Reverse immunological discovery takes the opposite route, beginning with a set of candidate peptides and testing whether donor-derived T cells recognise them. This approach does not require the prior isolation of a reactive T cell population and is therefore well-suited for systematic high-throughput screening of large antigen repertoires. Prediction of these peptides draws on multiple techniques. Genomic and transcriptomic analysis can highlight non-synonymous SNPs, insertion-deletions or structural variants mismatched between donor-recipient pairs as well as genes that are selectively expressed in leukaemia [152, 153]. *In silico* algorithms are also used, either in the prediction of potential epitopes themselves, such as SNEP, or to further filter peptides using HLA-binding algorithms, such as NetMHCpan [154, 155].

Immunopeptidomics can provide empirical confirmation of peptide presentation by eluting and sequencing peptides bound to HLA molecules on AML blasts [156, 157].

Predicted peptides are then tested for immunogenicity. This has been performed functionally, often via peptide-pulsed target cells, but other techniques are also employed [158]. Large-scale DNA-barcoded peptide-MHC multimer libraries have been used to screen thousands of peptides in parallel [159, 160].

Despite numerous technological advances, the number of molecularly defined, clinically validated GvL antigens remains small. Most studies rely on peripheral blood sampling and focus on class I HLA-restricted antigens. Overcoming these

limitations will be essential for improving the landscape of GvL targets.

1.8.2 Tumour-Derived Antigens in AML

Tumour-derived antigens encompass a heterogeneous group of targets generated through mutation, altered gene expression or abnormal processing restricted to cancer cells. Although these antigens can also be recognised in the autologous setting, they remain relevant to GvL as donor-derived immunity can mount a response against them post-alloSCT [161].

Tumour-associated antigens (TAAs) are non-mutated self-proteins that are absent or expressed at low levels in normal tissues but aberrantly expressed or overexpressed in AML. They may be lineage-restricted or oncofoetal antigens re-expressed during malignant transformation.

One of the most studied TAAs in AML is WT1, a zinc finger transcription factor that is essential during embryogenesis, but in adults is normally expressed only at low levels in a few tissues, including kidney podocytes and haematopoietic stem cells.

In AML, *WT1* can be overexpressed by 10- to 1000-fold compared with normal tissues, driving subsequent immune recognition [162, 163]. Therapies targeting WT1 have been shown to demonstrate anti-leukaemic effects both in the context of peptide vaccination and engineered WT1-specific T cells [164–166].

Another well-characterised example is PR1, a peptide derived from neutrophil elastase and proteinase-3, both of which are highly expressed in AML [167]. PR1-targeted strategies have also shown *in vivo* anti-leukaemic efficacy [164, 168].

While TAAs benefit from relatively broad applicability across AML patients, as self-antigens, they are subject to both central and peripheral tolerance. Effective T cell responses against them may therefore require an appropriate inflammatory context or high antigen loads. Additionally, low-level expression in normal tissues carries risks of off-target toxicities, underscoring the importance of careful target

selection [169].

Neoantigens are peptides generated by somatic mutations that are unique to cancers and, by definition, absent from normal tissues. In AML, the overall mutational burden is low relative to most solid tumours, severely limiting the pool of potential targets [170]. Nevertheless, recurrent mutations in leukaemia driver genes have been shown to generate shared neoantigenic epitopes.

One of the most promising examples are neoantigens derived from mutations in *NPM1*, an oncogenic driver present in approximately 30% of adult cases. *NPM1* mutations most commonly involve alterations in the C-terminus that generate a novel nuclear export signal, resulting in a unique peptide sequence that is absent from the wild-type protein. Studies have demonstrated presentation of this mutant C-terminal peptide by HLA class I and recognition by $CD8^+$ T cells [171, 172]. Moreover, NPM1-specific T cell responses have been detected in both autologous and post-alloSCT settings [173].

Another illustrative example is the *CBFB-MYH11* fusion gene found in core-binding factor AML with inv(16) or t(16;16). This fusion transcript encodes a novel junctional region that is absent from the normal proteome and peptides spanning this breakpoint have been shown to elicit T cell responses in the *in vitro* setting [174].

Tumour-exclusive expression of neoantigens minimises the risk of off-target toxicities, but their clinical utility is constrained by the rarity of recurrent, immunogenic mutations in AML, inter-patient HLA diversity as well as immune evasion. Neoantigens derived from driver genes may represent more stable and therapeutically relevant targets [175].

Non-canonical antigens represent an emerging and diverse category within cancer and AML immunology, arising from atypical genomic and proteomic processes. These include aberrant splicing-derived peptides, such as those generated by exon skipping or intron retention that create novel junctional epitopes [176]; post-translationally modified peptides, including phosphopeptides, that modulate TCR

recognition [177]; and peptides derived from endogenous retrotransposons, arising from de-repression of normally silenced genomic sequences such as from human endogenous retroviruses [178]. Although these antigens expand the potential GvL antigen repertoire, they remain at an early stage of translational development, with few candidates that have been validated in the clinical setting of AML, let alone post-alloSCT [179].

1.8.3 Allorecognition

Allorecognition describes the process by which donor T cells respond to self-peptides presented in the context of non-self HLA molecules. Because donor thymic selection occurs only against self-HLA, the donor T cell repertoire is not tolerised to novel peptide-HLA combinations encountered post-alloSCT. Recognition may be mediated by direct contact with polymorphic residues of the non-self HLA, or by engagement of self-peptides bound within its groove. It is this allorecognition that drives GvHD and rejection in the solid organ transplantation setting [180, 181].

As previously discussed, in the alloSCT setting, extensive HLA matching is employed to reduce the number of novel peptide–HLA complexes introduced at transplantation, thereby minimising the risk of uncontrolled alloresponses. HLA mismatches still occur however, such as in permissive HLA mismatches in MUD transplantation and in haploidentical transplantation, which introduces an entire non-shared haplotype. This mismatched haplotype markedly broadens the landscape of potential T cell targets, and is thought to contribute both to the potent graft-versus-leukaemia effects observed in haploidentical transplants and to the elevated risk of graft-versus-host disease that requires mitigation by additional immunosuppression such as PTCy [82, 182].

Despite its likely importance in alloSCT, allorecognition has been less systematically studied here than in solid organ transplantation. Historically, the catastrophic

consequences of HLA mismatching discouraged mechanistic dissection, reinforcing a focus on prevention through matching strategies. However, with haploidentical transplantation now widely adopted, there is increasing interest in characterising how allo-HLA restricted recognition contributes to GvL and how it might be modulated to limit GvHD [69].

1.8.4 Minor Histocompatibility Antigens (miHAs)

Minor histocompatibility antigens (miHAs) are peptides derived from polymorphic proteins in the human proteome that differ between individuals due to germline genetic variation. These variations most commonly arise from non-synonymous SNPs but can also result from small insertion-deletions or splice variants. A miHA mismatch occurs when the donor and recipient differ at such a locus, leading to the presentation of a peptide in the recipient that is absent in the donor.

In the post-alloSCT setting, these mismatches can be recognised as foreign by donor T cells. This can mediate GvL when the miHA is expressed on malignant haematopoietic cells, but can also cause GvHD if expressed in non-haematopoietic tissues [183]. Haematopoietically-restricted miHAs are therefore of particular interest as they offer the potential for selective GvL without off-target toxicities.

HA-1, encoded by *HMHA1*, remains the most extensively characterised miHA and a prototype for the clinical translation of miHA-targeted immunotherapy. It is a 9-mer peptide that is presented by HLA-A*02:01 or A*02:06, with expression largely confined to haematopoietic cells, including AML blasts, and minimal or absent expression in non-haematopoietic tissues [184]. HA-1-specific T cells have undergone extensive functional and clinical testing. *In vitro*, they are able to lyse HA-1-positive AML blasts [185, 186]. In HLA-matched but HA-1-mismatched transplant settings, HA-1-specific T cells can emerge after DLI, with responses temporally associated with AML remission [148]. A multicentre study of more than

800 patients demonstrated that mismatches in the graft-to-host direction of HA-1 were significantly associated with a reduced risk of AML relapse [187].

Several translational strategies have targeted HA-1, including phase I/II clinical trials of HA-1-specific T cell infusions and TCR gene transfers, each demonstrating safety, immunogenicity and preliminary signals of efficacy [188, 189].

Recent high-throughput, reverse immunological approaches have expanded the catalogue of molecularly defined GvL miHAs to several hundred antigens. The vast majority of these are HLA class I-restricted, with far fewer class II-restricted miHAs identified. Only a minority of these antigens have been functionally validated, and an even smaller set, primarily those with haematopoietically restricted expression have been evaluated clinically [152, 153].

Examples of candidate class II-restricted miHAs include LB-PIP4K2A and LB-ECGF, but technical challenges such as the promiscuity of the class II peptide groove, the lack of a strict peptide length constraint, the influence of flanking peptide residues and the complexity of $CD4^+$ T cell assays have limited their characterisation [190, 191].

Although most molecularly-defined GvL antigens to date are presented by HLA class I molecules and recognised by $CD8^+$ T cells, there is increasing evidence that class II-restricted $CD4^+$ T cell responses play an important role in mediating durable anti-leukaemic immunity [40, 192, 193]. In contrast to class I, class II expression is normally restricted to professional APCs and haematopoietic cells, offering the theoretical advantage of more selective targeting of leukaemia and limiting off-target toxicity [194]. Overcoming the current barriers to class II GvL antigen discovery will be a key step in fully defining the GvL repertoire and exploiting the therapeutic potential of $CD4^+$-mediated responses.

Though the expansion of the miHA repertoire is an important advance, there is a pressing need for prospective validation of candidate antigens. Most reported correlations between miHA mismatching and clinical outcome derive from retrospective or

observational datasets, which may capture statistical associations without proving mechanistic or functional relevance. Furthermore, many putative GvL-associated miHAs have not been tested for natural processing, stable presentation or *in vivo* relevance. Without further study, it remains uncertain which miHAs genuinely drive GvL *in vivo*, let alone which would prove to be consistently safe, immunogenic and clinically effective.

1.9 Translational Potential of GvL Antigen Discovery

The discovery and validation of molecularly defined GvL antigens and their cognate TCRs has direct clinical implications that extend beyond mechanistic insight.

Validated GvL antigens could potentially inform donor selection, which currently focuses on HLA matching. Various studies have investigated whether mismatches in confirmed miHAs can predict clinical outcome with conflicting results. One study, which examined six known miHAs, found no significant change in relapse rates when mismatched. However, mismatching was associated with reduced overall survival due to GvHD [195]. Conversely, two larger studies covering 24 antigens and more than 1000 patients reported that mismatching for one or more miHAs, whether haematopoietically restricted or ubiquitously expressed, was associated with longer relapse-free survival, although for some antigens, this benefit was only observed in the presence of active GvHD [187, 196].

The predictive accuracy of such approaches currently remains limited, partly due to the limited number of miHAs interrogated to date and the confounding effects of GvHD. Broadening the repertoire of characterised antigen targets and delineating the contribution of selective GvL antigens could substantially refine predictive algorithms for GvL and GvHD, thereby enabling more precise donor selection.

The identification of antigen-specific TCR sequences enables longitudinal tracking of GvL clonotypes. This monitoring could complement MRD assays and measurements of donor engraftment to inform post-alloSCT responses by providing a direct readout of the anti-leukaemic immune repertoire, where a decline in GvL clonotype abundance could precede molecular relapse. Detection of waning GvL activity could enable timely intervention, such as withdrawal of immunosuppression, DLI or maintenance chemotherapy [197]. As an example, in a study of 327 miHA-mismatched patients, peptide-MHC multimers were used to identify T cells specific for 15 miHAs, with the detection of antigen-specific T cell populations being correlated with improved relapse-free survival [196].

Finally, validated GvL antigens, particularly those with a broad HLA restriction, high population mismatch frequency and haematopoietically restricted expression, can be attractive targets for selective immunotherapy. Trials of adoptive transfer of HA-1-specific cells and peptide vaccination for WT1 have already been discussed (section 1.8), but further expansion of the antigen repertoire could broaden the range of therapeutically actionable targets capable of inducing selective GvL.

1.10 Previous Studies Within Our Laboratory of GvL in AML patients

The work contained within this chapter was performed by previous lab members Connor Sweeney and Gerda Mickute and presented within their DPhil theses [198, 199].

Previous work in the laboratory employed a reverse immunological approach to identify novel GvL responses in a cohort of 12 patients with AML who achieved sustained remission with alloSCT. Full clinical details for these patients are provided within the appendix (Figure A.1 - A.5). These patients were selected on the basis of clinical characteristics associated with a low likelihood of long-term remission

using chemotherapy alone, thereby maximising the probability of detecting a potent GvL response (Figure 1.5a).

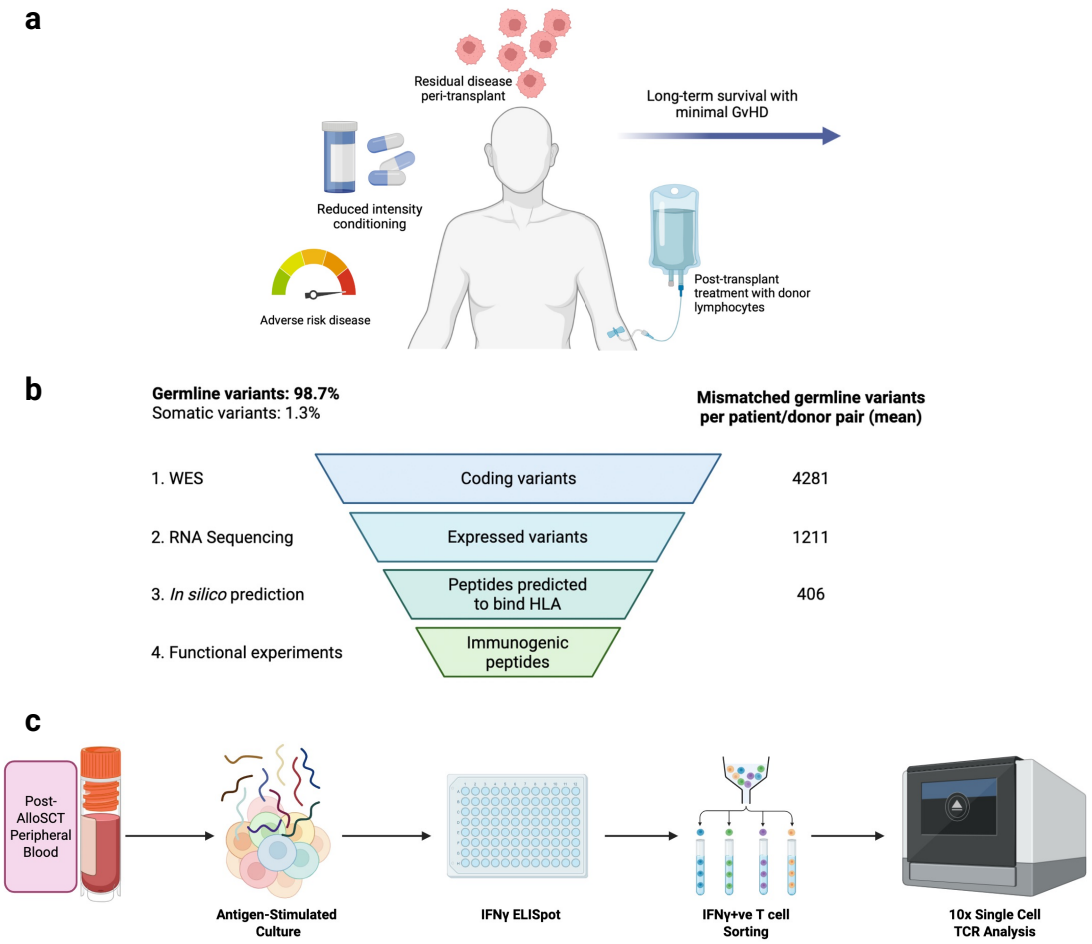

Figure 1.5: Summary of approach used to identify novel GvL responses. a. Overview of criteria used in selection of "GvL-enriched" patient cohort. **b.** Filtering steps used to generate candidate peptide library of mismatched patient-donor variants. **c.** Experimental schema demonstrating functional screening of candidate peptide library. *Data generated by Connor Sweeney* [198].

Of the 12 patients, ten patients underwent reduced-intensity conditioning, and seven experienced pre-transplant relapse necessitating salvage chemotherapy. Notably, one patient relapsed early post-alloSCT (3 months) but achieved remission after treatment with DLIs. At the time of analysis, all patients had sustained durable remission for 7-13 years (8-13 years of follow-up). To preferentially enrich for GvL over GvHD, patients were selected for minimal GvHD, with only two

experiencing acute GvHD greater than grade 1 or chronic GvHD more severe than mild.

To identify putative GvL antigens, the 12 patient-donor pairs underwent a multi-step filtering strategy (Figure 1.5b). Whole-exome sequencing of donor DNA, patient AML cells and healthy patient cells was first used to identify protein-encoding mismatches, the vast majority (98.7%) of which were germline. These were then restricted to transcriptionally active variants using bulk RNA sequencing of AML cells, generating a library of peptides spanning the relevant polymorphic regions. *In silico* HLA-binding prediction, with NetMHCpan 4.0 and NetMHCIIpan 3.0, was subsequently applied to select peptides with the highest predicted affinity (top 0.5%) for either class I or class II HLA molecules [200, 201]. This process yielded a candidate peptide library for functional screening with cryopreserved post-alloSCT peripheral blood mononuclear cells (PBMCs) collected 2-7 years after transplantation.

Screening was performed using a cultured IFNγ ELISpot assay (Figure 1.5c). Patient PBMCs were cultured with peptide pools to preferentially expand antigen-specific T cells, then tested for activation using IFNγ ELISpot. Positive peptide pools were deconvoluted to individual peptides, and antigen-specific T cells were subsequently isolated via IFNγ-Catch assays and analysed by 10x Genomics single-cell RNA sequencing with V(D)J enrichment to identify their TCR sequences.

Using this approach, 22 antigen-specific T cell responses were identified, all targeting non-synonymous, mismatched SNPs (Appendix Figure B.1).

One of these antigens, peptidylarginine deiminase 4 (PADI4), was selected for further validation due to its expression being largely restricted to the haematopoietic compartment, thereby minimising the risk of off-target effects. The cognate PADI4 TCR was introduced into third-party T cells, and its function was evaluated in a number of key contexts.

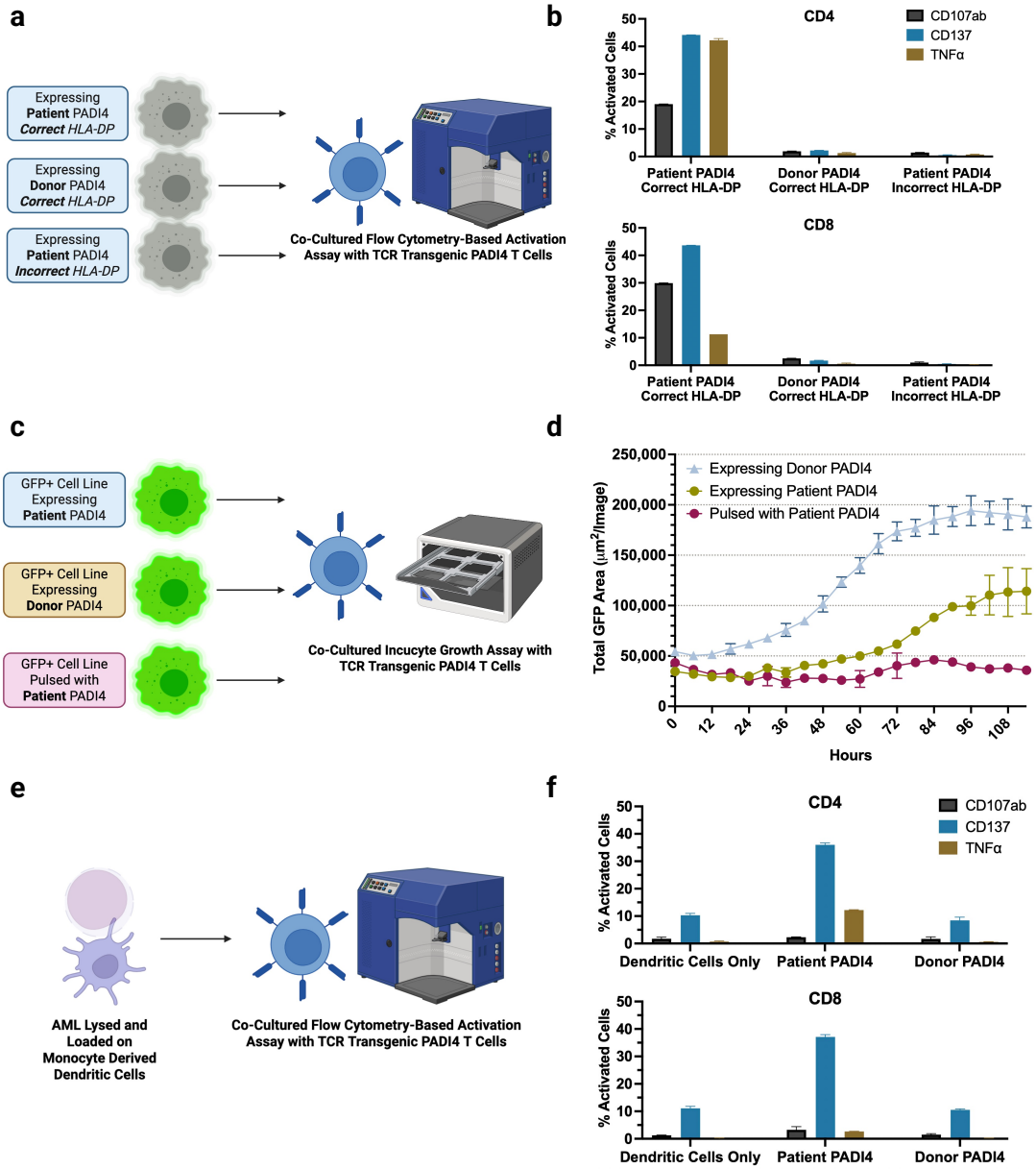

Figure 1.6: Functional validation of the PADI4-specific TCR a. Schematic of activation assays utilising transgenic PADI4-expressing cell lines. **b.** Flow cytometry analysis of $CD4^+$ and $CD8^+$ PADI4 T cells showing activation only in response to patient PADI4 with correct HLA-DP. **c.** Schematic of live-cell imaging assay using GFP^+ target cells. **d.** Quantification of GFP^+ target cell growth showing inhibition only for patient PADI4-expressing cells. **e.** Schematic of dendritic cell cross-presentation assays with primary AML lysate. **f.** Flow cytometry analysis of $CD4^+$ and $CD8^+$ PADI4 T cells only in response to dendritic cells loaded with lysate from AML expressing patient PADI4. *Data generated by Gerda Mickute [199]*

First, cancer cell lines were used to confirm both physiological antigen presentation and T cell activation. Monomac-1 (AML) and Boleth (B lymphoblastoid) cells, expressing the relevant restricting HLA-DP allele and engineered to express the PADI4 variant protein, elicited specific activation of transgenic PADI4 T cells in response to endogenously processed peptide (Figure 1.6a and b). This response was both SNP-specific and HLA-specific. Second, the PADI4 T cells exerted a growth-inhibitory effect on these target cells (Figure 1.6c and d). Finally, although autologous AML blasts from the patient were not available, blasts from other AML patients carrying the relevant PADI4 SNP and restricting HLA-DP allele were used. In this setting, direct activation or cytotoxicity against AML blasts was not observed, but activation occurred when AML lysate was processed and presented by monocyte-derived dendritic cells (Figure 1.6e and f). This indicates that while direct presentation by AML may be insufficient in this experimental system, PADI4-specific responses could still be engaged via professional antigen-presenting cells, with cross-presentation potentially contributing to GvL activity.

1.11 Thesis Aims

As described above, our laboratory previously established a high-throughput pipeline for the identification of putative GvL antigens in late post-alloSCT peripheral blood samples.

Despite compelling evidence for GvL, the composition, frequency and phenotype of GvL T cells in the early post-alloSCT bone marrow remains poorly defined. The bone marrow serves as both the anatomical niche of leukaemia stem cells and an important reservoir for memory T cell responses, making it a critical compartment in which to interrogate GvL immunity [202, 203]. The early post-alloSCT period is widely considered the most clinically crucial window for GvL activity, coinciding both with the highest risk of AML relapse and occurring in closest proximity to

the antigenic challenge of AML, when residual malignant cells and their associated antigens are most likely to be encountered by donor-derived T cells [197, 204].

We hypothesise that rare GvL clonotypes are established early in the marrow but are missed by standard approaches. Targeting this compartment not only addresses a critical biological question but also capitalises on the available material, as the majority of remaining cryopreserved samples from the GvL-enriched cohort are BMMNCs collected within the first 12 months post-alloSCT.

The overarching aim of this thesis is to adapt and extend the existing discovery framework from the peripheral blood to the biologically and clinically relevant early bone marrow compartment, to detect, isolate and characterise GvL-reactive T cell responses, with the following objectives:

1. To optimise *in vitro* culture protocols for early post-alloSCT BMMNCs to balance T cell expansion, functional capacity and repertoire diversity.
2. To apply these optimised methods to the GvL-enriched cohort, aiming to identify both novel and previously described GvL responses from the early bone marrow.
3. To define and validate candidate GvL T cell responses, by utilising single-cell transcriptomics to pair TCR identity with transcriptional phenotype and by conducting functional validation using TCR-engineered transgenic T cells.
4. To explore alternative strategies, including *ex vivo* approaches, to identify rare GvL clonotypes and confirm their *in vivo* persistence without prior *in vitro* expansion.
5. To characterise the persistence, phenotype and transcriptional states of identified GvL T cells during the first year post-alloSCT to inform models of early GvL surveillance.

2

Materials and Methods

Contents

2.1 Sample Collection, Processing and Ethical Approval

Post-alloSCT peripheral blood and bone marrow samples were obtained with informed consent under ethically approved studies HaemBio (REC 17/SC/0572) and COSI (REC 19/NW/0135). Healthy blood or bone marrow samples were obtained with informed consent from the MARCH study (REC 17/YH/0382) or NHS Blood and Transplant (non-clinical issue account T255).

Samples were processed immediately via Ficoll density gradient separation for isolation of mononuclear cells (MNCs). Briefly, fresh blood or BM was diluted in phosphate-buffered saline (PBS) at a 1:1 ratio. The blood/BM-PBS solution was layered on top of Ficoll-Paque (Sigma-Aldrich) at a 2:1 ratio, followed by centrifugation at 400G with minimal acceleration and no brake. The MNC fraction was collected and washed twice with PBS. Samples were either used immediately or cryopreserved in a solution of heat-inactivated foetal bovine serum (HI-FBS) with 10% dimethyl sulfoxide (DMSO) and stored in liquid nitrogen.

2.2 Cell Culture

Unless otherwise stated, cells were cultured in sterile-filtered T cell media: RPMI-1640 (Gibco) with 5% heat-inactivated human AB serum (Sigma-Aldrich), 1% sodium pyruvate (Sigma-Aldrich), 1% MEM non-essential amino acids (Gibco), 1% GlutaMAX (Gibco), 1% HEPES buffer (Sigma-Aldrich), 1% penicillin/streptomycin (Sigma-Aldrich) and 0.1% β-mercaptoethanol (Gibco). Cells were cultured under sterile conditions at 37°C with 5% CO_2, passaged every 2-3 days and where possible maintained at a concentration of 1-2 million cells/ml in a 24-well tissue-culture-treated plate (Corning) with 1-2 ml per well.

Cell counting and viability assessments were performed using the NucleoCounter NC-3000 automatic cell counter (ChemoMetec) with Solution 13 – Acridine Orange and 4',6-diamidino-2-phenylindole (DAPI).

For the thawing of frozen samples, samples were incubated in a 37°C water bath until almost entirely thawed and then diluted dropwise with 1 ml of HI-FBS. Samples were subsequently washed with media prior to downstream applications.

Where cell culture conditions were being tested or optimised, specific cell culture supplements are outlined in their respective figures. Cell culture protocols that are repeatedly used are outlined below:

2.2.1 Polyclonally-Stimulated T Cell Culture

Following thaw, cells were cultured in T cell media supplemented with 1000 units/ml of IL-2 (PeproTech), 10 ng/ml of IL-15 (PeproTech) and anti-CD3/CD28-conjugated magnetic Dynabeads (Gibco) at a 1:1 bead-to-cell ratio. From day 3 onwards, cells were passaged in T cell media supplemented with 10 ng/ml of IL-7 (Bio-Techne) and 10 ng/ml of IL-15. Dynabeads were magnetically removed on day 5.

2.2.2 Antigen-Stimulated T Cell Culture

Following thaw, cells were cultured in T cell media supplemented with 25 ng/ml of IL-7 and 2 µg/ml each of the peptides of interest. Peptides were synthesised at crude purity (GenScript), reconstituted in DMSO and stored at -80°C until use. From day 3 onwards, cells were passaged in T cell media supplemented with 1,800 units/ml of IL-2.

2.2.3 Joint APC and T Cell Culture

At thaw, cells were instead diluted and washed with X-VIVO 15 media (Lonza). Cells were resuspended in X-VIVO 15 supplemented with 2000 IU/ml of granulocyte-macrophage colony-stimulating factor (GM-CSF, R&D Systems), 1000 IU/ml of IL-4 (R&D Systems) and 100 ng/ml of FLT3L (R&D Systems). Cells were plated at a concentration of 0.5 million cells/ml in 96-well U-bottomed plates with a volume

of 200 µl/well. On day 1, cells were passaged with X-VIVO 15 supplemented with 20 µM R848 (InvivoGen), 200 ng/ml of LPS (InvivoGen), 20 ng/ml of IL-1β (R&D Systems) and 2 µg/ml each of the peptides of interest.

On Day 2 and every 2-3 days following, cells were passaged in sterile-filtered R10 media: RPMI-1640 with 10% heat-inactivated human AB serum, 1% GlutaMAX, 1% HEPES buffer, 1% penicillin/streptomycin. This R10 media is supplemented with 20 IU/ml of IL-2, 20 ng/ml of IL-7 and 20 ng/ml of IL-15.

2.2.4 Culture of HEK 293T Cells

HEK 293T cells were taken from frozen lab stocks. Cells were cultured in DMEM (Gibco) with 10% HI-FBS, 1% GlutaMAX, 1% sodium pyruvate and 1% penicillin/streptomycin. Cells were cultured in tissue-culture-treated T75 flasks (Corning) and passaged on confluency. Cells were dissociated with 3 ml of Trypsin-EDTA 0.25% with phenol red (Gibco).

2.3 Flow Cytometry and Sorting of T Cells

Antibodies used for all flow cytometry analyses and sorting experiments are listed in the appendix (Figure B.2). Data analysis was performed using FACSDiva v9.0 and FlowJo v10.10.0.

Frozen samples were thawed as previously described in section 2.2, then resuspended in FACS buffer: IMDM with 10% HI-FBS and 20 µg/ml of DNAse (Thermo Fisher). Samples were then filtered through a 70 µm cell strainer, centrifuged at 350G for 10 minutes and resuspended in Trustain-FcX block (BioLegend) at 1:100 dilution in PBS (Trustain-PBS). After a 10-minute incubation, the cells were surface stained with CD3 (PECy7), CD4 (APC) and CD8 (FITC) for a further 30 minutes. Cells were then washed and resuspended in FACS buffer with DAPI.

For analysis alone, cells were acquired on a BD Fortessa X20. Cell sorting was performed on a Sony MA900 with a 100 µm nozzle. Following exclusion of dead cells and doublets, live $CD3^+$ cells were sorted into FACS buffer. Post-sort T cell purity was confirmed by re-analysis of sorted cells.

2.4 TCR Repertoire Analysis

RNA was first extracted from up to 1 million T cells utilising the Qiagen RNeasy Mini kit. TCR repertoire library preparation was undertaken utilising the Takara SMART-Seq Human TCR kit with Unique Molecular Identifiers (UMIs) according to manufacturer instructions. The RNA input amount was 10 ng with a corresponding 18 PCR1 cycles and 20 PCR2 cycles.

TCR libraries were purified using double-sided selection with NucleoMag Clean Up and Size Select Beads (Takara Bio). Library quality was assessed using the High Sensitivity DNA Bioanalyzer kit (Agilent) and quantified using the Qubit dsDNA High Sensitivity Assay kit (Thermo Fisher) prior to pooling.

Next-generation sequencing (NGS) was performed at the Weatherall Institute of Molecular Medicine sequencing facility using an Illumina NextSeq Mid-Output 500/550 v2.5 kit with 150 bp paired-end reads. Demultiplexing and FastQ generation was undertaken using Illumina BaseSpace Sequence Hub. Preprocessing, UMI-based error correction, assembly and clonotype calling were performed utilising the Cogent NGS ImmuneProfiler v1.5 pipeline. UMI-collapsed clonotypes were used for downstream analysis with further normalisation via data downsampling to ensure a comparable number of UMI-corrected reads per sample across different timepoints. Both TCRα and TCRβ chains were used in calculations of diversity. Chord diagrams were generated using Cogent NGS ImmuneViewer v1.0.

2.5 IFNγ, IL-2 and IL-4 ELISpot

96-well plates with polyvinylidene fluoride (PVDF) membranes (Merck Millipore) were activated with 70% ethanol, washed with PBS and coated with 10 µg/ml of coating antibody: either anti-IFNγ (1-D1K, Mabtech), anti-IL-2 (MT2A91/2C95, Mabtech) or anti-IL-4 (IL4-1, Mabtech). Plates were incubated overnight at 4°C and subsequently washed with PBS and blocked with warm T cell media for 3 hours.

Prior to ELISpot testing, T cells were rested for 24 hours in cytokine-free T cell media prior to plating. 200,000 cells/well were used, suspended in T cell media. Phytohaemagglutinin (PHA) was used as a positive control at a concentration of 10 µg/ml. DMSO was used as a negative control at a concentration of 1%. $CD8^+$ T cell-targeted Cytomegalovirus (CMV)/Epstein-Barr Virus (EBV)/Influenza (Flu) peptide pools (CEF, Mabtech) and $CD4^+$ T cell-targeted CMV/EBV/Flu/Tetanus/Adenovirus peptide pools (CEFTA, Mabtech) were used at a concentration of 2 µg/ml for each peptide. Peptides of interest were used at 2 µg/ml. Each condition was tested in duplicate or greater.

ELISpot plates were developed after 20 hours of incubation at 37°C. The plates were washed with PBS/0.05% Tween (Sigma) and subsequently incubated with 1µg/ml of biotinylated antibody solution: anti-IFNγ (7-B6-1, Mabtech), anti-IL-2 (MT8G10, Mabtech) or anti-IL-4 (IL4-II, Mabtech). Each antibody was diluted in PBS/0.5% bovine serum albumin (BSA, Sigma-Aldrich) and sterile-filtered.

After a 4-hour incubation at room temperature, the plates were washed with PBS/0.05% Tween. Avidin-peroxidase conjugate (Vector Laboratories) was then applied to the wells with a 1-hour incubation. The plates were then washed with PBS/0.05% Tween followed by PBS alone prior to the application of 3-amino-9-ethylcarbazole (AEC, Sigma-Aldrich) substrate.

AEC substrate was prepared using the following mixture, sterile-filtered through a 0.45 µm filter: an AEC tablet dissolved in 2.5 ml of dimethylformamide (DMF), 43.7 ml of deionised water, 3.5 ml of 0.1M acetic acid, 280 µl of 3M sodium acetate

and 25 µl of 30% hydrogen peroxide. The AEC substrate was applied to the wells for 3 minutes prior to washing with water.

Plate analysis was performed using an AID Multispot Reader with their bespoke ELISpot Reader 7.0 software.

2.6 IFNγ, IL-2 and IL-4 Cytokine Catch Assays

T cells were rested for 24 hours in cytokine-free T cell media prior to functional testing. Cells were pulsed with 10 µg/ml of peptide and incubated at 37°C for 6 hours. PHA was used as a positive control and DMSO as a negative control as previously described.

Following incubation with peptide, the cells were washed with cold buffer (PBS/0.5% BSA/2mM EDTA), centrifuged at 4°C and 300G for 10 minutes, resuspended in Cytokine Catch reagent (Miltenyi) and incubated on ice for 5 minutes. Warm T cell media was then added to the cells, followed by a cytokine secretion period of 45 minutes at 37°C under intermittent agitation. Cells were then washed further with cold buffer, centrifuged as previously described and resuspended in Trustain-PBS. After 10 minutes, the cell suspension was incubated with either IFNγ, IFNγ with IL-2 or IFNγ with IL-4 detection antibodies in conjunction with surface staining for CD3 (PE-Cy7), CD4 (APC) and CD8 (FITC) for 30 minutes at 4°C in the dark. Cells were then washed, resuspended in FACS buffer with Hoechst 33342 (Thermo Fisher) and acquired with a BD Fortessa X20.

2.7 T Cell Subset Analysis

Cells were washed, resuspended in Trustain-PBS and incubated at room temperature for 10 minutes. This is followed by staining with Live/Dead Fixable Aqua (Thermo Fisher) at a 1:500 dilution for 15 minutes. Cells were washed and surface stained for CD25 (BUV395), CD4 (BUV563), CD3 (BUV805), CD127 (BV421), CCR7

(BV650), CCR6 (BV785), CD28 (FITC), CXCR3 (PE), CCR4 (PE-Cy7), CD45RA (APC) and CD8 (APC-Cy7) for 15 minutes.

Cells were then fixed and permeabilised with eBioscience Foxp3/Transcription Factor Fixation/Permeabilisation solutions (Thermo Fisher) as per manufacturer instructions. This was followed by intracellular staining for FOXP3 (PE-Cy5) for 30 minutes.

Cells were then washed, resuspended in PBS and acquired on a BD Fortessa X50.

2.8 Analysis of Public Datasets

Protein expression across healthy tissues was assessed using data from the publicly available Human Protein Atlas (HPA) [205, 206]. Protein expression levels were retrieved from the Tissue Atlas module, which integrates immunohistochemistry data generated from tissue microarrays. Semi-quantitative protein expression scores were derived from staining intensity and the fraction of immunoreactive cells, as evaluated by expert pathologists using validated antibodies.

Gene expression data for healthy tissues was obtained from the HPA Consensus Expression Dataset [205, 207], which integrates RNA-seq data from multiple sources. Expression values were pre-analysed and reported as normalised transcripts per million (nTPM).

Gene expression data for AML and healthy haematopoietic cells was derived from the BloodSpot database [208, 209]. Pre-processed consensus $\log_2$ expression values were used for all comparisons. AML datasets included gene expression profiles from the BEAT-AML [210], TARGET-AML [211], TCGA [212] and MILE studies [213]. Expression data from healthy haematopoietic cell subpopulations was obtained from the HemaExplorer database [214].

2.9 Isolation and Identification of Antigen-Specific T Cells through Functional Testing

2.9.1 Sorting of IFNγ-Positive T Cells

Post-alloSCT samples were thawed and cultured for at least 12 days using the previously described antigen-stimulated T cell culture method. Cells were rested for 24 hours in cytokine-free media, and a cytokine catch assay for IFNγ was performed as previously described. IFNγ^+ and IFNγ^- fractions were sorted using a Sony MA900.

2.9.2 Sorting of T Cells Following Joint APC-T Cell Culture

Post-alloSCT samples were thawed and cultured utilising the previously described joint APC and T cell culture method and then rested for 24 hours in cytokine-free media. Cells were pooled, resuspended in R10 media at a concentration of 1 million cells/ml and then stimulated with 2 µg/ml of anti-CD28 (BD Biosciences), 2 µg/ml of anti-CD49d (BD Biosciences) and 2 µg/ml of peptide. Immediately after stimulation, cells underwent initial surface staining for CD40L (BUV805), CD107a (BV421), CD107b (BV421) and 4-1BB (BV650), followed by Golgi blockade with 2 µM Monensin after an hour. Following an 8-hour incubation, cells were washed, kept on ice, and resuspended in TruStain-PBS followed by staining with Live/Dead Fixable Aqua at a 1:500 dilution for 15 minutes. Cells were washed, followed by surface staining for CD8 (FITC), CD3 (APC) and CD4 (APC-Cy7) for 30 minutes. Cell sorting was performed utilising a BD FACSDiscover S8 with a 100 µm nozzle.

2.9.3 Preparation and Sequencing of Single-Cell Libraries

Single-cell whole transcriptome and V(D)J libraries were generated utilising the 10X Genomics Gel-Beads-in-Emulsion-X (GEM-X) Single-Cell 5' v3 system according to manufacturer instructions.

In brief, up to 20,000 cells were loaded into a 10X Chromium GEM-X chip, with GEM generation and barcoding run on a Chromium X. Following reverse

transcription and GEM cleanup, cDNA was amplified via 12-17 cycles of PCR dependent on input cell number.

Whole transcriptome libraries were generated from cDNA utilising Library Construction Kit C with sequencing indexes taken from Dual Index Kit TT Set A. V(D)J libraries were generated from cDNA following an initial V(D)J enrichment with the Chromium Single-Cell Human TCR Amplification kit, followed by library construction as above. Quality control and quantification during and following library preparation was undertaken using the Agilent High Sensitivity DNA Bioanalyzer and the Qubit dsDNA High Sensitivity Assay.

Pooled library sequencing was provided by Novogene UK, a commercial vendor. Libraries were sequenced to a depth of 20,000 reads/cell for whole transcriptome and 5,000 reads/cell for V(D)J. Sequencing was performed on the NovaSeq X platform, with 75bp paired-end reads and 10% PhiX.

2.9.4 Processing and Analysis of 10X Single-Cell Data

Single-cell whole transcriptome and V(D)J data was received as demultiplexed FASTQ files from Novogene UK. Joint whole transcriptome and V(D)J analysis was performed utilising CellRanger v8.0.1 software. The 'multi' command was used, with the Homo sapiens reference genome GRCh38. This pipeline aligns and filters sequencing reads, counts barcodes and UMIs, and performs paired clonotype calling on the V(D)J libraries. Cell calls from the V(D)J dataset are discarded if they are not simultaneously called in the whole transcriptome data. Data from the same patient was aggregated using the CellRanger 'aggr' command.

Using the 10x Loupe v8.0.0 software, quality control filtering was undertaken, including only cells with >1000 UMIs/cell, 500-7000 genes/cell and <10% mitochondrial transcripts. K-means clustering was performed within the Loupe platform.

Subsequent analysis was performed within a Python 3.12.1 environment. Scanpy v1.11.1 was used to perform Leiden clustering, UMAP visualisation and differential

gene expression. Statistical significance in differential gene expression was performed in Scanpy utilising the Wilcoxon Rank-Sum test with the Benjamini-Hochberg correction for false discovery rate (FDR). Gene expression heatmaps were generated using Scanpy, utilising normalised Z scoring.

Automated cell annotation was performed using the CellTypist v1.6.3 package, using the Immune_All_Low v2 dataset, which comprises immune sub-populations combined from 20 tissues in 18 studies [215]. Comparison of TCR clonotypes with known public TCRs was performed using the Immunarch v1.0 package, cross-referencing against the publicly available VDJdb [216, 217].

2.10 MHC Binding Predictions

HLA class II binding predictions were performed using two state-of-the-art algorithms to evaluate the binding affinities of potential METTL22-derived epitopes to donor HLA-DR alleles. All possible 15-mer peptide windows from the 20-mer METTL22-1 peptide were analysed using both tools. Predictions were conducted against the four HLA-DR alleles expressed by the donor (HLA-DRB1*04:01, HLA-DRB1*15:01, HLA-DRB4*01:03 and HLA-DRB5*01:01) as they would have been the alleles present during functional screening.

The first of these algorithms, MixMHC2pred v2.02, was executed in no-context mode to avoid incorporating flanking sequence information which would have been absent in the prior functional testing [218, 219]. The second algorithm was NetMHCIIpan 4.0 which was run using default parameters [155]. In both cases, the percentile rank score was taken as the primary output metric.

2.11 Production of Transduced Primary T Cells

2.11.1 Construction of Recombinant pHRsin Plasmid

The strategy for lentiviral plasmid construction is taken from Gerda Mickute's thesis and is outlined in Figure 2.1 [199]. The pHRsin plasmid map is outlined in the appendix (Figure B.3)

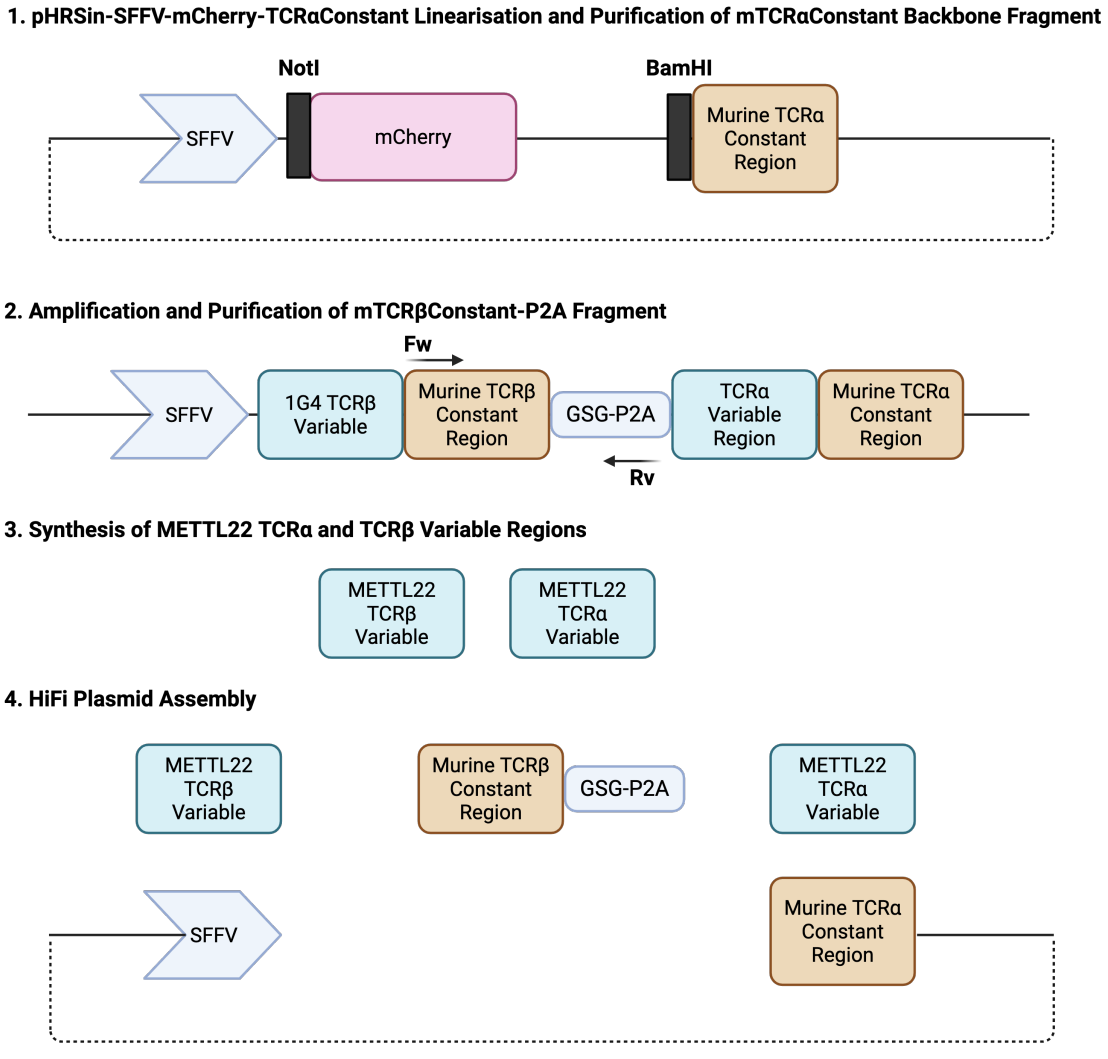

Figure 2.1: Strategy for generation of recombinant pHRSin transfer plasmid. Example growth curve for paired PBMC and BMMNC samples utilising antigen-stimulated culture from the prior GvL pipeline for a single patient.

The α and β variable regions of METTL22 Clonotypes 1,2 and 5 were codon-optimised and synthesised by Twist Bioscience with 20-30 bp overhangs for plasmid

assembly. The plasmids pHRsin-SFFV-mCherry-TCRαConstant and pHRsin-SFFV-1G4 were taken from frozen laboratory stocks.

The pHRSin-SFFV-mCherry-TCRαConstant plasmid was linearised using BamHI-HF(NEB) and NotI-HF (NEB) and gel purified using the QIAquick Gel Extraction Kit (Qiagen), generating a mTCRαConstant-Backbone fragment. The pHRsin-SFFV-1G4 plasmid was used to amplify a mTCRβConstant-P2A fragment using custom primers (forward: GAAGATCTACGTAACGTGACACCAC, reverse: CGGGGTTTTCCTCCACATCT) and Q5 High-Fidelity DNA Polymerase (NEB). The mTCRβConstant-P2A fragment was gel-purified as previously described.

For each clonotype, the TCRαVariable fragment, TCRβVariable fragment, mTCRβ-P2A fragment and mTCRαConstant-Backbone fragment were joined via Gibson assembly using the NEBuilder HiFi DNA Assembly Kit (NEB).

The assembly product was transformed into NEB 10-β Competent *E. coli* via heat shock, with a 1-hour outgrowth in NEB 10-beta/Stable Outgrowth Medium followed by overnight culture in Luria-Bertani (LB) medium with ampicillin selection at 30°C. Small-scale plasmid purification was performed using the QIAPrep Spin Miniprep Kit (Qiagen) with plasmid sequence confirmation via Nanopore sequencing performed by commercial vendor Plasmidsaurus.

2.11.2 Lentiviral Plasmid Production

Sequence-confirmed pHRsin transfer plasmids were re-transformed into NEB 10-β competent *E. coli* expanded as above. The control pHRSin-SFFV-PADI4 plasmid was taken from laboratory stocks that were originally purified by Gerda Mickute. For pMDG (VSV-G envelope) and Q8.91 (viral packaging) plasmids, frozen glycerol stocks of transformed *E. coli* were expanded.

Large-scale plasmid purification was performed using the NucleoBond Xtra Midi Kit (Macherey-Nagel) as per manufacturer instructions with sequence confirmation via Nanopore sequencing as above.

2.11.3 Lentiviral Production

HEK 293T was cultured and passaged as outlined in section 2.2. The day prior to transfection, HEK 293T cells were seeded in 6-well plates, with 1 million cells per well at a concentration of 0.5 million cells/ml.

A transfection master mix was prepared, containing per well: 100 µL of OptiMEM Medium (Thermo Fisher), 1 µg of pHRsin, 0.25 µg of pMDG and 0.5µg of pQ8.91. After thorough pipette-mixing, 4.5 µl/well of Turbofectin (OriGene) was added directly to the liquid, followed by a 30-minute incubation at room temperature.

The completed transfection master mix was then applied dropwise to the HEK 293T with gentle agitation, followed by a 48-hour culture period.

The viral supernatant was harvested, followed by centrifugation at 250G to remove debris. Lentivirus was used immediately for T cell transduction.

2.11.4 T Cell Transduction and Culture

48 hours prior to transduction, PBMCs were sourced from healthy donors as described in section 2.1. Following isolation, they were resuspended in T cell media supplemented with 1000 IU/ml of IL-2, 10 ng/ml of IL-15 and anti-CD3/CD28-conjugated magnetic Dynabeads at a 1:1 bead-to-cell ratio. Additionally, a RetroNectin-coated plate was prepared. In brief, 24-well, non-treated, flat-bottomed plates (Corning) were coated with 300 µl/well of 25 µg/ml of RetroNectin solution (Takara Bio) and refrigerated.

For the transduction, the RetroNectin solution was removed, wells blocked with PBS/2% BSA and washed with PBS. 3 ml of viral supernatant was then applied to each well and virus was bound via centrifugation at 2000G at 4°C for 90 minutes. Following centrifugation, the viral supernatant was removed, and 1 million pre-stimulated PBMCs were applied at a concentration of 0.5 million cells/ml. Spinoculation onto RetroNectin-bound virus was performed at 450G for 1 minute. Transduced cells were passaged every 2-3 days in T cell media with cytokines as above, with removal of Dynabeads at 3 days post-transduction.

2.11.5 FACS Sorting of Transduced T Cells

At least 5 days following transduction, T cells were sorted to enrich for transduced T cells expressing a murine TCR constant region. Cells were washed and resuspended in Trustain-PBS for a 10-minute incubation. Cells were subsequently surface stained for CD3 (PE-Cy7), CD4 (APC), CD8 (FITC) and mTCRβ (BV711) for 30 minutes at room temperature. Cells were washed and resuspended in FACS buffer with DAPI. Live, $CD3^+$, $mTCR\beta^+$ cells were sorted using a Sony MA900 with a 100 µm nozzle.

2.12 Functional Testing of Transgenic T Cells

2.12.1 Expansion of Target Cells from Frozen PBMCs

For use as target cells in peptide-pulsed activation assays, cells were expanded from frozen PBMCs using an adapted joint APC and T cell culture. Cells were thawed and cultured as stated in section 2.2, however, Day 1 stimulation was performed using activating UltraLEAF Purified anti-CD3 (OKT3, BioLegend) and anti-CD28 in place of peptide.

2.12.2 T Cell Activation Assays

Transduced effector T cells and expanded target cells were washed and rested in cytokine-free T cell media for 24 hours prior to experimental setup.

For conditions involving HLA-blockade, cells were incubated with anti-HLA antibodies for 2 hours at 37°C. These antibodies were: anti-HLA-I (W6/32, BioLegend), anti-HLA-II (Tu39, BioLegend), anti-HLA-DP (B7/21, AbCam), anti-HLA-DQ (Tu169, BioLegend) and anti-HLA-DR (L243, BioLegend).

Target cells were plated into V-bottomed 96-well plates, with 200,000 cells per well, and pulsed with peptide at a default concentration of 2 µg/ml unless otherwise stated. PHA was used as a positive control and DMSO as a negative

control, as previously stated. Effector cells were then plated onto target cells at a 1:2 effector-to-target ratio. Cell mixes were then co-stimulated with 2 µg/ml of anti-CD28 and 2 µg/ml of anti-CD49d, with initial surface staining for CD40L (BUV805), CD107a (BV421), CD107b (BV421) and 4-1BB (BV650). After 1 hour of co-culture, 2 µM Monensin was added for Golgi blockade, followed by a further 8-hour co-culture period.

At the end of the 9-hour co-culture, cells were washed and resuspended in Trustain-PBS for 10 minutes, followed by staining with Live/Dead Fixable Aqua at a 1:500 dilution for 15 minutes. Cells were washed, and further surface-stained for mTCRβ (BV711), CD8 (FITC), CD3 (AF700), CD4 (APC-Cy7) and CD69 (APC) for 15 minutes at room temperature. Cells were subsequently fixed and permeabilised using the BD Cytofix/Cytoperm Fixation and Permeabilisation Kit according to manufacturer instructions. Cells were then intracellularly stained for PD-L1 (BUV395), 4-1BB (BV650), OX40 (BB700), CD25 (PE) and IFNγ (PE-Cy7) for 30 minutes at 4°C, washed, resuspended in PBS and acquired with a BD Fortessa X50.

2.13 *Ex vivo* Single-Cell T Cell Sequencing

2.13.1 Sorting and Fixation of T Cells from Frozen BMMNCs

Frozen BMMNC samples were thawed and live, $CD3^+$ cells sorted as outlined in section 2.3. Fixation was carried out utilising the Parse Biosciences Evercode Cell Fixation v3 kit. In brief, post-sort samples were transferred into Protein Lo-Bind Tubes (Eppendorf), centrifuged at 450G for 10 minutes at 4°C, resuspended in Pre-Fixation Master Mix and filtered through a 70 µm cell strainer. Cell Fixative Master Mix and Cell Permeabilisation Solution were then added to the sample, followed by Stop Buffer. Once fixed and permeabilised, cells were again centrifuged at 450G for 10 minutes, resuspended in Cell Storage Master Mix and then stored at -80°C prior to barcoding.

2.13.2 Cell Barcoding and cDNA Library Preparation

Cell barcoding was performed using the Parse Biosciences Evercode TCR Mega Kit as per manufacturer recommendations.

To generate more than 1,000,000 barcodes, the Evercode TCR Mega Kit utilises multiple rounds of *in situ* split-pool combinatorial barcoding. In brief, fixed and permeabilised cells are loaded onto a 96-well barcoding plate. In Round 1 barcoding, RNA is reverse transcribed using oligo-dT and random hexamers tagged with sample-specific barcodes. These cells are then pooled, and then loaded into the Round 2 barcoding plate, where a second well-specific barcode is ligated. A similar pooling and ligation occurred in Round 3 barcoding, which incorporates a further biotinylated barcode.

Following Round 3 barcoding, cells are split into 16 sublibraries and lysed. Sublibraries are processed in parallel and recombined during pre-sequencing library pooling.

Biotinylated cDNA was then captured utilising magnetic streptavidin beads. cDNA libraries are then amplified using a template-switching adapter. Size selection was performed utilising AMPure XP (Beckman Coulter), with quality control using the Agilent High Sensitivity DNA Bioanalyzer and the Qubit dsDNA High Sensitivity Assay as previous.

2.13.3 Preparation and Sequencing of *Ex Vivo* Single-Cell Libraries

Amplified cDNA is then split for the preparation of whole transcriptome and TCR libraries.

For whole transcriptome library preparation, cDNA is fragmented, followed by end-repair, A-tailing and adapter ligation. The fourth, sublibrary-specific barcode is incorporated during amplification using the UDI Plate – WT.

For TCR library preparation, cDNA underwent two targeted PCR amplifications of the V(D)J segment, where the first incorporates sequencing adapters and the second incorporates the fourth, sublibrary-specific barcode using the UDI Plate – EC.

Pooled library sequencing was performed by Novogene UK. Libraries were sequenced to a depth of 20,000 reads/cell for whole transcriptome and 5,000 reads/cell for V(D)J. Sequencing was performed on the NovaSeq X platform with 10% PhiX and 150 bp paired-end reads. The cycle configuration was 242-8-8-58 and read 1 of the whole transcriptome library was data-trimmed in house at Novogene UK to 64bp.

2.13.4 Processing and Analysis of Parse Evercode Single-Cell Data

Single-cell gene expression and TCR data was received as data-trimmed FASTQ files from Novogene UK, demultiplexed into 16 sequencing sublibraries.

Initial processing was performed by the Parse Split-Pipe pipeline v1.5.1. First, an indexed reference genome was created using Split-Pipe's 'mkref' function on the Homo sapiens genome assembly GRCh38.

Gene expression data from each sublibrary was then individually processed with Split-Pipe. The Split-Pipe 'all' function was used for pre-processing, alignment, molecule information extraction and generation of a count matrix. This resulted in gene expression data that was demultiplexed further into sample-specific gene expression libraries. Gene expression data was then used in conjunction with the TCR analysis module of the 'all' function for immune-specific alignment and clonotype detection.

Upon analysis of all sublibraries, the Split-Pipe 'comb' function was used to aggregate cells into individual sample-specific libraries for downstream analysis.

Cell clustering, UMAP generation, differential gene expression, automated cell annotation and annotation of public TCRs were performed as described in section 2.9.

Gene signature enrichment analysis was performed utilising Scanpy. The Reactome TCR Signalling Signature (REACTOME_TCR_SIGNALING) was downloaded from mSigDB and comprises canonical TCR signalling components such as ZAP70 and LCK [220, 221]. The gene signature for neo-antigen specific

anti-tumour T cells was taken from transcriptional profiling of tumour-infiltrating lymphocytes reported by Rosenberg *et al.* [222]. AUCell scoring was performed utilising the AUCell v1.24.0 package run in R v4.3.2. Gene sets for AUCell scoring were selected based on curated literature-derived signatures including marker genes from CellTypist [215], Azimuth [223] and transcriptomic studies of $CD4^+$ T cell polarisation [224] or differentiation state [225]. Statistical significance was tested utilising the Wilcoxon Rank-Sum test with the Benjamini-Hochberg correction for multiple comparisons. Full details of genes used for enrichment analysis and AUCell scoring are outlined in the appendix Figure B.4.

2.14 Data Analysis and Visualisation

Experimental schematics were generated using BioRender. Flow cytometry analysis and representative plots were generated in FlowJo v10.10.0. Basic data analysis and presentation was conducted with GraphPad Prism v10.4.0. Where graphs with error bars are shown, this represents the mean value (M) $\pm$ standard deviation (SD). Plasmid design and map generation were performed in SnapGene v8.1.

3

Culture and Screening Methods for Post-AlloSCT Bone Marrow T Cells

Contents

3.1 Overview

The initial experimental workflow that was used to isolate the 22 putative GvL antigens utilised exclusively peripheral blood samples from the late (2-7 years) post-alloSCT period. These experimental techniques had not previously been successfully performed on BMMNCs from the early ($\leq$12 months) post-alloSCT period and as such, this chapter focuses on developing and validating methods for use in this setting.

In contrast to the late post-alloSCT peripheral blood, use of the early post-alloSCT bone marrow from the high-risk cohort poses a number of challenges.

Logistically, given the invasive nature of the BM aspirate procedure, the availability of BMMNC samples is limited by the number of timepoints sampled and is constrained further by the volume of aspirate and therefore cell number taken. In addition to this, the early post-alloSCT period is complicated by delayed T cell recovery as a result of conditioning, ongoing immunosuppressive therapy and other patient-specific factors [226–228]. Given the considerable numbers of candidate peptides that need to be screened, these methods must generate large numbers of cells for testing and utilise screening approaches that are both efficient and scalable.

The first part of this chapter therefore focuses on culturing methods that would successfully expand T cells from these early BMMNC samples, ensuring that the culturing process maintained both functional competence and the diversity of the TCR repertoire. The remainder of this chapter explores strategies that attempt to enhance our ability to detect potential GvL T cells. This was undertaken through trials of culture-based enrichment and through alternative readouts for assessing T cell activation.

3.2 Development of a Polyclonally-Stimulated Culture Method for the Expansion of T cells from BMMNCs

Previous attempts in our laboratory to culture BMMNCs utilising the original antigen-stimulated T cell culture (outlined in section 2.2) were unsuccessful, with the cells failing to expand with a progressive reduction in viability when compared to PBMCs taken from the same patient (Figure 3.1).

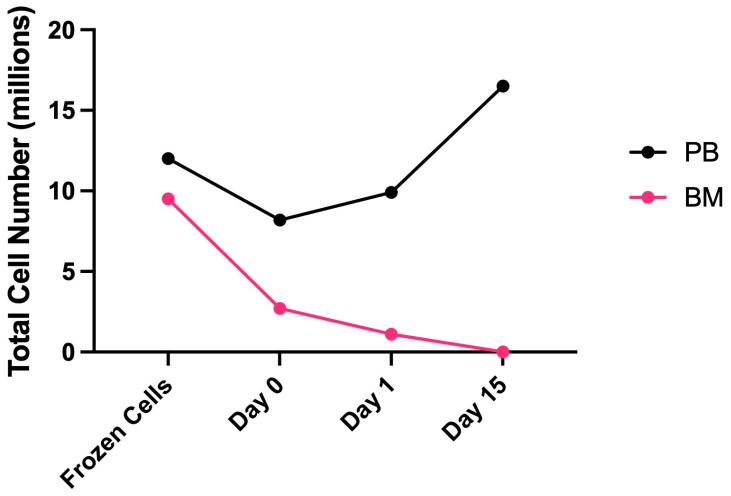

Figure 3.1: The prior antigen-stimulated culture method failed to expand BMMNCs. Example growth curve for paired PBMC and BMMNC samples utilising antigen-stimulated culture from the prior GvL pipeline for a single patient. *Data generated by Connor Sweeney.*

Though the discrepancy between the performance of PBMC and BMMNC cultures in previous experiments could be attributed to the absence of antigen-specific T cells in the tested BMMNC samples, given the prior non-viable cultures, limited cell stocks and the high numbers of candidate peptides to be tested (an average of 406 peptides per patient-donor pair), it was clear that the original antigen-stimulated method would be insufficient for the needs of this project.

The first priority, therefore, was to establish a culturing method that would be reliably able to expand T cells from post-alloSCT BMMNCs to a sufficient degree

that would allow for downstream testing. Unfortunately, the literature on culturing T cells from BMMNCs is limited, and in the post-alloSCT setting is essentially absent, necessitating the development and optimisation of a novel method.

Rather than attempting modifications to the antigen-stimulated approach, it was instead theorised that a polyclonally-stimulated culture method may be required, where broader T cell activation could drive proliferation and survival through paracrine signalling or T cell-T cell help. Two new culturing methods were therefore tested against a cytokine-only culturing method (named for work performed by Connor Sweeney, CS), on both PBMC and BMMNC samples from post-alloSCT patients taken from the first 12 months post-transplant (Figure 3.2a). Each vial was thawed and divided into three equal aliquots for parallel testing with each method.

The first of these two methods (Transduction-Like, TL) was adapted from a T cell expansion protocol used in the Vyas lab for lentiviral transduction of PBMCs. The second of these, (Cieri-Herda, CH) was an adapted approach from two papers focused on expanding T cells from BMMNCs in a non-alloSCT setting. Both these methods utilise superparamagnetic anti-CD3/anti-CD28 Dynabeads to provide simultaneous TCR and co-stimulatory activation (Figure 3.2b) [229, 230].

Both the polyclonally-stimulated TL and CH cultures expanded well across all the early post-alloSCT timepoints in samples derived from both PBMCs and BMMNCs. This is in stark contrast to the CS method, which recapitulated earlier experiments with the antigen-stimulated method and universally resulted in cell death following thaw (Figure 3.2c).

As the MNC samples used in the expansion trials were not CD3-selected prior to cryopreservation, flow cytometry was used to assess the percentage of $CD3^+$ cells at various timepoints over the culture period (Figure 3.2d). Though the starting percentage of $CD3^+$ cells was low and variable at thaw ($M = 21.4\%$, $SD = 17.5\%$), this increased markedly over the course of the culture duration so that $CD3^+$ cells comprised almost all cells by day 17 ($M = 95.7\%$, $SD = 6.5\%$). This enrichment

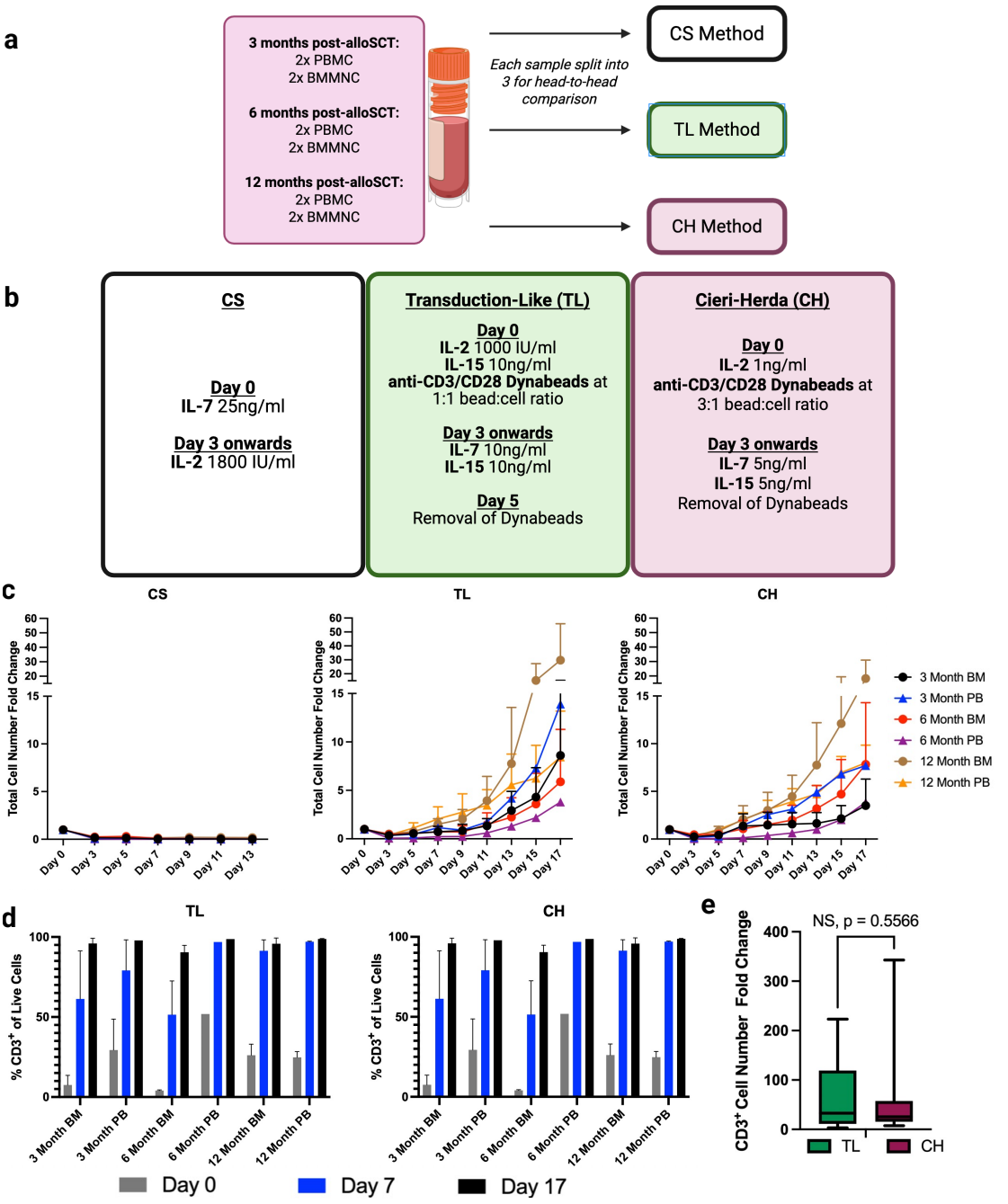

Figure 3.2: Head-to-head testing of culture methods for the expansion of post-alloSCT BMMNCs. a. Simplified schema showing samples used and experimental structure. **b.** Summary of cytokines and stimulation used for each culturing method in addition to routine culture maintenance. **c.** Growth curves showing total cell number fold change at each timepoint compared to Day 0 for each of the culturing methods (Day 0 = thaw). **d.** Graph showing the change in $CD3^+$ cells represented as a percentage of all live cells for TL and CH methods. **e.** Graph showing fold change of $CD3^+$ cell number from thaw to Day 17 utilising all samples tested. p value calculated using paired Wilcoxon test.

suggests that the culture conditions both promote T cell expansion and selectively favour T cell survival over non-T cell populations.

It is worth noting that the starting percentage of $CD3^+$ cells in BMMNCs taken from 3 and 6 months ($M = 5.81\%$, $SD = 2.45\%$) was significantly lower than in PBMCs taken from equivalent timepoints ($M = 40.7\%$, $SD = 15.9\%$, $p = 0.038$). This discrepancy did however equalise by the 12-month timepoint within this tested cohort. Additionally, in all cultures, there was a reduction in absolute cell number between thaw and day 3, which was accompanied by an increase in overall cell viability. This is likely to represent the loss of cells that were compromised by thaw combined with the non-proliferation of $CD3^-$ cells.

Overall, when considering the aggregate fold change of $CD3^+$ cells for all samples between the TL and CH methods, there was no statistically significant difference (Figure 3.2e). As a result of this, given the laboratory's shared experience with the TL protocol and its overall lower reagent cost, the TL protocol was taken forward for further experimentation.

3.3 Assessing the Effect of the Polyclonally-Stimulated Culture on TCR Repertoire

Having established a method that would reliably expand T cells from BMMNC samples, the next step was to ensure that these expanded T cells would remain suitable for use in screening for GvL responses.

The TCR repertoire has previously been shown to become altered over the course of cell culture, even in cases with a polyclonal stimulation [231, 232]. A direct assessment of the TCR repertoire was therefore undertaken, in order to ascertain whether the polyclonally-stimulated culture method would maintain sufficient TCR repertoire diversity to allow for broad and effective functional screening.

Four BMMNC samples from the early post-alloSCT period were selected for assessment and the TCR repertoire assessed at two timepoints (Figure 3.3a). Firstly, at thaw, and secondly, at day 12 of the polyclonally-stimulated culture. Day 12 was selected as a representative timepoint at which downstream functional testing would occur, to balance the need for sufficient expansion whilst avoiding late-stage culture effects. As with the prior use of the polyclonally-stimulated culture, all four of the samples successfully expanded following thaw, with enrichment of the $CD3^+$ cell fraction (Figure 3.3b).

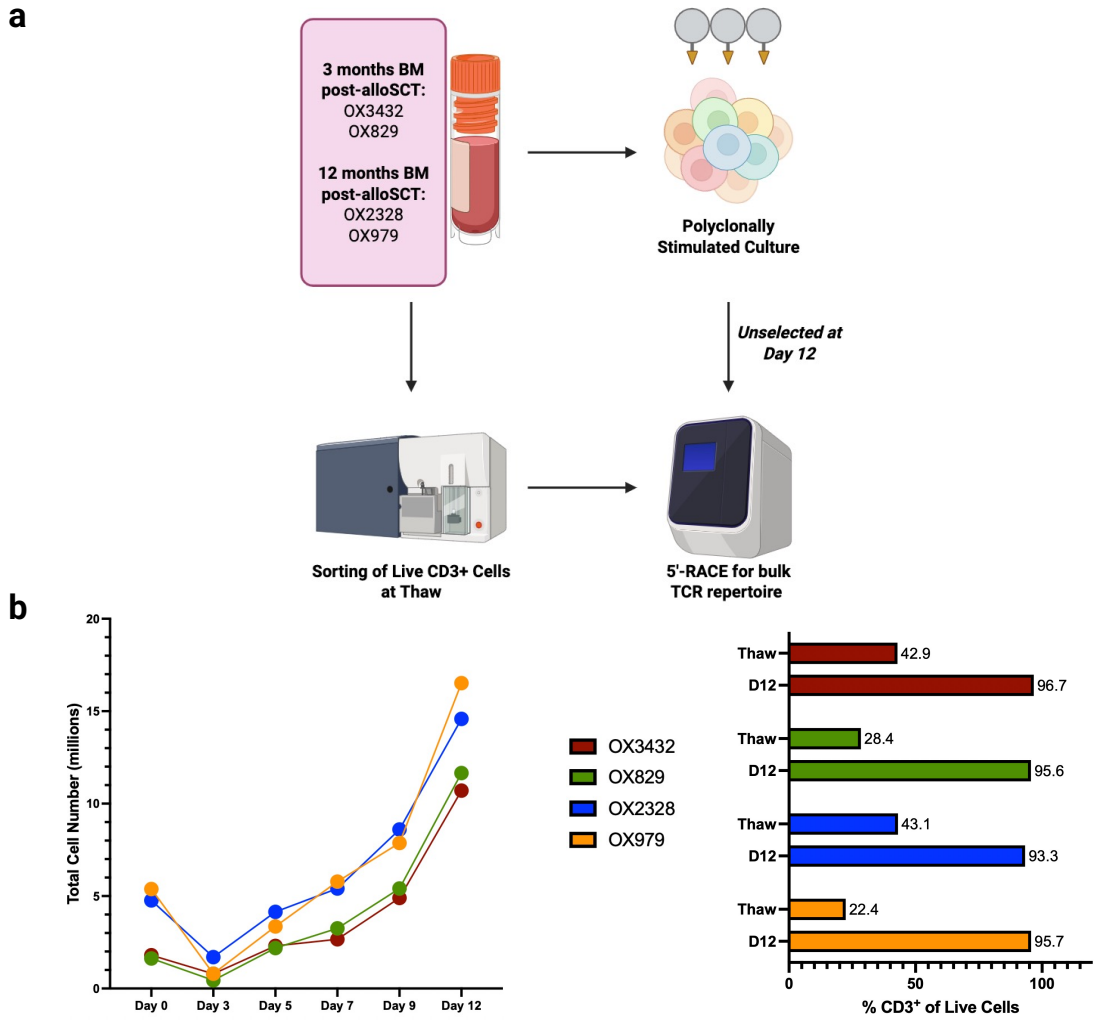

Figure 3.3: Assessment of TCR repertoire following polyclonally-stimulated culture. a. Simplified schema showing samples used and experimental structure. **b.** Absolute cell numbers and $CD3^+$% plotted over the course of the polyclonally-stimulated culture.

For the purposes of TCR library preparation, initial attempts were made to generate TCR libraries from thawed samples following magnetic selection for CD3 (data not shown). This, however, was unsuccessful due to the low cell viability (50.4 – 69.3%) and therefore poor RNA integrity. FACS sorting for live, $CD3^+$ cells was therefore undertaken at thaw prior to RNA purification.

Cell sorting was not necessary for the day 12 timepoint, given the high percentage of $CD3^+$ cells and excellent viability in culture (>95% in all cases).

TCR libraries were prepared utilising 5'-rapid amplification of cDNA ends (5'-RACE), with UMIs, which then underwent next-generation sequencing (NGS). This strategy was selected for a number of reasons that aim to improve sensitivity and fidelity.

By using universal 5' primers rather than pools of variable region-specific primers, the method avoids multiplex PCR. This mitigates primer-specific amplification bias which is further eliminated via UMI-based correction collapsing PCR duplicates. Additionally, given the increased sensitivity compared to multiplex PCR, the required RNA input amount is much reduced, which is particularly relevant in the context of BMMNCs at thaw, where $CD3^+$ cell quantity and quality are both particularly low. Finally, the method captures full-length TCR sequences which allows for precise clonotype identification which is of particular importance for the assessment of repertoire complexity [233].

As 5'-RACE with UMIs does not include cell barcoding, to robustly compare TCR repertoires across samples and timepoints, careful normalisation was required.

As the number of live $CD3^+$ cells at thaw was variable between samples, the analysis of TCR diversity was normalised to both input cell number and RNA amount. Following sequencing, samples which were sequenced more deeply were downsampled to ensure parity across timepoints.

It was possible to derive a number of diversity metrics from analysis of these libraries (Figure 3.4). The total number of clonotypes detected, normalised to cell

input, at day 12 was higher in all four samples when compared to thaw. There are multiple explanations for this difference. Firstly, it could be due to the expansion of low frequency clonotypes that are pushed over the limit of the assay's detection. Secondly, at thaw, many T cells may be in a functionally quiescent, low-mRNA state. As the culture process involves polyclonal T cell activation, this could push more clonotypes into a transcriptionally active state where TCR mRNA is more freely available. Finally, the improved viability, cell number and RNA integrity likely contributed to clonotype detection.

Though the total number of detected clonotypes was of a comparable order of magnitude in three out of the four samples, this is not the case for the sample from patient OX829. This is likely to be a consequence of the sample characteristics at thaw. This sample had the lowest viability and cell number of all samples tested, and this likely led to under-sampling bias and therefore an artificially reduced clonotype count.

To assess skewing of the TCR repertoire, the Shannon equitability index was calculated for each sample. This is a metric which represents the evenness of the repertoire, normalised to population size [234]. In each case, the Shannon equitability index was not significantly different between samples tested at thaw and post-expansion, suggesting that the repertoire does not become skewed over the course of the culture period. This indicates that no dominant clones disproportionately outcompeted others during culture. This maintenance of repertoire evenness is of paramount importance for avoiding selection bias and allowing for the screening of a broad range of TCR clonotypes during functional screening.

In summary, it appears that the polyclonally-stimulated culture does not adversely affect the TCR repertoire. This, in conjunction with the reproducible expansion of T cells using the culture, provides a basis upon which large numbers of TCR-diverse T cells for downstream GvL screening could be expanded.

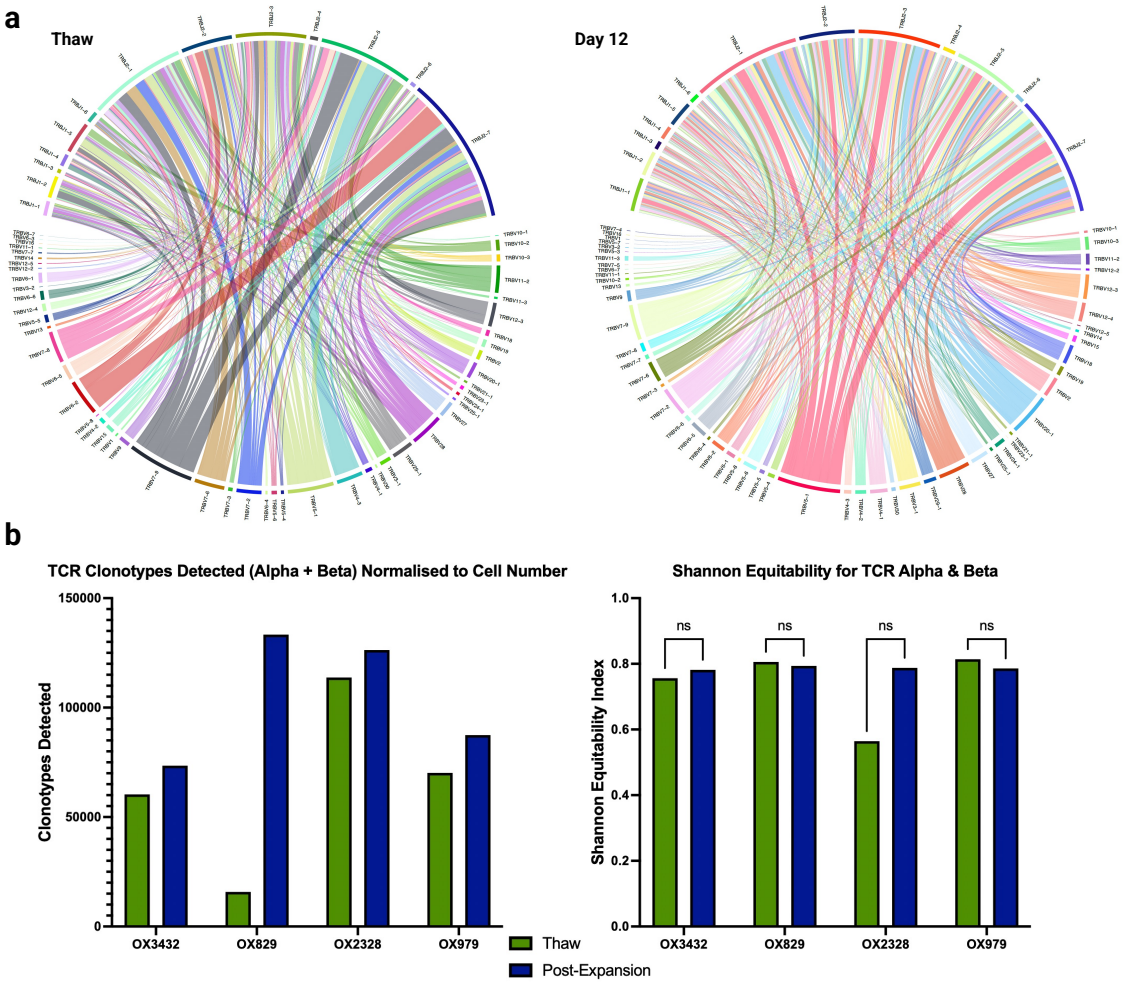

Figure 3.4: The polyclonally-stimulated culture does not adversely affect TCR repertoire. a. Example chord diagrams used as a visual representation of diversity. Here, the TCRβ repertoire at pre-and post-expansion for OX979. Outer arcs on the bottom of the diagram represent V segments, and arcs on the upper diagram represent J segments. Chord widths represent the pairing frequency. **b.** Graphs demonstrating total TCR clonotypes normalised to cell number and Shannon equitability index for samples pre- and post-expansion. p value calculated using 2-way ANOVA with Sidak correction for multiple comparisons.

3.4 Trialling Sequentially-stimulated Cultures to Screen for Antigen-Specific T Cells

Generating a viable pool of T cells from a frozen BMMNC sample is only the first step in screening for GvL antigens. To identify T cell responses to the peptide library, these cells must be capable of mounting a detectable level of activation during functional screening. In addition to this, unlike the prior antigen-stimulated culture method, a polyclonal stimulation would not result in the enrichment of antigen-specific T cells.

As a result of this, the next objective was to determine firstly whether T cells retained their ability to activate in response to peptide following the polyclonally-stimulated expansion, and secondly to assess whether a sequential enrichment for antigen-specific T cells was feasible.

Based on this rationale, the polyclonally expanded T cells were sequentially stimulated with the intent to enrich for antigen-specific T cells via preferential proliferation (Figure 3.5a).

Comparative IFNγ ELISpot could then be performed before and after the sequential stimulation, utilising spot-forming ability to assess activation potential and as a surrogate measure for the enrichment of antigen-specific T cells. IFNγ ELISpot was chosen to maintain consistency with the prior pipeline, and for its high throughput and high sensitivity, enabling rapid parallel testing of large peptide pools using limited patient material.

To maximise the probability of having antigen-specific T cells in the initial culture pool, screening was performed for viral-specific responses, utilising commercially available pooled viral peptides. The CEF pool comprises a panel of short peptides derived from CMV, EBV and influenza that are restricted to common class I HLA alleles and therefore is designed to stimulate $CD8^+$ T cell responses. The CEFTA pool, contains longer peptides from CMV, EBV, influenza, tetanus and adenovirus and is optimised for presentation by class II HLA molecules to drive

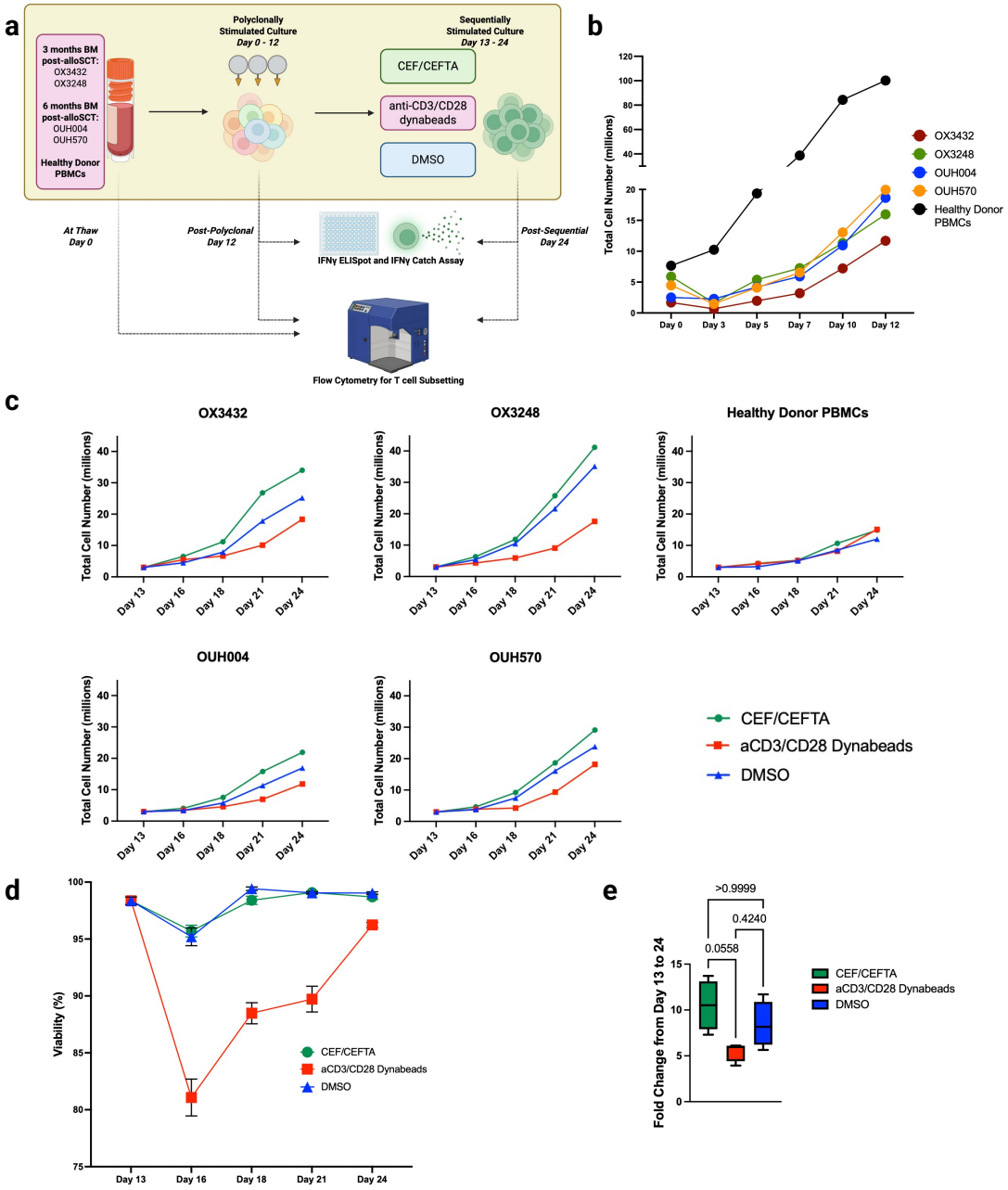

Figure 3.5: Trialling a sequential stimulation following the polyclonally-stimulated culture a. Simplified schema demonstrating samples used and experimental structure. Highlighted area indicates subset of experiments contributing to data in this figure. **b.** Absolute cell number of each sample plotted over the course of the initial polyclonally-stimulated culture. **c.** Growth curves for each sample during the sequentially-stimulated culture, showing respective performance of each stimulant. (Day 13 = day of sequential stimulation). **d.** Graph demonstrating mean viability across all samples for each stimulant used in the sequential stimulation. **e.** Graph showing absolute fold change of cells over the sequential stimulation utilising all samples. p value calculated using Kruskal-Wallis test.

$CD4^+$ T cell responses. Together, these pools provide broad HLA coverage across the population and serve as reliable positive controls for detecting pre-existing antiviral T cell immunity.

CEF/CEFTA-reactive T cells are expected to be present at high frequencies, even in the post-alloSCT setting [235, 236]. This made the use of CEF/CEFTA peptides suitable for proof-of-concept validation. This strategy, however, does not permit the assessment of the method's ability to detect low-frequency antigen-specific T cell responses.

Unfortunately, a suitable experimental model that would guarantee the presence of these responses in the post-alloSCT BMMNC setting could not be identified. Spike-in systems were considered, where transgenic T cell clones of a known specificity could be added to test sensitivity, however this would not faithfully recapitulate the behaviour of thawed early post-alloSCT T cells in culture due to differences in cell viability, differentiation state and polarisation.

Four BMMNC samples from within the first 6 months post-alloSCT and one healthy donor PBMC sample were selected for assessment. These patients were chosen based on confirmed clinical exposure to one of these viruses, as assessed by a positive viral-specific PCR titre, as well as having an HLA type that is covered by the commercial CEF/CEFTA pools.

These samples were then cultured using the polyclonally-stimulated method (Figure 3.5b), demonstrating a reproducible expansion consistent with previous experiments. As anticipated, the healthy donor PBMCs expanded to a greater extent than samples derived from post-alloSCT BMMNCs, by five- to ten-fold by the end of the 12-day period.

The samples were then sequentially stimulated with the CEF/CEFTA peptides. DMSO was used as a negative control, and anti-CD3/CD28 Dynabeads (at a 1:2 bead-to-cell ratio) provided a high-strength polyclonal stimulation that acted as a positive control (Figure 3.5c).

Several key observations emerged concerning the growth of these cells over the sequentially-stimulated culture period (days 13-24).

Firstly, compared to other conditions, BMMNCs stimulated by Dynabeads grew at a reduced rate. This was accompanied by a marked decrease in viability in the initial period following stimulation (Figure 3.5d). As the cells were cultured with only IL-7 initially, compared with IL-7 and IL-15 for the remainder of the culture period, some of this decrease in viability could be due to a lack of cytokine support. However, the difference between the Dynabeads-stimulated cultures compared with DMSO or CEF/CEFTA instead suggests an alternate mechanism, which in the context of the strong polyclonal stimulation that Dynabeads provide is likely to represent T cell over-activation with activation-induced cell death [237].

Secondly, the CEF/CEFTA-stimulated BMMNC conditions marginally outgrew the unstimulated DMSO conditions although this difference was not statistically significant ($p > 0.999$). One possible explanation for this minor difference could be the activation of CEF/CEFTA-reactive T cells, resulting in increased proliferation.

Finally, the growth of the healthy donor PBMC sample in this sequentially-stimulated phase was unexpectedly reduced compared to the BMMNC samples, regardless of stimulation used. The reasons for this are unclear but could be attributed to proliferative exhaustion following the extensive expansion during the polyclonal phase.

IFNγ ELISpot was performed at day 12, prior to the sequential stimulation, and day 24, at the end of the sequentially-stimulated culture period (Figure 3.6).

All BMMNC samples were able to mount a positive response to CEF/CEFTA following the polyclonal stimulation (in grey), signifying that the polyclonally-stimulated culture does maintain the activation potential of CEF/CEFTA-reactive cells. Interestingly, there does not appear to be a direct correlation between a sample's growth kinetics, when stimulated by CEF/CEFTA in the sequential-stimulation phase, and a sample's spot-forming ability.

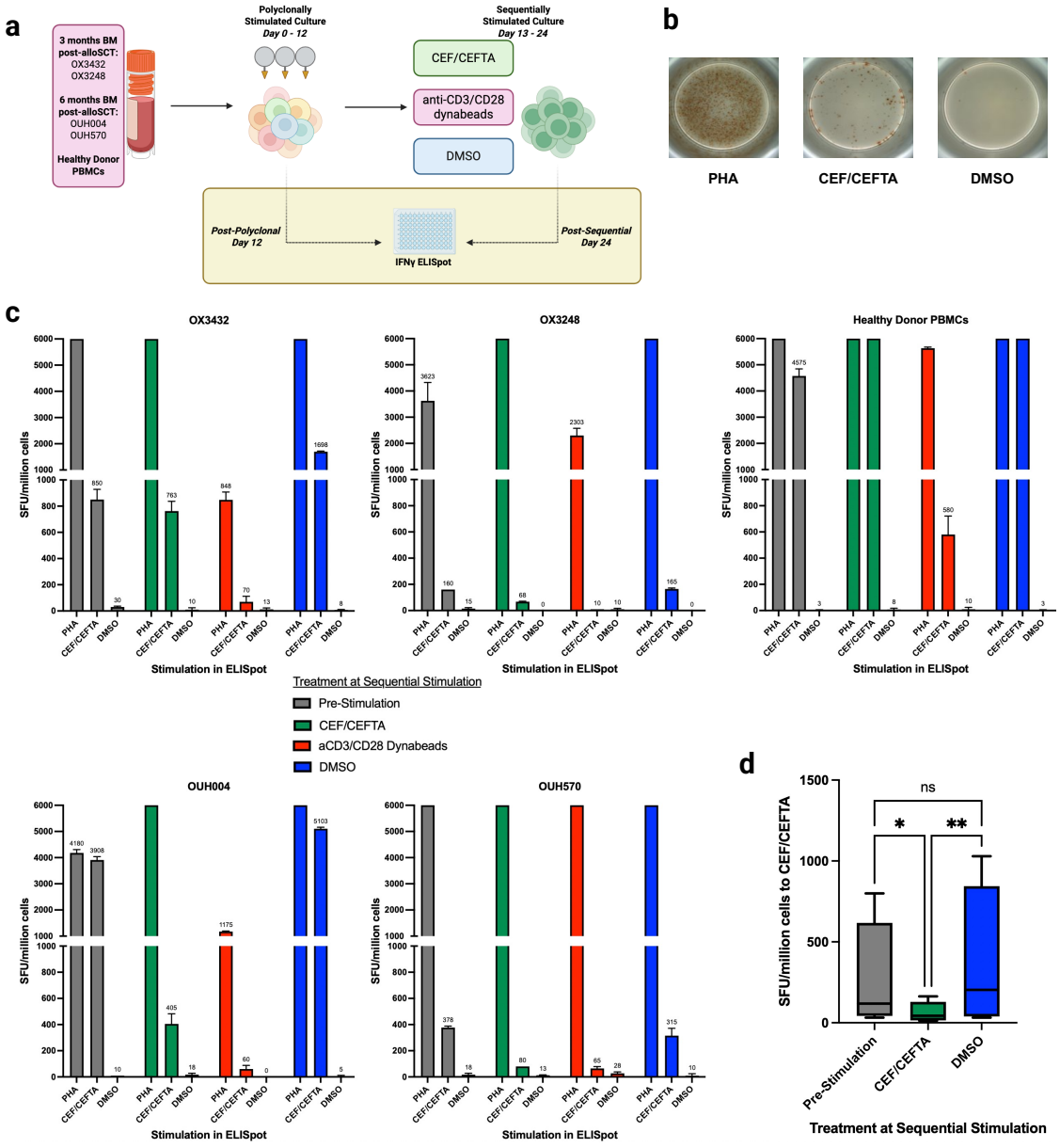

Figure 3.6: Sequential activation and culture with peptide results in reduced spot-forming ability at IFNγ ELISpot. a. Simplified schema demonstrating samples used and experimental structure. Highlighted area indicates subset of experiments contributing to data in this figure. **b.** Example ELISpot wells, taken from the post-polyclonal ELISpot performed on OX3432. **c.** IFNγ ELISpot results for each sample. Pre-Stimulation results are ELISpots taken at Day 12 of polyclonally-stimulated culture. Remaining conditions are taken from ELISpot at end of sequentially-stimulated culture period. ELISpot results are displayed as a maximum of 6000 SFU/million cells for readability. **d.** Graph showing aggregate response of all BM samples to CEF/CEFTA at IFNγ ELISpot, grouped by their stimulation in culture. p value calculated using Friedman test followed by Dunn's Test for multiple comparisons.

For all Dynabeads-stimulated conditions (in red), spot-forming ability is substantially reduced when compared to all other conditions, including in response to activation by PHA. This suggests that in addition to activation-induced cell death that there is an element of T cell exhaustion or anergy from repetitive and strong *in vitro* TCR stimulation [238, 239].

Surprisingly, despite the increased growth observed in the CEF/CEFTA-stimulated cultures, the ability of these cells to spot-form in response to a further exposure to CEF/CEFTA is significantly reduced when compared to both the post-polyclonal timepoint ($p = 0.033$) and the unstimulated DMSO cultures ($p = 0.0018$, Figure 3.6d).

While definitive enrichment of CEF/CEFTA-specific T cells over the course of the sequentially-stimulated culture could not be assessed using the current experimental methods, it is clear that the sequential stimulation negatively impacts the ability of these cells to activate again.

This emphasises that proliferation is not a good surrogate for functionality, and points towards a T cell-overstimulation analogous to, but less marked than, the effect in conditions stimulated with Dynabeads. These findings imply that a sequential *in vitro* stimulation would hamper attempts to isolate functional antigen-specific responses and is therefore unsuitable for GvL response detection. It is, however, certainly possible that a longer period of rest prior to stimulation, or a weaker stimulation, could mitigate this effect. Although directed TCR repertoire analyses could have provided direct insights into antigen-specific enrichment, these were not pursued given the overarching observation of diminished T cell activation potential.

In contrast, IFNγ ELISpot results from a prolonged unstimulated culture (the DMSO condition, in blue) result in comparable spot-forming ability when compared to the initial post-polyclonal IFNγ ELISpots ($p = 0.32$). This suggests that following the initial polyclonal stimulation, that T cells are able to proliferate for extended periods whilst maintaining the capacity for activation upon encountering antigen.

While IFNγ ELISpot enabled rapid and high-throughput screening for antigen-specific responses, as a bulk method, it does not allow for the direct isolation and therefore characterisation of reactive T cells. To address this, the prior pipeline utilised the IFNγ-Catch assay, a flow-based cytokine capture approach which therefore assesses activation at a single-cell resolution. Additionally, the method does not require fixation and therefore allows for the sorting of live, activated cells, preserving their transcriptomic integrity for downstream single-cell RNA sequencing.

To assess if the sequential stimulation had a similarly detrimental effect on the ability to identify antigen-specific cells using the IFNγ-Catch assay, the assay was run on two of the expanded BMMNC samples and the healthy donor PBMCs (Figure 3.7).

Due to the stringent time constraints that are inherent to the assay workflow, unfortunately only two BMMNC samples could be processed concurrently.

In a manner comparable to the IFNγ ELISpot results, BMMNC samples that had been sequentially-stimulated with CEF/CEFTA (in green), demonstrated a reduced percentage of $IFN\gamma^+$ cells following re-stimulation with peptide, compared to the unstimulated DMSO cultures (in blue).

PHA-induced IFNγ responses were more variable. Though IFNγ release in response to PHA was consistent between culture conditions in patient OX3248, this was not the case for patient OX3432, where the CEF/CEFTA sequentially-stimulated condition showed reduced IFNγ production. It is therefore unclear if the functional impairment seen in the sequentially-stimulated cultures is antigen-specific or reflects a global loss of cytokine competence.

Regardless, these findings reinforce the conclusion that the sequential stimulation impairs T cell functionality, corroborating the IFNγ ELISpot data.

In conclusion, these results collectively suggest that the current protocol for a sequential stimulation imposes significant functional constraints on T cell responsiveness, and that proliferation in culture is not a guarantee of subsequent

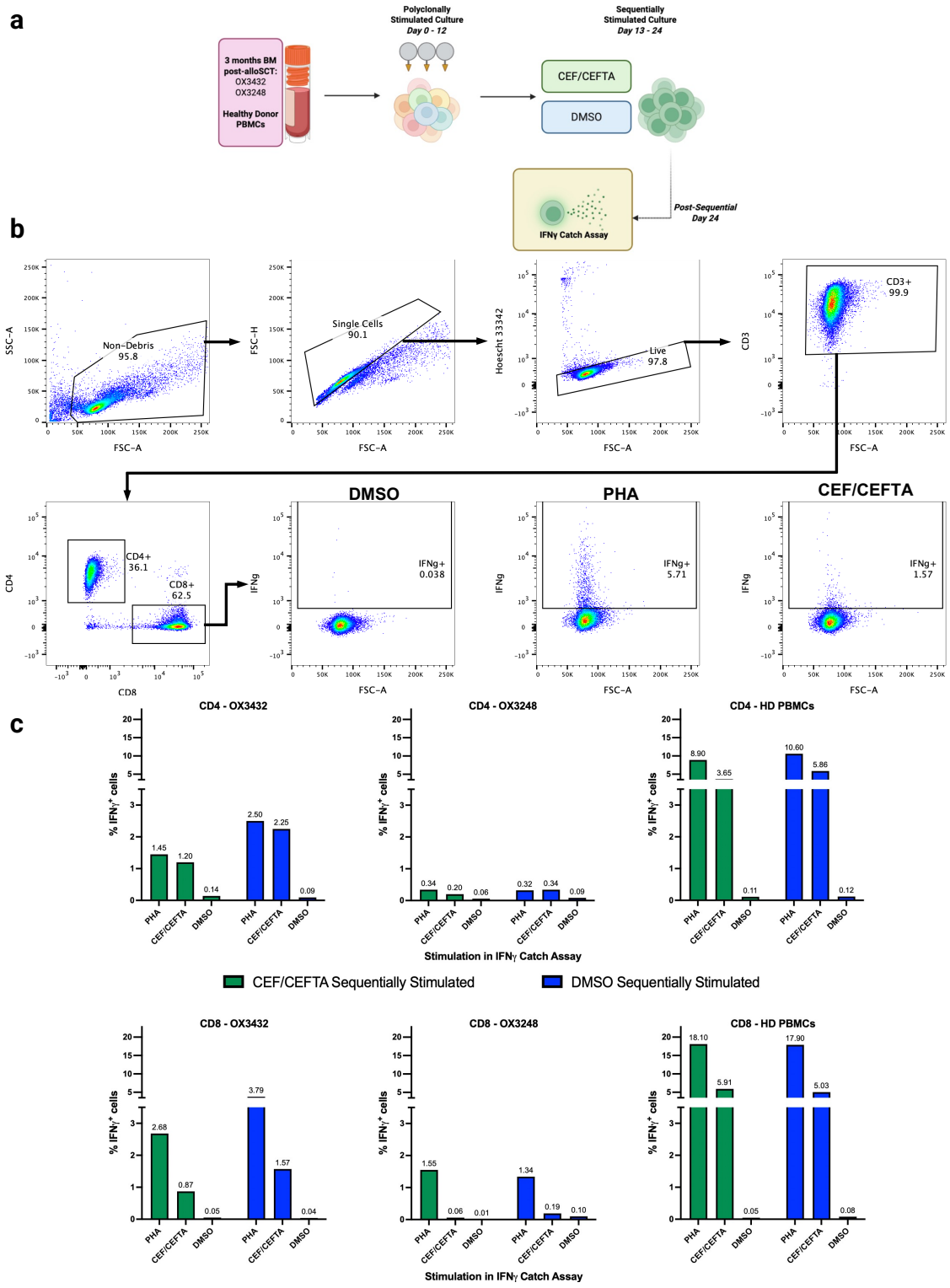

Figure 3.7: Sequentially-stimulated culture with peptide does not improve percentage of IFNγ^+ cells at cytokine release assay. **a.** Simplified schema demonstrating experimental structure. Highlighted area indicates subset of experiments contributing to this figure. **b.** Example gating strategy shown here for CD8$^+$ cells from patient OX3432 which have been sequentially stimulated in culture with DMSO. IFNγ^+ gate set based on negative DMSO control. **c.** Graphs demonstrating results of IFNγ release assays for 3 samples following sequentially-stimulated culture. Percentage of IFNγ^+ cells are shown as a proportion of total CD4$^+$ and CD8$^+$ cells respectively.

functionality. Though further optimisation is possible, such as through reducing the intensity of stimulation or extending rest phases, a single polyclonal stimulation at thaw appears to be sufficient to maintain a pool of functionally active T cells with which to undertake downstream screening.

3.5 Assessing T Cell Differentiation State over the Course of the Polyclonally-Stimulated Culture

Having selected the polyclonally-stimulated culture as a starting point for screening post-alloSCT BMMNC samples, to better understand the nature of the T cells expanded using these conditions and to refine our strategy for GvL antigen screening, further immunophenotypic characterisation was undertaken. Multiparameter flow cytometry was performed on the four BMMNC samples and the PBMC sample across three timepoints over the course of the prior culture period (Figure 3.8a). The panel was designed to assess the expression of canonical T cell markers for differentiation and functional polarisation (Figure B.5). Antigen experience was assessed on the basis of CD45RA and CCR7, and effector polarisation on surface expression of CXCR3, CCR4, CCR6, FOXP3, CD25 and CD127.

Gaining insight into the T cell differentiation state of the culture could inform the timing of functional screening as well as offer direction for the design of other forms of functional screening beyond IFNγ release.

The distribution of T cell subsets at thaw for the healthy donor PBMCs was compared to established adult reference ranges (Figure 3.8b) [240]. Though the majority of subsets were within the expected range, there was a reduction in the naïve compartment of $CD8^+$ cells (11.2% vs 14.0-62.0%) with an associated expansion of the effector memory compartment (46.2% vs 9.0-33.9%). The clinical background of the healthy donor was not made available, however these findings

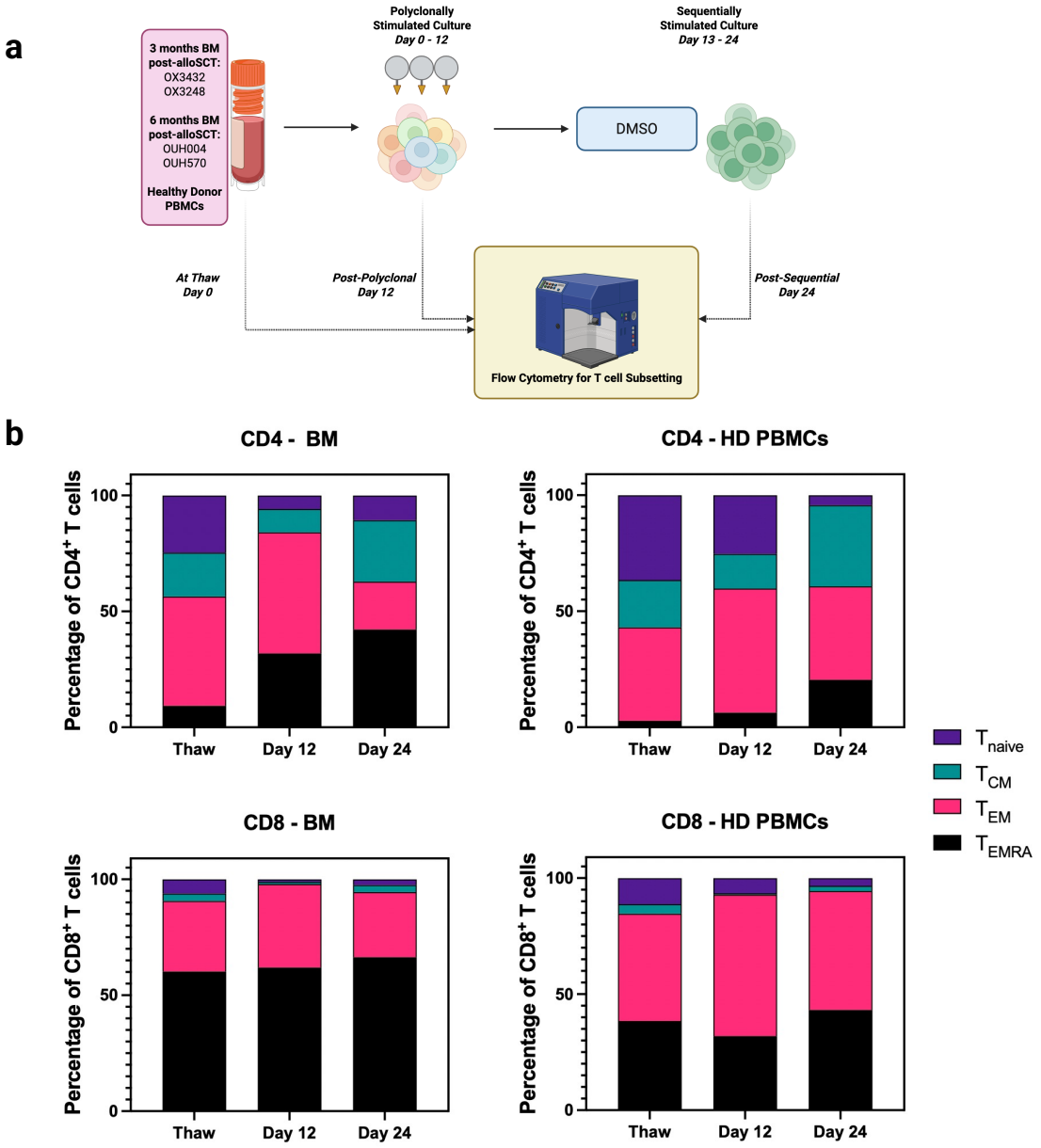

Figure 3.8: Overview of the CD4$^+$ and CD8$^+$ T cell phenotypes over the course of the polyclonal expansion. a. Simplified schema demonstrating samples used and experimental structure. Highlighted area indicates subset of experiments contributing to this figure. **b.** Frequency of the $T_{Naïve}$ (CD45RA$^+$, CCR7$^+$), T_{CM} (CD45RA$^-$, CCR7$^+$), T_{EM} (CD45RA$^-$, CCR7$^-$) and T_{EMRA} (CD45RA$^+$, CCR7$^-$) cells in the CD4$^+$ and CD8$^+$ populations. The 4 BMMNC samples are shown as an aggregate and the mean frequency displayed. Day 0 = thaw; Day 12 = at end of polyclonal expansion; Day 24 = at the end of the sequential stimulation with DMSO.

would be consistent with changes seen in either older adults or CMV$^+$ patients with associated immune-skewing [241].

The interpretation of results for the post-alloSCT BMMNCs is more challenging, as prior work in the post-alloSCT setting is focused on T cell subsets within the peripheral blood [236, 242], and work in the bone marrow is focused on healthy adults [243]. Overall, the T cell differentiation state of these samples at thaw is comparable to the findings in the peripheral blood of CMV$^+$ post-alloSCT patients, who have been shown to have expanded CMV-directed T_{EM} and T_{EMRA} populations with a corresponding reduction in the naïve compartment.

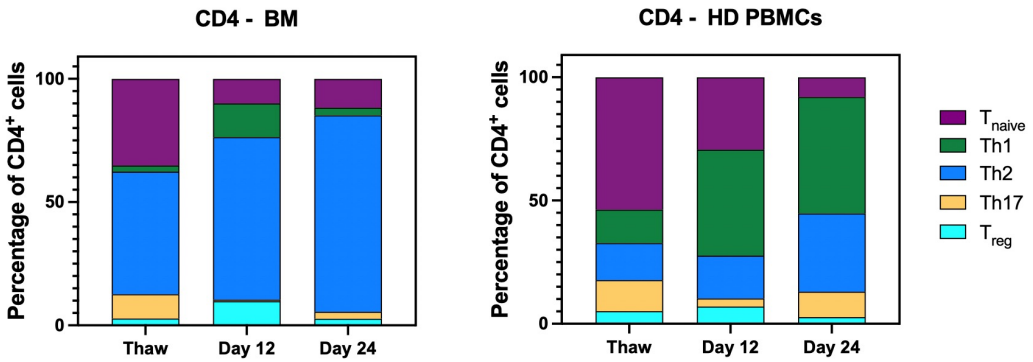

Figure 3.9: Overview of CD4$^+$ effector phenotypes over the course of the polyclonal expansion. Frequency of the $T_{Naïve}$, Th1 (CXCR3$^+$, CCR6$^-$, CCR4$^-$), Th2 (CXCR3$^-$, CCR6$^-$, CCR4$^+$), Th17 (CXCR3$^-$, CCR6$^+$, CCR4$^+$), and Treg (FOXP3$^+$, CD25$^+$, CD127lo) subsets represented as proportion of total CD4$^+$ cells. Untyped and transitional cells not shown. Day 0 = thaw; Day 12 = at end of polyclonal expansion; Day 24 = at the end of the sequential stimulation with DMSO.

Over the course of the culture period, there is an expected overall advancement in T cell antigen-experience. For the post-alloSCT BMMNCs, the proportion of T_{EMRA} cells rises for CD4$^+$ T cells (9.2% to 31.8% to 41.2%) and to a lesser extent in CD8$^+$ T cells (60.2% to 62.0% to 66.4%). This observation is likely to be multifactorial. It is in keeping with the strong TCR stimulation provided by the initial polyclonal stimulation driving the cells towards terminal differentiation. Additionally, the cytokine milieu may be contributing. For CD8$^+$ T cells in particular, the use of

IL-15 in culture is likely to contribute to the outgrowth of the T_{EMRA} fraction.

The effector memory compartment similarly rises from thaw to day 12 but appears to contract between day 12 and 24 (47.2% to 52.3% to 20.6% in $CD4^+$ and 30.4% to 36.0% to 28.0% in $CD8^+$). This is particularly relevant when considering the functional readout of IFNγ secretion as T_{EM} cells robustly and persistently produce IFNγ in response to repeat TCR stimulation, in contrast to T_{EMRA} cells, which demonstrate a comparatively reduced capacity to secrete IFNγ [244].

The effector polarisation of the $CD4^+$ fraction also varies over the culture period (Figure 3.9). From the results shown, however, it is not possible to draw conclusions as to whether this is due to the preferential expansion, or the alteration of their phenotype in culture. Regardless, the culture conditions appear to be Th2-polarising, with the Th2 percentage rising slowly over the period of culture from 49.7% at thaw, to 65.9% at day 12 and finally 79.7% at day 24. This is somewhat surprising, as the IL-7 and IL-15 used in culture should promote survival and expansion but have minimal roles in instructing effector polarisation. However, in the absence of other polarising cytokines, such as IL-12, T cells *in vitro* have been shown to default to a Th2-like phenotype [245, 246]. Whether these cells represent fully polarised Th2 effectors or a more transitional Th2-like phenotype that exists as an artefact of *in vitro* culture is unclear without deeper cell phenotyping.

The proportion of Th1 cells peaks at day 12 (2.51% at thaw, to 13.7% at day 12, to 3.1% at day 24). As the Th1 subset is the largest producer of IFNγ amongst $CD4^+$ cells, it also suggests that the yield of IFNγ ELISpot would be higher at day 12 when compared with later in the culture period. These findings raise questions regarding the optimal timing and modality of GvL response screening. In the case of IFNγ-based readouts, they suggest that functional screening would be best performed earlier in the culture period, rather than following a prolonged expansion.

3.6 Trialling IL-2 and IL-4 Cytokine Secretion Assays to Screen for Antigen-Specific T cells

Having observed the shifts in $CD4^+$ T cell polarisation and antigen experience over the course of the polyclonally-stimulated culture, one of the prevailing concerns was that utilising IFNγ as a marker of activation would underestimate antigen-specific responses, especially in the context of the emerging Th2 fraction.

To address this limitation, cytokine secretion assays for IL-2 and IL-4 were trialled to determine whether this could enhance the sensitivity of screening beyond IFNγ alone. IL-2 was chosen as a broad early marker of T cell activation, especially in $CD4^+$ cells that are not fully polarised, as may be the case in our culture system. IL-4 was further selected as a Th2-specific cytokine, that has been demonstrated to play roles in AML control both *in vitro* and in humanised mouse models [42, 43].

To explore if screening for IL-2 and IL-4 secretion would improve on IFNγ secretion alone, four further post-alloSCT samples were thawed, cultured for 12 days by the polyclonally-stimulated method and then tested for reactivity to CEF/CEFTA using ELISpot for IFNγ, IL-2, IL-4 or a combination of IFNγ, IL-2 and IL-4 together Figure 3.10. The individual assays would enable the quantification of IL-2 and IL-4-secreting cells while the multiplexed condition would assess if using the three cytokines in tandem would increase the overall detection of antigen-reactive cells compared to the prior IFNγ ELISpot alone.

Of the different conditions tested, the IFNγ ELISpot consistently provided the strongest and most consistent signal across all donors in response to both PHA and to CEF/CEFTA.

The individual IL-2 and IL-4 results were variable between samples, but overall much lower than IFNγ ELISpot alone. Based on responses to PHA, the incidence of IL-2-secreting cells was between 3- to 12-fold lower than IFNγ-secreting cells. IL-4 responses were similarly lower, and in the case of patient OX2328, IL-4 responses were undetectable in the IL-4 ELISpot.

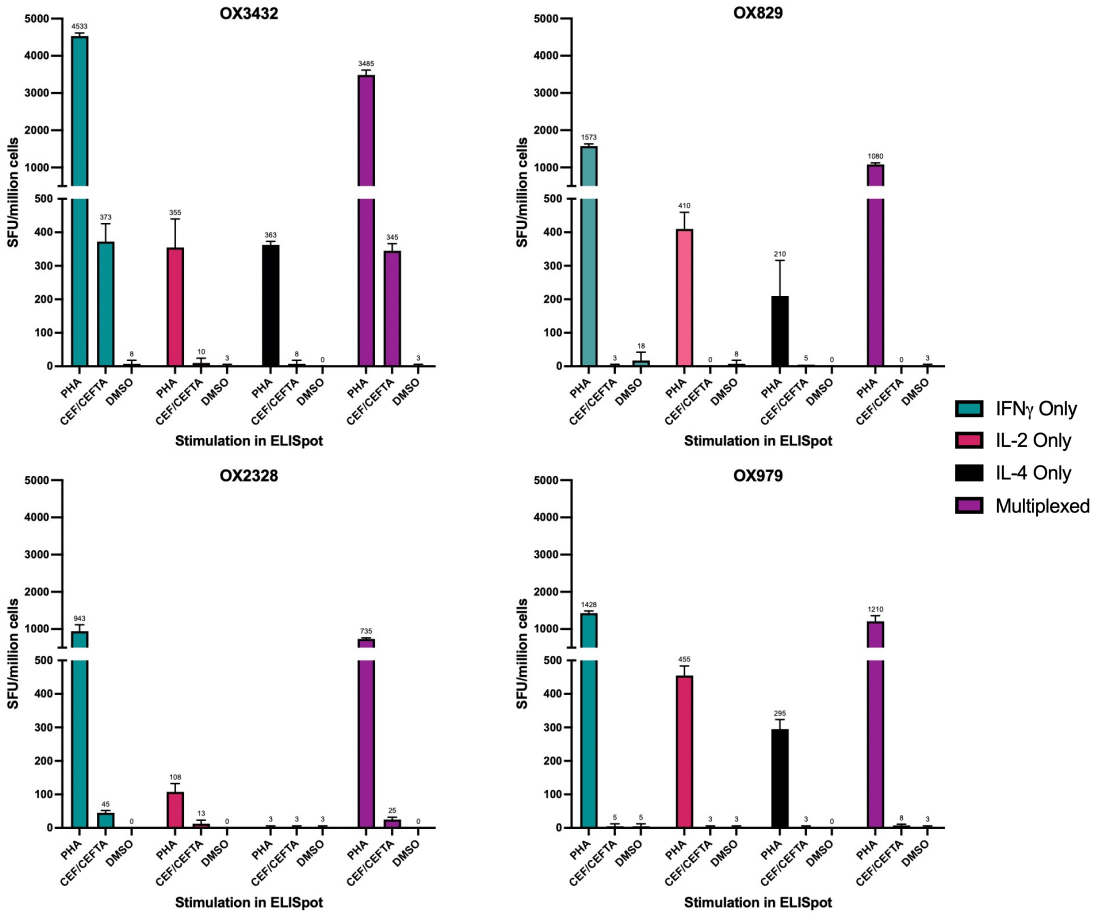

Figure 3.10: Screening for IL-2 and IL-4 release through ELISpot do not improve on IFNγ alone. ELISpot results for 4 BMMNC samples expanded via a polyclonally-stimulated culture. Each graph represents a single sample and each colour represents the cytokines screened for at ELISpot (Multiplexed utilises IFNγ, IL-2 and IL-4 antibodies).

Only two patients, OX3432 and OX2328 had a positive response to CEF/CEFTA. This patient cohort was not preselected for exposure to these viruses or restricting HLA and these responses are likely to simply be absent in the other two patients.

Surprisingly, the IFNγ ELISpot also outperformed the multiplexed combined-cytokine ELISpot. There are a number of possible explanations for this. Firstly, it may be that the majority of IL-2-secreting activated cells also co-secrete IFNγ, resulting in redundancies in signal-capture between these cytokines. Biologically, the intersection between IL-4 and IFNγ production would be unusual, however. Alternatively, there are experimental reasons such as spatial competition for antibody binding on the limited surface area of the ELISpot plate, or the cytokine capture

effect, where antibody-mediated capture of IL-2 would prevent paracrine IL-2-driven signalling and dampen overall cytokine release. Regardless of the explanation, the results suggest no benefit in multiplexing in this context. Similarly, as cell numbers are a limiting factor for functional screening, running multiple separate ELISpots does not appear to be a viable strategy.

When considering ELISpot, it appears that IFNγ as a sole functional readout appears to be the most sensitive of the assays, despite the prior observation of Th2-skewing or advanced differentiation. Additionally, there was an unexpected mismatch between the prior phenotypic evidence of Th2-skewing and the lack of IL-4 secretion. This could suggest that the cells in our culture system characterised as Th2 based on surface marker expression ($CXCR3^-$, $CCR4^+$, $CCR6^-$) may not truly reflect stably polarised, cytokine-competent Th2 effectors but may instead represent transient or partially polarised phenotypes. Alternatively, this could reflect the experimental design, where a secretion window of 0-20 hours was assessed. As IL-4 secretion only peaks after 24 hours, this could have led to a relative underestimation of activating IL-4-producing cells [247].

Cytokine Catch assays for IL-2 and IL-4 were performed on the samples for OX3432 and OX2328 to assess if they corroborated the prior ELISpot results Figure 3.11. Given the overlap between the limited fluorophores that were commercially available for the IL-2, IL-4 and IFNγ, the Cytokine Catch assays were tested in parallel configurations as IFNγ alone, IFNγ with IL-2 and IFNγ with IL-4.

As with the ELISpots, IFNγ secretion was detected most reliably in the IFNγ-only condition. Unexpectedly, the background IFNγ signal in the DMSO condition was elevated in the dual-staining panels. The cause for this elevated background is not clear but could reflect non-specific antibody capture or non-specific T cell activation by the Cytokine Catch reagents themselves when used in combination. Regardless, this makes the detection of truly positive responses more challenging.

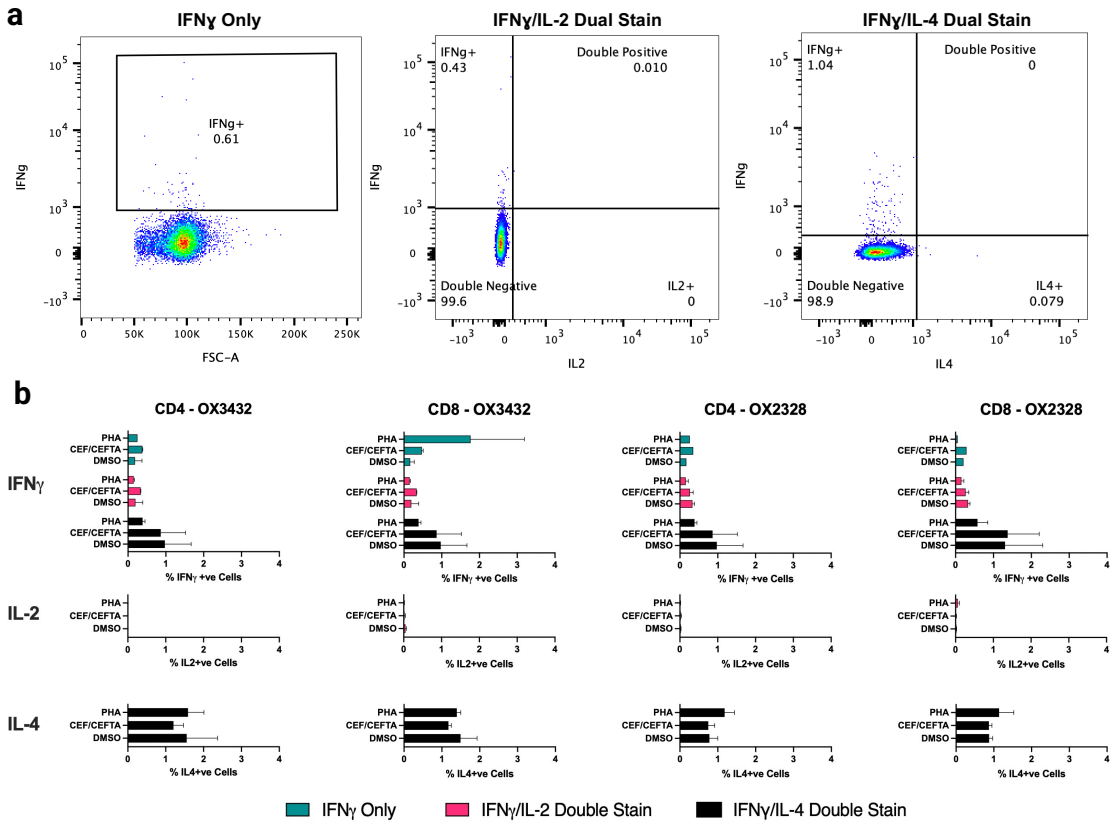

Figure 3.11: Staining for IL-2 and IL-4 release through Cytokine Catch assays do not improve on IFNγ alone. a. Example FACS plots taken from Cytokine Catch assays from OX3432 stimulated by CEF/CEFTA utilising IFNγ only, IFNγ with IL-2 and IFNγ with IL-4 antibodies respectively. **b.** Summary results of cytokine release assays demonstrating percentage of $CD4^+$ or $CD8^+$ cells secreting IFNγ, IL-2 and IL-4, as measured in the different Cytokine Catch assay conditions. The cytokine secreted is indicated on the left of the panel, and the different Cytokine Catch assay conditions are delineated by colour.

IL-2 secretion was essentially undetectable, including during stimulation with PHA. This is not in keeping with the IL-2 ELISpot results. This discrepancy is likely due to differences in the methodology. Whereas ELISpot assesses the total accumulated secretion of IL-2 from 0-20 hours post-stimulation, the Cytokine Catch assay captures only surface-bound cytokine over a 45-minute period, 6 hours post-activation and may therefore not capture the IL-2 secretion that would be expected at this timepoint, which would be on the rise and typically occurs in transient bursts. Additionally, as the Cytokine Catch assay requires surface binding and retention, it may underestimate the highly soluble and rapidly internalised IL-2. The sensitivity of the flow-based Cytokine Catch assay could therefore be limited both by duration

of cytokine secretion, and the threshold of secretion required for a positive response.

When assessing IL-4 production, there was little difference in the percentage of activated cells between conditions stimulated by PHA, CEF/CEFTA and DMSO. This suggests both a high level of background signal that renders the results difficult to interpret, as well as a lack of positive responses that may be due to the low abundance of IL-4. Similarly, the kinetics of the Cytokine Catch assay are not ideal for the detection of IL-4 release and these results therefore do not aid in clarifying the nature of the previously described Th2 phenotype seen in culture.

Finally, overall there were very few cells that were IFNγ/IL-2 double-positive or IFNγ/IL-4 double-positive. Given the lack of overall responses to IL-2 and IL-4 it is difficult to comment whether this is a true finding or a result of the methodology.

Taken together, despite our initial reservations, the addition of IL-2 or IL-4 did not enhance the ability to detect antigen-reactive cells when compared to IFNγ-based functional screening. Though it would be possible to trial alternate experimental approaches, including longer incubation windows, to improve on and broaden the readouts for T cell activation, the IFNγ ELISpot and IFNγ Cytokine Catch were selected as appropriate assays to carry forward to sample screening.

3.7 End of Chapter Discussion

Taken together, the experiments presented in this chapter establish a reproducible method for expanding T cells from early post-alloSCT BMMNCs utilising a polyclonally-stimulated culture. These expanded T cells retain both TCR repertoire diversity and activation potential, providing a suitable pool of cells that enable functional screening from the small starting pool of T cells that is typical of this clinical setting. The early post-alloSCT period is a critical window for immune surveillance and no prior published system has enabled functional screening in this manner.

Attempts were made to enrich for antigen-specific responses via sequential stimulation. Though conceptually appealing, this resulted in loss of functionality, emphasising the importance of carefully selecting the magnitude of T cell stimulation to balance proliferation and functional integrity.

The polyclonally-stimulated culture was further interrogated through multi-parameter flow cytometry. This revealed a phenotypic skewing over the culture period towards more antigen-experienced cells as well as the generation of a Th2-like population, which may be an artefact of the culture conditions, which lack polarising cytokines. With this in mind, attempts to broaden functional screening to the secretion of IL-2 and IL-4 were undertaken, without a clear benefit when compared to IFNγ alone.

The key limitation of the current study was the use of CEF/CEFTA peptides, as it was not possible to identify an experimental system that would guarantee the presence of low-frequency T cell responses that are present *in vivo* in the tested post-alloSCT BMMNCs.

So though the method appears sufficient in the detection of higher frequency viral responses, it is not clear whether it would be equally successful in the GvL setting. There is no clear consensus in the field as to the reported incidence of GvL-reactive T cells, with frequencies varying widely depending on the antigen, timepoint, clinical background and techniques used in identification. Selective GvL responses, however, are considered to constitute only a small fraction of the total T cell repertoire, with frequencies as low as $<0.1\%$ being reported in many studies [40, 248, 249].

It may be that further optimisation may be required for the detection of rarer GvL-reactive T cells. This could involve alternate culture methods, where T cell enrichment could occur, or during the functional screening itself. IFNγ ELISpot has been chosen given the ability to screen sensitively in a high-throughput manner. Though it was not possible to improve on utilising IFNγ as our functional readout, it is inherently biased towards Th1 and cytotoxic clones, and the ability to resolve very low-frequency responses is limited. Other modalities for the identification of

antigen-specific T cells, such as flow-based activation-induced marker (AIM) assays, which are expanded upon in later sections, or peptide-MHC multimer staining could be used for the detection of rare cells, but these methods would come at a significant cost in terms of throughput and would be better suited for a narrower and targeted peptide screening than what is currently envisioned.

An additional concern is raised by the changes in T cell phenotype that occur over the course of the culture period. Given ongoing changes in T cell antigen experience and polarisation, it raises questions as to the overall validity of the experimental model.

Though a cell's TCR sequence and antigen-specificity would not be affected, it is clear that there are substantial changes that occur in overall gene expression. These changes would mask *in vivo* cell states, and therefore whole transcriptome analysis of cells that are generated by this expansion will need to be interpreted with caution. If it is possible, however, to identify TCR clonotypes that are relevant, the stability of the TCR over the course of the culture could allow us to directly analyse these cells if they are detectable *ex vivo*.

In addition to its use for the identification of putative GvL responses from the early post-alloSCT BMMNCs, the polyclonally-stimulated T cell expansion may have applications in other settings. Most antigen discovery platforms rely on testing on PBMCs. This culture protocol opens up access to bone marrow-resident T cells, which may demonstrate different antigen-specificities or functional phenotypes.

The polyclonally-stimulated expansion facilitates the *in vitro* expansion of T cells from what is a sparse and immunologically compromised setting, and in addition to interrogating the bone marrow, with optimisation, it could be expanded for use in other lymphopenic settings, such as in hypoplastic marrow disorders or in other post-chemotherapy settings.

In conclusion, the work presented in this chapter establishes a reproducible method for T cell expansion and functional screening from early post-alloSCT bone

marrow. While certain limitations do remain, particularly in the detection of low-frequency responses and phenotypic changes in culture, the polyclonally-stimulated method offers a scalable method for functional T cell screening. This method not only facilitates the screening of candidate GvL peptides in our cohort but could have broadly applicable uses in exploring the bone marrow T cell compartment.

4

Applying Stimulated T Cell Culture for the Identification of GvL T Cells

Contents

4.1 Overview

Having established the polyclonally-stimulated culture and IFNγ ELISpot as a method for screening early post-alloSCT BMMNCs for GvL responses, the next step was to apply the pipeline to the high-risk, GvL-enriched patient cohort.

This chapter begins by detailing the application of the pipeline to two patients (OX717 and OX747) who were both previously shown to exhibit putative GvL responses that were detected in late peripheral blood samples. These patients were selected to increase the likelihood of detecting antigen-specific T cells. These attempts, however, did not result in the identification of any positive responses from the early post-alloSCT bone marrow.

To explore if these negative results were a methodological limitation rather than a true absence of antigen-specific T cells in the early post-alloSCT bone marrow, the polyclonally-stimulated culture was used on a late peripheral blood sample from patient OX747 at a timepoint where GvL responses were previously detected. This was chosen as an internal positive control to validate the sensitivity of the polyclonally-stimulated approach and enable direct comparison to the previous antigen-stimulated method. Further investigation into the differences between these two culture methods was undertaken with bulk TCR sequencing.

Subsequent testing identified a candidate GvL response against a peptide derived from METTL22, which was isolated using an IFNγ-Catch assay and fluorescence-activated cell sorting in conjunction with single-cell TCR and whole transcriptome sequencing via the 10x Genomics platform. Bulk TCR sequencing was then employed on serial samples to longitudinally track these putative antigen-specific clonotypes.

The chapter concludes with the functional validation of the identified METTL22-reactive TCRs, employing lentivirally transduced, TCR-engineered T cells to confirm antigen reactivity and specificity.

4.2 Applying the Polyclonally-Stimulated Method to the GvL-Enriched Cohort

To conserve limited patient material, the polyclonally-stimulated method was initially applied to a single BMMNC sample from the GvL-enriched cohort, taken at 9 months post-alloSCT from patient OX717.

This selection was based not only on sample availability, but also on the prior detection of putative GvL responses in the late peripheral blood. These samples were considered more likely to harbour antigen-specific T cell responses when compared to patients in whom no responses had been detected at late timepoints.

In total, 149 peptides were identified by the reverse immunological pipeline and had previously undergone screening in the peripheral blood of patient OX717 at 5.5 years post-alloSCT. At that time, putative GvL responses were detected against two overlapping peptides (RHOT2-1 and RHOT2-2) that encompass the same non-synonymous SNP in RHOT2. All 149 peptides from the original library were subsequently used for screening of the bone marrow sample (Figure 4.1a).

Following thaw, the sample expanded robustly, growing from a day 3 nadir of 1.9 million cells to more than 21 million cells at day 12 (Figure 4.1b). Similarly, the $CD3^+$ fraction rose from 17.8% of live cells at thaw to 90.2% at the end of the expansion (Figure 4.1c). These results recapitulated those observed during the development of the method, confirming the reproducibility of the T cell expansion and enrichment seen in a polyclonally-stimulated culture.

After the expansion, cells were rested in cytokine-free media to reduce non-specific activation and then tested via IFNγ ELISpot (Figure 4.1d). As in previous ELISpot assays, PHA, DMSO and CEF/CEFTA were used as controls. The previously identified RHOT2 peptides were tested individually, and the remaining 147 peptides were tested in pools of 20-25 peptides.

a

Patient	Timepoint Post-AlloSCT	Sample Type	Alloreactive Peptides Previously Identified	Total Peptides in GvL Pipeline Library to Screen
OX717	9 months	BM	RHOT2	149

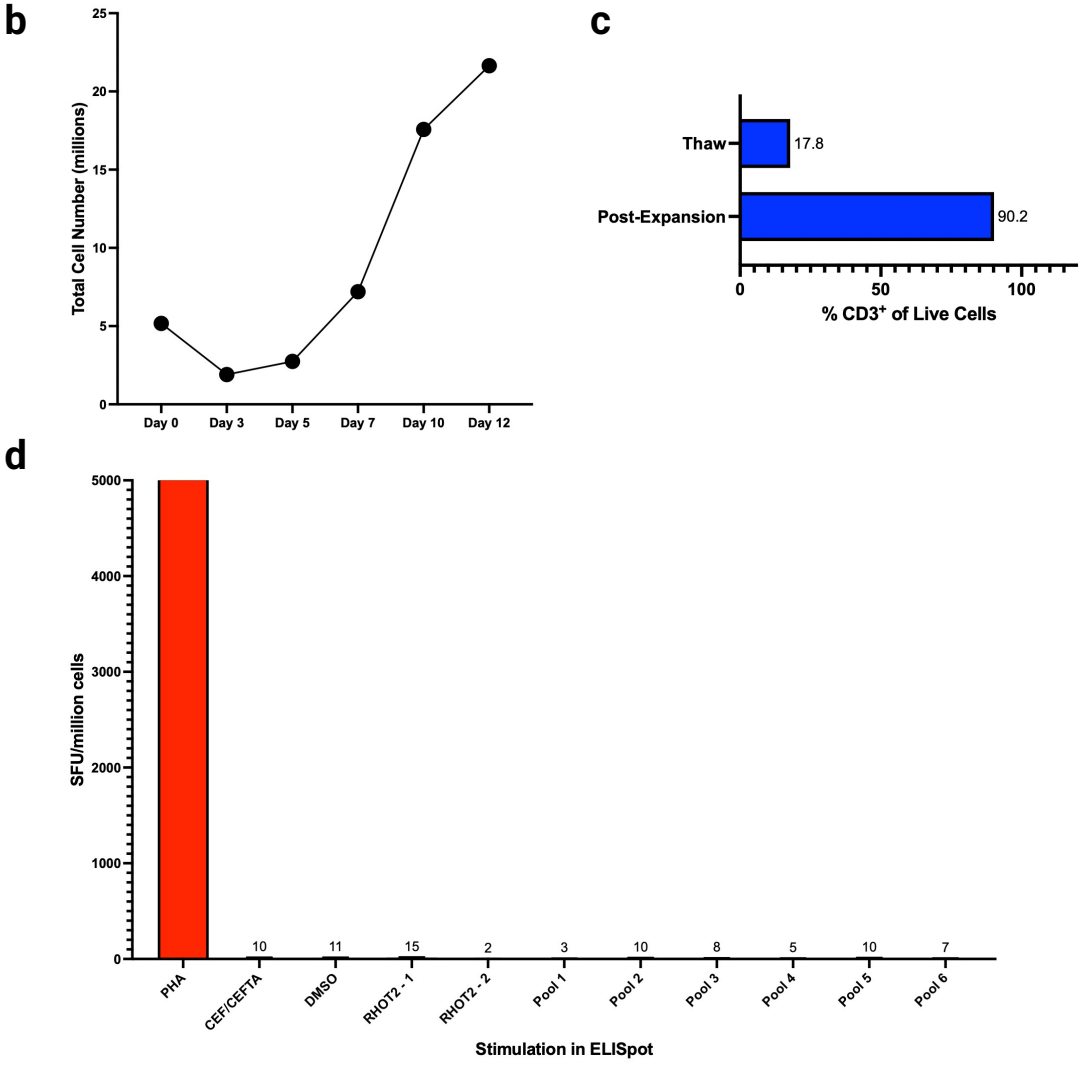

Figure 4.1: Applying the screening method to patient OX717. **a.** Table describing sample characteristics. **b.** Growth curve demonstrating absolute cell count over course of polyclonally-stimulated culture. **c.** Description of $CD3^{+}$% as a proportion of all live cells assessed by flow cytometry pre- and post- culture. **d.** IFNγ ELISpot results. RHOT2-1 and RHOT2-2 refer to two separate peptides spanning the same SNP in RHOT2. Pools comprise 20-25 peptides each. ELISpot results are displayed as a maximum of 5000 SFU/million cells for readability.

Other than a positive response to PHA, there were no responses above background to any of the six peptide pools or to the RHOT2 peptides.

Rather than drawing firm conclusions from a single tested sample, the polyclonally-stimulated approach was extended to four additional BMMNC samples taken from 3-12 months post-alloSCT from a second patient, OX747. Patient OX747 similarly had putative GvL responses detected at 6 years post-alloSCT in the peripheral blood. These were responses against three different non-synonymous SNPs, in DOCK8, METTL22 and DCAF13. For METTL22, there were two overlapping peptides (METTL22-1 and METTL22-2) encompassing the same non-synonymous SNP. The peptide library for screening totalled 252 candidate peptides (Figure 4.2a).

a

Patient	Timepoint Post-AlloSCT	Sample Type	Alloreactive Peptides Previously Identified	Total Peptides in GvL Pipeline Library to Screen
OX747	3 months	BM	DOCK8	252
	6 months		METTL22	
	9 months		DCAF13	
	12 months			

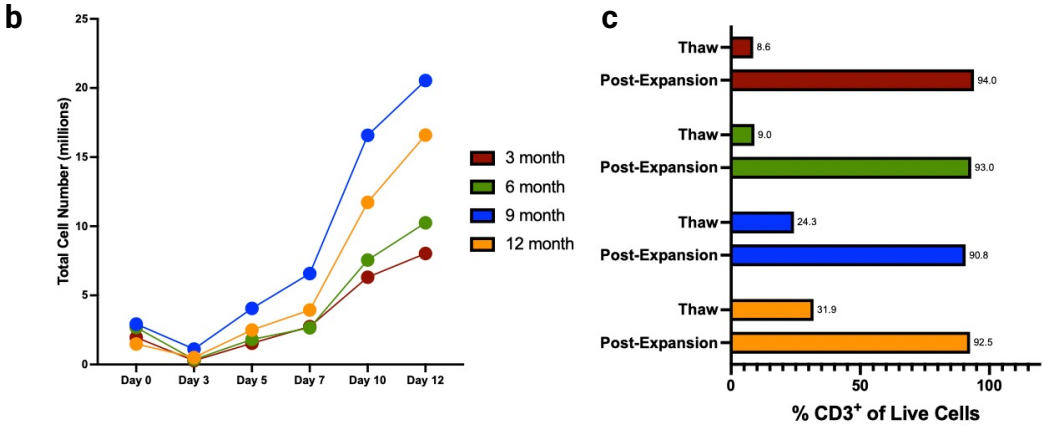

Figure 4.2: Applying the polyclonally-stimulated culture to patient OX747. **a.** Table describing sample characteristics for timepoints tested. **b.** Growth curve demonstrating absolute cell count over course of polyclonally-stimulated culture. **c.** Description of $CD3^{+}$% as a proportion of all live cells assessed by flow cytometry pre- and post- culture.

Reassuringly, all four BMMNC samples expanded robustly following the polyclonal stimulation (Figure 4.2b), with a corresponding enrichment in the $CD3^{+}$% over the expansion period (Figure 4.2c). The 3-month and 6-month samples did

not expand as greatly, likely as a product of both a lower starting cell number and a lower starting $CD3^{+}$% (8.6% and 9.0% respectively, compared to 24.3% and 31.9% for the 9-month and 12-month samples).

For the IFNγ ELISpot, DOCK8, METTL22-1, METTL22-2, and DCAF13 peptides were tested individually, and the 248 other peptides were tested in ten pools of 20-25 peptides (Figure 4.3). As was the case with the previous patient, no responses above background were detected apart from the expected positive control response to PHA.

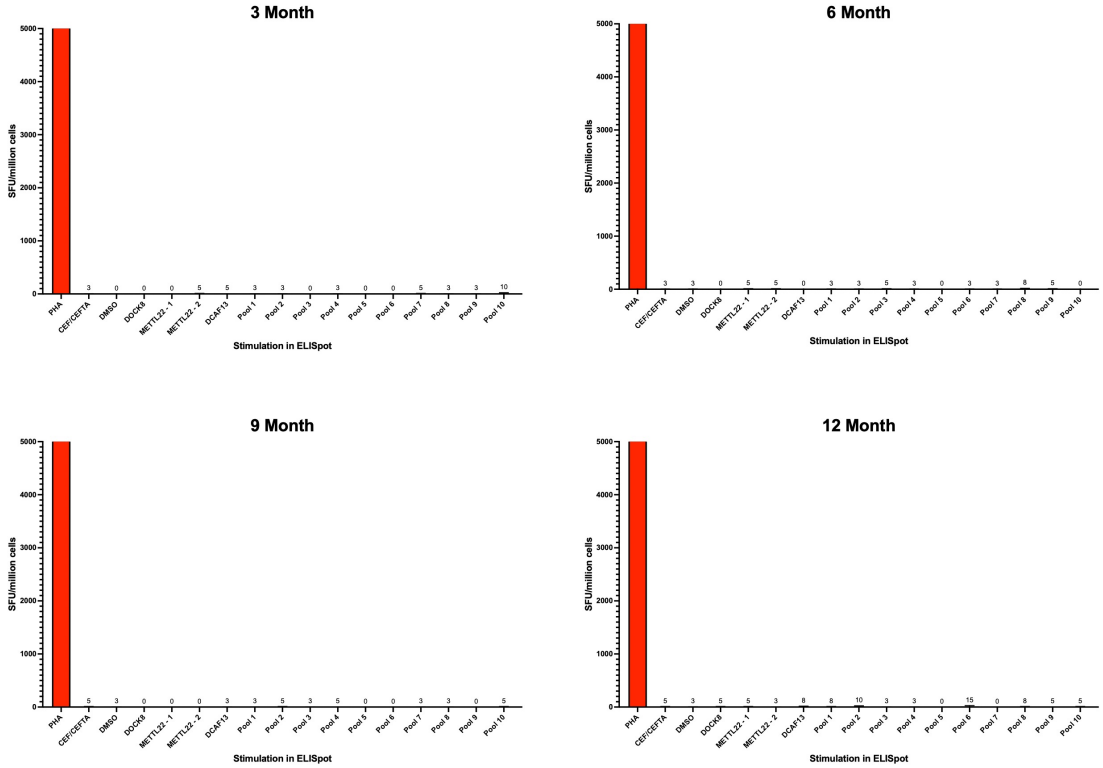

Figure 4.3: IFNγ ELISpot results for patient OX747. IFNγ ELISpot results for the four samples and timepoints tested. METTL22-1 and METTL22-2 refer to two separate peptides spanning the same SNP in METTL22. Pools comprise 20-25 peptides each. ELISpot results are displayed as a maximum of 5000 SFU/million cells for readability

Following the absence of detectable positive responses during the testing of a total of 5 BMMNC samples spread across two patients, the potential causes for this were carefully examined.

Firstly, it was certainly possible that no antigen-reactive cells of interest were present in the early post-alloSCT bone marrow. Though putative GvL responses

were detected in the late peripheral blood of these patients, little is known about the kinetics of these responses and there is no guarantee the same responses are present in this setting. In the 3-6 month window, the presence of antigen-specific T cells is expected to be minimal due to reconstitution being dominated by the homeostatic peripheral expansion of passenger T cells, with limited antigen-driven activity. Similarly, though the timing of T cell reconstitution is patient-specific and context-dependent, ongoing immunosuppression, delayed thymopoiesis and incomplete haematopoietic recovery would be expected to impair the emergence of antigen-experienced T cells in the 6-12 month post-alloSCT period [227, 250, 251].

Secondly, in contrast to the prior antigen-stimulated method, which utilised a peptide-driven expansion phase that would selectively enrich for antigen-reactive T cells, the polyclonally-stimulated method applies a single round of non-specific stimulation prior to IFNγ ELISpot. Though previous work in chapter 3 suggests that these T cells would be maintained at similar relative frequencies in the repertoire, this could substantially limit the detection of rarer clones given the concurrent expansion of bystander and naïve populations. As a result of this, the sensitivity of this approach may be insufficient for identifying low-frequency T cells, particularly in the context of the early post-alloSCT where the relevant clones may not yet have expanded.

Finally, though the activation potential of viral-reactive T cells was shown to be maintained in prior experimentation with the polyclonally-stimulated method, this was not explicitly demonstrated in GvL T cells, whose *ex vivo* phenotype and responsiveness in culture may differ markedly.

For these reasons, rather than proceeding to screen further patients within the cohort, a direct assessment was undertaken to determine whether the polyclonally-stimulated method could detect GvL-reactive responses in a PBMC sample from a late timepoint where responses had previously been detected.

4.3 Comparative Screening Using Polyclonally-Stimulated and Antigen-Specific Cultures

To assess the methodology of the polyclonally-stimulated method in a more granular fashion, it was applied to a peripheral blood sample from patient OX747 taken at 6 years post-alloSCT. This was the timepoint where GvL responses against DOCK8, METTL22 and DCAF13 peptides had previously been detected. This sample was therefore chosen to serve as an internal positive control, allowing for a direct comparison between the polyclonally-stimulated and antigen-stimulated culture methods. In doing so, this provided a means of evaluating the relative sensitivity of the polyclonally-stimulated method for detecting antigen-specific GvL responses.

In order to account for inter-experimental variability, a single vial of 6-year post-alloSCT peripheral blood from OX747 was thawed, split in half, and then cultured concurrently with either the polyclonally-stimulated or antigen-stimulated culture methods (Figure 4.4a).

As expected, the polyclonally-stimulated and antigen-stimulated methods performed very differently over the course of the culture period. In terms of absolute cell number, the polyclonally-stimulated expansion rose from 3.3 million cells at thaw to 51.2 million cells at day 12, compared to the 6.1 million cells at day 12 of the antigen-specific stimulation (Figure 4.4b). Similarly, the $CD3^+$ fraction of the polyclonally-stimulated culture was larger, with the percentage of $CD3^+$ cells rising from 53.9% of live cells to 93.8% at day 12, compared with the 77.6% seen in the antigen-stimulated culture (Figure 4.4c). The lower $CD3^+$ percentage observed in the antigen-stimulated culture primarily reflects the reduced expansion of $CD3^+$ cells, which, when compared against the $CD3^-$ fraction appears proportionally diminished.

Taken together, the polyclonally-stimulated method resulted in a ten-fold greater number of $CD3^+$ cells at day 12 when compared to the antigen-stimulated method.

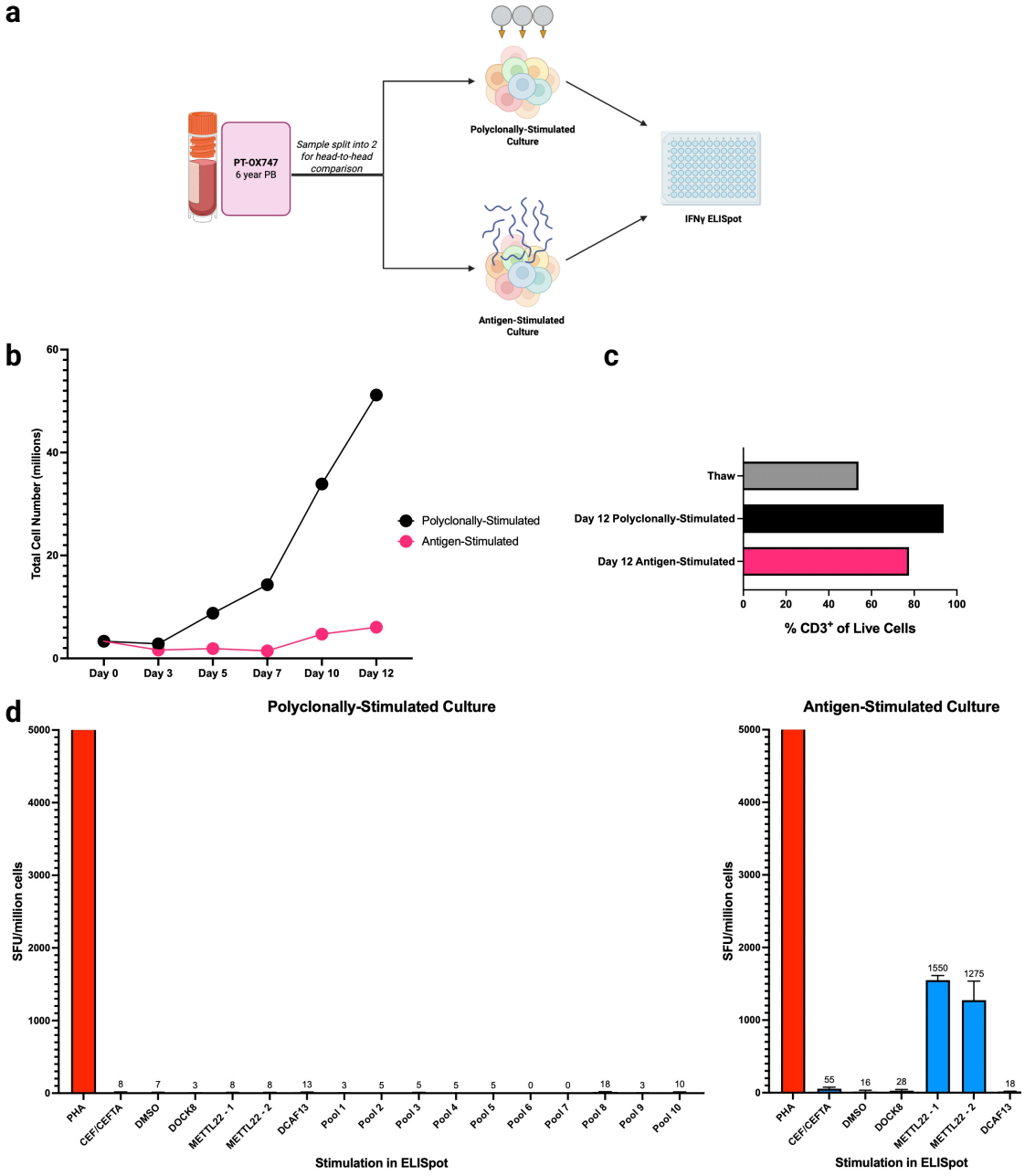

Figure 4.4: Previously detected responses in late peripheral blood are present following antigen-stimulated, but not polyclonally-stimulated culture. a. Simplified schema showing experimental structure. **b.** Growth curve demonstrating absolute cell count comparing polyclonally-stimulated and antigen-stimulated culture. **c.** Description of $CD3^{+}$% as a proportion of all live cells assessed by flow cytometry at thaw and at Day 12. **d.** IFNγ ELISpot results following either polyclonally-stimulated or antigen-stimulated culture. METTL22-1 and METTL22-2 refer to two separate peptides spanning the same SNP in METTL22. Pools comprise 20-30 peptides each.

At the end of the culture period, cells from both culture conditions were assessed by IFNγ ELISpot (Figure 4.4d). Given the limited overall cell number of the antigen-stimulated culture, screening was restricted to targeted testing of the previously identified GvL peptides, rather than the full peptide library.

Consistent with the earlier findings of the early post-alloSCT bone marrow, the polyclonally-stimulated culture yielded no detectable responses against any peptide. In contrast, the antigen-stimulated culture demonstrated substantial responses against both METTL22 peptides. METTL22-1 elicited 1550 SFU/million cells (SD = 63.6) and METTL22-2 elicited 1275 SFU/million cells (SD = 185).

Several additional observations warrant discussion. Despite prior detection of responses against DOCK8 and DCAF13 in this patient, neither peptide elicited a response in this assay. Importantly, when originally identified, the response against DOCK8 was of equivalent intensity to METTL22, while the DCAF13 response was even greater, highlighting that their subsequent absence was not attributable to weaker baseline immunogenicity. As the sample used here was an aliquot from the same blood draw in which the original responses were identified, this emphasises the inherent stochasticity and variability in T cell sampling and detection across these cryopreserved vials. Additionally, given that high-frequency TCR clonotypes would be more likely to be found across multiple sample vials, this lends further credence to the low starting frequency of our cells of interest.

Secondly, aside from the expected response to PHA, the only other detectable signal was a weak response to the CEF/CEFTA viral peptide pool, which produced a response approximately threefold above background. Importantly, this response was observed in the antigen-specific culture without any prior expansion with CEF/CEFTA peptides, indicating the presence of pre-existing CEF/CEFTA-reactive T cells at sufficient frequency to be detectable under these conditions. In contrast, no such response was detected in the parallel polyclonally-stimulated culture, suggesting that these virus-specific T cells were not of sufficiently high frequency to be detected in the presence of global T cell proliferation. This result mirrors prior testing in the

peripheral blood by Connor Sweeney, where a CEF/CEFTA response was detected at a similar magnitude [198].

These findings provide evidence that the polyclonally-stimulated culture method was unable to detect antigen-specific GvL responses that are readily seen following the antigen-stimulated expansion.

While the polyclonally-stimulated culture did result in a significantly higher total number of $CD3^+$ T cells for functional testing, this came at the expense of sensitivity.

The most likely explanation is that the antigen-stimulated expansion increased the relative frequency of rare, antigen-specific GvL clones to levels above the threshold of detection, whereas in the polyclonal culture these same clones remained obscured within the background of actively proliferating bystander cells. An additional possibility is that polyclonal stimulation imposed a degree of functional impairment, reducing the capacity of GvL T cells to respond even if present.

Taken together, these results emphasise the limited utility of the polyclonally-stimulated method alone in detecting these low-frequency GvL responses. Future approaches would therefore need to balance enrichment of our T cells of interest with maintaining a requisite degree of stimulation that maintains the survival of these cells.

4.4 METTL22 as a Candidate Minor Histocompatibility Antigen

Having identified patient-specific responses against METTL22, its expression was examined to evaluate its potential immunological relevance in the post-alloSCT setting. Expression across both healthy tissues and haematopoietic compartments was assessed through the interrogation of public datasets.

Protein expression profiling using immunohistochemistry data from the Human Protein Atlas (HPA) demonstrated positive staining across a broad range of tissues, with no marked enrichment in the haematopoietic system (Figure 4.5a) [205, 206].

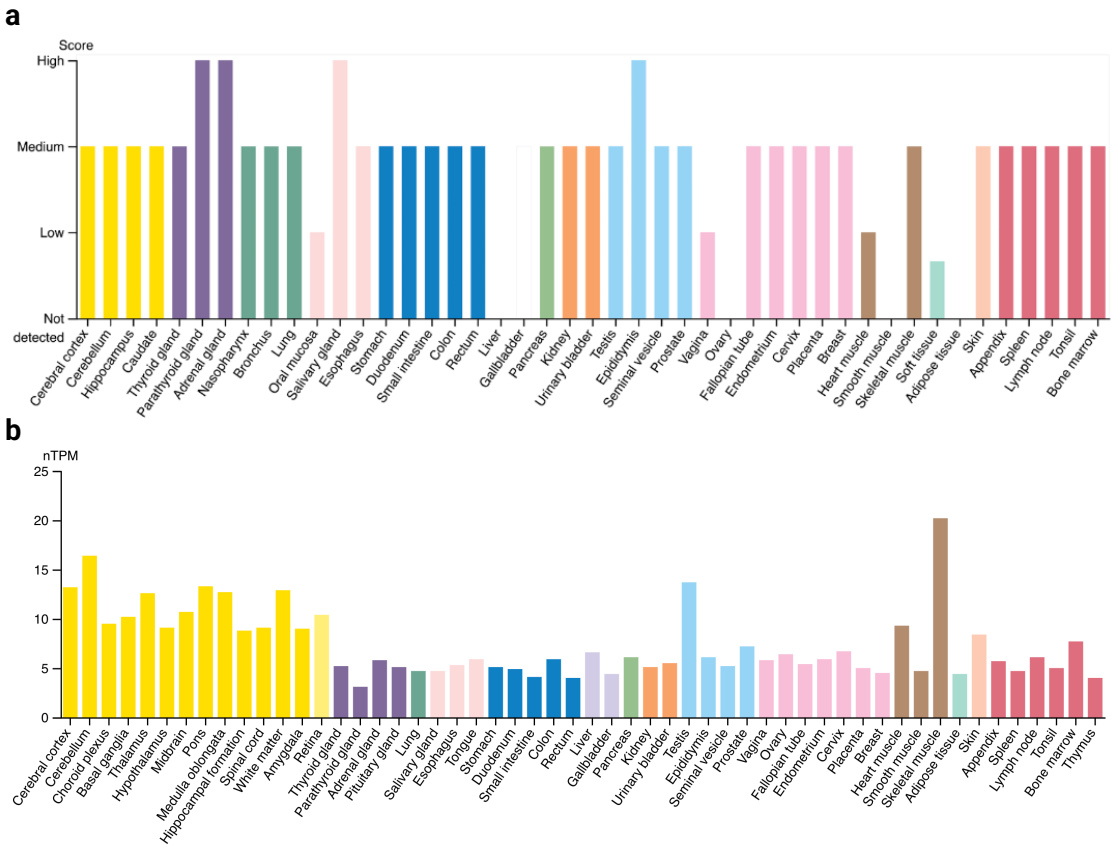

Figure 4.5: Expression of METTL22 across tissues. a. Semi-quantitative protein expression scores for METTL22 across healthy tissues taken from the Human Protein Atlas (HPA) [205, 206]. Scoring reflects analysis of staining intensity and proportion of stained cells in immunohistochemistry data evaluated by expert pathologists. **b.** mRNA expression levels of METTL22 in healthy tissues taken from the HPA Consensus dataset, expressed as normalised transcripts per million (nTPM) [207].

mRNA expression analysis using the HPA Consensus dataset similarly demonstrated widespread expression of METTL22 (Figure 4.5b) [205, 207].

Although protein expression scoring is semi-quantitative and dependent on operator interpretation, antibody performance and histological quality, several tissues such as the liver or smooth muscle, demonstrate marked discrepancies between mRNA and protein levels. This reflects well-known post-transcriptional regulatory mechanisms.

Gene expression within the haematopoietic compartment and AML was further assessed using publicly available microarray and RNA-sequencing datasets via the BloodSpot platform (Figure 4.6) [208, 209].

Four separate AML datasets were surveyed from the BEAT-AML, TARGET-AML, TCGA and MILE studies [210–213]. Across all four AML datasets, METTL22 was consistently expressed at a detectable level, though this was lower for the BEAT-AML and TARGET-AML datasets, this may reflect methodological differences, where these datasets were sourced from RNAseq whereas the remainder were sourced from microarray data.

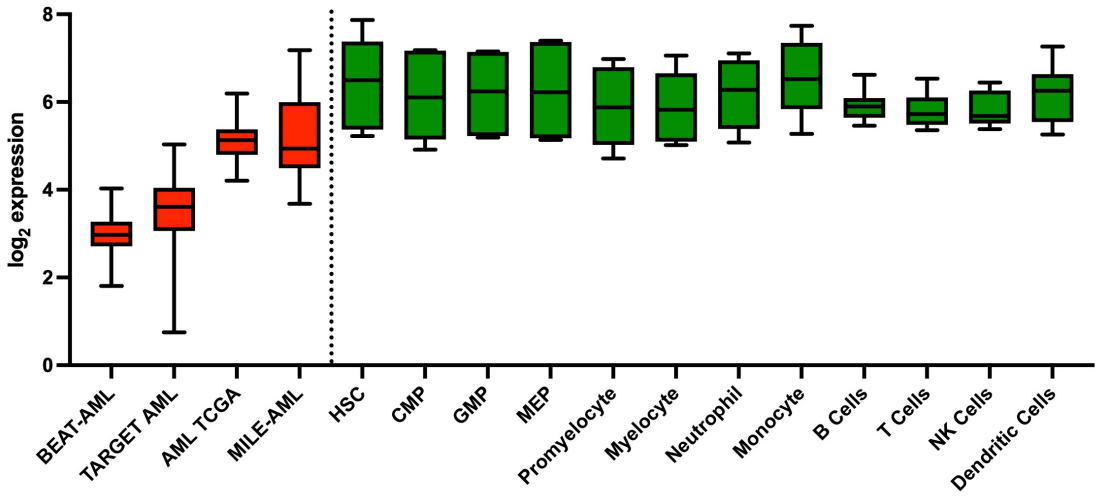

Figure 4.6: Gene expression of METTL22 in AML and healthy haematopoiesis. Gene expression shown as $\log_2$-transformed consensus expression values. AML datasets in red include BEAT-AML, TARGET-AML, TCGA and MILE studies [210–213]. Healthy subpopulations in green are derived from the HemaExplorer dataset [209]. HSC = Haematopoeitic stem cell. CMP = Common myeloid progenitor. GMP = Granulocyte-monocyte progenitor. MEP = Megakaryocyte-erythroid progenitor. NK = Natural killer.

Taken together, this data shows that METTL22 is not haematopoietically restricted. It may, however, still act as a GvL antigen despite its ubiquitous expression, potentially through selective antigen processing and presentation of class II HLA within the haematopoietic compartment. Alternatively, METTL22-specific T cell responses may also target non-malignant host tissues, acting as a joint GvL/GvHD response.

4.5 Isolation and TCR Sequencing of METTL22-specific T cells

As the TCR sequences mediating METTL22-specific responses had not previously been identified, isolation of these cells was undertaken using an IFNγ-Catch assay in conjunction with single-cell sorting and 10x Genomics-based methods.

This strategy enables the retrieval of TCRα/β sequences for downstream applications, including functional validation through activation or cytotoxicity assays. Furthermore, knowledge of these sequences could be used in conjunction with bulk sequencing to refine our previous assessments of the differences in clonal enrichment between the polyclonally-stimulated and antigen-stimulated cultures by progressing from functionality to true TCR clonotype analysis.

Cells from the antigen-stimulated culture (as performed in section 4.3) were rested for 24 hours in cytokine-free medium and then re-stimulated separately with METTL22-1 and METTL22-2 peptides. Following a 45-minute cytokine secretion period, IFNγ-producing cells were labelled using the IFNγ-Catch assay and sorted (Figure 4.7a).

To maximise cell retention, IFNγ$^+$, CD3$^+$ T cells were sorted irrespective of CD4/CD8 status, although surface expression for both markers was simultaneously assessed during flow cytometry.

Stimulation with either METTL22-1 or METTL22-2 resulted in a notable global increase in IFNγ fluorescence across the entire CD3$^+$ population compared to the DMSO control. This likely reflects either paracrine activation of bystander cells or non-specific capture of secreted IFNγ on non-activated cells from the culture milieu. Due to this change in background fluorescence, sorting gates for IFNγ$^+$ and IFNγ$^-$ populations were set individually for each condition on the basis of the fluorescent intensity of the background population. Notably, METTL22-1 induced a higher degree of IFNγ expression than METTL22-2, in agreement with the differential response observed in the prior IFNγ ELISpot.

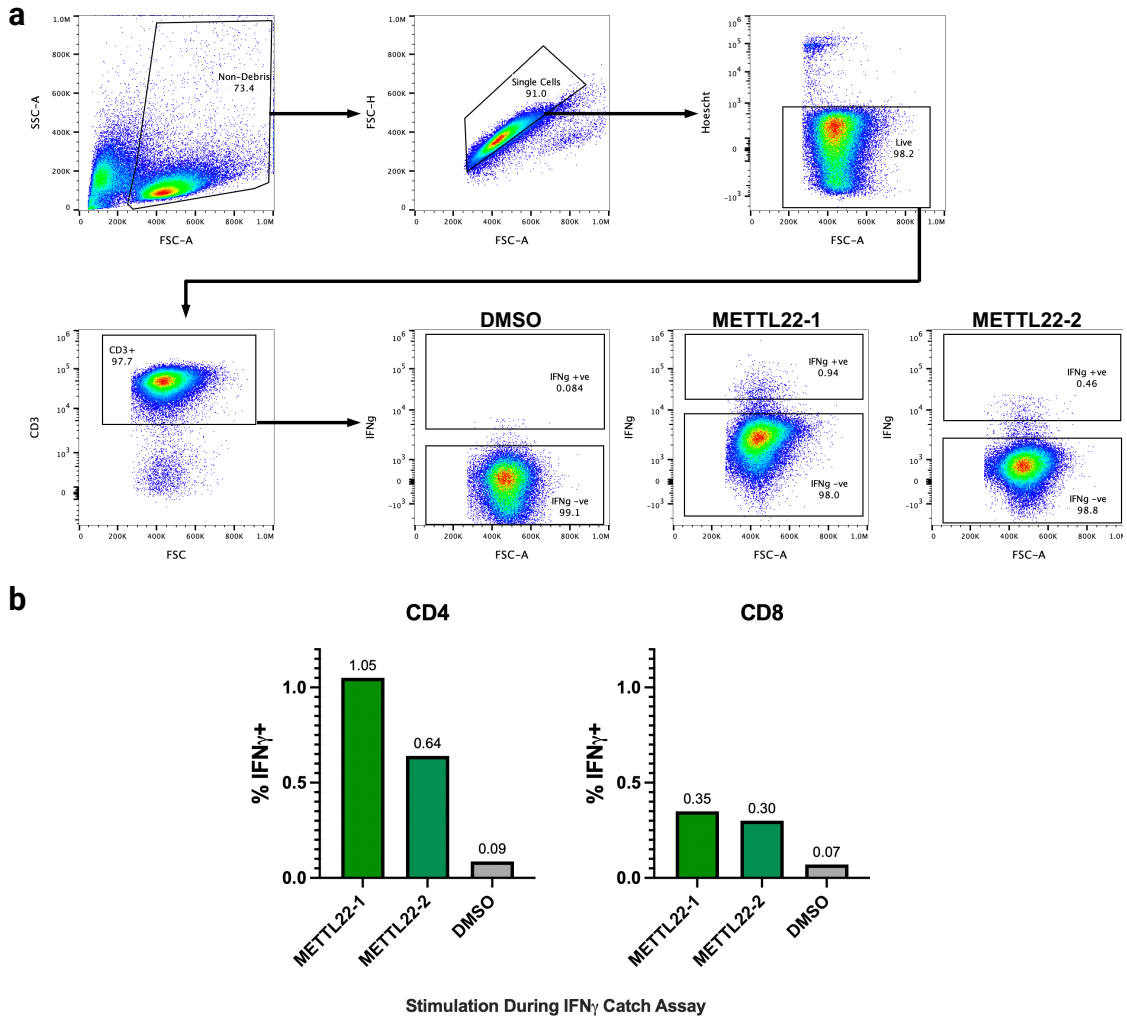

Figure 4.7: Isolation of METTL22-reactive T cells utilising IFNγ Catch assay. a. Gating strategy for the sorting of IFNγ$^+$ and IFNγ$^-$ T cells following an antigen-stimulated stimulation. Numbers on plots display percentage of parent population. Headings on the final three flow plots outline stimulation used at IFNγ-Catch assay. Due to low cell yield, CD3$^+$ T cells were sorted as a bulk population without further subdivision into CD4$^+$ or CD8$^+$ subsets. **b.** Summary analysis of flow cytometry data, showing the percentage of CD4$^+$ and CD8$^+$ cells which express IFNγ in response to stimulation by peptides METTL22-1, METTL22-2 and DMSO.

In both stimulated conditions, $CD4^+$ T cell activation exceeded that of $CD8^+$ cells, suggesting a predominance of $CD4^+$-driven responses (Figure 4.7b). It is unclear to what extent the observed $CD8^+$ activation represents true antigen-specific stimulation rather than background activation, however this can be further clarified through downstream transcriptomic profiling.

Following cell sorting, TCR and whole transcriptome library preparation was undertaken for $IFN\gamma^+$ and $IFN\gamma^-$ fractions for cells stimulated by METTL22-1 and METTL22-2 (n = 2,382). By concurrently analysing gene expression and TCR data, V(D)J calling accuracy was improved by excluding cell barcodes that were not simultaneously called in both modalities, mitigating the risk of V(D)J overcalling. Additionally, analysis of the $IFN\gamma^-$ fraction provides a background for the identification of enriched clones and activation-specific transcriptional states.

Unfortunately, given the lower cell number sorted for the $IFN\gamma^+$ fraction for METTL22-2, the quality of the cDNA library was insufficient to carry forward and as such only conditions stimulated by METTL22-1 underwent full library preparation and sequencing. While it cannot be entirely excluded that distinct TCRs may preferentially recognise peptides with differing N- or C-terminal overhangs, the most plausible explanation is that METTL22-1 and METTL22-2 stimulate the same clonotypes, with the reduced responsiveness to METTL22-2 reflecting weaker peptide-HLA binding. Consequently, the $IFN\gamma^+$ fraction stimulated by METTL22-1 was deemed likely to be representative for the characterisation of antigen-specific clonotypes.

Analysis of the TCR repertoire within the $IFN\gamma^+$ fraction revealed a skewed TCR repertoire, consistent with clonal expansion in response to stimulation by METTL22 peptide (Figure 4.8).

Eight clonotypes were present at a frequency of greater than 2% within the $IFN\gamma^+$ population, together comprising 46.1% of the total repertoire. In contrast, these same clonotypes were either undetectable (Clonotypes 1, 5 and 8), or present

a

Clonotype	Frequency in IFNγ +ve Fraction (%)	Frequency in IFNγ -ve Fraction (%)	Fold Enrichment Between Negative and Positive Fractions	TCRa CDR3 Sequence	TCRb CDR3 Sequence
1	13.23			CAAILQGAQKLVF	CSARTHSDEAFF
2	9.92	1.70	5.8	CAFAISNYQLIW	CSAIVGTGVFDEQFF
3	5.25	0.50	10.5	CAVNFGNEKLTF	CSARASQGDTQYF
4	4.86	0.10	48.6	CAASYTGFQKLVF	CASTDTSGDTEAFF
5	4.28			CAVEAEGQNFVF	CSASGGGAPGELFF
6	3.31	1.90	1.7	CLVGASLNDYKLSF	CASSGPGELFF
7	3.11	0.10	31.1	CAASHLQGAQKLVF	CASSLMGQGLQPQHF
8	2.14			CAVGNSGNTPLVF	CASSSGGYSVVFF
Sum of Unpaired and Low Frequency	53.89	95.70			

b

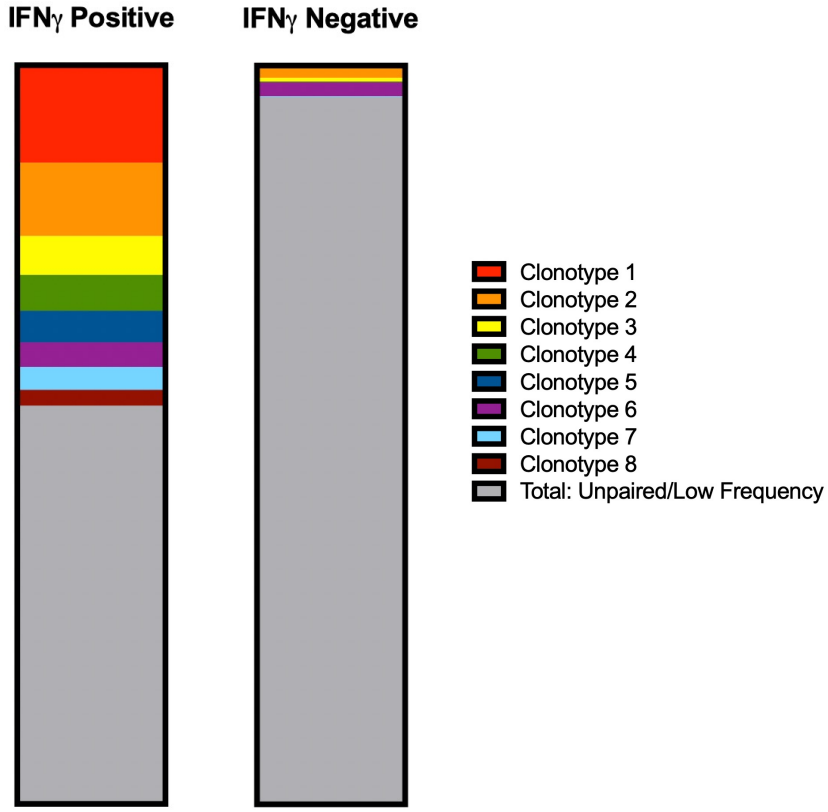

Figure 4.8: Eight enriched TCR clonotypes were identified in the IFNγ^+ fraction of cells stimulated by peptide METTL22-1. a. Table outlining the high frequency clonotypes identified in the IFNγ^+ fraction with their degree of enrichment and their CDR3 sequences. Low frequency clonotypes are defined here as <2% of the total repertoire. **b.** Visual representation of clonotypes isolated. Each large bar represents all T cell clones identified from the IFNγ^+ and IFNγ^- fractions. Y-axis represents the percentage of all sequenced cells. The grey portion of each bar represents the sum of all low frequency clonotypes and clonotypes without fully paired TCRα and TCRβ chains.

at a lower frequency in the IFNγ^- fraction, which was predominantly comprised of low frequency clonotypes. The extent of enrichment of clonotypes detectable in both fractions was variable, with fold-change ranging between 1.7-fold and 48.6-fold.

Clonotypes exhibiting high enrichment in the IFNγ^+ fraction are more likely to represent *bona fide* antigen-specific T cell responses to METTL22. In particular, Clonotypes 1, 5 and 8 were of particular interest as they are absent in the IFNγ^- fraction altogether. Conversely, Clonotype 6, which was only modestly enriched at 1.7-fold, may represent a non-specifically activated or bystander population. However, as the peptide-stimulated culture system is itself designed to promote the expansion of METTL22-specific cells, even these clonotypes with minimal differential abundance should not necessarily be discounted outright. Functional validation remains of paramount importance in the confirmation of definitive antigen specificity.

Comparison of these TCR sequences against publicly available TCR databases confirmed that all these sequences were private, which is consistent with a T cell response against a minor histocompatibility antigen in this clinical context [216].

Having identified a selection of expanded clones within the METTL22-reactive IFNγ^+ fraction, the next step was to investigate their transcriptional phenotype, both to elucidate their effector function, as well as further inform which of these clonotypes should be prioritised for downstream functional validation.

4.6 Transcriptional Profiling of METTL22-specific T cells

To investigate the phenotypic identity of the METTL22-specific T cells, transcriptomic analysis was performed on the paired whole transcriptome libraries generated from the sorted IFNγ^+ and IFNγ^- populations. This approach enabled the integration of TCR clonotype and gene expression data, allowing for the mapping of antigen-specific clones onto discrete transcriptional states.

Dimensionality reduction was performed on log-normalised gene expression data using principal component analysis (PCA) followed by unbiased clustering via k-means, chosen given the overall modest cell number. This process demarcated six transcriptionally distinct clusters, which were visualised on UMAP plots (Figure 4.9a). Clusters were annotated *post hoc* on the basis of canonical marker gene expression of the majority of cells within each cluster [215, 223].

The majority of cells fell into three dominant clusters: conventional $CD4^+$ T cells, $CD8^+$ T_{EM}/T_{EMRA} and $CD8^+$ $T_{Naïve}/T_{CM}$. Two smaller clusters comprised double-negative T cells and an unclassified group that did not map clearly to a defined T cell lineage. Finally, there was a clearly demarcated population of activated cytotoxic $CD4^+$ T cells.

In order to validate these annotations, expression of CD4 and CD8A was visualised using violin plots (Figure 4.9b). As expected, CD4 transcript expression was restricted to the $CD4^+$ T cell and activated cytotoxic $CD4^+$ clusters. However, expression within these clusters was heterogeneous and in some cells appeared low or undetectable. CD4 is a low-abundance transcript that can be downregulated during T cell activation and effector differentiation [252]. Furthermore, transcript drop-out, particularly in the case of low-expression genes, is a well-recognised limitation of droplet-based single-cell RNA-seq platforms such as the 10x Chromium platform used here, arising from inefficient capture and amplification [253].

CD8 expression was similarly restricted to the $CD8^+$ T_{EM}/T_{EMRA} and $CD8^+$ $T_{Naïve}/T_{CM}$ clusters.

To further support these functional annotations, the expression of a curated panel of functional and differentiation-associated genes was projected onto the UMAP (Figure 4.9c). Markers associated with naïve and memory-like states, *TCF7*, *LEF1* and *IL7R* were most highly expressed in the $CD8^+$ $T_{Naïve}/T_{CM}$ cluster. Cytotoxic markers *NKG7*, *GZMB* and *PRF1* were highly expressed in both the $CD8^+$ T_{EM}/T_{EMRA} cluster and the activated cytotoxic $CD4^+$ cluster. This activated cytotoxic $CD4^+$ cluster also showed high expression of effector molecules, such as

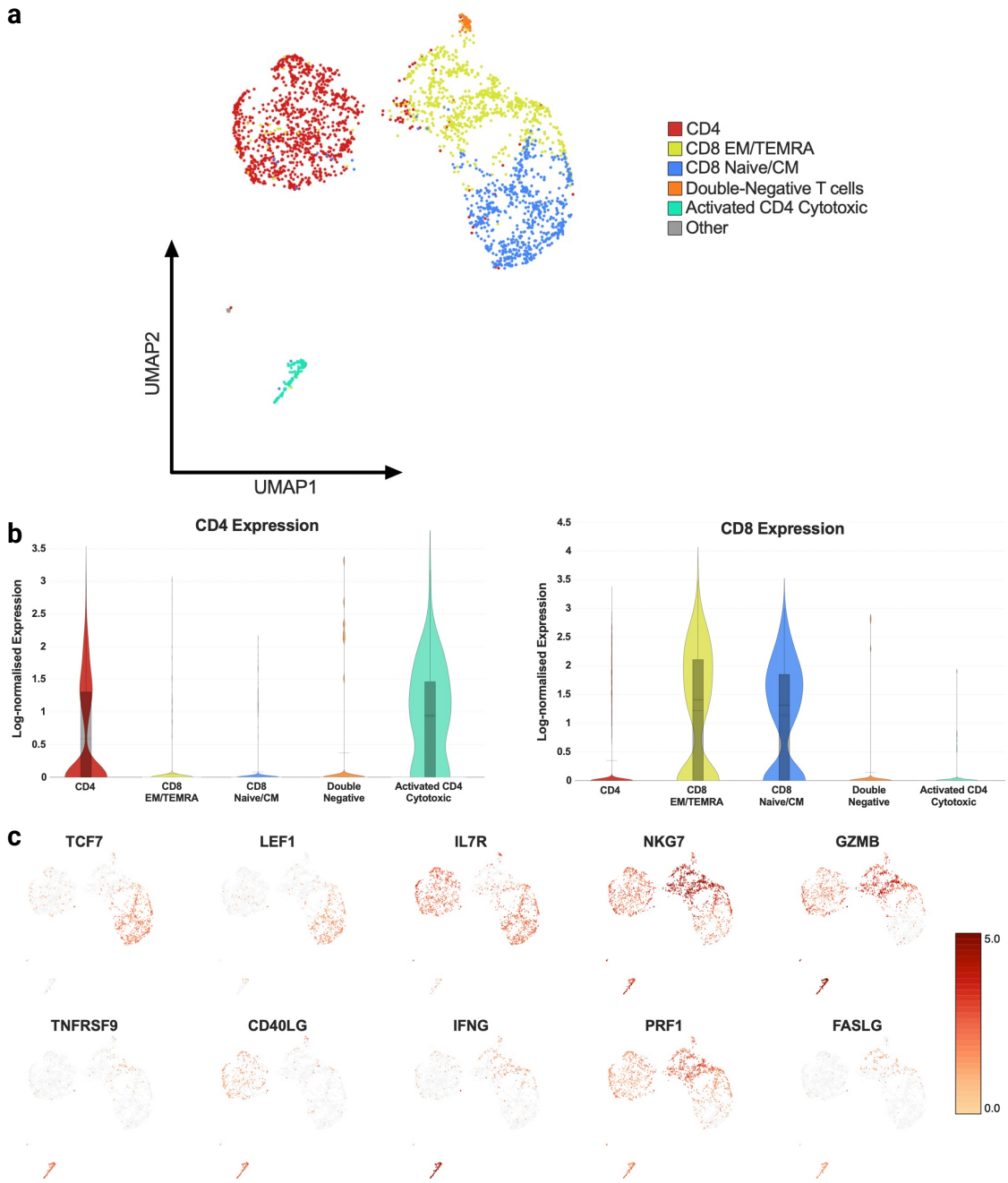

Figure 4.9: Single cell transcriptomics for all sorted T cells from patient OX747 a. UMAP plot derived from transcriptomic profiles of both IFNγ^+ and IFNγ^- cells ($n = 2382$) following dimensionality reduction and clustered via K-means. Clusters annotated *post hoc* via expression of canonical marker genes. **b.** Violin plots demonstrating log-normalised expression of CD4 and CD8 for each cluster as outlined above. Where appropriate, each box represents the mean with interquartile range. **c.** UMAP plots displaying log-normalised expression (colour-scale) for selected T cell marker genes.

IFNG and *FASLG*, alongside co-stimulatory and activation markers *TNFRSF* (OX40) and *CD40LG*, consistent with a transcriptionally activated state.

To examine the relationship between functional activation and transcriptional state, IFNγ$^+$ and IFNγ$^-$ cells were overlaid onto the UMAP (Figure 4.10). IFNγ$^+$ cells were disproportionately enriched in the activated cytotoxic CD4$^+$ cluster, and to a lesser extent, within the conventional CD4$^+$ cluster. Interestingly, not all cells that were sorted into the IFNγ$^+$ fraction have detectable IFNγ transcripts, lending credence to our previous hypothesis of background capture of IFNγ on the surface of non-activated cells during the IFNγ-Catch assay.

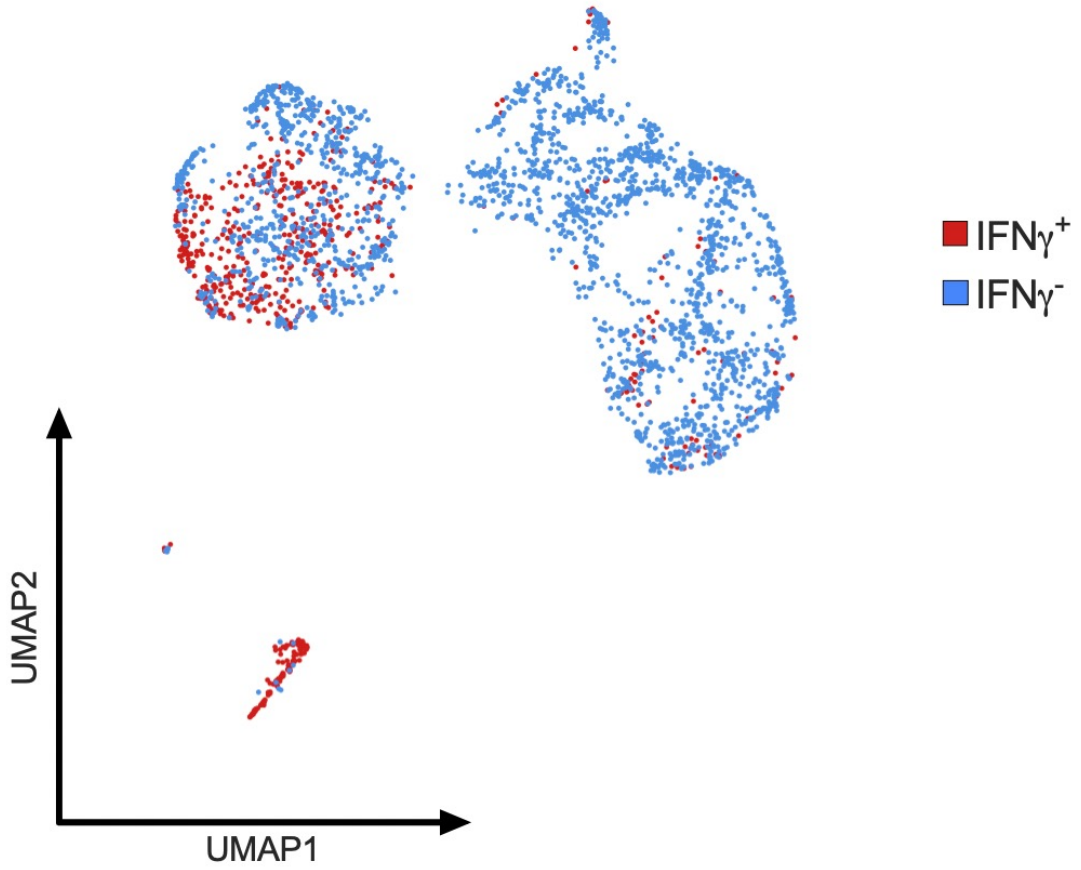

Figure 4.10: Distribution of IFNγ$^+$ and IFNγ$^-$ T cells. UMAP plots demonstrating distribution of IFNγ$^+$ and IFNγ$^-$ T cells coloured by IFNγ status.

The eight clonotypes that were enriched in the IFNγ^+ fraction were mapped onto the UMAP and coloured by their annotated cluster (Figure 4.11a). All of these clonotypes were CD4$^+$ restricted, consistent with the higher proportion of activated CD4$^+$ cells during the IFNγ-Catch assay.

Clonotypes 1 and 5, which were both highly enriched and absent in the IFNγ^- population, were localised entirely within the activated cytotoxic CD4$^+$ cluster. This contrasts with the remainder of the clonotypes, which were more largely scattered within the conventional CD4$^+$ cluster.

To explore the molecular signatures that underpinned the distinct activated cytotoxic CD4$^+$ cluster, differential gene expression analysis was performed, comparing Clonotypes 1 and 5 with all other cells (Figure 4.11b).

This analysis revealed a total of 578 significantly differentially expressed genes ($p < 0.05$ and $|\log_2$ Fold Change$| > 2$). Among the differentially expressed genes were non-coding RNAs and broadly expressed transcripts with limited interpretive value in T cell biology.

Downregulated genes included *TCF7*, *CCR7*, *KLF2* and *IL7R*, indicative of transition away from a naïve phenotype to a more differentiated effector phenotype. Upregulated genes included genes associated with a cytotoxic effector profile – such as *IFNG*, *PRF1*, *FASLG* and *GZMB* – and genes associated with T cell co-stimulation or activation – such as *TNFRSF9*, *CD40LG*, *IL2RA*, *CD70* or *LAG3*.

It is unclear, however, to what extent this cytotoxic phenotype reflects the *in vivo* phenotype of these T cells. The use of exogenous, unopposed IL-2 throughout the antigen-stimulated culture, in combination with TCR activation, can itself drive effector differentiation and cytotoxic gene expression [254].

Together, this signature indicates a robust cytotoxic effector program with evidence of recent activation. This further supports the relevance of Clonotypes 1 and 5 as *bona fide* METTL22-specific T cells.

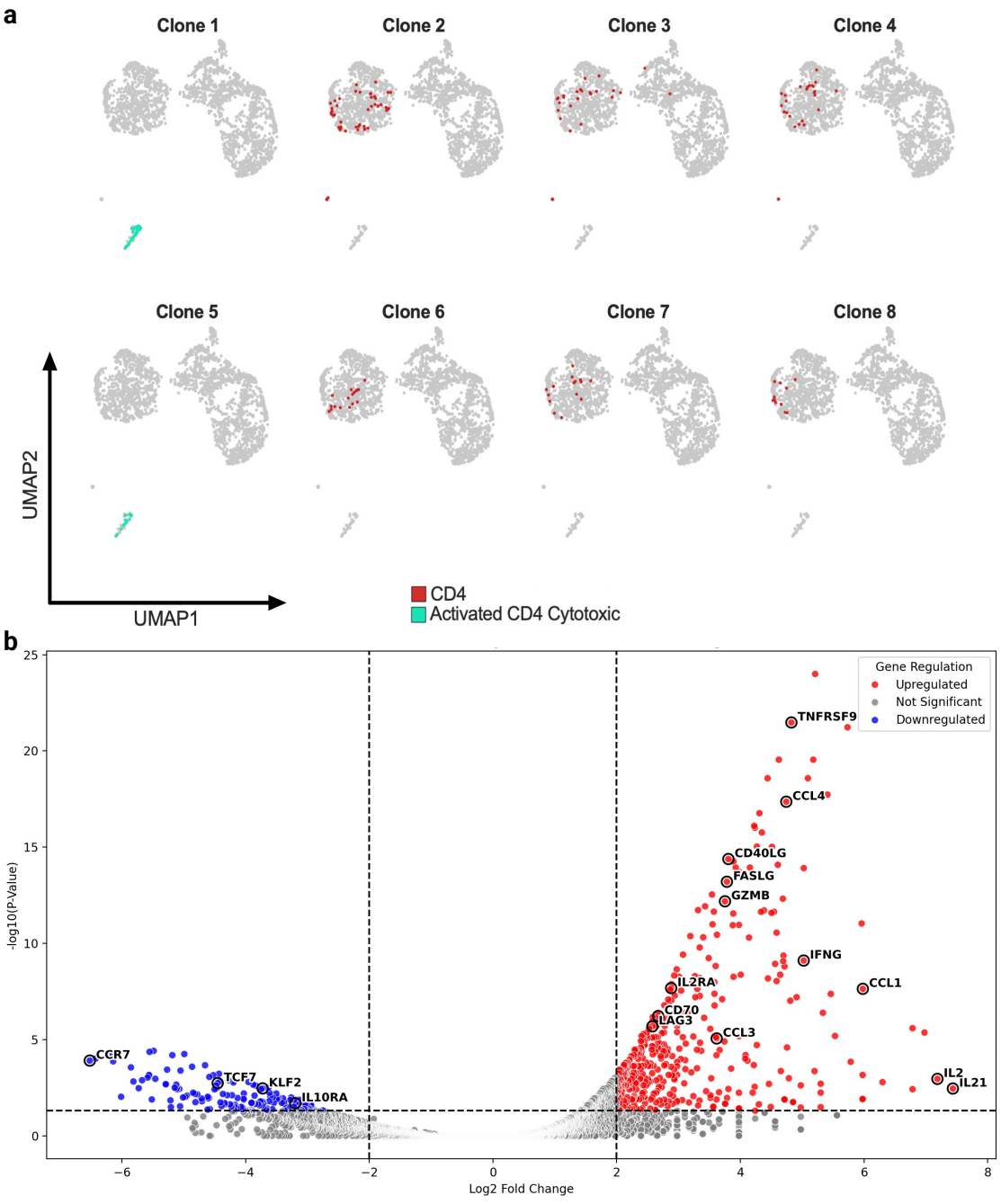

Figure 4.11: Clones 1 and 5 are transcriptionally distinct and sit in an activated CD4 cytotoxic cluster. a. UMAP plots demonstrating distribution of TCR clonotypes of interest that were enriched in the sorted IFNγ^+ cell fraction. Cells are coloured by their annotated cell type. **b.** Volcano plot demonstrating differentially expressed genes for clonotypes 1 and 5 compared against all other cells. Significantly differentially expressed genes (p<0.05 and $|\log_2 FC|$) are highlighted in colour with genes of interest annotated. Statistical testing was performed utilising the 10x Loupe platform, using a variant negative binomial exact test with the Benjamini-Hochberg FDR correction.

4.7 Bulk Repertoire Sequencing of OX747

To further assess the frequency of METTL22-specific TCR clonotypes beyond the single-cell context, bulk TCR sequencing was performed on cultured T cells from patient OX747.

This complementary approach would allow for a more direct and quantitative assessment of the abundance of these clonotypes across culture conditions, independent of their activation potential.

Bulk TCR sequencing was performed on both the antigen-stimulated and polyclonally-stimulated cultures derived from 6-year post-alloSCT peripheral blood (as performed in section 4.3). As previously described in section 2.4 and section 3.3, this was performed utilising 5'-RACE followed by NGS, with UMI-corrected read counts serving as a proxy for clonotype frequency. As the cell and RNA input was equivalent across conditions, further normalisation with downsampling was not required.

By focusing on the eight enriched TCR clonotypes within the IFNγ^+ fraction, it was possible to evaluate their frequency relative to the broader repertoire in both the culture conditions and therefore assess their divergence over the culture period (Figure 4.12a). Although ideally, this analysis would have extended to the *ex vivo* TCR repertoire at thaw, this was not feasible given the limited cell numbers and the decision to prioritise functional screening over baseline profiling.

As expected, all eight clonotypes were detectable in the antigen-stimulated culture, where these clones had originally been identified, with frequencies from 0.31% to 7.61%. However, in keeping with the limitations of bulk RNA sequencing, pairing of the TCRα and TCRβ chains could not be directly established.

Notably, save for Clonotypes 3 and 8, the frequency of each clonotype's TCRα and TCRβ chains was discordant. This was most striking in Clonotype 2, where its TCRα was detected at a frequency of 0.82% and its TCRβ at 7.36%.

a

Clonotype	Frequency in IFNγ +ve Fraction (%)	Antigen-Stimulated Culture		Polyclonally-Stimulated Culture	
		Inferred TCRα Frequency (%)	Inferred TCRβ Frequency (%)	Inferred TCRα Frequency (%)	Inferred TCRβ Frequency (%)
1	13.23	1.46	0.47		
2	9.92	0.82	7.36	0.00204	0.02375
3	5.25	0.91	1.25		
4	4.86	0.87	2.37		
5	4.28	0.10	0.53		
6	3.31	7.61	3.76	0.00131	0.00043
7	3.11	1.50	0.68		
8	2.14	0.42	0.31	0.00015	0.00043

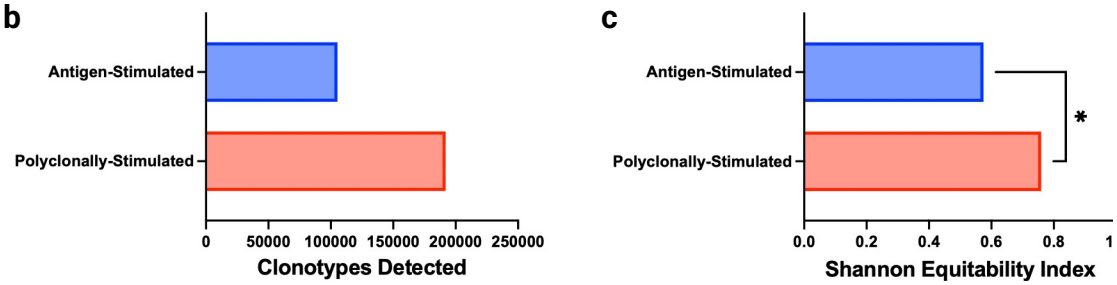

Figure 4.12: IFNγ-enriched clonotypes detected in late peripheral blood fall below limits of detection in a polyclonally-stimulated culture. a. Description of the inferred TCRα and TCRβ clonotype frequencies from bulk sequencing of antigen-stimulated and polyclonally-stimulated culture of late peripheral blood from patient OX747. Inferred frequency calculated utilising fraction of all UMI-collapsed reads sequenced. **b.** Graph depicting number of TCR clonotypes detected via bulk sequencing from a 1 million cell aliquot of antigen-stimulated and polyclonally-stimulated cells. **c.** Shannon equitability indices of the antigen-stimulated and polyclonally-stimulated repertoires. p value is calculated via Student's t test.

Several factors could account for this discordance. Firstly, this could reflect alternative TCRα pairing. Unlike TCRβ, which is subject to strict allelic exclusion during early thymic development, the TCRα locus instead undergoes successive recombination without enforced allelic exclusion, permitting expression of dual TCRα chains in a subset of mature T cells [255, 256]. Indeed, single-cell sequencing for Clonotype 2, revealed expression of an alternate TCRα chain, supporting this explanation.

Secondly, one of the detected chains may be utilised in one or more other TCRs of differing specificity, in that the apparent imbalance at sequencing reflects contributions from unrelated clonotypes sharing that chain.

Thirdly, as clonotype frequency is inferred from UMI-collapsed read count, differences in initial mRNA abundance between TCRα and TCRβ transcripts could

lead to frequency discrepancies.

Finally, technical biases in mRNA capture and amplification can occur. Despite the use of UMIs to control for PCR bias, SmartSeq-based approaches remain sensitive to transcript length and GC content, particularly during reverse transcription, which can result in chain-specific dropout or preferential amplification. Despite these limitations, bulk TCR sequencing offers a powerful and high-throughput method for tracking known TCR clonotypes within large populations of cells. However, the observed frequency discrepancies reinforce the value of single-cell-based methods for high-confidence clonotype calling with αβ chain pairing.

Unexpectedly, only Clonotypes 2, 6 and 8 remained detectable following the polyclonally-stimulated culture. Interestingly, the skewed TCRα/TCRβ ratio was consistent for both Clonotypes 2 and 6, suggesting a reproducible feature to these clonotypes' pairing dynamics or technical performance. As both the polyclonally-stimulated and antigen-stimulated cultures originated from the same vial split in half, this suggests that these missing clonotypes likely exist at frequencies below 0.00014%, based on the rarest detected clonotype. It is possible that increasing sequencing depth could result in the identification of the remaining clonotypes. However, sampling was already performed to a depth of 1 in 700,000, based on a starting input of 1,000,000 cells, making deeper analysis unlikely to yield additional benefits. This suggests that the absence of detection reflects true biological rarity, rather than insufficient technical resolution.

Although it is not possible to determine whether individual clonotypes expanded to equal extents during the polyclonally-stimulated culture, data presented in chapter 3 has shown that the overall repertoire diversity remains stable over the culture period. This supports the hypothesis that the initial frequency of these GvL clonotypes is extremely low, being both consistent with and lower than the reported incidences of <0.1% seen in some studies [40, 249, 257]. These findings echo earlier

concerns raised during the development of the polyclonally-stimulated method and emphasise the importance of selective enrichment for GvL clonotypes during culture.

In keeping with these observations, the number of distinct clonotypes detected in the polyclonally-stimulated culture was almost double the number detected in the antigen-stimulated expansion (Figure 4.12b). Furthermore, the Shannon equitability index confirmed a significantly lower diversity in the antigen-stimulated culture compared to the polyclonal expansion (Figure 4.12c). This suggests that irrelevant clonotypes are retained at high levels in the polyclonally-stimulated method, hampering the detection of desired GvL T cell responses, where a focused expansion is more valuable than broad maintenance of diversity.

Clonotype	3 months post-alloSCT		6 months post-alloSCT		9 months post-alloSCT		12 months post-alloSCT	
	Inferred TCRα Frequency (%)	Inferred TCRβ Frequency (%)	Inferred TCRα Frequency (%)	Inferred TCRβ Frequency (%)	Inferred TCRα Frequency (%)	Inferred TCRβ Frequency (%)	Inferred TCRα Frequency (%)	Inferred TCRβ Frequency (%)
1								
2	0.0071	0.1300	0.0092	0.1463	0.0068	0.0598	0.0002	0.0054
3								
4								
5								
6			0.0046	0.0030	0.0076	0.0028	0.0149	0.0073
7								
8								

Figure 4.13: Clonotypes 2 and 6 are detectable through bulk sequencing of polyclonally-stimulated early Bone Marrow. Description of the inferred TCRα and TCRβ clonotype frequencies from bulk sequencing of polyclonally-stimulated cultures of early BM from patient OX747. Inferred frequency calculated utilising fraction of all UMI-collapsed reads sequenced.

Bulk TCR sequencing was also applied to the polyclonally-stimulated bone marrow cultures from 3, 6, 9 and 12-month post-alloSCT from patient OX747 (Figure 4.13). As with the polyclonally-stimulated peripheral blood, most of the eight enriched clonotypes were not detected at any of the bone marrow timepoints. Clonotype 2 was consistently detected at a low frequency across all four timepoints, while Clonotype 6 was present from 6-12 months. In both cases, the previously observed TCRα to TCRβ frequency imbalance was maintained.

Taken together, these findings suggest that any approach aiming to identify GvL-reactive T cells will likely require pre-enrichment before functional screening.

Additionally, the persistence of Clonotypes 2 and 6 across multiple timepoints and both peripheral blood and bone marrow compartments strengthens the case for prioritising their functional validation in future assays.

4.8 Developing a Strategy for Functional Validation of METTL22-specific T cells

Having identified candidate METTL22-reactive TCR clonotypes through single-cell sequencing and characterised their clonal dynamics through bulk approaches, the next objective was to functionally validate their antigen specificity. This step is essential to confirm that these TCRs are not merely present within the activated IFNγ^+ fraction but were in fact directly responsible for METTL22 recognition.

Successful functional validation required three key components: firstly, the generation of transgenic T cells expressing our clonotypes of interest. Secondly, the identification of appropriate target cells which would be able to present METTL22 in the context of the correct restricting HLA. Finally, the development of a robust and sensitive *in vitro* activation assay.

As it was not logistically feasible to simultaneously test all eight clonotypes identified in the IFNγ^+ single-cell fraction, three clonotypes were selected for validation. In the context of the prior data, Clonotypes 1 and 5 were prioritised based on their exclusive localisation within the transcriptionally-defined activated cytotoxic CD4$^+$ cluster and their complete absence from the IFNγ^- fraction. Clonotype 2 was chosen not only as the second most frequent clone, but due to its repeated detection across multiple post-alloSCT bone marrow and peripheral blood samples, suggesting sustained *in vivo* relevance.

The generation of transgenic T cells was performed using a lentiviral transduction strategy. Briefly, a recombinant pHRSin lentiviral transfer plasmid encoding the codon-optimised METTL22-specific TCRα and TCRβ chains was synthesised as outlined in section 2.11, and all constructs were sequence-confirmed prior to

use. Murine constant regions were utilised in order to minimise mispairing with endogenous TCR chains and to facilitate downstream detection using antibodies against the murine TCRβ [258].

Lentivirus was generated via transient transfection of HEK 293T cells with the pHRSin transfer construct and associated packaging plasmids. Viral supernatant was harvested and used to transduce activated PBMCs from healthy donors, with spinoculation performed onto RetroNectin-bound virus to enhance transduction efficiency (Figure 4.14). Following transduction, cells were expanded and subsequently sorted for mTCRβ expression to generate a high-purity transgenic T cell population for functional testing.

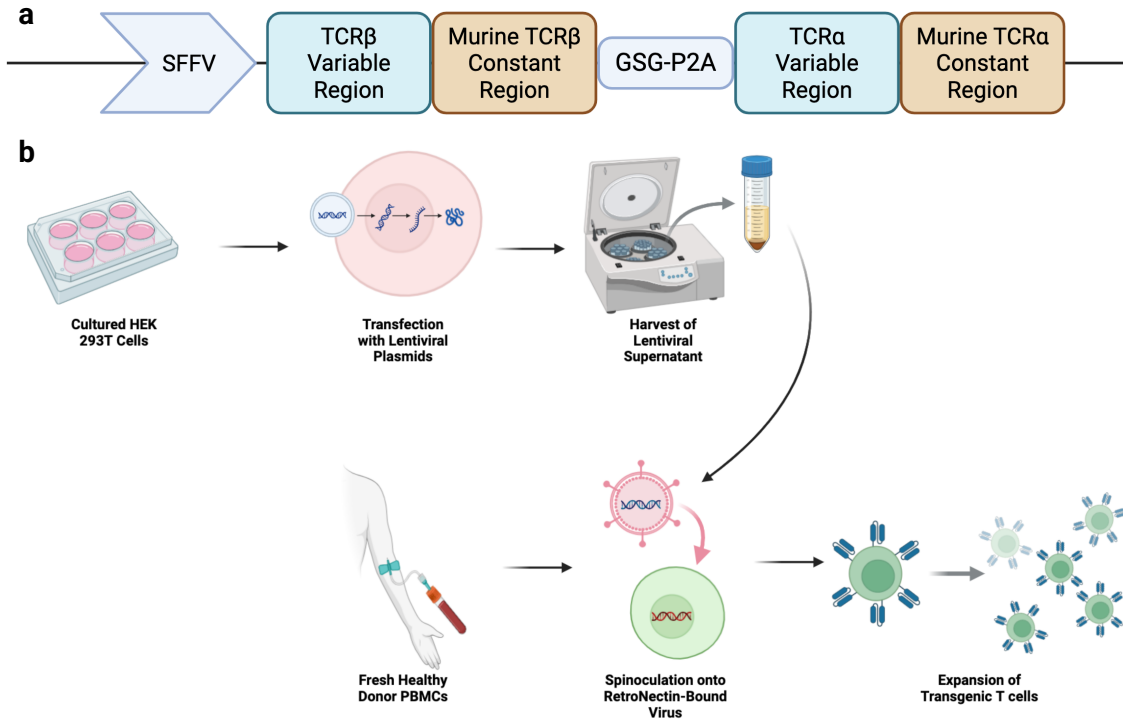

Figure 4.14: Generation of METTL22 TCR transduced T cells. a. Outline of TCR insert within pHRSin Lentiviral plasmid. Full plasmid map available in appendix (Figure B.3). **b.** Simplified experimental schema showing method for generating TCR transgenic T cells.

Determining the restricting HLA allele was essential for the selection of a suitable target cell population for co-culture. METTL22-1 and METTL22-2 peptides were

designed as 20-mer peptides, with the donor incorporating a variant non-synonymous A to T substitution (Figure 4.15).

The predominance of $CD4^+$ cells in the activated IFNγ-secreting fraction during IFNγ-Catch assay suggested class II HLA restriction. Additionally, prior experimental data during the initial use of the GvL pipeline by Connor Sweeney included dedicated functional HLA-blocking studies during IFNγ ELISpot of cultured peripheral blood from late post-alloSCT (Figure 4.15b).

a

Peptide	"Patient" Amino Acid Sequence (Reference)	"Donor" Amino Acid Sequence (Variant)
METTL22-1	LELGAGTGL**A**SIIAATMART	LELGAGTGL**T**SIIAATMART
METTL22-2	AGTGL**A**SIIAATMARTVYCT	AGTGL**T**SIIAATMARTVYCT

b

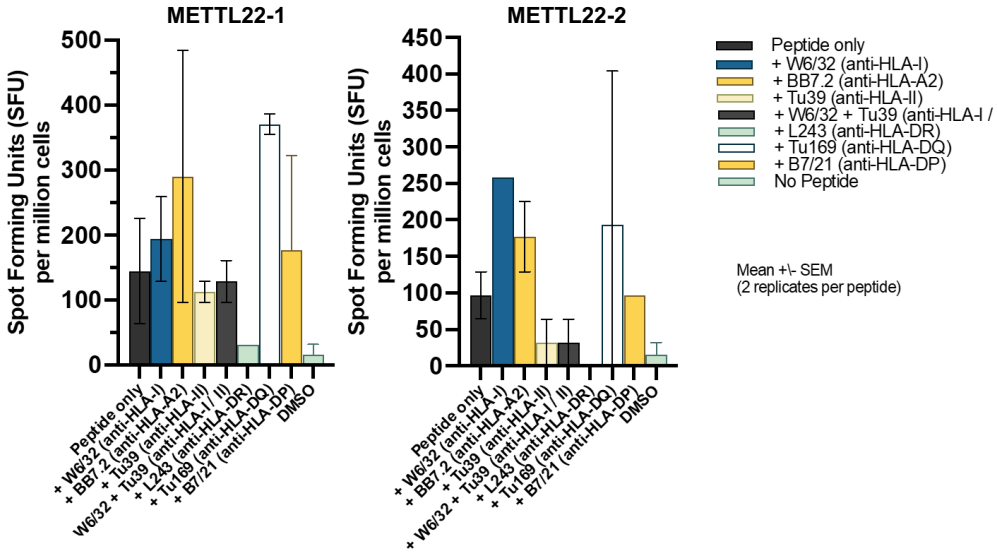

Figure 4.15: Previous HLA restriction studies of METTL22-specific responses in patient OX747. a. Description of METTL22-1 and METTL22-2 20-mer peptides derived from the "patient" and "donor" variants. Amino acid substitutions distinguishing the two sequences are highlighted in red. **b.** HLA-blocking studies performed during IFNγ ELISpot of cultured peripheral blood from patient OX747, stimulated by either METTL22-1 or METTL22-2. Bars represent mean spot forming units with the standard error. The DMSO condition is an unstimulated condition with no METTL22 peptide and no antibody blockade. *Data and figure generated by Connor Sweeney* [198].

Antibody-mediated blockade of HLA-DR resulted in the abrogation of positive responses to both METTL22-1 and METTL22-2. In contrast, blockade of HLA-I, HLA-DQ or HLA-DP had no effect. Interestingly, pan-HLA-II blockade, either alone or in combination with HLA-I blockade, was sufficient to repress responses to

METTL22-2, but not METTL22-1. This discrepancy is likely attributable to the higher levels of activation seen consistently with METTL22-1 and the comparatively reduced efficacy of the pan-HLA-II antibody Tu39 relative to the HLA-DR-specific antibody L243. Taken together, these findings strongly supported an HLA-DR-restricted presentation of METTL22.

To narrow down the specific restricting HLA-DR allele, patient and donor HLA-types were compared (Figure 4.16a). Patient OX747 received a haploidentical alloSCT transplant and had established 100% donor chimerism at all sampled timepoints. As the METTL22-specific response was detected via peptide-pulsed haematopoietic cells, it is reasonable to assume that antigen presentation occurred in the context of donor-derived HLA class II. The full complement of donor HLA-DR alleles included DRB1*04:04, DRB1*15:01, DRB4*01:03 and DRB5*01:01. Of these, only DRB1*04:04 and DRB4*01:03 were shared between donor and patient and therefore be capable of acting as clinically relevant presenting HLA on the surface of the patient's AML to mediate GvL.

To further refine the likely restricting allele, two independent *in silico* HLA class II binding prediction tools, MixMHC2pred and NetMHCIIpan, were utilised (Figure 4.16b). Sliding 15-mer frames from the METTL22-1 sequence were assessed against all donor HLA-DR alleles. The percentile rank score (% Rank Score) was used as the primary output metric, with conventional thresholds defining strong binders as having a %Rank Score of <2% and weak binders as <10%.

Neither algorithm predicted strong binding of any 15-mer to any allele. MixMHC2pred predicted weak binding to DRB1*04:04, DRB1*15:01 and DRB5*01:01, while NetMHCIIpan predicted only DRB5*01:01 as a weak binder.

Though both tools did agree that the GTGLASIIAATMART 15-mer peptide was the most likely presented fragment, the predictions across algorithms were only partially concordant, with no clear single HLA-DR proving to be the likely restricting allele.

a

Locus	Patient		Donor	
	First Allele	Second Allele	First Allele	Second Allele
HLA-A	*01:01:01:01		*31:01:02	*01:01:01:01
HLA-B	*51:01:01	*40:01	*51:01:01	
HLA-C	*03:04:01	*06:02:01	*15:02/10/62	*06:02/83/70/30
HLA-DRB1	*04:04:01	*13:02:01	*04:04:01	*15:01
HLA-DRB3	*03:01			
HLA-DRB4	*01:03		*01:03	
HLA-DRB5			*01:01:01	
HLA-DQB1	*03:02:01	*06:04:01	*06:02:01	*03:02:01
HLA-DPB1	*10:01	*03:01:01/*104:01	*10:01	*04:01:01

b

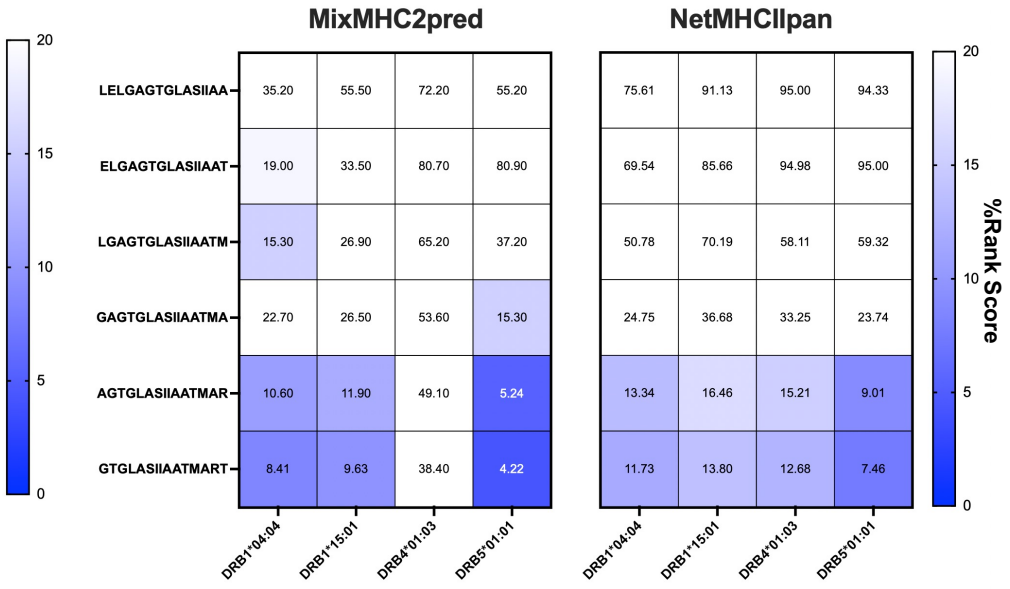

Figure 4.16: ***In silico*** **assessment of patient-specific METTL22 peptide presentation.** **a.** HLA typing of both patient and donor. HLA loci not listed are not routinely typed in clinical practice. Absent alleles are shaded in grey and shared alleles in green. **b.** Heatmaps showing predicted HLA class II binding of overlapping 15-mer peptides derived from the METTL22-1 sequence, using MixMHC2pred v2.0.2 and NetMHCIIpan 4.0. Values indicate the %Rank score (lower = stronger predicted binding) for each peptide-HLA combination.

These inconsistencies are reflective of the known limitations in HLA class II binding predictions, which include variability in the alignment of a peptide's binding register, a lack of model training data and the inherent promiscuity of the open class II binding groove. Given the equivocal nature of these computational results and the potential for underrepresentation of minor histocompatibility antigens in model training datasets, the decision was made to not rely on these algorithms for allele selection. Instead, an inclusive approach was adopted that would functionally

screen all donor-derived HLA-DR alleles as candidates.

Several strategies were considered for achieving comprehensive HLA-DR coverage. One option was to use single-HLA-expressing cell lines, which would allow for the unambiguous determination of HLA-restriction [259]. This approach however, would require parallel testing with four separate target cell lines, and was considered logistically infeasible.

A second possibility was to leverage existing HLA-typed cell lines that coincidentally expressed the donor HLA-DR alleles of interest. In practice, however, the limited availability of class II HLA-typed cell lines in public repositories, in conjunction with the promiscuity of peptide-HLA class II binding, made this approach unreliable [260].

Ultimately, autologous patient material was selected as the optimal target cell source. This strategy would ensure expression of all relevant HLA-DR alleles without the inclusion of any irrelevant alleles. Ethical constraints precluded the immortalisation of patient samples, such as through the generation of EBV-transformed lymphoblastoid cell lines, and *in vitro* expansion of cryopreserved patient PBMCs was therefore undertaken to generate a pool of target cells for functional screening.

Finally, to optimise conditions for a robust activation assay, a validated PADI4-specific TCR was employed in conjunction with healthy donor PBMCs expressing the relevant restricting allele, HLA-DPB1*04:01. This system provided a well-characterised positive control with which to assess our culture parameters and readouts, prior to testing the METTL22-specific TCRs. A 9-hour co-culture duration was selected to capture early activation whilst limiting non-specific activation and delayed marker downregulation.

Following co-culture, activation of transduced T cells, defined by mTCRβ expression, was assessed by flow cytometry using a panel of eight activation-induced markers: 4-1BB, CD40L, CD107a/b, OX40, CD25, CD69, IFNγ and PD-L1 (Figure 4.17.

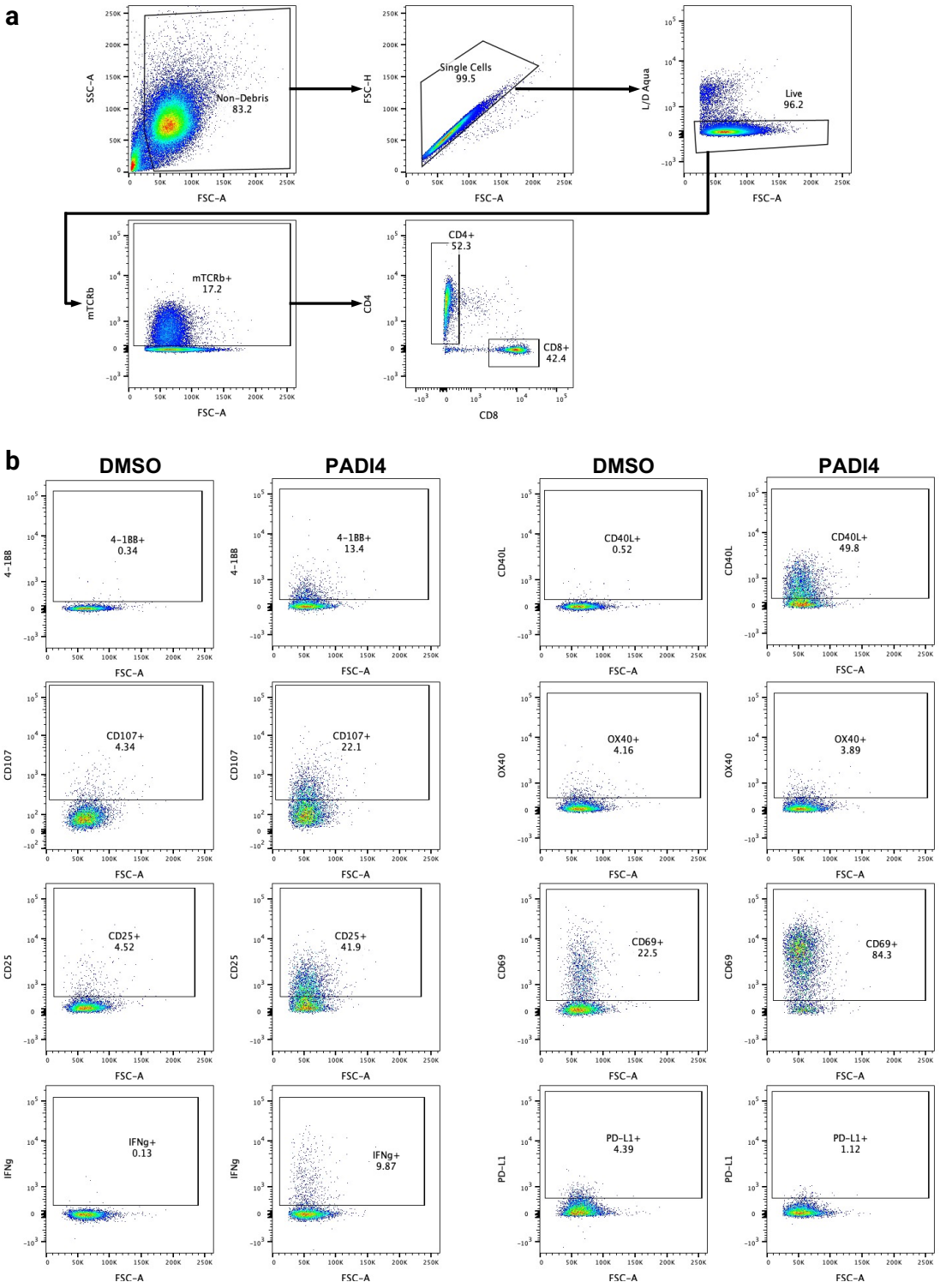

Figure 4.17: Optimising a T cell activation assay utilising PADI4-specific transgenic T cells. a. Gating strategy for the identification of live transgenic $CD4^+$ and $CD8^+$ T cells during a 9-hour co-culture activation assay. Transduced T cells are identifiable through fluorescent staining of the murine TCRβ constant chain. **b.** Flow cytometry plots for transgenic $CD4^+$ cells gated as above. Each column represents either cells stimulated with either DMSO or PADI4 peptide respectively. Positive gates set based on DMSO controls.

Of these markers, OX40 and PD-L1 were not appreciably upregulated compared to background at this timepoint, consistent with prior reports showing that expression of these markers typically peaks beyond 24 hours post-stimulation [261, 262]. These markers were therefore not taken forward in future experimentation.

Although CD69 was clearly upregulated in response to PADI4, its high baseline expression in DMSO controls complicates interpretation. In $CD4^+$, $mTCR\beta^+$ cells, CD69 expression increased from a background level of 22.5% to 84.3% upon stimulation with PADI4. However, $CD8^+$, $mTCR\beta^+$ cells exhibited a higher baseline of CD69 expression of 46.7%, consistent with CD69 classically being more expressed within the $CD8^+$ subset. It is unclear why the background level of CD69 expression is so high, but this may in part reflect residual activation from the transduction process, which involves potent stimulation via anti-CD3 and anti-CD28 during T cell expansion.

With these considerations, 4-1BB, CD40L, CD107a/b, CD25 and IFNγ were selected as the most robust and interpretable readouts for downstream functional validation of METTL22-specific TCRs.

4.9 Functional Validation of Putative METTL22-specific TCRs

Following the development of a strategy for TCR validation, this approach was applied to the three candidate clonotypes that were identified in previous analyses: Clonotypes 1, 2 and 5. Each clonotype was individually expressed in transgenic T cells generated via lentiviral transduction of healthy donor PBMCs. In parallel, cryopreserved PBMCs from patient OX747 were thawed and expanded for use as target cells (Figure 4.18a).

These target cells were then pulsed with either patient-derived METTL22-1 and METTL22-2 peptides in combination, or the equivalent donor-derived variants. T cell activation was assessed as previously outlined in section 4.8, utilising multiparametric flow cytometry following a 9-hour co-culture period.

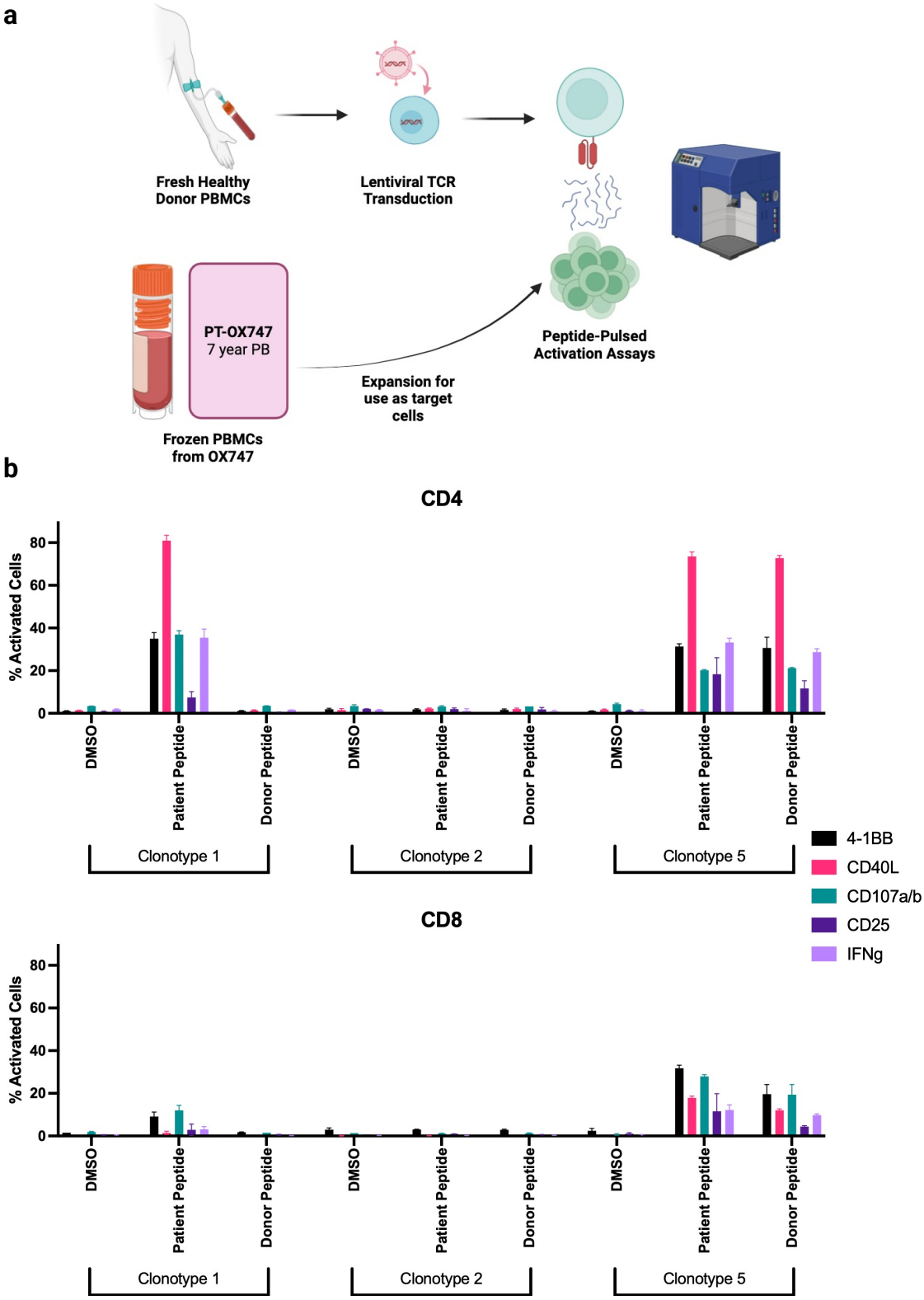

Figure 4.18: T cells transduced with Clonotype 1 and 5 activate in response to METTL22 peptide. a. Experimental schema for functional validation of METTL22-specific T cells. **b.** Summary of flow cytometry data assessing activation of mTCRβ$^+$ transgenic T cells following 9-hour co-culture with target cells from patient OX747, pulsed with either patient or donor METTL22 peptides respectively. CD4$^+$ and CD8$^+$ cells are displayed separately. Each coloured bar represents a single activation marker.

This allowed for a direct evaluation of antigen specificity and functional competence for each clonotype, with a particular emphasis on distinguishing recognition of patient-specific METTL22 peptides, which would be presented by the patient's AML, rather than the recognition of shared donor sequences.

Of the three clonotypes tested, Clonotype 1 was the only one to exhibit specific activation in response to patient-derived METTL22 peptides (Figure 4.18b). In response to patient METTL22, $CD4^+$ T cells from Clonotype 1 demonstrated clear upregulation of all five activation markers 4-1BB, CD40L, CD107a/b, CD25 and IFNγ. In contrast, no appreciable activation was observed in response to the donor peptides, with levels comparable to the DMSO control, confirming strict specificity for the patient variant.

Activation was largely limited to $CD4^+$ T cells, with $CD8^+$ T cells showing only modest upregulation of activation markers in response to patient peptide. While reduced expression of CD40L and CD25 would be expected in $CD8^+$ cells, the similarly low levels of CD8-associated markers such as 4-1BB and CD107a/b suggest the importance of the CD4 co-receptor in facilitating efficient TCR signalling in this context. These findings are consistent with both the increased activation of $CD4^+$ cells seen at IFNγ-Catch and the transcriptional identity of Clonotype 1 as mapping on to an activated cytotoxic $CD4^+$ subset.

Clonotype 5, which was within the activated cytotoxic $CD4^+$ cluster, exhibited clear activation toward METTL22-derived peptides. However, in contrast to Clonotype 1, this activation occurred in response to both patient- and donor-derived METTL22 peptides, with no appreciable difference in magnitude between conditions.

As before, activation in $CD4^+$ T cells was greater than in $CD8^+$ T cells, but this disparity was less marked here than in Clonotype 1.

The lack of allelic discrimination for Clonotype 5 suggests that the polymorphism that distinguishes the patient and donor METTL22 peptide does not discernibly affect TCR recognition.

Given that the target cells were derived from post-transplant patient PBMCs under conditions of confirmed 100% donor chimerism, all HLA molecules presenting in this assay were donor derived. The observed dual reactivity can therefore not be explained by allorecognition arising from HLA mismatches. This data instead suggests that Clonotype 5 recognises a self-antigen, raising questions regarding the physiological relevance and validity of this response.

One possible explanation is that the METTL22 peptide recognised by Clonotype 5 is not naturally processed and presented *in vivo*. The initial selection of peptides utilised *in silico* HLA-binding predictions which did not incorporate features of antigen processing, intracellular localisation or proteasomal cleavage. It is therefore entirely possible that the identified 20-mer peptide is not endogenously presented at the cell surface, and that Clonotype 5's reactivity reflects engagement with an artefactual epitope that is not encountered under physiological conditions.

An alternative explanation is that Clonotype 5 does recognise a self-antigen, but in a manner that is physiologically tolerated *in vivo*, such as due to mechanisms of peripheral tolerance or insufficient co-stimulation. In contrast, the *in vitro* conditions used for lentiviral transduction and activation include a number of stimulants that may artificially lower the activation threshold. Under such permissive conditions, self-reactive TCRs that would ordinarily remain quiescent could exhibit overt activation. Additionally, the concentration of peptide used in this assay (2µg/ml, or 1.04 nmol), likely exceeds physiological levels, potentially enabling activation that would not occur during endogenous antigen presentation. It is conceivable that lower concentrations could reveal selective recognition of the patient variant, although this interpretation remains speculative.

Finally, it is conceivable that Clonotype 5 was a previously naïve T cell *in vivo*, which acquired partial effector function over the course of the *in vitro* expansion protocol. This explanation, however, is less likely given the short culture duration of 12 days and the fact that cells were only subject to a single round of antigen-specific stimulation.

Despite its high clonal abundance and persistence across multiple post-alloSCT timepoints, Clonotype 2 failed to exhibit any detectable functional reactivity to METTL22 peptides in this assay system. Neither $CD4^+$ nor $CD8^+$ T cells showed appreciable upregulation of activation markers relative to the DMSO background, indicating a lack of peptide-specific activation.

The most likely explanation for this is that Clonotype 2 recognises an unrelated antigen, and that its original presence within the $IFN\gamma^+$ fraction during single-cell profiling reflects bystander activation, either within the original culture milieu or as a paracrine phenomenon during the IFNγ-Catch assay.

This highlights the importance of functionally validating candidate TCRs, particularly in the context of activation-based screening, non-specific labelling of bystander clones can lead to the identification of false-positives.

Additionally, Clonotype 2 was not enriched within the transcriptionally-defined activated cytotoxic $CD4^+$ cluster but instead mapped to a broader $CD4^+$ T cell population. This supports the added value of utilising gene expression to refine clonotype prioritisation and suggests that the phenotype of candidate TCR clonotypes may help discriminate true antigen-specific responses from non-specifically activated T cell populations.

Given these experimental findings, subsequent functional assays focused solely on Clonotype 1. To evaluate its antigen sensitivity, a peptide titration was next performed, spanning five orders of magnitude from 10^{-4} to 10 µg/ml (Figure 4.19a).

Clonotype 1 exhibited a dose-dependent activation profile in response to patient peptide, with detectable expression of activation markers at concentrations as low as 10^{-2} µg/ml. Among $CD4^+$ T cells, CD40L and IFNγ expression reached an apparent plateau at ≥1 µg/ml, while 4-1BB, CD107a/b and CD25 appeared to demonstrate continued dose responsiveness across the tested range. This differential pattern is consistent with the concept of graded TCR signalling thresholds, where different activation markers are induced at different levels of stimulation [263].

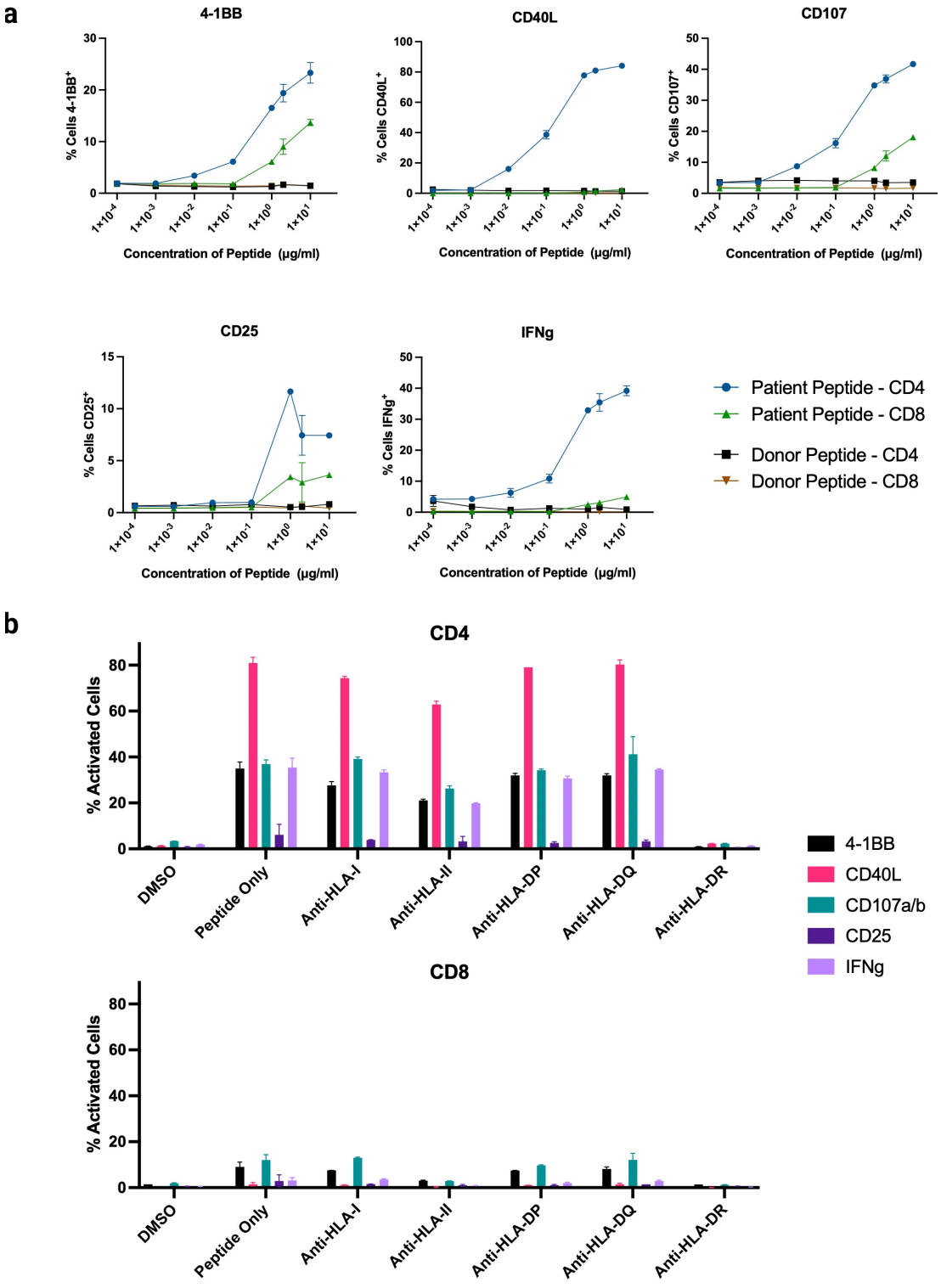

Figure 4.19: Peptide titration and HLA-blocking studies for Clonotype 1. a. Graphs demonstrating activation of mTCRβ$^+$ T cells following 9-hour co-culture with target cells from patient OX747 pulsed with varying concentrations of patient or donor METTL22 peptides. Each graph represents a single activation marker. **b.** Summary of HLA blocking studies. Prior to the 9-hour co-culture and activation assay, target cells were incubated with HLA-blocking antibodies for 2 hours, prior to being loaded with 2µg/ml of patient METTL22-1 and METTL22-2 peptides. The DMSO condition included neither HLA-blocking antibodies nor METTL22 peptides.

$CD8^+$ T cells showed lower overall levels of activation, consistent with earlier findings, but did display appreciable upregulation of classical $CD8^+$-associated markers 4-1BB and CD107a/b at higher peptide concentrations.

Importantly, no activation was observed in response to donor-derived METTL22 peptide at any tested concentration, further confirming that Clonotype 1 selectively recognises the patient-specific variant.

To confirm the HLA restriction of Clonotype 1, a panel of HLA-blocking antibodies was employed during the activation assay, where transgenic T cells were stimulated with patient-derived METTL22 peptides. Antibodies targeting pan-HLA-I, pan-HLA-II, HLA-DP, HLA-DQ and HLA-DR were tested individually, in addition to an unstimulated DMSO condition (Figure 4.19b).

Blockade of HLA-DR resulted in the complete abrogation of Clonotype 1 activation across all tested activation markers, indicating a strict requirement for HLA-DR-mediated antigen presentation. Though this is most visible in the $CD4^+$ T cell compartment, this is also the case for $CD8^+$ T cells, where the low levels of activation seen in other conditions falls to background levels.

Interestingly, blockade of pan-HLA-II did also appear to reduce activation, but it was substantially less effective than the HLA-DR specific antibody, consistent with prior reports of low efficacy of the Tu39 antibody in functional assays in section 4.8.

These findings reinforce the conclusion that Clonotype 1 is $CD4^+$ dependent, HLA-DR restricted and selectively reactive to the patient-specific METTL22 peptide variant.

4.10 End of Chapter Discussion

This chapter described the systematic application and evaluation of a polyclonally-stimulated culture combined with an IFNγ ELISpot assay for the detection of GvL responses post-alloSCT. Whilst the method was effective at expanding T cells from early post-transplant bone marrow samples, it failed to detect any antigen-specific

responses in either of the patients tested from the high-risk GvL-enriched cohort. This was the case even when testing peripheral blood from late post-alloSCT timepoints where known GvL responses had previously been detected.

In contrast, the previously established antigen-stimulated culture method successfully identified METTL22-specific responses in the peripheral blood of patient OX747. This led to the identification and subsequent functional validation of a $CD4^+$ TCR clonotype which was allele-restricted, patient-specific and HLA-DR-restricted.

Collectively, these comparative experiments clearly demonstrated that although the polyclonally-stimulated method yields a higher total number of $CD3^+$ cells, it lacks the sensitivity required to detect low-frequency, antigen-specific T cells. This is likely due to the proliferation of irrelevant bystander cells. This limitation was supported not only by the absence of functional responses in polyclonally-stimulated samples but by direct TCR repertoire analyses utilising bulk sequencing, where relevant clonotypes fell below the limit of detection following a polyclonal stimulation.

The ongoing inability to detect antigen-reactive clonotypes in the early post-alloSCT marrow highlights a challenging clinical and experimental context. This could reflect a true biological absence, technical limitations with the methods used in their detection, or both.

The early post-alloSCT period is complicated by ongoing immunosuppression and the delayed dynamics of immune reconstitution. Early T cell repopulation is dominated by the peripheral expansion of pre-existing memory cells, with delayed emergence of de novo thymic output and limited antigen-driven clonal selection in the first 12 months post-alloSCT, complicating efforts to isolate rare, antigen-specific GvL T cells during this window [227, 250].

There are also intrinsic limitations in the current approaches to isolate antigen-reactive T cells from the early post-alloSCT period. Given the apparent rarity of such cells, targeted enrichment is essential to raise them above the threshold of detection. However, our prior antigen-stimulated cultures were incompatible with

early post-alloSCT BM samples due to poor survival and proliferation post-thaw. Antigen-specific expansion remains essential, but would benefit from additional strategies such as cytokine modulation, feeder cell support or the use of professional antigen-presenting cells [264, 265].

Given the intent to screen hundreds of possible candidate peptides, approaches such as multimer-based screening remain logistically unfeasible. Alternate strategies, such as T cell library methods, which expand naïve T cells, are very sensitive but address a different question and do not capture the antigen-experienced populations most relevant to the early post-alloSCT setting [266].

Among the candidate peptides tested, METTL22 emerged as a putative minor histocompatibility antigen. METTL22 (Methyltransferase-Like 22) belongs to the diverse methyltransferase-like family of proteins. The 33 members of the vertebrate METTL family have a broad range of substrates and roles, but they all share a highly conserved seven-β-strand (7BS) catalytic domain [267]. METTL22 is a lysine methyltransferase which currently has one experimentally validated target to date, the DNA-binding protein Kin17 [268]. Methylation of Kin17 by METTL22 impairs the ability of Kin17 to bind to chromatin and therefore promotes its localisation in the cytoplasm.

Though little is known as to the targets and biological functions of METTL22, it has been implicated in the differentiation of embryonic stem cells (ESCs) to haematopoietic stem cells (HSCs). Knockdown of METTL22 in zebrafish has been shown to reduce the expression of *Runx1* and *c-myb* during HSC development, key transcription factors in HSC emergence. Knockdown of METTL22 in human umbilical cord blood similarly resulted in a phenotypic reduction in HSC number [269].

However, for minor histocompatibility antigens, functional importance is not a prerequisite for immunogenicity. Immunological relevance instead depends on factors such as differential expression, the immunogenicity of the polymorphism between patient and donor, and the ability to undergo intracellular processing and

HLA presentation.

The identification of METTL22 as a candidate minor histocompatibility antigen and the validation of Clonotype 1 as a patient-specific TCR prompts broader reflection on the methods used for the identification and validation of potential GvL TCRs.

Though the use of IFNγ-Catch, cell sorting and single-cell sequencing was instrumental in isolating Clonotype 1, there are clear methodological limitations.

The detection of the functionally inert Clonotype 2, despite its high abundance and presence in the activated IFNγ$^+$ fraction, highlights the potential for artefactual capture of irrelevant T cells, underscoring the importance of robust downstream validation. Encouragingly, the integration of transcriptomic data with TCR clonotype, appears to be a good strategy for prioritising clonotypes for validation. The reactive Clonotypes 1 and 5 both were located within a transcriptomically distinct cluster of activated cytotoxic CD4$^+$ cells, suggesting that transcriptomic context may improve the predictive yield of functional screening.

Conversely, the detection of Clonotype 5, a TCR that was not specific for patient-derived METTL22, raises questions as to the physiological validity of the *in vitro* screening system given its apparent recognition of a potential self-antigen. The pipeline used to identify candidate GvL peptides does not account for antigen processing or presentation, and the activation assays rely on peptide-pulsed targets, lentivirally-transduced effectors and artificial co-culture conditions with activating cytokines and antibodies. While these conditions facilitate this initial screening, they may overestimate functional relevance and they should be considered a starting point for more stringent and physiologically representative validation.

It is also possible that the apparent dual reactivity of Clonotype 5 reflects a difference in sensitivity rather than true lack of specificity, with activation by the donor peptide occurring only at supraphysiological concentrations. If selective responses to the patient peptide were to occur at low or intermediate concentrations, the relevance of this TCR cannot be excluded outright.

Clonotype 1 was validated as an allele-specific, HLA-DR-restricted TCR in this experimental setting. Further studies could aim to define the exact restricting HLA-DR allele, such as through the use of cell lines engineered to express a single HLA [259]. If the restricting HLA allele is shared between patient and donor, this would support the physiological plausibility of this TCR's activity post-transplant.

Confirming that METTL22-derived peptides are naturally processed and presented is also critical. This would require the careful selection of appropriate target cells which co-express the relevant HLA-DR allele and the correct METTL22 SNP. Systems overexpressing METTL22 in appropriate cell lines, such as those used for the validation of the PADI4 TCR in section 1.10, could serve this purpose. Ideally, these experiments would then be extended to the original patient AML, though sample availability is very limited. AML immunopeptidomics may also provide supportive evidence, although such analyses are often limited by sensitivity [157].

The *in vitro* transcriptional phenotype of Clonotype 1 resembles that of a cytotoxic $CD4^+$ T cell, marked by the high expression of cytotoxic markers such as *GZMB*, *IFNG* and *PRF1*. While some of this phenotype may reflect culture conditions, particularly the effects of IL-2, cytotoxic $CD4^+$ T cells have been increasingly recognised in tumour immunity. Although their role in GvL responses post-alloSCT has still not been established, these findings raise the possibility that $CD4^+$ cytotoxicity may contribute to AML control in the post-transplant setting [254, 270, 271].

The widespread expression of METTL22 across haematopoietic and non-haematopoietic tissues, at both the mRNA and protein levels, raises potential concerns for off-target effects.

Clonotype 1 is, however, HLA-DR-restricted, and HLA class II molecules are generally restricted to APCs and haematopoietic cells in non-inflammatory settings. This may confer tissue specificity, even when targeting a widely expressed antigen, though the risk of on-target, off-tissue effects remains [194].

4. Applying Stimulated T Cell Culture for the Identification of GvL T Cells

Studies have shown that purified $CD4^+$ donor lymphocyte infusions can mediate GvL in the absence of GvHD, highlighting the crucial role of class II-restricted responses in the therapeutic setting [192].

It is certainly possible that Clonotype 1 could represent a shared GvL/GvHD response rather than a GvL-specific response and further work using non-haematopoietic target cells or *in vivo* models will be required to assess potential toxicity. Notably, clinical trials of miHA-targeted therapy have focused on class I-restricted antigens [40]. The METTL22 TCR therefore offers a potential avenue to extend GvL immunotherapy into the class II space.

In conclusion, these findings highlight both the promise and limitations of culture-based screening approaches for the identification of rare, antigen-specific T cells in the post-alloSCT setting. Despite the successful validation of a METTL22-specific TCR using these techniques, the failure of the polyclonally-stimulated culture to detect known responses in conjunction with TCR repertoire sequencing reveals a critical bottleneck in the detection of GvL responses in the patient setting. Without targeted enrichment, the relevant clonotypes remain below the threshold of detection, with frequencies $\leq 0.1\%$.

Overcoming this challenge will require orthogonal strategies that do not rely solely on bulk expansion and enhance sensitivity for low-frequency T cells. The following chapter explores these next steps, applying both modified culture systems and *ex vivo* approaches to interrogate these rare T cell responses in early post-transplant samples.

5

Alternative Approaches to Identify Post-AlloSCT Bone Marrow GvL T Cells

Contents

5.1 Overview

The early post-alloSCT bone marrow presents a particularly challenging setting for the detection of putative GvL T cell responses. Clonotypes of interest exist at extremely low frequencies, and conventional *in vitro* expansion strategies have been limited by poor cell survival and the non-specific proliferation of irrelevant clones. To address these challenges, this chapter investigates several complementary approaches to enhance the detection of GvL responses from the early post-alloSCT bone marrow.

First, modified *in vitro* culture systems were employed. These incorporated an antigen-specific stimulation in combination with either enhanced cytokine support or professional antigen-presenting cells. These adaptations aimed to support the selective expansion of low-frequency, antigen-reactive T cells and successfully enabled the re-identification of previously isolated GvL clonotypes.

In parallel, an orthogonal *ex vivo* single-cell approach was used to detect known GvL-associated clonotypes directly from primary patient bone marrow, without the effects of prior *in vitro* culture. This method leveraged a high-throughput platform to overcome the low frequency of target T cell populations. This enabled both the confirmation of *in vivo* persistence and true transcriptional phenotyping of these putative GvL T cells. While this approach was limited to the interrogation of pre-characterised TCRs, it provided critical insight into their presence and transcriptional profile in the *in vivo* setting.

5.2 Trialling Cytokine-Supported Protocols with Delayed Polyclonal Stimulation

To investigate whether alternative approaches in culture could simultaneously allow for the survival and enrichment of antigen-specific bone marrow-derived T cells, two complementary approaches were explored: firstly, the use of enhanced

cytokine regimens during antigen stimulation, and secondly, the use of a delayed polyclonal stimulation to act as a "rescue" to rapidly expand cells following an initial period of enrichment.

Three distinct cytokine-based culture strategies were tested over the course of the initial 10-day antigen-stimulation phase (Figure 5.1a). The CS method, used in previous experiments, served as a baseline. A second "polyclonal-like" condition utilised the same cytokines as the prior polyclonally-stimulated cultures (IL-2, IL-7 and IL-15), designed to support broad T cell survival and expansion. The third condition introduced sustained high-dose IL-2, adapted from protocols designed to expand antigen-specific T cells from tumour-infiltrating lymphocytes [264].

Four cryopreserved post-alloSCT bone marrow samples were selected for analysis (Figure 5.1b). Two samples (from patients OX717 and OX747) were from the high-risk GvL-enriched cohort who had previously exhibited T cell responses to predicted peptides. These patients were included to assess whether low-frequency, GvL-reactive clones could be selectively expanded using these approaches. However, given that these antigen-specific clones had not been empirically confirmed to be present in this context, the existence of reactive T cells within the starting cryopreserved sample could not be guaranteed.

The remaining two samples (OUH501 and OUH570) were selected based on previously documented IFNγ ELISpot responses to CEF/CEFTA viral peptides following a polyclonally-stimulated culture. These served as a functional control cohort where the presence of antigen-reactive cells could be guaranteed, albeit at a higher frequency than our target population. This therefore provided a means to assess whether any observed limitations with expanding the GvL-targeted cultures were attributable to methodological constraints rather than the intrinsic absence of antigen-specific cells.

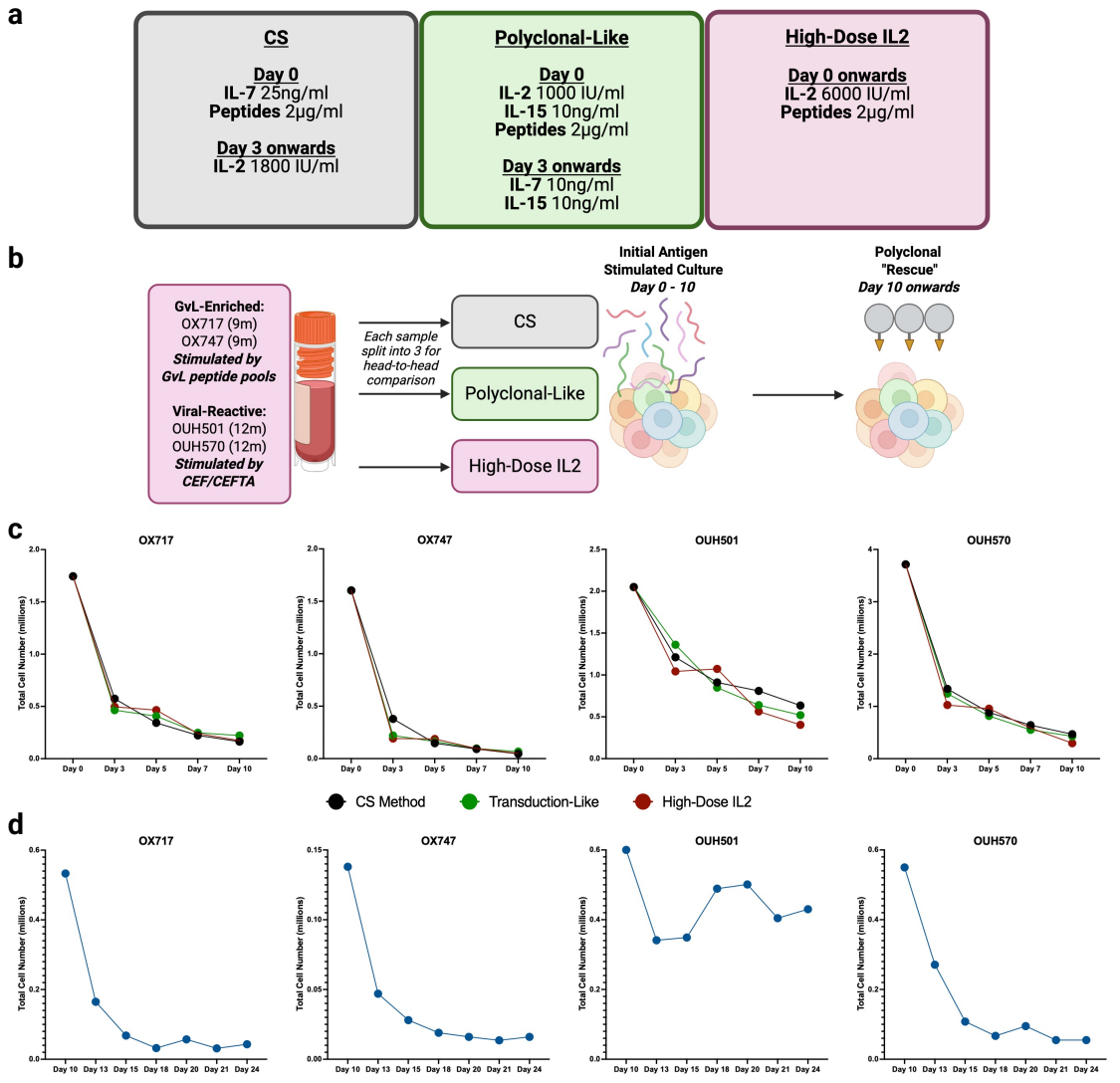

Figure 5.1: Alternative antigen-stimulated methods with a polyclonal "rescue" do not allow for expansion of early post-allograft bone marrow. a. Graphic outlining the three separate cytokine mixes for the initial antigen stimulated culture. **b.** Simplified experimental schema demonstrating samples used and workflow. "GvL Enriched" samples are from the high-risk cohort and are stimulated by their respective putative GvL peptide pools. "Viral-Reactive" samples are samples which have had a previous positive response to CEF/CEFTA at IFNγ ELIspot following a polyclonal expansion. Timepoint listed in brackets. **c.** Growth curves for the initial antigen-stimulated culture. Each graph is a sample, and each colour a condition. **d.** Growth curves for the subsequent polyclonal "rescue." Individual samples were pooled following the initial antigen-stimulated culture given low cell number.

Following stimulation with the relevant peptide pools under each of the three cytokine regimes, total cell counts were monitored over the 10-day period (Figure 5.1c). Across all samples and conditions, the total absolute cell number declined substantially over time. This trend was anticipated, given that the antigen-stimulated cultures are designed to selectively support the proliferation of antigen-specific T cells at the expense of non-specific T cells and non-T lymphoid populations, which would lack survival signals.

Importantly, no consistent differences in cell number were observed between the three cytokine regimens at this stage, indicating that none conferred a selective advantage under antigen-specific stimulation.

Unexpectedly, the kinetics of cell loss were comparable between the GvL-enriched and viral-reactive samples, despite prior evidence of robust, high-frequency viral responses in the latter. This observation suggests that even relatively abundant antigen-specific T cells within the post-alloSCT bone marrow may fail to appreciably proliferate under these early culture conditions, or remain present at such low absolute numbers that minor proliferative increases do not translate into a discernible change in overall culture growth.

Given the low cell yields from each of the three cytokine regimens, conditions were pooled by patient prior to the polyclonal "rescue" with CD3/CD28 stimulation (Figure 5.1d). This step aimed to assess whether a stronger polyclonal stimulus could recover proliferative capacity following a period of antigen-specific priming, during which antigen-reactive T cells would, in theory, have been selectively enriched relative to the total culture.

Polyclonal stimulation resulted in modest proliferative recovery in only one sample, OUH501. However, even in this case, total cell numbers did not exceed the original input over the subsequent two-week culture period. The remaining three samples showed a continual and progressive decline in cell counts, indicating that the delayed polyclonal stimulation was insufficient to restore T cell expansion in

this phase.

Taken together, these findings demonstrate that neither alternative cytokine support nor a delayed polyclonal stimulation is sufficient to drive meaningful expansion of bone marrow-derived T cells from post-alloSCT patients.

The inclusion of viral-reactive samples, where antigen-specific T cells are known to be present, further supports the interpretation that this is a generalised impairment of the post-transplant T cell compartment, requiring alternate strategies for their survival and expansion.

5.3 Utilising a Joint APC-T cell Culture Method on the GvL-Enriched Cohort

A joint APC-T cell co-culture method, adapted from a PBMC culturing method from the Bhardwaj laboratory, was subsequently applied to a sample from the GvL-enriched cohort [265]. This method was developed and optimised by Maria Barbanti for use with early post-alloSCT bone marrow samples, and as such data regarding its validation and optimisation is not presented here. This approach combined staged cytokine support and adjuvant stimulation to first promote the maturation of professional antigen-presenting cells prior to T cell-directed stimulation with peptide antigens and pro-survival cytokines (Figure 5.2a).

This approach was applied to a BMMNC sample obtained 12 months post-alloSCT from patient OX885 (Figure 5.2b). This patient had previously been identified as harbouring two putative GvL T cell responses targeting peptides in GSTZ1 and WASHC4, as detected in peripheral blood samples taken at 4 years post-alloSCT.

During the 27-day culture period, an initial contraction in total cell number was observed, followed by a delayed expansion commencing at approximately 3 weeks (Figure 5.2c). Relative to other applications of this protocol, this represented a delay of approximately 7 days in the onset of proliferation, potentially reflecting

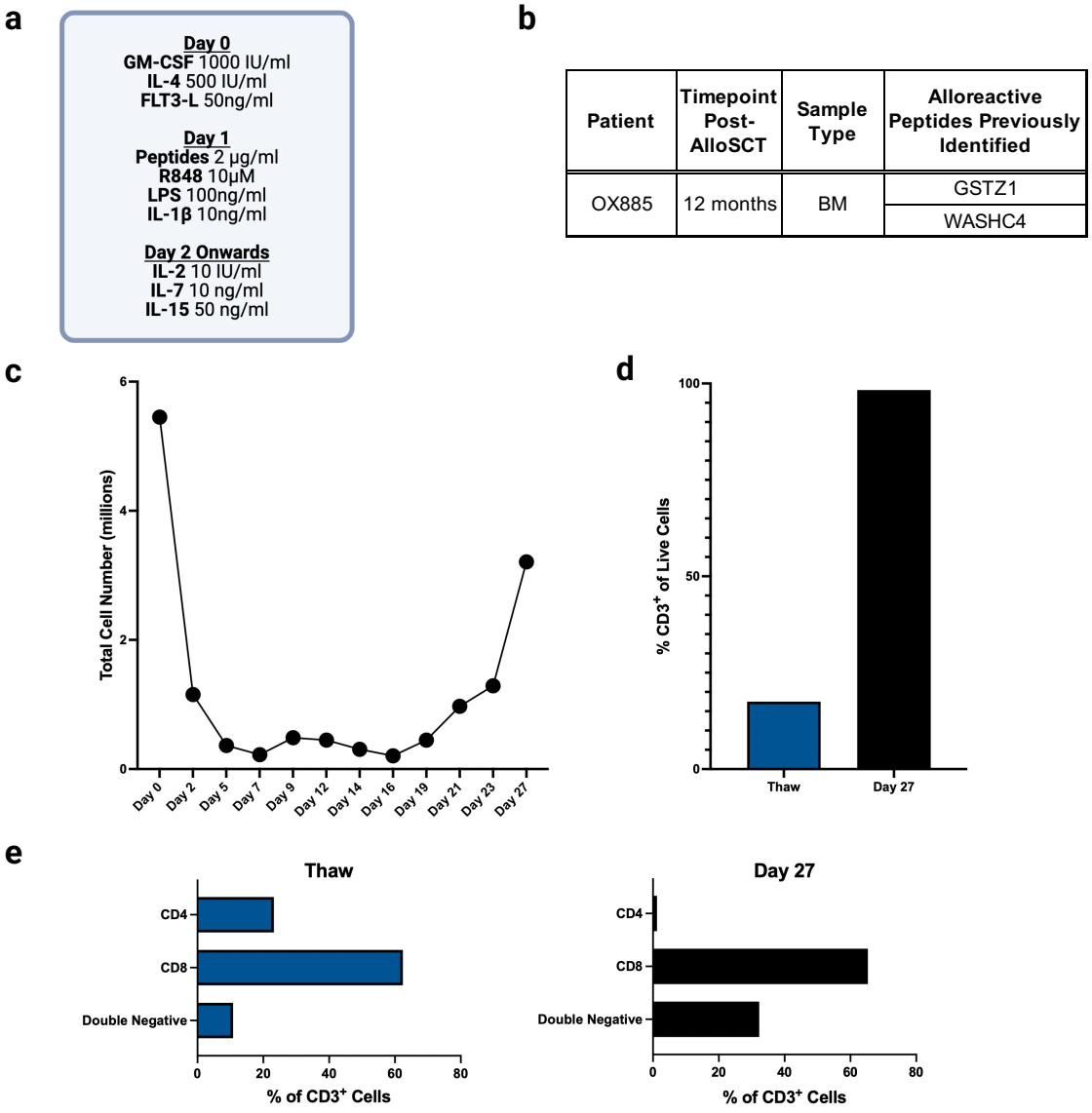

Figure 5.2: A joint APC-T cell culture method allows for the expansion of early post-alloSCT BMMNCs from patient OX885. a. Graphic describing cytokines and stimulants used in joint APC-T cell culture method. **b.** Characteristics of sample tested. **c.** Growth curve demonstrating absolute cell count over course of culture period. **d.** Description of $CD3^{+}$% as a proportion of all live cells assessed by flow cytometry at thaw and end of culture period. d. Phenotypic distribution of $CD3^{+}$ T cells based on CD4 and CD8 expression assessed at flow cytometry. GM-CSF = Granulocyte-monocyte colony stimulating factor. FLT3-L = FMS-like tyrosine kinase 3 ligand. R848 = Resiquimod. LPS = Lipopolysaccharide. IL-1β = Interleukin-1β

a comparatively lower starting frequency of antigen-specific T cells, requiring a prolonged expansion to reach detectable levels.

Flow cytometric analysis demonstrated a substantial enrichment of $CD3^+$ T cells, increasing from 18% at thaw to 98.3% of live cells by day 27, indicating successful expansion of the T cell compartment from the early post-alloSCT marrow utilising this method (Figure 5.2d). Interestingly, the proportions of $CD4^+$, $CD8^+$ and double-negative T cells shifted markedly over the course of the culture. This shift was not observed in four prior applications of this culture system performed by Maria Barbanti (not shown), but may reflect CD4 downregulation in the context of chronic activation or alternatively, the preferential expansion of unconventional T cell subsets [252]. The application of single-cell gene expression analysis in downstream experimentation does, however, provide a means to clarify the identity of these populations.

At the end of the culture period, cells were restimulated with DMSO, GSTZ1 or WASHC4 peptide to assess antigen-specific activation. Rather than relying on cytokine-secretion assays such as the IFNγ-Catch, activated $CD3^+$ cells were identified and sorted based on the expression of CD40L and 4-1BB (Figure 5.3). This combination was chosen on the basis of previous optimisation experiments (performed by Maria Barbanti, data not shown), which identified these markers as optimal for detecting early activation across both $CD4^+$ and $CD8^+$ subsets. To enhance activation, the stimulation assay included co-stimulatory antibodies against CD28 and CD49d. A key limitation of this assay, however, is the degree of background activation observed in the absence of peptide. In the DMSO control, 1.86% of $CD3^+$ cells fell within the $CD40L^+$ and $4\text{-}1BB^+$ activation gate. Peptide-stimulated conditions yielded only marginally higher frequencies, with 1.98% for GSTZ1 and 1.91% for WASHC4. Although downstream single-cell TCR sequencing enables the exclusion of non-specifically activated clonotypes, the modest differences from background observed at the flow cytometry level present challenges when attempting to screen multiple samples or multiple peptides.

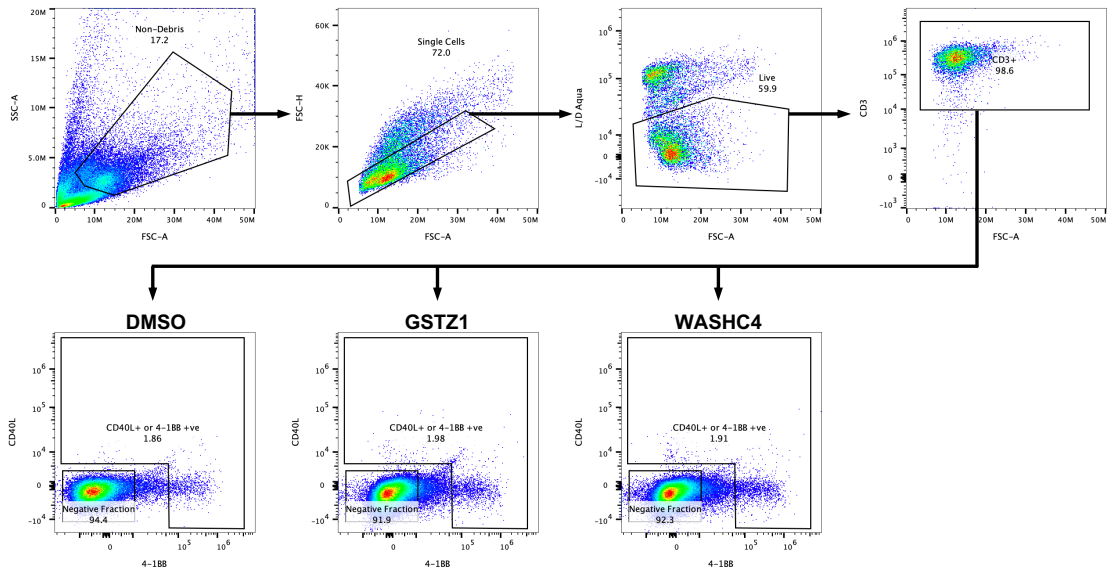

Figure 5.3: Gating strategy for activation-induced marker based sorting of OX885. Example flow plots demonstrating gating strategy used in the sorting of activated cells based on expression of CD40L and 4-1BB. The CD3 gate was set broadly to capture activated cells in which CD3 expression is downregulated. The second row demonstrates three separate conditions, where each condition was stimulated by DMSO (negative control), GSTZ1 peptide or WASHC4 peptide.

To overcome the limitations imposed by background activation and to definitively identify antigen-specific T cell clonotypes, single-cell TCR and gene expression sequencing was performed on sorted $CD3^+$ cells that were $CD40L^+$ or $4\text{-}1BB^+$ from each peptide-stimulated condition.

Background clonotypes, interpreted as reflecting non-specifically activated or bystander cells, were defined based on recurrence across multiple activated fractions, their presence in the activated DMSO-stimulated fraction or their enrichment within non-activated fractions.

Following the exclusion of these background clonotypes, a single dominant clonotype remained within the GSTZ1-stimulated activated fraction, designated as GSTZ1-Clone 1 (Figure 5.4a). This clonotype accounted for 33.7% of the activated cell population.

Notably, GSTZ1-Clone 1 was identical at the nucleotide level to a previously characterised GSTZ1-reactive TCR clonotype detected in peripheral blood from the same patient at 4 years post-alloSCT (Figure 5.4b). GSTZ1-Clone 1 was

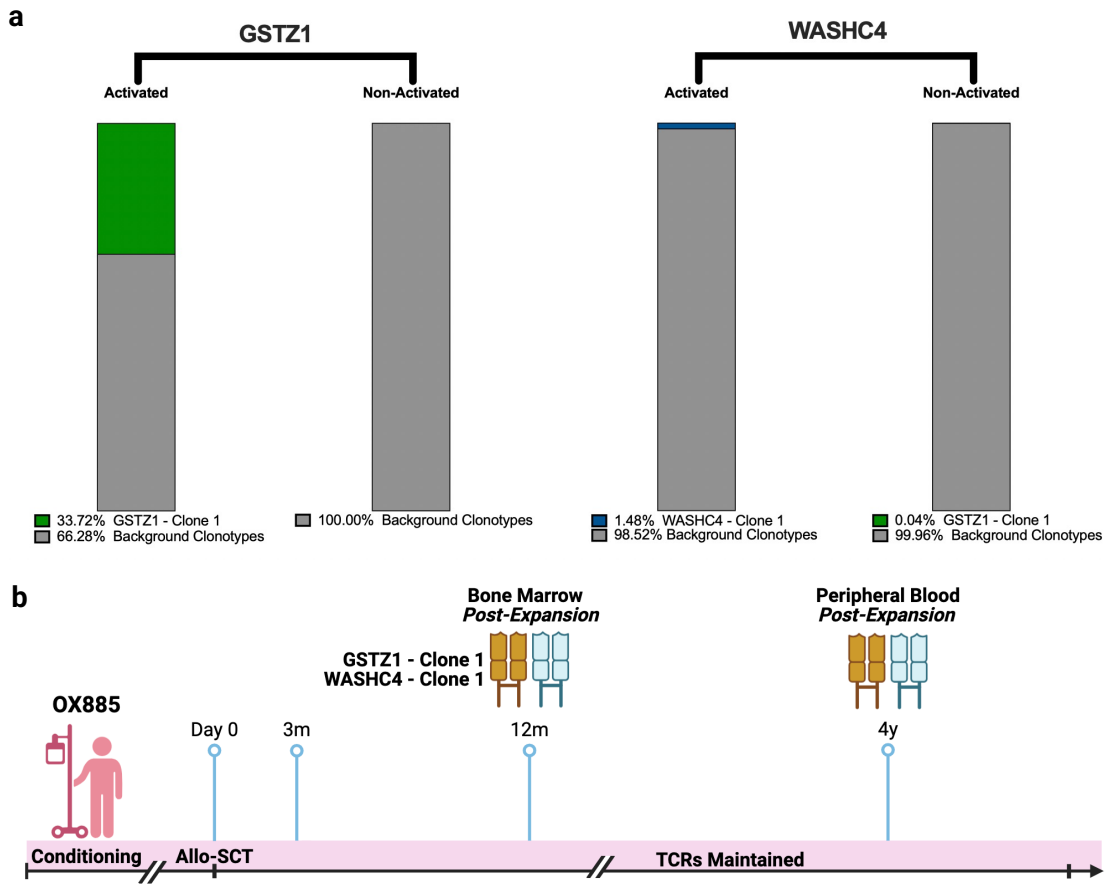

Figure 5.4: The same GSTZ1 and WASHC4-reactive TCR clonotypes are detected in the early bone marrow and late peripheral blood of patient OX885. **a.** Single cell TCR repertoire analysis of activated and non-activated fractions stimulated by GSTZ1 and WASHC4. GSTZ1 Clone 1 and WASHC4 Clone 1 are both TCR clonotypes that were previously identified in the late peripheral blood of patient OX885. Background clonotypes represent a combination of low frequency clonotypes and non-specifically activated clonotypes shared across multiple activated fractions. **b.** Visual schematic outlining timepoints and methods by which the same TCR clonotypes were identified in patient OX885.

also detected at a low frequency (0.04%) within the non-activated fraction of the WASHC4-stimulated condition, consistent with its baseline prevalence in the culture milieu. Its lack of enrichment in the WASHC4-activated fraction supports the specificity of its response to GSTZ1.

This analysis was repeated for the WASHC4-stimulated activated fraction. Similarly, a single non-background clonotype was identified, designated as WASHC4-Clone 1, which accounted for 1.48% of the activated $CD3^+$ population. This

clonotype also exactly matched a previously characterised WASHC4-reactive TCR from the peripheral blood at 4 years post-alloSCT.

The identification of these two antigen-specific clonotypes, each matching previously characterised peripheral blood TCRs, highlights two key principles. Firstly, their presence in the bone marrow at 1 year post-alloSCT demonstrates their early post-transplant establishment. Secondly, the persistence of these clonotypes over at least a three-year period supports their potential physiological relevance with implications for long-term antigen-specific immune surveillance.

To characterise the phenotypic identity of the GSTZ1- and WASHC4-reactive T cell clonotypes, single-cell gene expression data from all sorted populations were jointly analysed and visualised using UMAP embedding following unsupervised clustering with the Leiden algorithm (Figure 5.5a). T cell identities were subsequently assigned using CellTypist without majority calling, resulting in per-cell annotation across clusters.

The dataset comprised a number of transcriptionally distinct T cell subsets, including CD8$^+$ T_{EM}/T_{EMRA} cells, CD8$^+$ $T_{Naïve}$/T_{CM} cells, cycling T cells and γδ T cells. Additional minor and transitional populations with limited cell numbers were aggregated into a general "Other" category.

To validate the robustness of these automated annotations, the expression of a curated panel of T cell identity and effector genes was visualised across the annotated subsets (Figure 5.5b).

This analysis confirmed expected expression patterns across subsets. *CD4*, *TBX21*, *IFNG* and *IL12RB2* were enriched in the type 1 helper T cell cluster. The CD8$^+$ $T_{Naïve}$/T_{CM} cluster showed high expression of homing and stemness-associated genes including *CCR7*, *SELL*, *LEF1* and *TCF7*, whereas CD8$^+$ T_{EM}/T_{EMRA} cells were enriched for cytotoxic effector genes *GZMB*, *PRF1* and *GNLY* along with cytotoxic regulator *NKG7*. Cycling T cells were marked by proliferative markers *PCNA* and *MKI67* and the remaining large subset, γδ T cells, was marked by

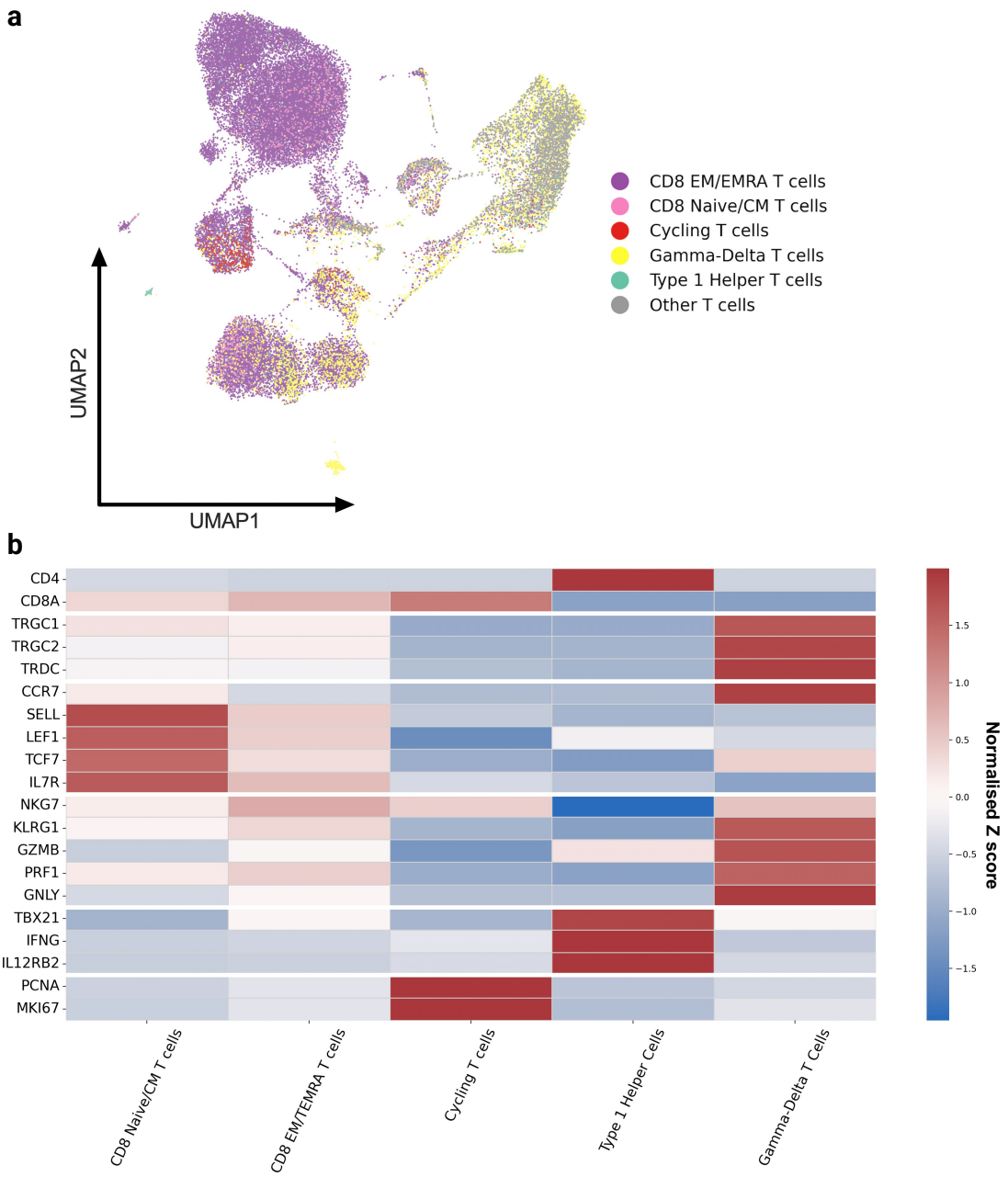

Figure 5.5: Single cell transcriptomics for all sorted T cells from patient OX885. **a.** UMAP plot of gene expression following Leiden clustering from all FACS-sorted populations from patient OX885 (GSTZ1-activated, GSTZ1-non-activated, WASHC4-activated, WASHC4-non-activated). $n = 32003$. Cell annotation performed on a per-cell basis, utilising CellTypist without majority calling. *b.* Heatmap showing the scaled gene expression of selected genes across the annotated T cell subsets. Gene expression values are normalised and presented as Z scores.

strong expression of TCR constant genes *TRGC1*, *TRGC2* and *TRDC* along with cytotoxic effectors.

These single-cell annotations align with the earlier flow cytometric findings of $CD4^+$ T cell depletion with a corresponding increase in the double-negative fraction. These double-negative T cells are shown here to be transcriptionally consistent with γδ T cells, clarifying their identity.

The spatial distribution of GSTZ1-Clone 1 and WASHC4-Clone 1 was projected onto the same UMAP embedding (Figure 5.6). Both clonotypes were exclusively localised to the type 1 helper T cell cluster, suggesting that the T cells that mediate these antigen-specific responses are $CD4^+$ T cells with a Th1-polarised phenotype.

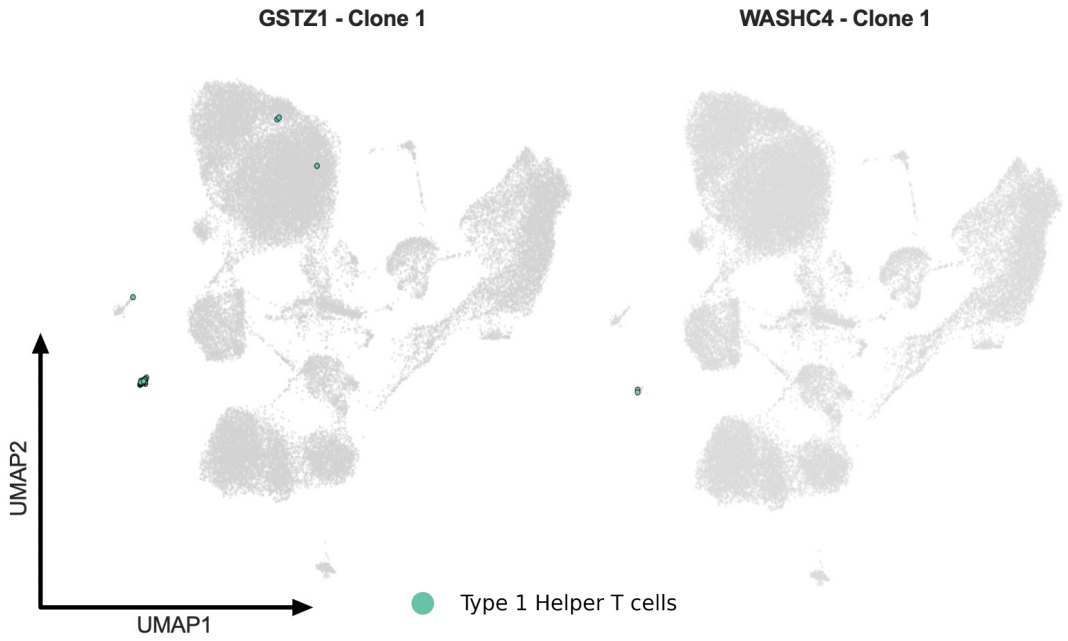

Figure 5.6: The GSTZ1 and WASHC4-reactive clones are Th1-polarised $CD4^+$ cells. UMAP plots demonstrating localisation of GSTZ1-Clone 1 and WASHC4-Clone 1 within the broader single-cell transcriptional landscape. Cells are coloured by their transcriptionally annotated cell type.

This contrasts with the previously described METTL22-Clonotype 1, which exhibited a transcriptional profile which was consistent with a cytotoxic $CD4^+$ phenotype. The observed phenotypic differences may reflect underlying variation between these patients and samples, or alternatively, the influence of the culture

conditions. While the METTL22 clones were expanded under unopposed IL-2, which can promote cytotoxic differentiation, the GSTZ1 and WASHC4 cultures included IL-7 and IL-15, which could support Th1 polarisation and memory potential over a cytotoxic phenotype [254, 272].

Together, these findings demonstrate that the joint APC-T cell co-culture is a viable strategy for the recovery and characterisation of antigen-specific T cells from early post-alloSCT bone marrow, albeit constrained by high background activation during flow cytometric assays. Further refinements aimed at reducing non-specific activation could expand the utility of this platform and reduce the reliance on single-cell sequencing to disentangle relevant TCR clonotypes. The detection of GSTZ1- and WASHC4-specific TCR clonotypes at both 12 months and 4 years post-alloSCT supports the early establishment and long-term persistence of putative GvL responses. These results underscore the potential for longitudinal tracking of clonotypes across compartments and timepoints and provide further support for the physiological importance of these T cells in immune surveillance.

5.4 High-Throughput Single-Cell Analysis of Post-AlloSCT Bone Marrow

In addition to the culture-based approaches employed to interrogate the post-alloSCT bone marrow, a parallel *ex vivo* strategy was undertaken. This approach was designed to confirm the *in vivo* presence of putative GvL T cell clones previously identified *in vitro*, therefore ensuring that these clonotypes were not artefacts of prolonged stimulation that were expanded in culture. Moreover, *ex vivo* profiling enables a more accurate assessment of the transcriptional and phenotypic landscape of these T cells, preserving signatures of antigen experience and lineage polarisation without the confounding effects of cell culture.

The principal technical challenge inherent to these *ex vivo* approaches is the inability to functionally enrich for antigen-specific GvL T cells. To resolve TCRα/β pairing and clonal identity, a single-cell based approach is required. Given the low inferred frequencies of GvL-reactive clones based on prior bulk TCR sequencing, this would necessitate a single-cell platform capable of capturing and processing very large numbers of cells in a scalable and cost-efficient manner.

Conventional droplet-based single-cell platforms, such as those developed by 10x Genomics, incur a relatively high cost when generating paired gene expression and TCR libraries, at approximately £0.10 to 0.20 per cell. While effective for moderate cell numbers, such as those used in earlier *in vitro* experiments, these costs become prohibitive when scaled to the hundreds of thousands of cells required to detect rare clonotypes with sufficient sensitivity.

To overcome this limitation, a novel combinatorial indexing method was employed, the Parse Evercode platform. In contrast to bead-in-emulsion-based systems, this approach relies on fixation and permeabilisation of cells followed by multiple rounds of *in situ* split-pool barcoding, enabling the generation of unique cell barcodes without the use of microfluidic systems. Crucially, this method dramatically reduces per-cell library preparation costs, to approximately £0.002 per cell, therefore enabling high-throughput profiling of these rare T cell populations across large cell volumes.

A total of 11 samples from six patients in the GvL-enriched cohort were selected for high-throughput single-cell analysis (Figure 5.7a). Patient selection was guided by sample availability, cryopreserved cell counts, and most critically, the prior identification of putative GvL TCRs in the peripheral blood at later timepoints [198]. Importantly, with the exception of the PADI4-specific response (section 1.10), these TCRs were identified on the basis of their enrichment within IFNγ^+ fractions following expansion and peptide stimulation, but their peptide specificity had not been formally confirmed through downstream functional testing. As such, they

should be considered candidate GvL TCRs pending definitive validation.

a

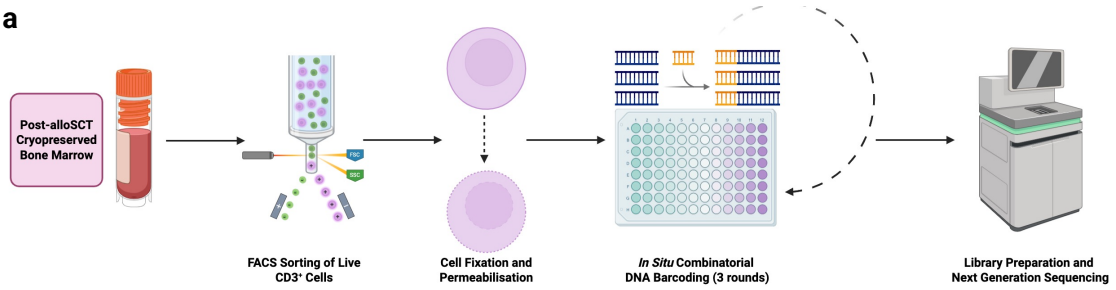

b

Patient	Timepoint Post-AlloSCT	Number of Alloreactive TCRs Identified in Late PB	Number of Cells Reported at Cryopreservation	Number of Cells Post-Thaw	Number of Live/CD3+ Cells Post-Sorting	Number of Cells Post-Fixation
OX289	6 months	20	4,500,000	1,960,000	59,800	53,400
OX628	3 months	3	20,000,000	11,240,000	29,300	12,210
	6 months		15,000,000	9,420,000	134,400	72,000
	12 months		15,000,000	12,130,000	328,500	272,000
OX747	3 months	8	10,000,000	4,970,000	8,500	4,000
	6 months		15,000,000	5,690,000	103,100	69,000
	9 months		19,000,000	7,120,000	183,200	94,500
OX866	11 months	3	18,000,000	7,020,000	510,000	333,000
OX885	3 months	3	18,000,000	10,910,000	73,000	45,600
	12 months		20,000,000	9,980,000	212,100	132,800
OX1149	3 months	3	9,300,000	4,460,000	200,640	98,000
		Total	163,800,000	84,900,000	1,842,540	1,186,510

Figure 5.7: High-throughput *ex vivo* single-cell analysis of post-alloSCT bone marrow using the Parse EverCode method. a. Simplified schema demonstrating experimental workflow. **b.** Summary of sample characteristics and cell processing metrics demonstrating cumulative cell losses from thaw to fixation.

Samples were thawed and immediately subjected to fluorescence-activated cell sorting to isolate viable $CD3^+$ T cells. This was followed directly by chemical fixation and permeabilisation. Post-permeabilisation, cells were stored at -80°C prior to pooled combinatorial barcoding. There were substantial cell losses at each key processing step, but as anticipated, these were greatest during thawing and sorting (Figure 5.7b). These losses reflect the combined effects of low post-thaw viability and the low proportion of $CD3^+$ cells characteristic of post-alloSCT bone marrow.

The recovery of live $CD3^+$ post-sort ranged from 0.3% to 7.3% of thawed input cells with an aggregate yield of 2.2%. Fixation-associated cell losses were comparatively modest, with sample retention ranging from 41.7% to 81.3% with

an aggregate retention of 64.4%. Notably, samples with larger initial cell inputs tended to exhibit higher overall retention, likely reflecting more efficient pelleting during the multiple centrifugation steps required during cell preparation.

Following fixation, cells underwent reverse transcription and three rounds of *in situ* barcoding. Barcoded cells were then distributed into 16 sublibraries for cell lysis, cDNA capture, and amplification. These sublibraries demonstrated the expected size distribution with minimal evidence of degradation (Figure 5.8a). However, a prominent early peak was observed in cDNA traces, consistent with primer-dimer formation. Given the relative novelty of the Parse Evercode platform and the limited overall experience with this platform, this finding was discussed with the Parse Biosciences Research and Development team. The early peak was deemed non-inhibitory to downstream reactions and would be expected to be removed during subsequent size selection. Accordingly, all cDNA sublibraries progressed to gene expression and TCR library preparation without further modification.

Gene expression libraries were synthesised without complication and displayed appropriate size distributions, with final concentrations ranging from 47.0 to 80.8 ng/µl. In contrast, TCR libraries, although of the correct expected size, displayed markedly low concentrations (1.53 to 3.32 ng/µl), insufficient for standard next-generation sequencing protocols.

Efforts to re-amplify the TCR libraries from remaining cDNA yielded similarly low concentrations. This issue was therefore re-escalated to Parse Biosciences, where extensive internal investigation revealed that the early primer-dimer peak had inadvertently been incorporated into the first round of TCR-specific PCR amplification. Although this non-specific product was not itself amplified during the second round of TCR-targeted PCR, given the use of nested TCR-specific primers, its presence effectively diluted the pool of *bona fide* TCR template, thereby lowering the final TCR library concentration. Furthermore, the contaminating product was removed during downstream size selection and was therefore not detected in the final library traces, masking the underlying cause of low library yield.

a

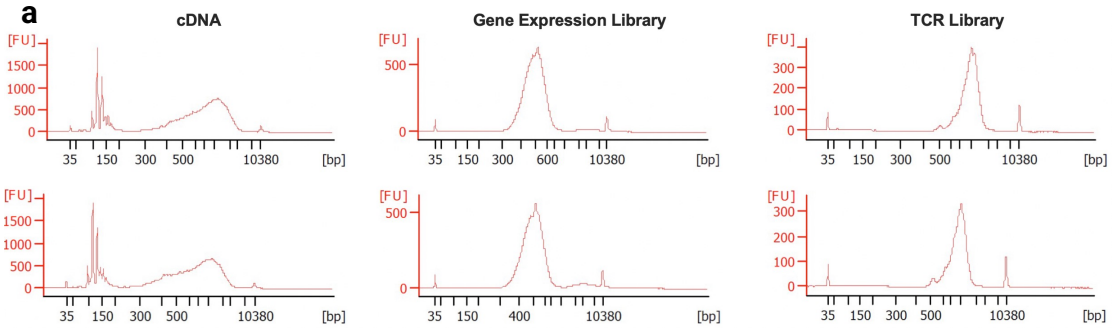

b

Patient	Timepoint Post-AlloSCT	Cell Number Entering Barcoding	Cell Number After Barcoding	Number of Cells Detected at Single Cell Sequencing
OX289	6 months	53,400	31,504	22999
OX628	3 months	12,210	7,203	5080
	6 months	72,000	42,478	34870
	12 months	272,000	160,471	105697
OX747	3 months	4,000	2,360	282
	6 months	69,000	40,708	28242
	9 months	94,500	55,752	34084
OX866	11 months	333,000	196,459	129118
OX885	3 months	45,600	26,902	7802
	12 months	132,800	78,347	69133
OX1149	3 months	98,000	57,817	47123
	Total	1,186,510	700,001	484,430

c

Median Transcripts/Cell	5002
Median Genes/Cell	2176
Mean Reads/Cell	33821
Sequencing Saturation	0.426
Barcode 1 (RT) > Q30	0.946
Barcode 2 > Q30	0.959
Barcode 3 >Q30	0.965
cDNA > Q30	0.915

d

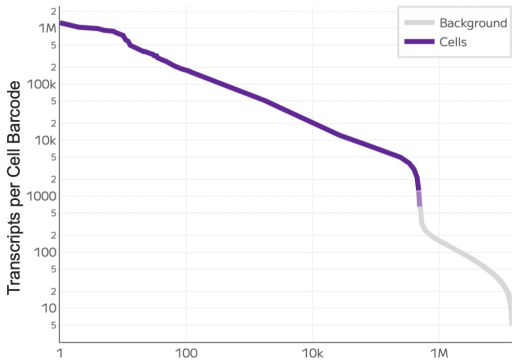

Figure 5.8: Single-cell library quality control and cell recovery metrics. a. Representative Bioanalyzer traces from two sublibraries from cDNA synthesis, complete gene expression libraries and TCR libraries, demonstrating size distribution of library products. **b.** Summary of cell recovery throughout the barcoding and sequencing pipeline for individual samples. Number of cells detected at single-cell sequencing reflects high-confidence transcriptome and TCR barcode calls. **c.** Summary table of quality metrics across all sublibraries. **d.** Log-scaled barcode rank plot showing transcript counts (UMIs) per cell barcode.

Following protocol optimisation and the removal of the primer-dimer peak prior to targeted TCR amplification, sublibraries of sufficient concentration were generated, pooled and successfully sequenced via multiplexed next-generation sequencing.

Further cell losses occurred during barcoding, library preparation and sequencing. A total of 1,186,510 fixed cells were input into the barcoding workflow, with 700,001 cells recovered post-barcoding but prior to cell lysis, corresponding to a retention of 59.0%. Following library preparation and sequencing, a total of 484,430 high-confidence cell barcodes were detected, yielding a final cell recovery rate of 26.3% across the entire Parse Evercode workflow, from sorted cell input to sequenced output (Figure 5.8b). This retention rate is consistent with previously reported benchmarks for the Parse Evercode platform [273].

Sequencing of the pooled sublibraries yielded over 16.3 billion reads, with a mean depth of 33,821 reads per cell (Figure 5.8c). The median transcript count per cell was 5,002, and a median of 2,176 genes per cell were detected. Although the overall sequencing saturation was relatively modest at 42.6%, barcode rank profiling revealed a well-defined inflection between true cell-containing barcodes and background, indicating that most recoverable cells had already been captured at the current sequencing depth (Figure 5.8d). Additional sequencing would therefore be unlikely to substantially increase cell yield, though it would be expected to improve transcriptome coverage and enable more sensitive detection of low-abundance transcripts.

Collectively, these metrics confirm the successful generation of high-quality, high-throughput single-cell transcriptomic and TCR libraries from *ex vivo* post-alloSCT bone marrow.

5.5 Dissecting the Reconstitution of the T Cell Repertoire in the Post-AlloSCT Period

In parallel to targeted efforts to identify putative GvL TCRs, the high-throughput Parse platform enabled the generation of a large paired-chain TCR dataset spanning six post-alloSCT patients, including three who underwent longitudinal sampling. While most studies in this setting focus exclusively on TCRβ sequences to define a clonotype, the availability of paired-chain data here allows for a more granular assessment of the post-alloSCT repertoire and of the dynamics of T cell reconstitution.

To evaluate antigen specificity, both the TCRα and TCRβ chains were cross-referenced against the VDJdb database to annotate clonotypes with known epitope reactivity (Figure 5.9) [216].

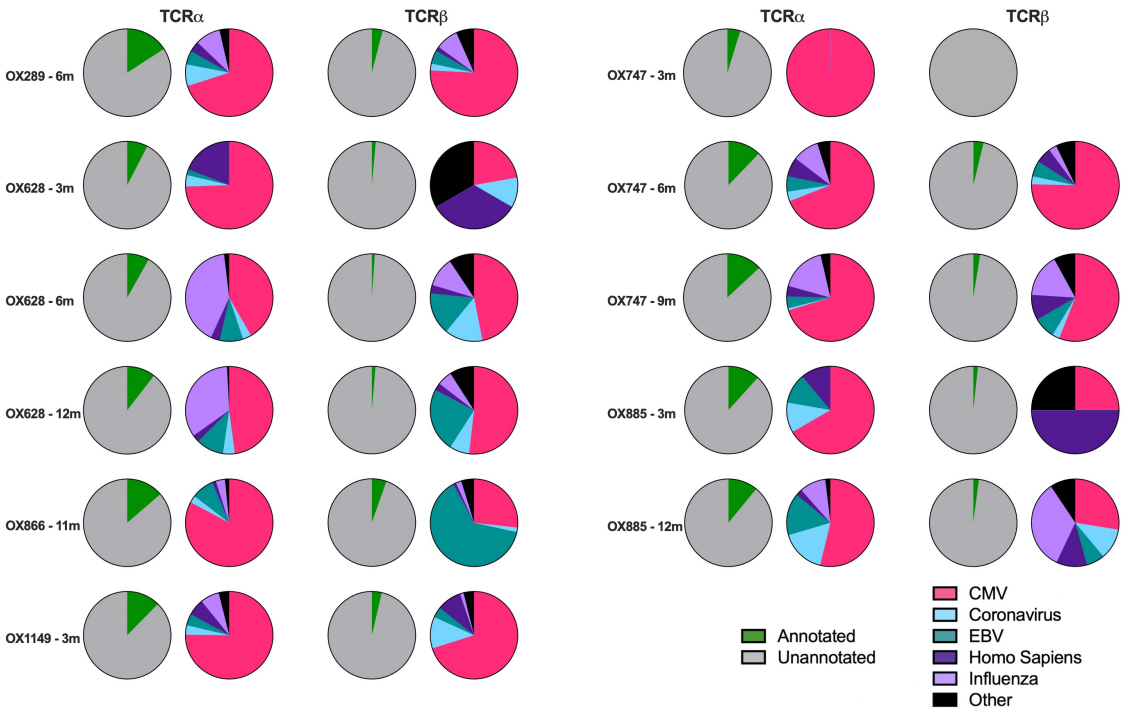

Figure 5.9: Annotation of *ex vivo* TCR repertoires. Graphs demonstrating the distribution of annotated and unannotated clonotypes for TCRα and TCRβ chains across individual patient samples and timepoints. The left pie chart for each sample and chain represents the proportion of each repertoire that was annotated successfully by VDJdb. The right pie chart displays the predicted antigen specificity of the annotated TCR chains, with colours indicating the antigen source. TCRs annotated as *Homo sapiens* correspond to known neoantigens, tumour-associated antigens, or autoantigens.

Consistent with the limited coverage of known TCR-peptide interactions in existing reference datasets, the majority of clonotypes remained unannotated. Across all samples, only 8.3% of clonotypes could be matched to a known antigen, ranging from 0.0% to 18.9% by sample. Interestingly, the annotation rate was higher in TCRα chains (13.7%) compared to TCRβ chains (3.5%), likely reflecting the increased combinatorial diversity and privacy of TCRβ sequences.

The majority of annotated clonotypes were directed against viral epitopes, with CMV-specific sequences accounting for 61.7% of annotations. This dominance may partially reflect biases in VDJdb and similar TCR-epitope databases, which are dominated by MHC class I-restricted responses to common viral epitopes, but is also consistent with previous reports demonstrating that CMV-specific TCRs can comprise over half the circulating $CD8^+$ T cell pool by 12 months post-alloSCT [102]. Smaller fractions of annotated sequences targeted EBV, influenza or coronavirus antigens. A minority of clonotypes matched epitopes derived from *Homo sapiens*, though it is not possible to determine the functional significance of these TCRs from database annotation alone.

To investigate the persistence, emergence and turnover of TCRs following alloSCT, the top five most abundant clones were tracked as paired TCRα/β clonotypes across all available timepoints in the three patients with longitudinal samples (Figure 5.10).

In patient OX628, the dominant clonotypes at 3 months collectively comprised over 30% of the total repertoire, reflecting the oligoclonal nature of early T cell reconstitution [228, 251]. All five of these clonotypes remained detectable at later timepoints, with 3m-4 notably persisting within the top five clonotypes throughout the first year. The remaining four clonotypes declined substantially over time, together representing only 1.5% of the repertoire at 12 months. One of these persistent early clonotypes, 3m-5, was CMV-specific, consistent with the well-documented longevity of CMV-reactive memory T cells in the post-alloSCT setting [102, 274].

OX628

Top Clonotypes		Frequency at: 3 months	6 months	9 months	Epitope
3 months	1	0.1120	0.0057	0.0032	
	2	0.0682	0.0002	0.0042	
	3	0.0422	0.0148	0.0054	
	4	0.0422	0.0265	0.0266	
	5	0.0276	0.0043	0.0023	CMV
6 months	1	0.0049	0.0811	0.0219	
	2	0.0032	0.0656	0.0150	
	3	0.0000	0.0627	0.1140	
	4	0.0032	0.0269	0.0260	Influenza
	5	Same Clone as 3m-4			
12 months	1	Same Clone as 6m-3			
	2	0.0000	0.0181	0.0645	
	3	Same Clone as 3m-4			
	4	Same Clone as 6m-4			
	5	Same Clone as 6m-1			

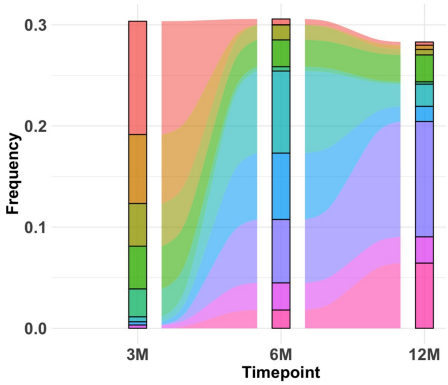

OX747

Top Clonotypes		Frequency at: 6 months	9 months	Epitope
6 months	1	0.0216	0.0199	CMV
	2	0.0173	0.0030	
	3	0.0157	0.0051	CMV
	4	0.0076	0.0003	
	5	0.0054	0.0020	
9 months	1	Same Clone as 6m-1		
	2	0.0043	0.0105	CMV
	3	0.0016	0.0071	
	4	0.0032	0.0054	
	5	0.0022	0.0051	CMV

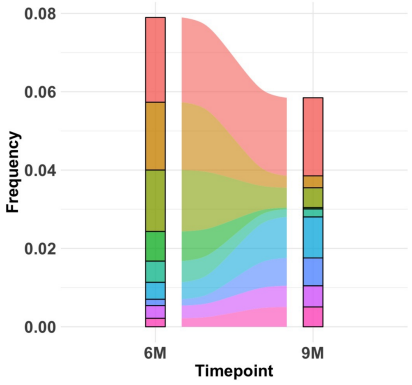

OX885

Top Clonotypes		Frequency at: 3 months	12 months	Epitope
3 months	1	0.0957	0.0065	
	2	0.0217	0.0087	
	3	0.0130	0.0004	
	4	0.0130	0.0000	
	5	0.0130	0.0000	
12 months	1	0.0000	0.0571	
	2	0.0000	0.0483	
	3	0.0000	0.0243	
	4	0.0000	0.0239	
	5	0.0000	0.0215	CMV

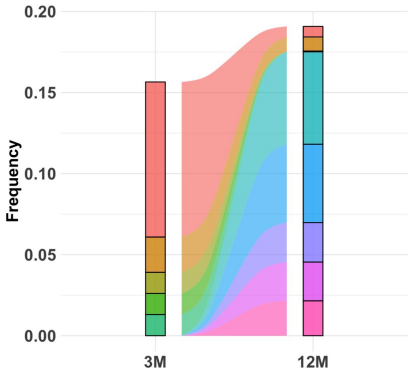

Figure 5.10: Longitudinal tracking of dominant TCR clonotypes. Top 5 clonotypes for patients with multiple assessed timepoints (OX628, OX747 and OX885) were ranked by abundance at each timepoint. Lineage tables display the frequency of each of these clonotypes across timepoints, with shared clones indicated. Epitope annotations were assigned by cross-referencing with VDJdb. Corresponding stacked area plots illustrate the relative contribution of each clonotype over time. The 3-month sample for OX747 was excluded given the low total cell recovery at this timepoint ($n = 282$).

At 6 months, four new dominant clonotypes emerged. Most were already detectable at low frequency at 3 months, suggesting early establishment followed by a later expansion. The exception to this was 6m-3, which was not detected earlier and likely represents a newly established clonotype. Among the remaining clonotypes, 6m-4 was annotated as influenza-specific, indicating expansion of virus-specific cells beyond CMV.

By 12 months, the top clonotypes were largely maintained from the 6-month timepoint, with 12m-2 notably expanding after 3 months to reach prominence.

The 3-month sample from patient OX747 was excluded due to low total cell recovery (n = 282), which led to an unrepresentative and highly skewed repertoire.

In contrast to OX628, the top five clonotypes at both 6 and 9 months from patient OX747 accounted for less than 8% of the repertoire, indicating a more polyclonal and evenly distributed T cell population.

Despite this, the TCR repertoire was clearly enriched by CMV-specific responses. The most abundant clonotype at both 6 and 9 months was CMV-directed, as were three additional top-five clones. All dominant clonotypes were present at both timepoints, demonstrating clonal stability. Although their relative frequencies fluctuated over time, the consistent presence of these virus-specific clones reinforces the importance of CMV-specific memory in shaping post-alloSCT T cell landscapes.

Unlike the previous patients, patient OX885 exhibited a highly dynamic clonal trajectory. At 3 months, the top five clonotypes accounted for 15.6% of the total repertoire. By 12 months, two of these (3m-4 and 3m-5) had declined to undetectable levels, while the other three clones persisted only at low frequencies, together totalling 1.5% of the repertoire.

Strikingly, all five dominant clonotypes at 12 months were not detected at 3 months, indicating substantial clonal replacement. Among these new clones, 12m-5 was also annotated as CMV-specific. This turnover pattern reflects the delayed establishment of new clones in the post-alloSCT period but may also be accentuated

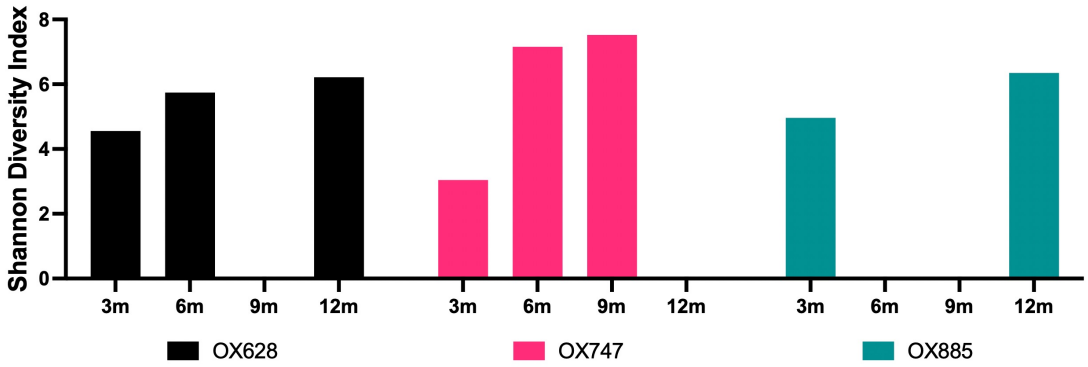

Figure 5.11: TCR repertoire diversity over time. Bar plot showing the Shannon diversity index of paired TCR clonotypes in patients OX628, OX747, and OX885 across serial timepoints post-alloSCT.

by the longer interval of 9 months between sampling.

Across all three patients, TCR repertoire diversity, as measured by the Shannon diversity index, increased over time (Figure 5.11), consistent with the transition from early oligoclonal reconstitution towards a more diverse, polyclonal repertoire. This pattern reflects the expected course of T cell recovery post-alloSCT, with initial homeostatic proliferation of donor-derived memory T cells followed by gradual thymus-dependent generation of *de novo* T cells [226, 251, 275].

These longitudinal analyses highlight substantial inter-patient heterogeneity in T cell clonal recovery post-alloSCT. Some clonotypes are established early and persist throughout the first year, while others undergo contraction or are replaced entirely. Still others emerge only at later timepoints, reflecting delayed expansion or thymus-dependent repertoire renewal. CMV-specific clonotypes featured prominently in all patients, emphasising the central role of CMV-specific immunity in shaping early post-alloSCT T cell repertoires.

The dynamic and individualised nature of these clonal trajectories likely reflects differences in clinical context, including infectious challenges, conditioning, graft composition and immunosuppression. These findings reinforce the importance of longitudinal tracking in understanding post-transplant immune reconstitution. Though many dominant clonotypes lacked known antigen specificity, future advances

in TCR-epitope inference, including machine learning approaches such as GLIPH2, DeepTCR or NetTCR2.0, could elucidate their functional relevance and deepen understanding of T cell responses in the post-alloSCT setting [276–278].

5.6 Detection and Profiling of GvL T cells in the Early Post-AlloSCT Bone Marrow

Building on the repertoire-wide observations presented in the previous section, the next step was to investigate whether putative GvL T cell clonotypes, which had been previously identified through functional assays using late post-alloSCT peripheral blood samples, could also be detected in the *ex vivo* dataset from the early post-alloSCT bone marrow. This analysis would assess whether these clones were established early post-alloSCT, and confirm they were not artefacts of *in vitro* expansion. To address this, a targeted search was performed within the single-cell TCR libraries generated from the Parse Evercode dataset, focusing specifically on the full-length, paired TCRα and TCRβ sequences previously assigned to GvL TCRs on a per-patient basis.

Candidate GvL clonotypes, previously identified in the late peripheral blood (by Connor Sweeney [198]), were successfully detected in two patients: OX289 at 6 months post-alloSCT and OX885 at 12 months (Figure 5.12a). For patient OX289, RNF123-Clone 1 and FTSJ3-Clone 1.1 were identified, and for OX885, GSTZ1-Clone 1 and WASHC4-Clone 1. Notably, the OX885 clonotypes matched those independently identified in section 5.3 through *in vitro* functional screening of this same timepoint, providing strong orthogonal cross-validation across these two methodologies.

Although the observed frequencies of these clones were low, ranging from 0.013% to 0.10%, they were consistent with estimates derived from prior bulk TCR sequencing and align with the lower range of reported GvL-reactive T cell frequencies in the literature [40, 249, 257]. No GvL clonotypes were detected in

a

Patient	Timepoint Post-Allo	Lower Limit of Clonotype Detection (%)	Known GvL TCRs Present at Timepoint?	Targeted Peptide	Clonotype ID	Clonotype Frequency (%)
OX289	6 months	0.034	Yes (2)	RNF123	1	0.10
				FTSJ3	1.1	0.067
OX628	3 months	0.017	No			
	6 months	0.16				
	12 months	0.012				
OX747	3 months	4.7	No			
	6 months	0.054				
	9 months	0.034				
OX866	11 months	0.0052	No			
OX885	3 months	0.043	No			
	12 months	0.013	Yes (2)	GSTZ1	1	0.082
				WASHC4	1	0.013
OX1149	3 months	0.048	No			

b

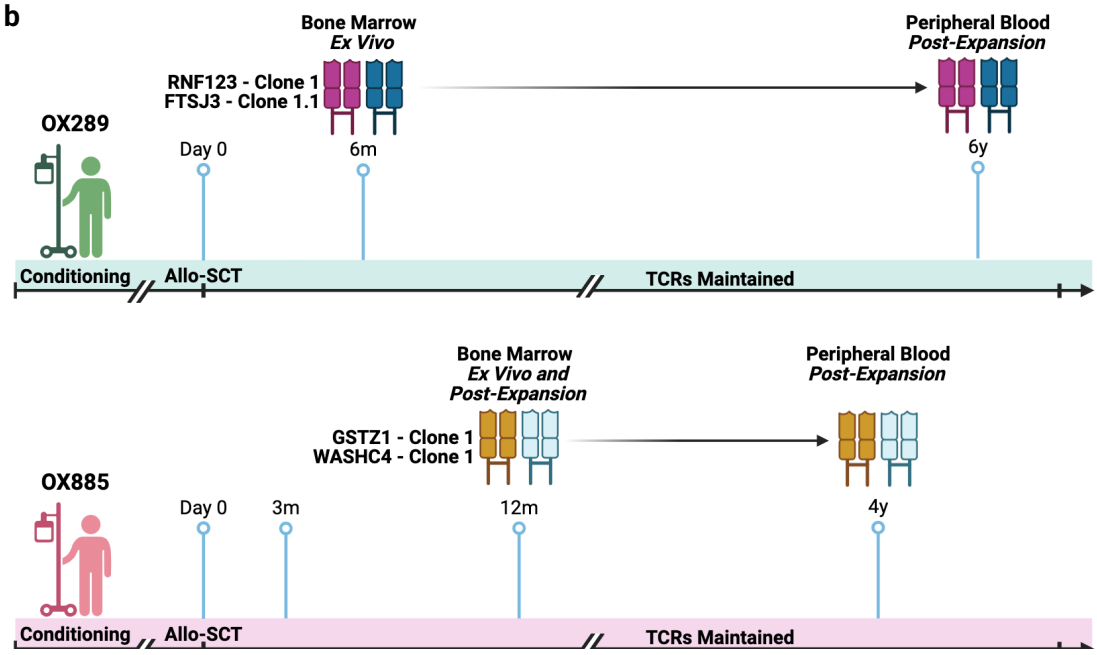

Figure 5.12: Four previously identified TCR clonotypes are detected in the early bone marrow using *ex vivo* TCR sequencing. a. Table summarising results of *ex vivo* TCR sequencing of post-alloSCT bone marrow at various timepoints. The lower limit of clonotype detection was defined utilising the lowest-abundance TCR clone identified in each sample. Known GvL TCRs refer to putative TCRs identified previously through functional screening of late peripheral blood. Clonotypes highlighted in green reflect identified TCRs that are identical to previously identified clones from the late peripheral blood. **b.** Visual schematic outlining timepoints and methods by which the same TCR clonotypes were identified in patients OX289 and OX885.

the remaining four patients nor in the 3-month sample from OX885. However, it remains unclear whether this absence reflects genuine biological absence or technical limitations. In this context, the effective limit of detection, which extends as low as 0.0052%, is defined by the lowest confidently called TCR within each dataset, and clonotypes below this threshold may have simply evaded capture.

Crucially, the four identified clonotypes were identified directly from *ex vivo* material, in the absence of any exogenous antigen or cytokine stimulation. This provides unambiguous evidence for their presence *in vivo*. Furthermore, their detection at these early post-alloSCT timepoints, several years prior to their original identification in the peripheral blood, suggests that GvL clones are established early in the post-alloSCT period with their persistence lending further credence to their physiological relevance (Figure 5.12b).

To characterise the transcriptional phenotype of the GvL clonotypes identified in the early post-alloSCT bone marrow, paired single-cell gene expression data was analysed.

In patient OX289, a total of 22,999 cells were recovered and visualised using UMAP projection (Figure 5.13a). Cell annotation was performed using the CellTypist classifier without majority voting, in order to preserve within-cluster cell heterogeneity [215]. The subset distribution was dominated by $CD8^+$ T_{EM}/T_{EMRA} cells, with $CD4^+$ $T_{Naïve}/T_{CM}$ also present at substantial, but lower, levels (Figure 5.13b). Regulatory and γδ T cells were detected at frequencies consistent with published reports, and the overall reversal of the CD4:CD8 ratio is in keeping with immune reconstitution at this 6-month post-alloSCT time point [93, 106, 228].

The validity of these annotations was confirmed through Z score-normalised expression of canonical marker genes, which aligned well with the annotated identities (Figure 5.13c).

Despite the detection of RNF123-Clone 1 ($n = 3$) and FTSJ3-Clone 1.1 ($n = 2$), the low number of clonotype-assigned cells in this sample precluded statistically

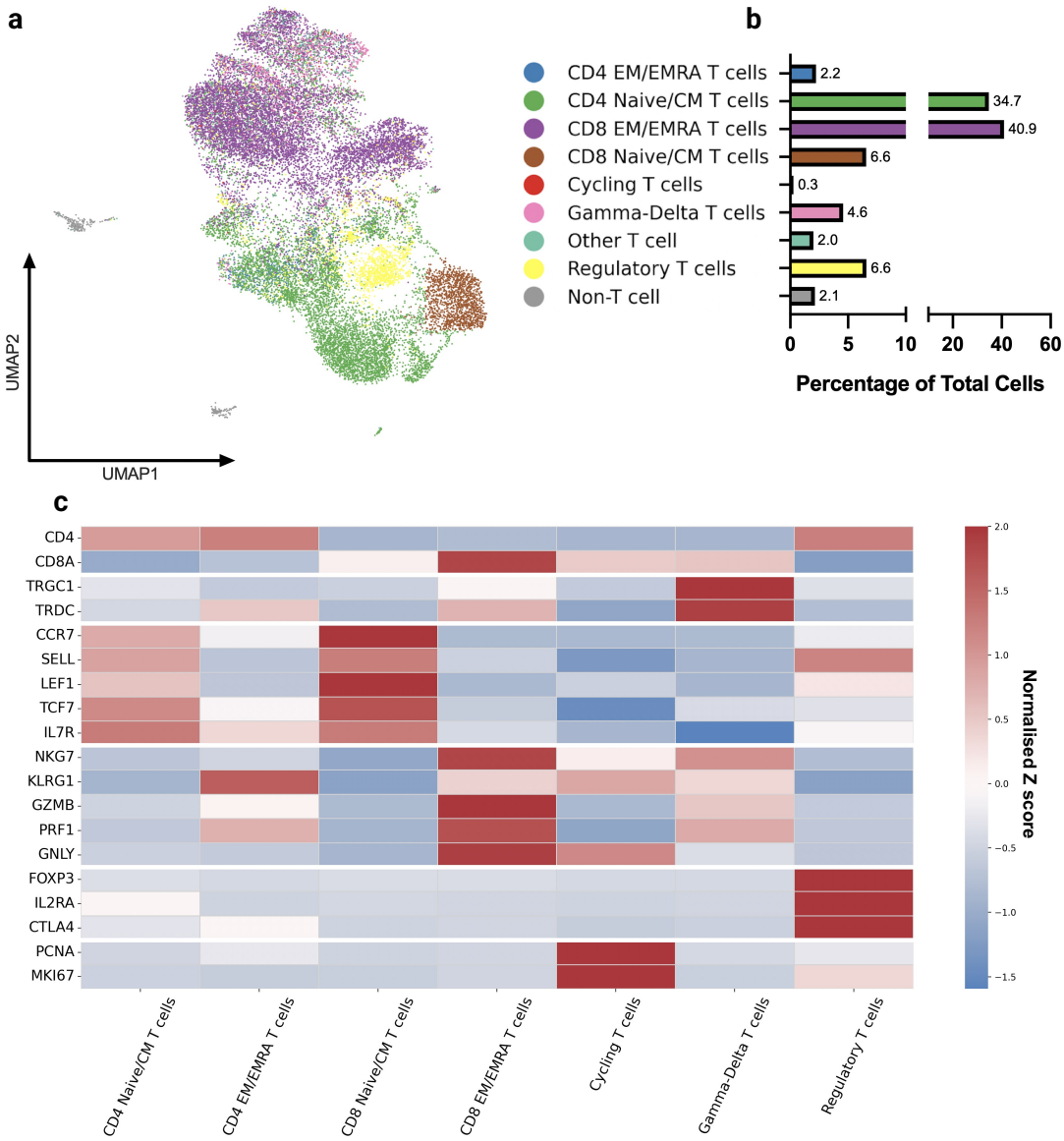

Figure 5.13: Transcriptional characterisation of cells at 6-months post-alloSCT from patient OX289. a. UMAP projection of single-cell gene expression from patient OX289 (n=22999). Cell annotation performed utilising CellTypist without majority voting. **b.** Bar plot showing the relative frequency of each annotated subset, expressed as a proportion of all cells. **c.** Heatmap displaying Z score normalised expression of selected marker genes across annotated T cell subsets.

robust analysis of differential gene expression or gene set enrichment. Nevertheless, projection of these cells onto the UMAP revealed that RNF123-Clone 1 localised within the CD4$^+$ $T_{Naïve}/T_{CM}$ subset, while FTSJ3-Clone 1.1 resided within the CD8$^+$ T_{EM}/T_{EMRA} compartment (Figure 5.14). These localisations are concordant with the phenotypes originally assigned during the functional screening of peripheral blood.

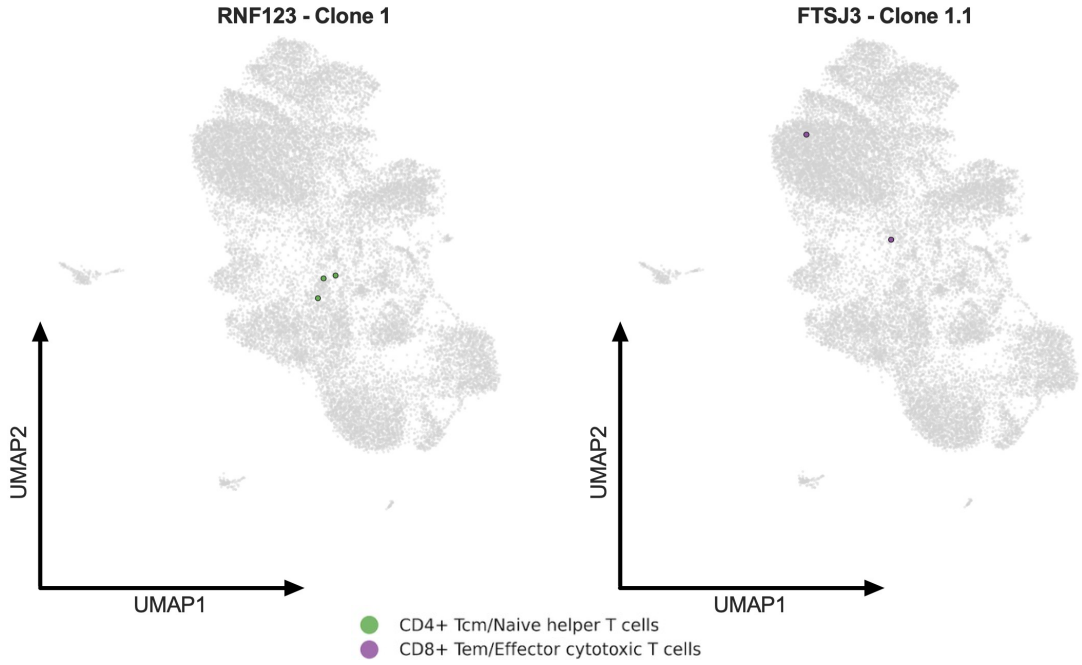

Figure 5.14: Localisation of alloreactive clonotypes for patient OX289. UMAP projections demonstrate the distribution of individual cells belonging to putative GvL clonotypes (RNF123-Clone 1 and FTSJ3-Clone 1.1) within the broader single-cell transcriptional landscape. Cells are coloured by their transcriptionally annotated subtype.

The T_{EM}/T_{EMRA} phenotype of FTSJ3-Clone 1.1 supports its classification as an antigen-experienced, functionally active GvL clone. In contrast, the transcriptional annotation of RNF123-Clone 1 is more ambiguous. As it has localised to a CD4$^+$ $T_{Naïve}/T_{CM}$ cluster, this transcriptional state may reflect either a truly naïve, antigen-inexperienced cell or a central memory cell that has undergone antigen priming, and without further investigation its functional relevance remains unresolved.

The 12-month post-alloSCT bone marrow sample from patient OX885 yielded 69,134 cells, including six cells corresponding to GSTZ1-Clone 1 and a single cell

assigned to WASHC4-Clone 1. Cell type annotation again identified a spectrum of subsets (Figure 5.15a). As in patient OX289, $CD8^+$ T_{EM}/T_{EMRA} cells were the dominant population, but the proportion of $CD4^+$ $T_{Naïve}/T_{CM}$ cells was comparatively lower despite the later timepoint (Figure 5.15b). In this patient, this pattern may plausibly have been influenced by the clinical context, where sufficiently low donor chimerism to require DLI may have perturbed the normal trajectory of immune reconstitution.

Canonical marker expression supported these annotations (Figure 5.15c). Both GSTZ1-Clone 1 and WASHC4-Clone 1 were annotated as $CD4^+$ $T_{Naïve}/T_{CM}$ cells (Figure 5.16a).

To further assess the phenotype of the identified GvL clonotypes, per-cell gene enrichment scores were calculated for two predefined transcriptional signatures (Figure 5.16b). The first was a proximal TCR signalling module curated from the Reactome pathway database, comprising genes such as *CD3E*, *ZAP70*, *LCK* and *LAT* [221]. This signature showed widespread enrichment across the T cell landscape, with maximal expression in $CD8^+$ T_{EM}/T_{EMRA} clusters, likely representing active antiviral effector responses. The clusters harbouring GSTZ1-Clone 1 and WASHC4-Clone 1 showed moderate enrichment for this signature, suggesting these clones may have undergone recent TCR engagement.

The second signature, defined by Rosenberg *et al.*, encompassed a composite activation and exhaustion program derived from neoantigen-specific tumour-infiltrating lymphocytes, including *PDCD1*, *IFNG*, *TOX* and *TBX21* [222]. The greatest enrichment of this signature was in a small subset of $CD8^+$ T_{EM}/T_{EMRA} cells and in the Treg cluster. Given the presence of canonical Treg genes within the signature, such as *CTLA4*, *ENTPD1*, *ICOS* and *ITGAE*, this is not surprising. The GvL clonotypes did not score highly for this signature, a result that may reflect both their non-exhausted memory status and the contextual limitations of using tumour-derived, neoantigen-specific T cell signatures to assess alloantigen-specific $CD4^+$ T cells in the bone marrow.

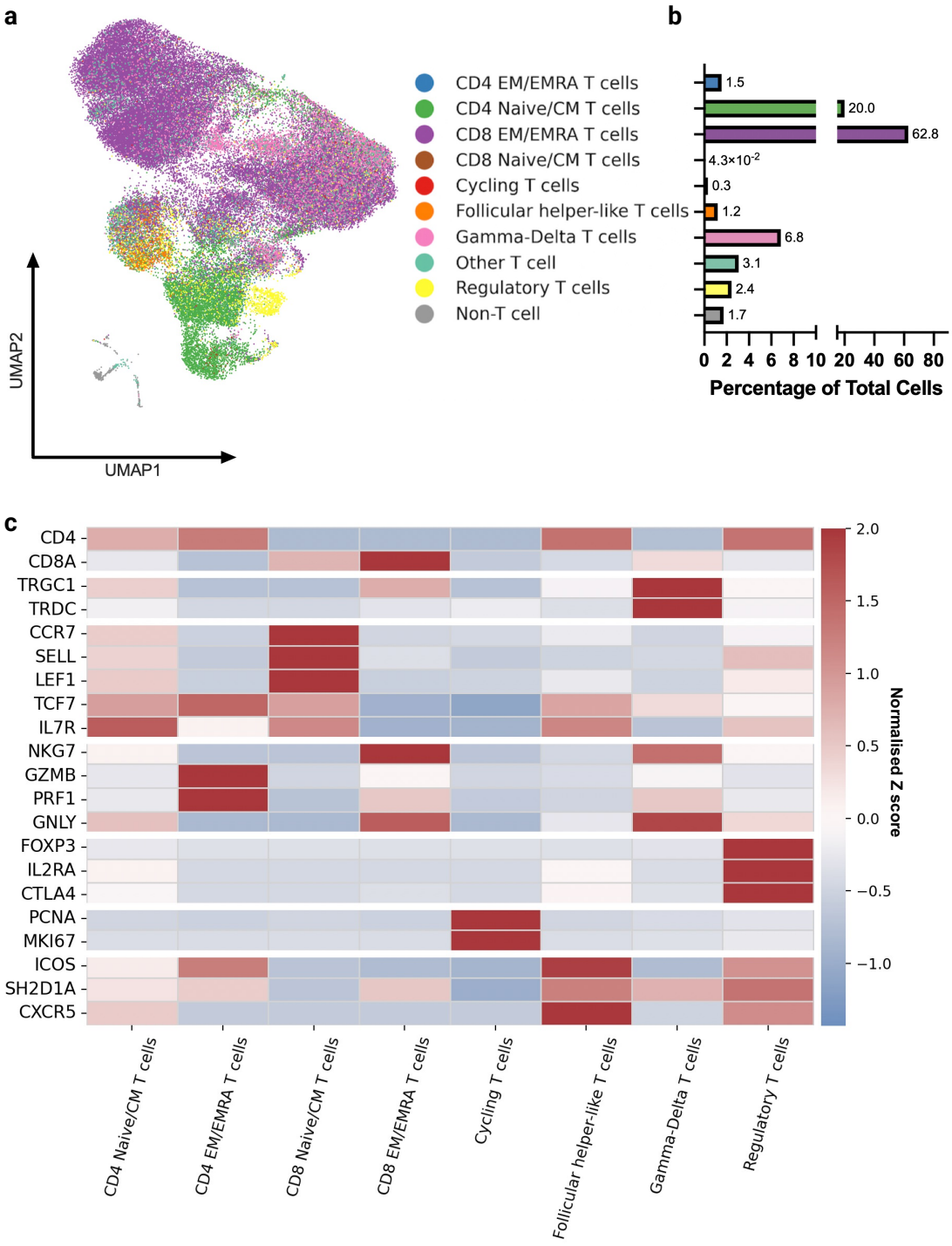

Figure 5.15: Transcriptional characterisation of cells at 12-months post-alloSCT from patient OX885. a. UMAP projection of single-cell gene expression from patient OX885 ($n = 69134$). Cell annotation performed utilising CellTypist without majority voting. **b.** Bar plot showing the relative frequency of each annotated subset, expressed as a proportion of all cells. **c.** Heatmap displaying Z score-normalised expression of selected marker genes across annotated T cell subsets.

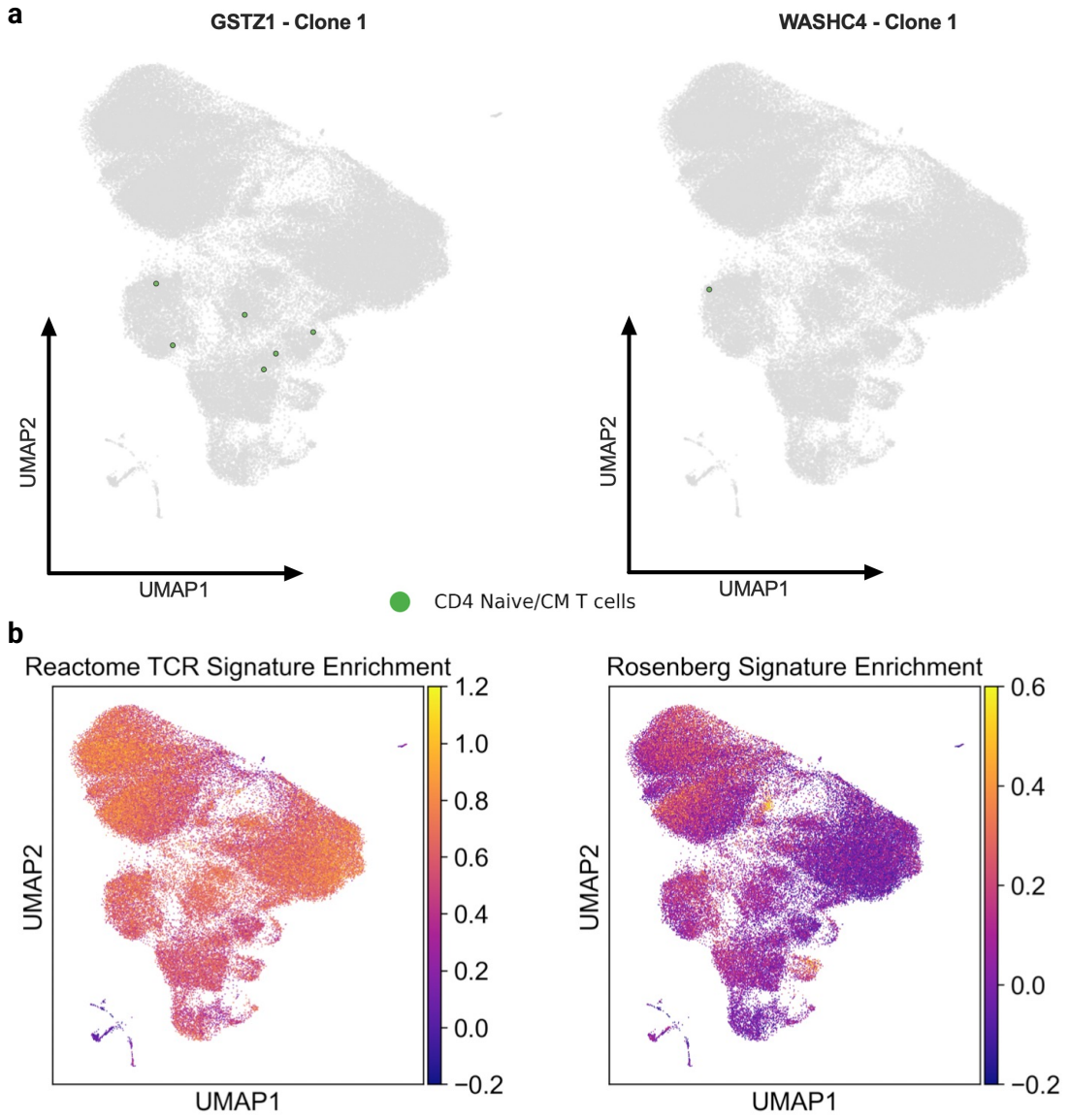

Figure 5.16: Phenotypic localisation and transcriptional signature enrichment of alloreactive cells from patient OX885. a. UMAP projections demonstrating distribution of GSTZ1-Clone 1 and WASHC4-Clone 1 within the broader single-cell transcriptional landscape. Cells are coloured by their transcriptionally annotated cluster. **b.** Gene signature enrichment scores visualised across the UMAP using single cell AUCell scoring for the Reactome TCR Signalling Signature [221], which comprises canonical TCR signalling components, and the T cell signature defined by Rosenberg *et al.* derived from neoantigen-reactive tumour-infiltrating lymphocytes [222].

As the most abundant GvL clonotype, GSTZ1-Clone 1 was further interrogated using AUCell scoring against curated gene sets representing T cell differentiation states and $CD4^+$ polarisation programs (Figure 5.17, with full gene lists available in appendix Figure B.4). Compared to all other $CD4^+$ T cells, GSTZ1-Clone 1 cells were significantly enriched for both T_{CM} and Th1-associated transcriptional profiles. No enrichment was observed for Th2, Th17, Treg, $CD4^+$ cytotoxic or exhaustion-associated programs. This suggests that GSTZ1-Clone 1 represents a Th1-polarised central memory population, a phenotype associated with antigen-experience, long-term persistence and sustained effector potential.

Although the small number of recovered putative GvL cells limits definitive phenotypic characterisation, their detection in this setting provides strong evidence for their *bona fide* establishment in the early post-alloSCT bone marrow. Moreover, the transcriptional profiles of several clonotypes, including localisation to effector or memory compartments and enrichment for TCR signalling programs, are consistent with prior antigen experience. Together, these findings support the physiological relevance of these persistent GvL clonotypes, suggesting that long-lived, antigen-experienced T cells may contribute to durable GvL surveillance in the post-alloSCT setting.

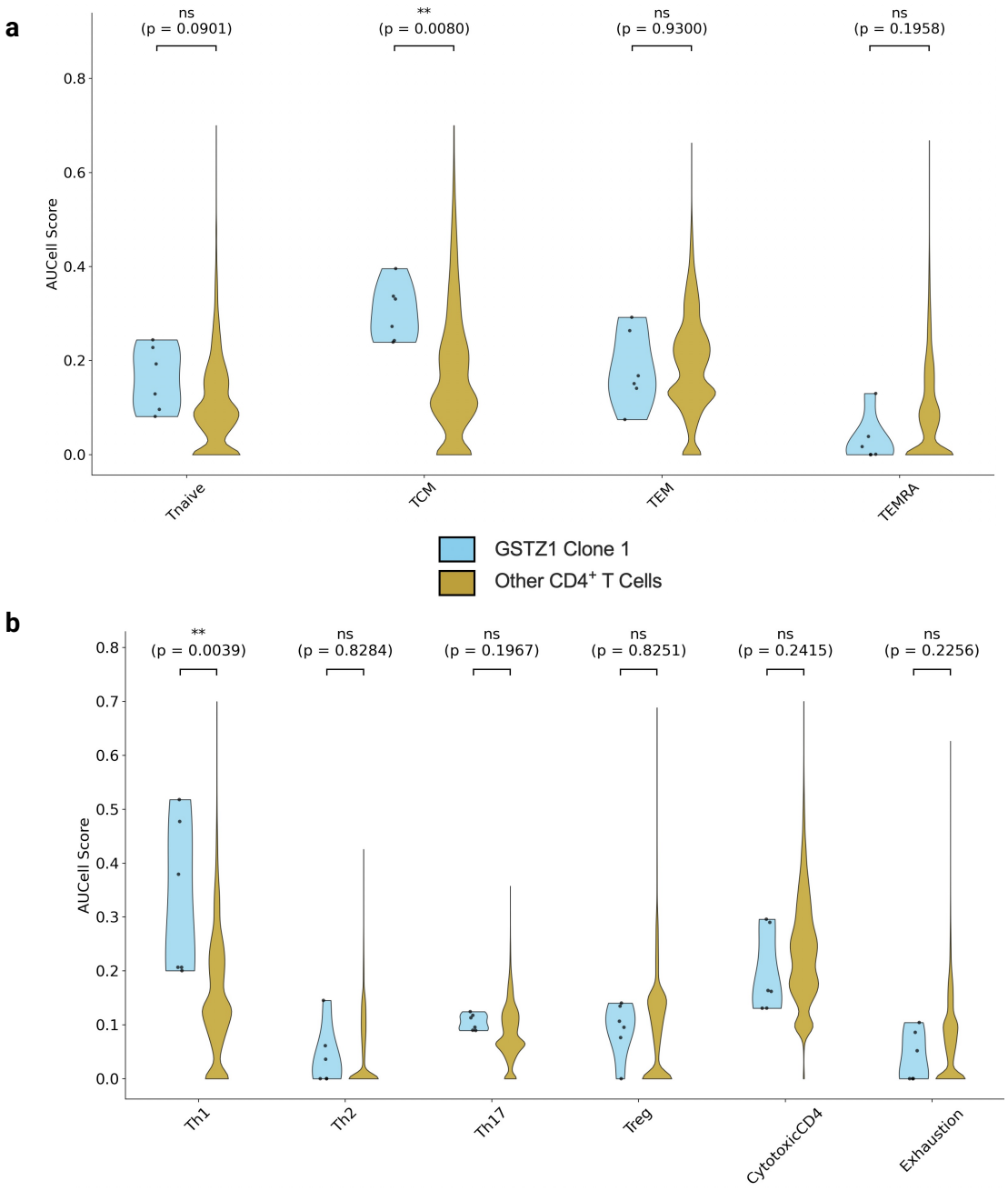

Figure 5.17: GSTZ1-Clone 1 comprises Th1-polarised central memory cells. a. Violin plots showing AUCell enrichment scores for T cell differentiation state. GSTZ1-Clone 1 cells are shown in blue with individual cells overlaid as dot plots. All other $CD4^+$ T cells are shown gold, without dot overlays for visual clarity. **b.** Violin plots showing AUCell enrichment scores for T cell polarisation and exhaustion-associated transcriptional programs. Statistical significance was calculated utilising the Wilcoxon Rank-Sum test with the Benjamini-Hochberg correction for multiple comparisons.

5.7 End of Chapter Discussion

This chapter utilised complementary *in vitro* and *ex vivo* methodologies for the identification and characterisation of antigen-specific T cell responses in the early post-alloSCT bone marrow, a setting complicated by T cell scarcity and fragility. The failure to expand even high-frequency, virus-specific T cells under a range of cytokine conditions highlights a generalised impairment in post-alloSCT T cell proliferation, extending beyond the GvL-reactive context.

In addition to enabling targeted searches for known GvL clonotypes, the high-throughput single-cell profiling undertaken here provides a broader view of the composition of T cells repopulating the bone marrow in the first year post-alloSCT. In the two samples analysed in detail, the overall subset distribution, including the dominance of $CD8^+$ T_{EM}/T_{EMRA} cells and the reversal of the CD4:CD8 ratio, align with published reports of post-alloSCT recovery ([87, 228]). Whilst these observations support models of immune reconstitution, they represent only a fraction of the available dataset. Single-cell data was generated using 11 samples from 6 patients, and a more systematic analysis of this larger cohort could yield a richer understanding of how bone marrow T cells reconstitute over time. Such analyses could complement existing studies of peripheral blood reconstitution and provide a deeper understanding of the post-alloSCT immune landscape. This context helps to frame the interpretation of candidate GvL clonotypes, which must be understood within the background of this dynamic and heterogeneous immune recovery.

Four GvL-associated clonotypes, originally identified in the late post-alloSCT peripheral blood, were successfully detected directly from the bone marrow of two patients via high-throughput single-cell sequencing, at frequencies ranging from 0.01% to 0.1%. Though one of these clonotypes was from the $CD8^+$ compartment (FTSJ3-Clone 1.1), the remainder were $CD4^+$ T cells. For one of these patients (OX885) two TCR clonotypes (GSTZ1-Clone 1 and WASHC4-Clone 1) were independently identified using a joint APC-T cell co-culture system, providing

robust orthogonal validation. Single-cell transcriptomic profiling revealed that GSTZ1-Clone 1 exhibited a Th1-polarised, central memory transcriptional signature, consistent with prior antigen exposure and long-term immunological persistence.

Taken together with prior peripheral blood findings, this data provides strong evidence that long-lived, antigen-experienced GvL T cells are established early post-alloSCT and may persist for years across blood and bone marrow compartments. These observations support a model in which GvL surveillance is maintained not only by $CD8^+$ cytotoxic T cells, but by long-lasting conventional $CD4^+$ responses with helper or memory-like function. This is consistent with the evolving paradigm in which both subsets play important roles in GvL control, and raise the possibility that HLA class II-restricted T cells could mediate selective anti-leukaemic effects due to limited expression of class II outside the haematopoietic compartment [140, 141, 193].

Despite these insights, each platform presented specific methodological constraints, predominantly reflecting the rarity of GvL T cells and the dual challenge of identifying unknown TCRs and their cognate antigens in an unbiased fashion.

The APC-T cell co-culture system offered a viable strategy for supporting the survival, expansion and enrichment of relevant T cells from the post-transplant bone marrow. Whilst this enabled sufficient expansion for downstream testing, the use of activation-induced marker assays to isolate peptide-responsive T cells was hindered by substantial background activation. Although it is possible to discriminate potential antigen-specific clonotypes from this activated pool using single-cell TCR sequencing, the cost and labour-intensiveness of this approach currently preclude its use outside of targeted screening of a few selected antigens. Technical refinements, such as the titration of co-stimulation, the incorporation of more selective activation markers or the development of alternate functional readouts may help to reduce non-specific signal and increase scalability.

The *ex vivo* single-cell strategy enabled the unbiased recovery of T cells at scale using the Parse Evercode platform. Whilst this method allowed for the high-throughput interrogation of over 400,000 single T cells, it was inherently limited to the detection of previously characterised GvL clonotypes, as the absence of functional readouts and paired antigen information restricts its capacity to identify novel GvL responses.

Additionally, the rarity of GvL-reactive T cells, even in this enriched cohort, means that biologically relevant clonotypes may remain undetected due to stochastic dropout or by having frequencies below the limits of assay detection.

Though a minority of clonotypes could be annotated to known epitopes via cross-referencing with VDJdb, the majority lacked linked antigen data. Nonetheless, the resulting, large-scale dataset offers a valuable potential future resource for TCR-epitope inference. As predictive algorithms such as GLIPH2, DeepTCR and NetTCR2.0 continue to improve, reanalysis of this dataset may enable identification of novel TCR-peptide interactions or convergent motifs shared across patients [276–278].

While the identification of four GvL clonotypes in the *ex vivo* bone marrow is a significant advance, the low number of recovered antigen-specific T cells limits downstream functional interpretation. Future approaches might include the use of large-volume marrow sampling, combined with a targeted enrichment specific to these TCRs, such as through the use of peptide-MHC multimers, allowing for the selective isolation of rare GvL-reactive T cells prior to single-cell sequencing [249, 279].

Although their transcriptional signatures suggest prior antigen priming, particularly for GSTZ1-Clone 1, transcriptional state alone cannot confirm antigen specificity or effector potential.

No functional validation has yet been directly performed on the TCR clonotypes that were identified in *ex vivo* analyses. Whilst their independent detection

through orthogonal approaches at multiple timepoints supports their physiological importance, definitive validation will require experimental confirmation. A logical next step would be the re-expression of these GvL TCRs in healthy donor-derived T cells via lentiviral editing as described in previous chapters. This could be followed by activation or even killing assays against patient-derived targets. Such validation would provide definitive evidence for antigen specificity and effector potential.

From a translational perspective, the absence of significant GvHD in the patients in whom these clonotypes were detected suggests that, at the low frequencies observed, they were not associated with overt deleterious host reactivity. However, this does not establish that the same TCRs would be safe if transferred at higher numbers in the setting of TCR-engineered cellular therapy. A critical requirement for translation is the selective induction of GvL without GvHD, and this cannot be assumed from the transcriptional profile alone. Additionally, though the transcriptional profile of the original cells may offer insight into GvL control, the behaviour of a TCR is not dictated solely by the phenotype of the cell in which it was originally isolated, since engineered TCRs can be expressed in diverse cellular subsets.

Clonotypes such as GSTZ1-Clone 1, whose persistence, memory-associated features and non-exhausted transcriptional profile are supportive of a role in GvL immunity, should therefore be regarded as candidates for further study rather than as potential therapies. Rigorous functional testing will be needed to confirm their anti-leukaemic activity and their safety profile.

In parallel, longitudinal tracking of these clonotypes in blood and bone marrow may provide novel biomarkers for immune surveillance, ultimately enabling patient stratification and dynamic monitoring of GvL competence post-transplant, though this application will also require prospective validation to determine its predictive value.

In conclusion, the work presented in this chapter demonstrates the feasibility of detecting rare, antigen-experienced GvL T cells from early post-alloSCT bone marrow using integrated *in vitro* expansion and high-throughput *ex vivo* profiling. Whilst technical limitations persist, the persistence and transcriptional phenotype of these identified clonotypes strongly support their biological relevance. These findings advance our understanding of the early post-alloSCT T cell landscape and offer further basis for the mechanistic exploration of GvL.

6 Discussion

Contents

6.1 Overview

AlloSCT remains the most effective curative therapy for AML in patients with adverse risk disease, yet relapse remains the leading cause of mortality. The GvL effect, mediated by donor-derived T cells recognising patient-specific or AML-associated antigens, plays a central role in maintaining durable post-transplant remission. Several important gaps continue to limit the understanding and clinical exploitation of this response. A comprehensive, experimentally validated catalogue of endogenously processed and presented GvL targets is still lacking. The antigenic and contextual determinants that separate GvL from GvHD remain poorly characterised, and the relative contributions of effector compartments beyond conventional cytotoxic $CD8^+$ cells remain poorly quantified. Moreover, most human studies have focused on peripheral blood, with little work addressing bone marrow-resident T cells during the first post-transplant year, when relapse risk is highest and GvL may be most crucial.

The work presented in this thesis set out to address two challenges in this field. Firstly, the technical limitations that have hindered the isolation and characterisation of rare antigen-specific T cells from early post-alloSCT bone marrow. Secondly, the absence of systematic, longitudinal, compartment-spanning data linking early marrow clonotypes to their persistence in later blood samples. Culture-based enrichment, functional testing, bulk and single-cell sequencing and high-throughput transcriptomics were integrated to develop a sensitive methodological framework for identifying, validating and characterising these cells.

A polyclonally-stimulated culture method was developed that was capable of reliably expanding T cells from cryopreserved early post-alloSCT bone marrow samples, overcoming the poor viability and lack of proliferation that had limited earlier antigen-specific expansion attempts. While this approach reliably enriched for $CD3^+$ cells and maintained TCR repertoire diversity, it was insufficiently sensitive to detect very low-frequency GvL-reactive clonotypes, which required

targeted enrichment to reach the threshold for detection. This highlighted the compromise between yield and specificity that is required when interrogating rare T cell populations.

Using antigen-specific stimulation of later peripheral blood samples, a $CD4^+$ TCR clonotype targeting a patient-specific METTL22 variant was identified and functionally validated, demonstrating strict HLA-DR dependence, representing, alongside the PADI4-specific TCR studied in prior, unpublished work by the Vyas lab (section 1.10, [198]), one of the few functionally validated class II-restricted GvL TCRs.

An APC-T cell co-culture system was subsequently applied to early post-alloSCT bone marrow, in combination with AIM-based FACS enrichment, to recover GSTZ1 and WASHC4-specific T cells expressing TCRs that had previously been detected in the late peripheral blood. These clonotypes were independently confirmed through high-throughput *ex vivo* single-cell profiling, which also identified clonotypes previously shown to be enriched in T cells reactive to two additional GvL miHAs. This platform enabled clonotypic identification and phenotypic annotation without the confounding effects of culture, confirming the low but true *in vivo* frequency of these clones, demonstrating that certain GvL clonotypes are established within the first year post-alloSCT and persist for years across compartments. Integration of transcriptomic data further revealed that the *ex vivo* phenotype of GSTZ1-specific T cells was consistent with Th1-polarised central memory, highlighting long-lived $CD4^+$ populations as potential key contributors to durable GvL surveillance alongside cytotoxic $CD8^+$ effectors.

The sections that follow discuss these findings within the broader context of post-alloSCT immunology, considering their implications for the dynamics of GvL immunity, the methodological challenges of detecting GvL-reactive clones, the diversity of GvL effector phenotypes *in vivo* and the translational potential of GvL

for therapeutic and diagnostic applications.

6.2 Dynamics of Immune Reconstitution and GvL Immunity

Analysis of the early post-alloSCT bone marrow revealed a number of TCR repertoire features that were broadly consistent with established models of immune reconstitution. In samples with longitudinal sampling, TCR repertoire diversity increased progressively over time, and the most abundant clonotypes seen were frequently virus-specific, particularly CMV, reflecting the well-documented dominance of CMV-specific immunity in shaping the post-alloSCT immune landscape and influencing the breadth of subsequent repertoire recovery [100–102].

Within this background of viral dominance, rare GvL-reactive clonotypes were detected directly *ex vivo* in bone marrow as early as six months post-alloSCT. The identification of GSTZ1-, WASHC4-, and RNF123-specific $CD4^+$ clonotypes in this setting represents a novel finding in a field dominated by $CD8^+$-mediated responses identified in the peripheral blood. The persistence of these clonotypes across years and compartments is highly suggestive of physiological significance. The presence of long-lived $CD4^+$ clonotypes also aligns with the increasing evidence that demonstrates the capacity of $CD4^+$ subsets to mediate durable anti-tumour immunity albeit in the solid tumour setting [46, 47]. These putative GvL clones have not yet been comprehensively functionally validated, and demonstrating they are able to effectively recognise endogenously processed and presented peptide in a specific manner will be crucial.

Given that immune reconstitution at six months post-alloSCT remains incomplete, especially for the slower-to-recover $CD4^+$ compartment, the ontogeny of these GvL T cells remains uncertain [90].

In patient OX289, GvL clonotypes were detectable at six months, raising the possibility that they were transferred with the graft, and maintained via homeostatic peripheral expansion. The clinical efficacy of DLI in the wider setting, where durable remissions can be achieved through adoptive transfer of donor T cells, supports a donor origin for at least some GvL cells [129, 130]. It is also plausible that these reflect donor-derived memory T cells that, though originally primed against unrelated antigens, cross-react with patient-specific GvL epitopes [280].

Within the GvL-enriched cohort, post-DLI GvL-reactive T cells were not detected. Patient OX866 experienced an early post-alloSCT relapse which was treated to a durable remission with salvage chemotherapy and DLI, and despite assessment of the post-DLI marrow with *ex vivo* high-throughput single-cell approaches, no corresponding GvL clone was seen, although assay sensitivity cannot exclude their presence.

In contrast, the delayed appearance of certain clonotypes suggests a possible contribution from *de novo* thymopoiesis, highlighting two potential sources of GvL immunity. In patient OX885, GvL clonotypes were only detectable at 12 months, but not three months, raising the question of whether they arose via thymic output, or whether they were present but undetected. Importantly, the apparent absence of these clonotypes at early timepoints cannot be assumed to represent true biological absence, as low cell input numbers and assay sensitivity may have caused these cells to fall below the thresholds of detection.

These findings also emphasise the technical limitations inherent to screening the early post-alloSCT bone marrow. T cell numbers are low, restricted by conditioning, immunosuppression and the biology of T cell reconstitution [227, 228]. With the functional methods used here, detection was constrained to previously defined antigens due to low cell numbers, and TCR detection was limited to known sequences, severely narrowing and biasing the search for GvL responses. Additionally, at this timepoint, diversity of the TCR repertoire is lower, potentially further narrowing the experimental remit.

While the *ex vivo* frequencies of GvL clones were not established in the late peripheral blood, ascertaining this would be a prudent next step. The relative comparative ease with which these clones were identified in the late peripheral blood does suggest a higher frequency, however. Direct quantification of *ex vivo* frequencies at this later timepoint could establish if these GvL clones become immunodominant in the fully reconstituted host.

These factors highlight a balance between the clinical importance of interrogating early timepoints and the substantial technical challenges of doing so. It is not clear whether experimental efforts to identify GvL responses are best directed at these early timepoints, or at later intervals, where it is experimentally less challenging and long-lived responses can be detected.

Despite these caveats, the recovery of rare, persistent $CD4^+$ GvL clonotypes in the early marrow provides important evidence for the timing and durability of anti-leukaemic immunity post-alloSCT. It suggests that GvL surveillance can be established early, and that long-lived $CD4^+$-mediated responses can occupy a stable and relevant niche despite the dominance of viral-specific clonotypes. The low frequencies of these cells (at 0.01-0.1%) demonstrate that scarcity does not necessarily preclude relevance. This principle echoes broader immunological observations of pathogen-specific responses that rare T cell populations can be stably maintained, expand upon encountering antigen and provide effective protective immunity [281, 282].

Should the detection of these clones at early timepoints become relevant in the prediction of relapse, this may be challenging given the depth required to detect them reliably. Establishing whether the presence or absence of early GvL clonotypes predicts outcome will require larger, longitudinal cohorts and a more diverse catalogue of GvL responses, addressing their utility as biomarkers of durable remission. Future studies could also aim to clarify the ontogeny of these cells by combining longitudinal sampling in patients to track T cell clones during immune reconstitution combined with donor repertoire analyses, determining whether these

T cells are graft-derived or thymically generated.

6.3 Identification of Rare GvL-Reactive T Cells

The detection of rare, antigen-specific GvL T cell populations in the post-alloSCT setting presents substantial methodological challenges. The low starting frequency of these cells, low viability and limited cell numbers available from bone marrow aspirates necessitate the use of a discovery platform that is both highly sensitive and selective.

In this work, four main approaches were employed, each with distinct advantages and drawbacks.

Polyclonally-stimulated T cell culture, whilst yielding high numbers of expanded cells, lacked targeted enrichment and produced cultures dominated by T cells of irrelevant specificities.

Antigen-specific stimulation, in contrast, did allow for enrichment of T cells of a desired specificity using late PBMC samples, but did not function in the setting of the early post-alloSCT bone marrow, where cryopreserved samples underwent early cell death following thaw. Notably, many trials with this approach also failed to recover even abundant virus-specific T cells from the early bone marrow, pointing to a more generalised defect in proliferative capacity in the early post-alloSCT compartment.

Co-culture of autologous APCs with T cells allowed sufficient stimulation for survival whilst mediating enrichment of antigen-specific cells. However, this method was hampered by high levels of background activation, resulting in difficulties in disentangling physiologically relevant GvL responses from non-specific background.

Finally, high-throughput *ex vivo* profiling provided an unbiased means of capturing TCR clonotypes directly, but the inability to infer cognate antigens from unknown TCR sequences restricted this approach to previously defined clonotypes, precluding the discovery of truly novel responses. Should there be significant advances in TCR antigen-prediction, straightforward *ex vivo* sequencing could in

future provide a powerful means to uncover novel GvL responses.

These approaches exemplify the tension between throughput and specificity, a broader theme common to antigen discovery across cancer immunology. Computational and multimer-based screens provide high throughput at the expense of physiological fidelity, as only a small fraction of predicted or enriched candidates prove to be immunogenic. Immunopeptidomics offers a physiologically derived catalogue of presented epitopes but suffers from high input requirements, technical noise, under-sampling of low-affinity peptides and a persistent validation bottleneck. Reverse immunological approaches, while valuable, are inherently uncoupled from physiological function, and therefore require rigorous functional validation [283, 284].

Lower-throughput, functional assays, such as the cultured IFNγ ELISpot, are more physiologically faithful but lack scalability. A central limitation of current functional discovery platforms is that they operate under highly permissive conditions, where peptide abundance and co-stimulatory signals are optimised to maximise sensitivity. These conditions are invaluable for detection but provide little insight into how TCRs behave *in vivo*, where antigen density, stromal interactions, inhibitory checkpoint engagement and the cytokine milieu all vary considerably. This limitation is particularly evident in the solid tumour setting, where many T cells identified as antigen-specific *ex vivo* prove to be exhausted or anergic *in situ* [285, 286]. Multimodal single-cell approaches that couple antigen specificity with cell phenotype, such as with the identification of GSTZ1-specific T cells as a non-exhausted Th1-polarised T_{CM} population, will be crucial to bridge this gap.

The net consequence across all these methods remains that only a minority of candidate antigens prove to be naturally processed, presented and capable of eliciting robust T cell activation. The paramount importance of functional validation can be seen in the identification of METTL22 clonotypes, where only one of three TCRs tested was able to activate specifically in response to the patient's SNP.

The small number of validated antigens and clonotypes recovered here is therefore partially a reflection of the wider field but also the methodology used.

The initial reverse immunological pipeline used to generate the peptide library used to screen for responses in the GvL-enriched cohort will not have generated an exhaustive list of candidates. The use of whole genome and exome sequencing to identify mismatches is limited by sequencing depth, and is restricted only to peptide-coding differences, and therefore would not screen for tumour-associated or cryptic antigens. Additionally, the *in silico* algorithms used at the time, NetMHCpan 4.0 and NetMHCIIpan 3.0, are imperfect, especially in the context of class II, and only the highest-affinity binders were selected for screening [201, 284]. These have since been updated and could yield further undiscovered GvL responses.

Combinatorial pipelines that integrate *in silico* prediction with immunopeptidomics can further help refine and prioritise candidates, further improving the selection of candidate peptides.

In summary, while the approaches used here enabled the identification of a number of rare GvL-reactive T cell clones, they also highlight the intrinsic limitations of current methods. Overcoming these barriers will require the development of discovery platforms that combine the sensitivity necessary to detect low-frequency populations with the specificity to distinguish genuine GvL responses from background. This reflects a fundamental challenge across cancer immunology, in that rare physiologically relevant T cells are embedded within a vast repertoire, and only a minority of predicted candidates withstand the scrutiny of functional validation [287, 288].

6.4 Phenotypic and Functional Heterogeneity of GvL T cells

T cells reactive to five GvL antigens were recovered and validated across the different methodological approaches, offering the opportunity to investigate their

transcriptional phenotype.

The METTL22-specific clonotype represented an activated population of $CD4^+$ T cells with robust cytotoxic activity. METTL22-Clonotype 1 was able to recognise a patient-specific SNP presented on HLA-DR and its transcriptional phenotype was enriched for cytotoxic markers *NKG7*, *GZMB*, *PRF1* and effector molecules such as *IFNG* and *FASLG*. However, the conditions under which this clonotype was recovered skew interpretation. The clonotype was first expanded in a cytokine-rich environment with high-dose IL-2 and repeated stimulation, conditions known to bias $CD4^+$ differentiation towards cytotoxic effector function [254]. As such, the cytotoxic phenotype demonstrated *in vitro* may not accurately reflect behaviour *in vivo*, where antigen density is lower and cytokine support limited. While the METTL22 clone demonstrates that these cells are able to differentiate into potent cytotoxic effectors, whether this occurs physiologically is uncertain.

Two further clonotypes, reactive to GSTZ1 and WASHC4, were also initially identified through culture-based approaches. These $CD4^+$ cells displayed a mature Th1-polarised effector profile but again, the culture conditions likely accentuated differentiation.

Unlike the *in vitro* conditions, the recovery of GSTZ1 and WASHC4-specific $CD4^+$ T cells from the *ex vivo* single-cell sequencing captures the phenotype of these cells as they exist in the marrow. Although limited by small sample numbers, these observations offer insight into the physiological states of these GvL T cells.

Among the *ex vivo* identified clones, GSTZ1 was the most robustly recovered, with sufficient cell numbers to allow for basic phenotypic annotations. GSTZ1-specific T cells expressed a Th1-polarised transcriptional programme, matching the effector function identified in the *in vitro* work. However, these cells were less differentiated *ex vivo*, harbouring a central memory phenotype. This implies that while GSTZ1-specific T cells are antigen-experienced, they retain proliferative potential and long-term persistence, rather than being terminally committed to effector differentiation. This poised state may underpin their ability to provide

durable surveillance and prevent relapse, as seen in the patient from which these cells were isolated.

The *ex vivo* recovery of $CD4^+$ clones reactive to WASHC4 and RNF123, although at much lower frequencies, reinforces the credibility of class II-restricted GvL T cells, even if their effector functions remain to be defined. Regardless, their presence across timepoints and compartments suggests that $CD4^+$-mediated immune surveillance may be a consistent and increasingly recognised feature of GvL.

The FTSJ3-reactive clonotype represented a more conventional GvL response. Identified as a $CD8^+$ T_{EM}/T_{EMRA} subset, these cells conformed to the established model of alloantigen-specific $CD8^+$ cytotoxicity. Their presence validates the contribution of canonical effectors, and though it was the sole $CD8^+$ effector, this is unsurprising as only four of the 22 previously identified GvL responses were not $CD4^+$-mediated, limiting the range of surveyed $CD8^+$ responses in the *ex vivo* dataset. Together, these findings reinforce that both $CD4^+$ and $CD8^+$ compartments contribute to GvL and highlight that CD4-restricted clonotypes may be an underappreciated arm of this immunity.

The prominence of CD4-restricted clonotypes in this work aligns with the growing importance of $CD4^+$-mediated immunity in immuno-oncology. $CD4^+$ T cells can act as active and versatile anti-tumour effectors, mediating tumour control through a number of mechanisms that include direct cytotoxicity, recruitment of alternate effectors and reshaping the tumour microenvironment [289, 290]. Though $CD4^+$ T cells are known to be important in GvL, the mechanism by which they control leukaemia is not yet fully elucidated.

GSTZ1, WASHC4 and RNF123 are all ubiquitously expressed proteins that are not enriched within the haematopoietic system [205–207]. Recognition of these antigens might be expected to precipitate GvHD, however, this was not observed in the clinical course of these patients. As HLA class II expression in steady state is largely confined to professional APCs and the haematopoietic compartment, GvHD

target tissues may be spared from $CD4^+$ T cell recognition [191, 194]. In this way, class II-restricted responses against widely expressed proteins can, in principle, mediate selective GvL without concomitant systemic GvHD, although it is unclear if this extends beyond this physiological setting, where these putative GvL cells are present at low frequencies.

Regardless, the functional impact of these clonotypes is ultimately determined by their *in vivo* context. AML blasts can evade GvL by escaping recognition, such as through downregulation of class II HLA, or by impairing T cell effector function via inhibitory interactions that drive exhaustion or anergy [140, 291]. Both mechanisms mean that T cells which appear potent *in vitro* may fail to exert clinically relevant effects *in vivo*.

These considerations highlight the added value of coupling antigen-specificity with transcriptional profiling. Whereas loss of HLA-mediated antigen presentation would render T cells ineffective irrespective of their state, phenotypic profiling can distinguish whether T cell clones retain non-exhausted, memory-like features consistent with durable GvL, or instead represent exhausted or anergic remnants. For example, in this work, the identification of GSTZ1-reactive T cells as a non-exhausted Th1-polarised T_{CM} phenotype supports their potential role as *bona fide* effectors.

Extending paired analyses across additional antigens will be key in discriminating durable GvL mediators from ineffective bystanders, and therefore prioritising which clonotypes represent the most promising candidates for further exploration.

Future work could build on these observations by moving beyond transcriptional signatures alone. Should larger numbers of GvL T cells be isolated, further insight could be gained through the use of deeper sequencing or multi-omic approaches that integrate chromatin accessibility and surface proteomics, providing a higher-resolution view of the differentiation states that underpin durable GvL. Additionally, spatial studies of bone marrow trephine biopsies could be used to define how these T cells are positioned relative to AML and the microenvironment, interrogating the

interactome and clarifying whether supportive niches drive GvL T cell persistence. Comparative studies across larger cohorts will also be needed to establish whether particular T cell populations recur consistently, and whether the predominance of $CD4^+$-restricted responses observed here is generalisable.

Together, these findings underscore that GvL immunity is both phenotypically diverse and context-dependent. The key challenge is to disentangle which clonotypes represent durable effectors, paving the way to gaining a deeper understanding of GvL and selectively harnessing these responses for therapeutic use.

6.5 Translational Applications of Validated GvL Responses

In addition to clarifying the underlying biology, the identification and validation of molecularly-defined GvL antigens and their cognate TCRs can potentially be leveraged for clinical benefit.

Previous studies examining limited panels of miHAs have yielded conflicting results on whether miHA mismatching predicts relapse outcomes, with an association between increased mismatching and the incidence of GvHD [187, 195, 196]. One of the main pitfalls of these studies is that in the selection of miHAs covered, all but three were HLA class I-restricted, and were not pre-selected on the basis of GvL exclusivity. The use of validated, GvL-reactive class II-restricted antigens, such as GSTZ1, alongside haematopoietically-restricted antigens, could generate a selective panel of mismatches that could predict durable GvL whilst avoiding prohibitive GvHD. A broader catalogue of validated responses will be essential if donor selection is to progress beyond HLA-matching alone.

This work has demonstrated that defined clonotypes can be recovered as early as six months post-alloSCT and persist across years and compartments at low,

but detectable frequencies. These features make them potential candidates as biomarkers for relapse surveillance, allowing for the direct measurement of the abundance of protective GvL clonotypes alongside conventional MRD monitoring, thereby assessing both anti-leukaemic immunity and disease burden. A decline in protective clones could therefore act as an early signal of impending relapse, allowing for early clinical interventions such as DLI or maintenance chemotherapy.

The identification of these selective GvL responses could also potentially shape therapy. $CD4^+$ DLIs have previously been shown to be able to enhance donor chimerism and promote GvL in the absence of GvHD [192]. Though historically DLI infusion products do not undergo filtering for T cells of known phenotypes or specificities, it is possible that future DLIs could be refined by enriching for central memory T cells or validated antigen-specific clonotypes, improving their capacity to promote durable remission.

Additionally, though transgenic miHA-specific T cells have been used with class I-restricted antigens, such as HA-1 and WT-1, the class II space has not yet been explored in the context of AML [166, 188]. Given the restricted tissue expression of class II, T cell therapies do not necessarily need to be limited to targeting haematopoietically-restricted or leukaemia-associated antigens, widening the pool of potential targets.

Regardless, a key limitation for translation is the need to account for population frequencies of antigen-HLA combinations. No matter how well-validated an individual TCR-antigen pair, their applicability is restricted to the fraction of patients carrying these mismatches. Overcoming this will require prioritising investigation of common HLA alleles and polymorphisms, assembling a broad panel of validated TCRs to broaden coverage. While limited by scale and constrained by rarity, detailed characterisation of individual GvL TCRs can nonetheless provide a foundation for developing practical strategies for improving post-alloSCT outcomes.

6.6 Concluding Remarks

The work outlined in this thesis demonstrates that rare GvL-reactive clonotypes can be detected in the early post-alloSCT bone marrow and persist across years and compartments, establishing them as genuine *in vivo* responses rather than artefacts of culture. Their predominance within the $CD4^+$ compartment, with transcriptional states consistent with Th1-polarised central memory, highlights a durable and underappreciated role for $CD4^+$ T cells in GvL surveillance alongside conventional $CD8^+$ cytotoxicity.

The methods employed underscore the challenges of recovering and validating such rare populations, with each platform requiring a balance between sensitivity, specificity, and scalability. Nevertheless, the persistence and phenotype of validated clones extend our understanding of the diversity of GvL immunity and contribute to the growing catalogue of clinically relevant minor histocompatibility antigens.

Appendices

A

Supplementary Clinical Data

Patient ID	Gender	Age at Diagnosis	ELN 2022 Genetic Risk	Cytogenetics	Mutations in Recurrently Mutated Genes
OX289	F	52	Intermediate	Normal	MPL, PARP4, SH2B3, SMC1A
OX607	F	50	Intermediate	Normal	NPM1, FLT3 ITD, DNMT3A, TET2
OX628	M	50	Favourable	Normal	NPM1, DHX15, IDH2, MED2
OX690	F	29	Adverse	47, XX, +21	ASXL1, IDH2, KMT2C, RUNX1
OX717	M	16	Favourable	Inv(16)	KRAS
OX747	F	48	Intermediate	46, XX, add(3)(q21), add(5)(q3?4)	FLT3 ITD, CUX1, KMT2D
OX802	F	48	Intermediate	Normal	DNMT3A
OX866	M	51	Intermediate	46, XY, t(5;11;9)	FLT3 ITD, ASXL2, KMT2C, WT1
OX885	F	42	Intermediate	Normal	FLT3 ITD CBL, STAT5B
OX993	M	59	Intermediate	Normal	ASXL2, CEBPA, CUX1, KMT2C, RIT1
OX1098	F	60	Intermediate	Not known	FLT3 ITD, DNMT3A, KIT
OX1149	M	41	Favourable	47, XY, +4	NPM1, IDH1, KIT

Figure A.1: Baseline characteristics of the GvL-enriched Cohort. The ELN 2017 genetic risk was determined according to cytogenetic and molecular genetic features of disease at diagnosis [9]. M = Male. F = Female. FLT3 ITD = FLT3 internal tandem duplication.

Patient ID	First-Line Chemotherapy	Refractory/ Relapsed Disease	Salvage Chemotherapy	Disease Status at Transplant	Donor Type	Conditioning	Relapse	Salvage Treatment	Donor Lymphocyte Infusions	Clinical Status
OX289	DA (x1)	-	-	CR1	Matched Sibling	RIC Flu/Mel	-	-	-	Alive (12 years)
OX607	DA (x1); DA + Lestaurtinib/Placebo (x1); HiDAC + Lestaurtinib/Placebo (x1)	-	-	CR1	Matched Sibling	RIC Flu/Mel with PTCy	-	-	-	Alive (13 years)
OX628	DA (x1); DA + Everolimus/Placebo (x1); HiDAC + Everolimus/Placebo (x1)	Molecular Relapse	FLAG-Ida (x1)	Morphological CR2	12/12 MUD	RIC Flu/Mel/Alem	-	-	Yes (x3, from 11 months) - For falling donor chimerism	Alive (12 years)
OX690	DA (x1); DA + Everolimus/Placebo (x1); HiDAC + Everolimus/Placebo (x1)	-	-	CR1	Matched Sibling	MAC Bu/Cy with PTCy	Morphological Relapse (11 years)	Ven/Aza (x4) to 2nd AlloSCT	-	Alive (13 years)
OX717	DA (x1); DA + GO (x1); HiDAC (x2)	Molecular Relapse	FLAG-Ida (x1)	MRD Positive	11/12 Sibling	MAC Thiotepa/Bu/Flu/ATG	-	-	-	Alive (12 years)
OX747	DA (x2)	-	-	CR1	Haploidentical Sibling, after failed MUD	RIC Cy/Flu/TBI	-	-	-	Alive (12 years)
OX802	DA (x1); HiDAC (x2)	-	-	CR1	Matched Sibling	RIC Flu/Mel with PT-MTX	-	-	-	Alive (12 years)
OX866	DA (x1)	Refractory Disease	FLAG-Ida (x2)	CR	Matched Sibling	RIC Flu/Mel	Morphological Relapse (3 months)	FLAG-Ida (x1); FLA (x1)	Yes (x3, from 7 months) - For relapse	Alive (11 years)
OX885	DA (x2); HiDAC (x1)	Morphological Relapse	FLAG-Ida (x1)	CR2	11/12 MUD	RIC Flu/Mel/Alem	-	-	Yes (x2, from 1 year) - For falling donor chimerism	Alive (11 years)
OX993	DA (x2); HiDAC (x1)	Morphological Relapse	FLAG-Ida (x1)	CR2	11/12 MUD	RIC Flu/Amsacrine/ Ara-C/Bu/ATG	Morphological Relapse (7 years)	Ven/Aza (x8)	Yes (x2 from 8 years) - For relapse	Alive (9 years)
OX1098	DA (x1)	Refractory Disease	FLAG-Ida (x1)	CR	12/12 MUD	RIC Flu/Amsacrine/ Ara-C/Bu/ATG	Morphological Relapse (7 years)	Ven/Aza (x6)	Yes (x3 from 9 years) - For relapse	Alive (9 years)
OX1149	DA + GO (x1); DA (x1); HiDAC (x2)	Molecular Relapse	FLAG-Ida (x1)	MRD Positive	Matched Sibling	RIC Bu/Cy with PT-MTX	-	-	-	Alive (8 years)

Figure A.2: Treatment summary for GvL-enriched cohort. Number of chemotherapy cycles in brackets next to regime. Number of years post-alloSCT in brackets in clinical status. Please refer to abbreviations for individual chemotherapeutic agents

Patient ID	Donor Chimerism	Acute GvHD	Chronic GvHD	Post-AlloSCT Systemic Immunosuppression
OX289	3 months: 84.9%; 4 months: 77.3%; Full from 5 months	Nil	Mild Mouth/GI	Budesonide (11 months); Ciclosporin (16 months)
OX607	Full throughout	Nil	Nil	Ciclosporin (5 months)
OX628	11 months: 46.1% - followed by DLI; 12 months: 67.9% followed by DLI; 14 months: 81.1% followed by DLI; Full from 16 months	Nil	Mild Skin	Ciclosporin (4 months)
OX690	5 months: 86.9%; 12 months: 92.5%; Full from 14 months	Grade 3 Liver	Moderate Liver	Prednisolone (6 months); Ciclosporin (15 months)
OX717	Full throughout	Grade 1 Skin	Nil	Ciclosporin (5 months)
OX747	Full throughout	Grade 1 Skin	Mild Mouth/Skin	Mycophenolate (4 months); Prednisolone (8 months); Ciclosporin (11 months)
OX802	Full throughout	Grade 1 Skin	Severe Mouth/Skin/Gut/ Liver/Ocular/Neutropenia	Ciclosporin (6 months, reintroduced at 11 months and stopped again at 3 years); Multiple prednisolone courses for flares
OX866	3 months: 80% with relapse followed by 3x DLI; Full from 5 months	Nil	Nil	Ciclosporin (3 months)
OX885	8 months: 13.5% followed by DLI; 13 months: 44%; 15 months: 62% followed by DLI; Month 20: 92%	Grade 1 Skin	Nil	Ciclosporin (4 months)
OX993	3 months: 90%; 5 months: 90%; 11 months: 90%	Grade 1 Skin	Mild Skin	Mycophenolate (2 months); Ciclosporin (6 months)
OX1098	14 months: 84%; 23 months: 83%; 44 months: 87%	Nil	Nil	Ciclosporin (5 months)
OX1149	Full throughout	Grade 1 Skin	Mild Mouth	Ciclosporin (6 months)

Figure A.3: GvHD, immunosuppression and chimerism data from the GvL-enriched Cohort. Timepoint of immunosuppression cessation is outlined in brackets.

Patient	A	A	B	B	C	C
OX289	*02:05	*23:01/05/06/08/10/11-19	*44:03/13/26/30/32/36-61	*58:01/04/11/13/15	*04:01/05/08/10/12/16-33	*07:01/06/16/18/20/21/24-57
OX607	*24:02/09N/11N/14/15/20-144	*26:01/08/11N/12/14-50	*27:05/13/28/37/38/45-67	55:01-03/05/10/11/15-43	*01:02/06/08/11/15-18/20-40	*03:03/13/18/20N/22Q-88
OX628	*24:02	*03:01:01	*44:02:01	*08:01	*07:01	*05:01
OX690	*24:02/09N/11N/15/17-144	*11:01/05/07/09/12/13-64	*13:02/03/14-16/19/30-38	*51:01/03/11N/12/14/17-96	*03:03/13/18/20N/22Q-88	*06:02/03/07/09/10/12-45
OX717	*68:01:01	*11:01:01	*55:01:01	*15:01:01	*03:04:01	*03:03:01
OX747	*01:01:01	-	*51:01:01	*40:01	*03:04:01	*06:02:01
OX802	*32:01-03/05/06/09-46	*11:01/05/07/09-13/21N-64	*35:01/05/17/23/30/32-202	*08:01/07/11/14/15/18-93	*04:01/05/08/10/12/16-127	*07:02/10/13/15/23/32N-262
OX866	*26:01/08/11N/12/14-77	*02:01/06/09/21/25/26-374	*27:05/13/28/37/38/45-87	*08:01/11/13-15/18/19-94	*07:01/06/16/18/20/21-263	*01:02/06/08/11/15-73
OX885	*02:05:01	*24:02	*18:01:01	*49:01	*07:01	-
OX993	*24:02	*02:01:01	*40:01	*18:01:01	*12:03	*03:04
OX1098	*02:01:01	-	*57:01:01	*40:01	*06:02	*03:04:01
OX1149	*34:02:01	*24:02	*55:01:01	*58:02	*06:02	*01:02

Figure A.4: Class I HLA typing for the GvL-enriched cohort.

Patient	DRB1	DRB1	DRB3	DRB3	DRB4	DRB5	DQA1	DQA1	DQB1	DQB1	DPB1	DPB1
OX289	*03:01	*07:01:01	*02:02/05/11/13/14/17-23	-	-	-	*02:02	-	*02:02	*02:01/02/04	*04:01:01	*02:01:02
OX607	*01:01:01	*13:02:01	*03:01-03	-	-	-	*01:02/06	-	*06:04/27/36/38/39	*05:01	*04:02	*02:01
OX628	*03:01	*11:01:01	*01:01/04	-	-	-	*01:02/06	*05:01	*02:01:01	*06:02:01	*04:01:01	-
OX690	*07:01:01	-	-	-	*01:01-04/07	-	*02:02	-	*02:02	*02:01/02/05	*17:01	*13:01
OX717	*14:54	*15:01	*02:02/28/29N	-	-	*01:01:01	*01:02/06	*01:01/04/05/07	*06:02:01	*05:03:01	*05:01	*04:01:01
OX747	*04:04:01	*13:02:01	*03:01-03	-	*01:03	-	*01:02/06/08/09	*03:01-03	*03:02:01	*03:02:01	*10:01	*03:01:01
OX802	*03:01	*11:01	*02:02/28/29N	-	-	-	*05:01	*05:05/08-11	*02:01	*03:03:01	*04:01/*121:01	-
OX866	*03:01	*08:01	*01:01/03-06/09/13/15	-	-	-	*04:01-04	*05:01	*02:01	*02:04:02	04:01/*120:01N/*121:01/*129:01/*134	-
OX885	*11:04:01	*04:05:01	*02:02/28/29N	-	*01:03	*01:01:01	*03:01-03	*05:05/08/09/11	*03:01:01	-	*04:01:01	-
OX993	*01:01	*11:01	*02:02/28/29N	-	-	-	*01:01/02/04-09/11/12	*05:05/08/09/11	*03:01:01	*05:03:01	*04:01:01	-
OX1098	*07:01:01	*15:01:01	-	-	*01:03:01:02N	*01:01:01	*01:02/06/08/09/11	*02:01	*06:02:01	*03:03:02	*04:01:01	-
OX1149	*13:01	*11:02:01	*02:02/28/29N	*01:01/04	-	-	*01:03/10	*05:05/08/09/11	*03:01:01	*06:03:01	*02:01:02	-

Figure A.5: Class II HLA typing for the GvL-enriched cohort.

B
Supplementary Figures

Patient	Timepoint post-alloSCT	Gene	Peptide ID	Patient Peptide Sequence	Donor Peptide Sequence	CD4/CD8 Response
OX289	6 years	*NAGPA*	1	ALAFLLLISIAANLSLLLSR	ALAFLLLISTAANLSLLLSR	CD8
		RNF123	1	EVQDCLKQLMMSLLQLYRFS	EVQDCLKQLMMSLLRLYRFS	CD4
		LLGL2	1	GYSPSLHILAIGTRSGAIKL	GYSPSLRILAIGTRSGAIKL	CD4
		ENDOD1	1	VATFPVYTMVAIPIVCKD	VATFPVYTMGAIPIVCKD	CD8
		HENMT1	1	PPLYRQRYQFIKNLVDQHEP	PPLYRQRYQFVKNLVDQHEP	CD4
			2	PLYRQRYQFIKNLVDQHEPK	PLYRQRYQFVKNLVDQHEPK	
		ACADS	1	VSRPELLRESISAFLVPMPT	VSRPELLREGISAFLVPMPT	CD4
			2	TDRALQNKSISAFLVPMPTP	TDRALQNKGISAFLVPMPTP	
		LRR1	1	EPPVDICLSKAISSSLKGFL	EPPVDICLSKANSSSLKGFL	CD4
		FTSJ3	1	GETGMFSLSTIRGHQYATY	GETGMFSLCTIRGHQYATY	CD8
		LGALS8	1	MNYVSKRLPFAARLNTPMGP	MNYVSKSLPFAARLNTPMGP	CD4
OX628	6 years	*LITAF*	1	ITVQTVYVQHLITFLDRPIQ	ITVQTVYVQHPITFLDRPIQ	CD4
			2	QTVYVQHLITFLDRPIQMCC	QTVYVQHPITFLDRPIQMCC	
		PGLS	1	PGLISMFSSSQELGAALAQL	PGLISVFSSSQELGAALAQL	ND
OX717	5.5 years	*RHOT2*	1	TQRSVLLCKVVGARGVGKSA	TQRSVLLCKVVGACGVGKSA	ND
			2	KVVGARGVGKSAFLQAFLGR	KVVGACGVGKSAFLQAFLGR	
OX747	6 years	*DOCK8*	1	APISLSSFFNVSTLEREVTD	APISLSSFFSVSTLEREVTD	CD4
		METTL22	1	LELGAGTGLASIIAATMART	LELGAGTGLTSIIAATMART	CD4
			2	AGTGLASIIAATMARTVYCT	AGTGLTSIIAATMARTVYCT	
		DCAF13	1	VPREYVRALNATKLERVFAK	VPREYIRALNATKLERVFAK	ND
OX802	5 years	*COA6*	1	GQKSPRFRRVSCFLRLGRST	GQKSPRFRRVTCFLRLGRST	CD4
			2	RFRRVSCFLRLGRSTLLELE	RFRRVTCFLRLGRSTLLELE	
OX866	6 years	*PADI4*	1	LTISLLDTFNLELPEAVVFQ	LTISLLDTSNLELPEAVVFQ	CD4
			2	ISLLDTFNLELPEAVVFQDS	ISLLDTSNLELPEAVVFQDS	
OX885	4 years	*GSTZ1*	1	WRVRIALALKGIDYETVPIN	WRVRIALALKGIDYKTVPIN	CD4
			2	VRIALALKGIDYETVPINLI	VRIALALKGIDYKTVPINLI	
		WASHC4	1	DRAEKFNRGIRKLGITPEGQ	DRAEKFNRGIRKLGVTPEGQ	CD4
			2	EKFNRGIRKLGITPEGQSYL	EKFNRGIRKLGVTPEGQSYL	
OX993	2 years	*DENND6B*	1	LHRDKALLKRLLKGMQKKRP	LHRDKALLKRLLKGVQKKRP	CD4
			2	KALLKRLLKGMQKKRPSDVQ	KALLKRLLKGVQKKRPSDVQ	
OX1149	1 year	*RNH1*	1	AASCEPLASVLRAKLTSRSS	AASCEPLASVLRAKPTSRSS	CD4
		SLC26A6	1	GAGPDPLRLHGHLPVRTSCP	GAGPDPLRLRGHLPVRTSCP	CD4

Figure B.1: Summary of alloreactive responses identified in the late peripheral blood Mismatched amino acid between patient and donor peptide sequences highlighted in red. ND = not determined.

Target	Fluorochrome	Parameter	Clone	Supplier	Dilution
4-1BB	BV650	405-670/30	4B4-1	BD	1:50
CCR4	PE-Cy7	561-780/60	L291H4	BioLegend	1:200
CCR6	BV785	405-780/30	G034E3	BioLegend	1:50
CCR7	BV650	405-670/30	G043H7	BD	1:25
CD107a	BV421	405-450/50	H4A3	BioLegend	1:250
CD107b	BV421	405-450/50	H4B4	BioLegend	1:250
CD127	BV421	405-450/50	A019D5	BioLegend	1:50
CD25	BUV395	355-379/28	M-A251	BD	1:100
CD25	PE	561-585/15	BC96	BioLegend	1:25
CD28	FITC	488-530/30	CD28.2	BD	1:100
CD3	BUV805	355-812/34	SK7	BD	1:100
CD3	PE-Cy7	561-780/60	HIT3A	BD	1:100
CD3	AF700	640-730/45	OKT3	BioLegend	1:100
CD4	BUV563	355-580/30	SK3	BD	1:100
CD4	APC	640-670/30	OKT4	BioLegend	1:200
CD4	APC-Cy7	640-780/60	OKT4	BioLegend	1:100
CD40L	BUV805	355-812/34	TRAP1	BD	1:200
CD45RA	APC	640-670/30	HI100	BioLegend	1:50
CD69	APC	640-670/30	FN50	BioLegend	1:50
CD8	APC-Cy7	640-780/60	SK1	BD	1:100
CD8	FITC	488-530/30	SK1	BioLegend	1:100
CXCR3	PE	561-585/15	G025H7	BioLegend	1:100
FOXP3	PE-Cy5	561-670/30	PCH101	ThermoFisher	1:100
IFNg	PE-Cy7	561-780/60	B27	BD	1:50
mTCRb	BV711	405-710/50	H57-597	BD	1:80
OX40	BB700	488-695/40	ACT35	BD	1:50
PDL1	BUV395	355-379/28	29E.2A3	BD	1:200

Figure B.2: List of antibodies used during flow cytometry.

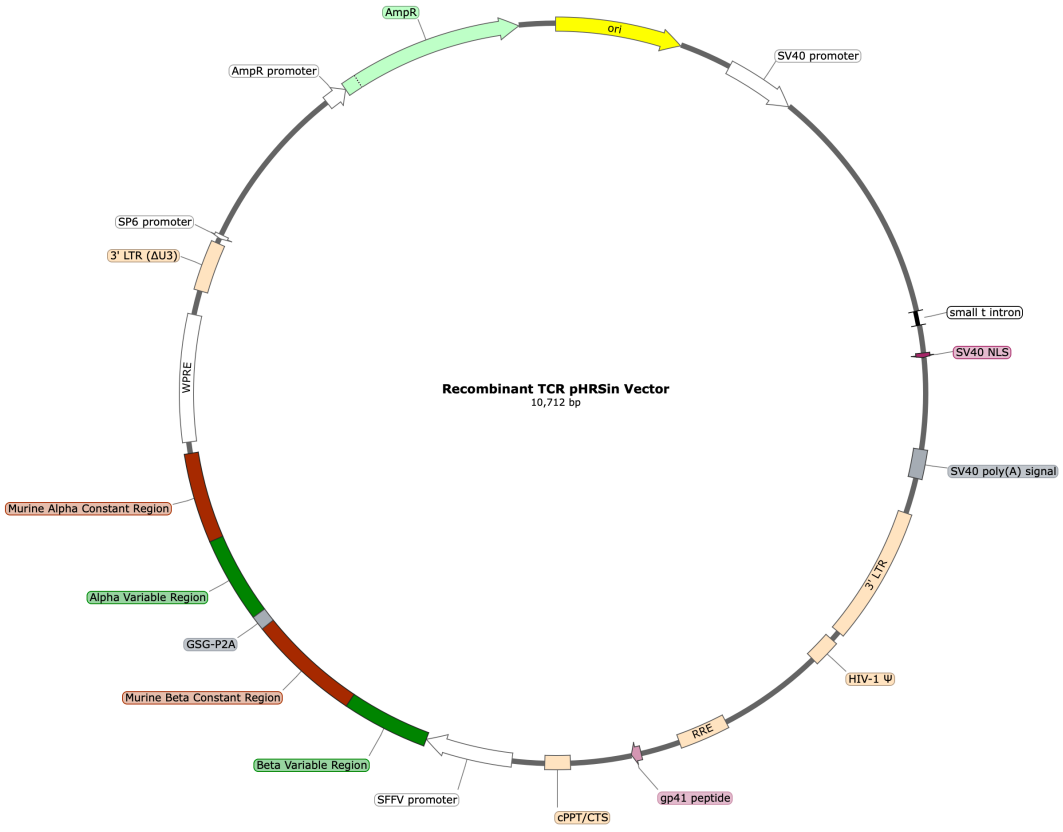

Figure B.3: Recombinant pHRSin vector map.

Geneset Name	Genes
Reactome	CD3D, CD3E, CD3G, CD247, LCK, FYN, ZAP70, LAT, LCP2, GRAP2, PLCG1, ITK, VAV1, RAC1, NCK1, NCK2, MAPK1, MAPK3
Rosenberg	CXCL13, PDCD1, LAG3, HAVCR2, TOX, CTLA4, ENTPD1, LAYN, TNFRSF9, CD38, GZMB, PRF1, IFNG, EOMES, TBX21, ICOS, HLA-DRA, ITGAE, CD69, IL7R
TNaive	SELL, CCR7, TCF7, IL7R, LEF1, BACH2, MAL, TCF7L2
TCM	CCR7, IL7R, TCF7, SELL, CD28, LTB, TRAC
TEM	GZMK, GZMA, CCL5, IL32, PRDM1, CXCR3, IFNG, CD69
TEMRA	GZMB, PRF1, GNLY, KLRG1, CX3CR1, ZEB2, TBX21, B3GAT1 (CD57)
Th1	TBX21, IFNG, STAT1, CXCR3, IL12RB2, CD40LG, IL2, TNF
Th2	GATA3, IL4, IL5, IL13, CCR4, STAT6, IL2RA, CCR8, MAF
Th17	RORC, IL17A, IL17F, IL23R, STAT3, CCR6, IL21, BATF, AHR, KLRB1
Treg	FOXP3, IL2RA, CTLA4, ENTPD1, IKZF2, TGFBR2, TIGIT, TNFRSF18, LRRC32
Cytotoxic CD4	GZMH, PRF1, GZMA, GNLY, EOMES, FGFBP2, RUNX3, ITGB1, CD4
Exhaustion	PDCD1, LAG3, HAVCR2, TIGIT, CTLA4, TOX, ENTPD1, EOMES, NR4A1, BATF

Figure B.4: Summary of gene sets used during AUCell scoring.

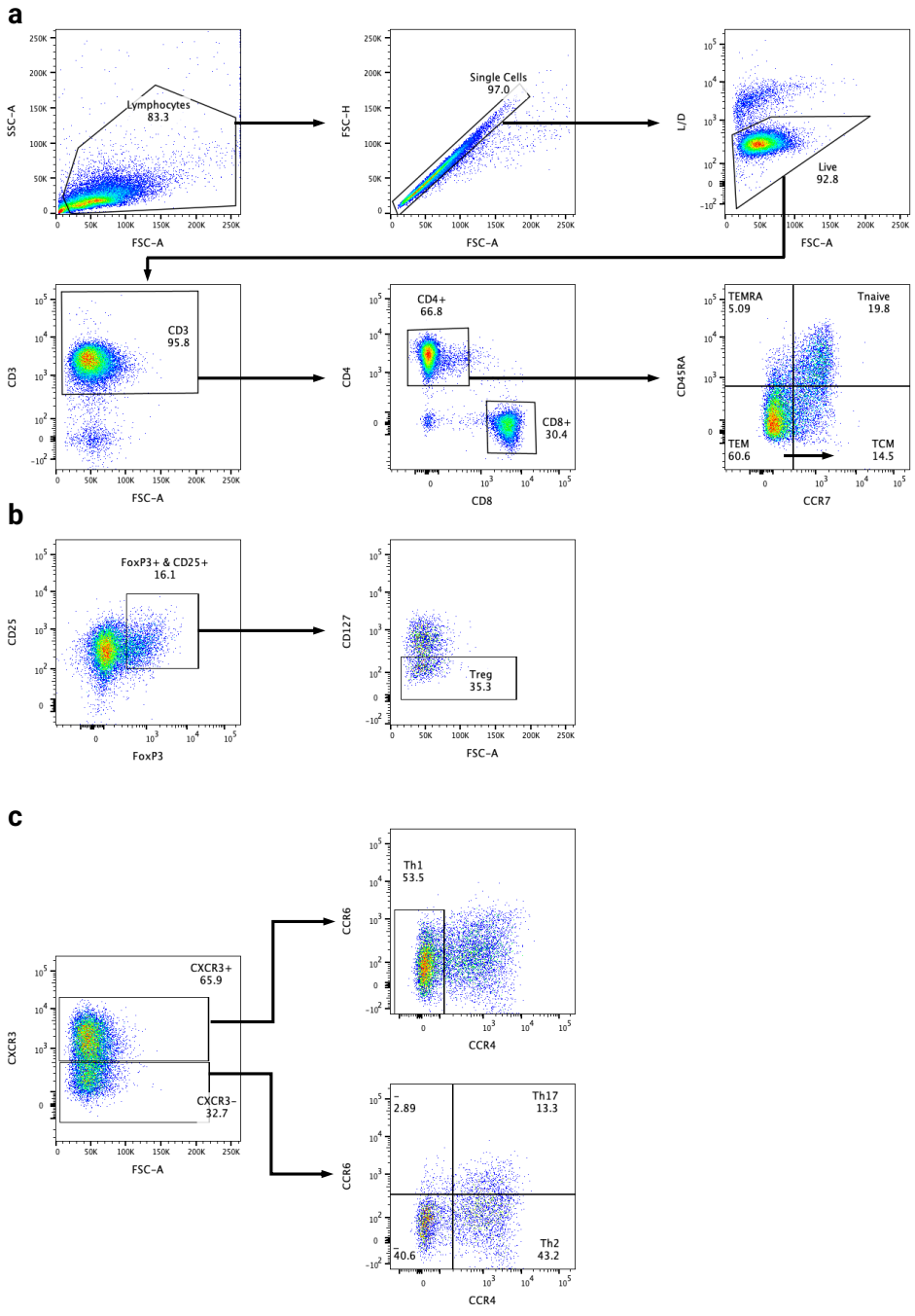

Figure B.5: T cell subset analysis. Example flow cytometry plots of healthy donor PBMCs demonstrating gating strategy for T cell subset analysis. Gating determined utilising FMOs on the same sample. **a.** Initial gating for $CD4^+$ and $CD8^+$ cells followed by antigen experience. **b.** Gating strategy for Tregs, starting from $CD4^+$ cells. **c.** Gating strategy for Th1, Th2 and Th17 effector polarisation, starting from of $CD4^+$ cells.

Patient	Peptide	TCR Clone	CDR3 TCRa	CDR3 TCRb
OX289	NAGPA	1	CVVDFYTSGTYKYIF	CSARDREAAGYGYTF
	RNF123	1	CALIPTGGGNKLTF	CSARLAHSGTNTGELFF
	LLGL2	1.1	CAVGAYSSASKIIF	CASRDRGSGANVLTF
		1.2	CAVGAYSSASKIIF	CSGGWGPNTGELFF
		2	CAVGHFSSRSSGSARQLTF	CASSLKVGVDSSYNEQFF
	ENDOD1	1.1	CAGLDDKIIF	CASSDPISGRGDEQFF
		1.2	CAVAGSNYQLIW	CASSDPISGRGDEQFF
	HENMT1	1	CAESPSDGQKLLF	CASSLRQGISPEQFF
		2.1	CAVEETSGSRLTF	CASSLRQGISPEQFF
		2.2	CAVEETSGSRLTF	CASSERQGITEAFF
		3.1	CAVSGTGANSKLTF	CASSDPISGRGDEQFF
		3.2	CAVSGTGANSKLTF	CASSFGGGAWNEQFF
	ACADS	1.1	CALRHKAAGNKLTF	CSASGPEKLFF
		1.2	CAALFDGGSQGNLIF	CSASGPEKLFF
		2	CASRGLAGETQYF	CAVIPNSGYALNF
		3	CALRGRNQGGKLIF	CSARLSSGGGYEQFF
	LRR1	1	CLVVPVYNQGGKLIF	CASSSGTSGMGETQYF
		2	CILRDVGGSEKLVF	CSAKGLENQPQHF
	FTSJ3	1.1	CVVNKATSGTYKYIF	CSARDREAAGYGYTF
		1.2	CVVNKATSGTYKYIF	CSARLAHSGTNTGELFF
OX628	LITAF	1.1	CAGHQIQGAQKLVF	CASSYSGMNTEAFF
		1.2	CAGANNNARLMF	CSVTPGGGVNTEAFF
		1.3	CAVSAGGTSYGKLTF	CASSQVLRGEQYF
OX747	METTL22	1	CAAILQGAQKLVF	CSARTHSDEAFF
		2	CAFAISNYQLIW	CSAIVGTGVFDEQFF
		3	CAVNFGNEKLTF	CSARASQGDTQYF
		4	CAASYTGFQKLVF	CASTDTSGDTEAFF
		5	CAVEAEGQNFVF	CSASGGGAPGELFF
		6	CLVGASLNDYKLSF	CASSGPGELFF
		7	CAASHLQGAQKLVF	CASSLMGQGLQPQHF
		8	CAVGNSGNTPLVF	CASSSGGYSVVFF
OX866	PADI4	1	CALSERPYGGATNKLIF	CASSERRTQPAYEQYF
		2.1	CALPAGNTPLVF	CASSLTGGNYGYTF
		2.2	CAVRGQAGTALIF	CASSLTGGNYGYTF
OX885	GSTZ1	1	CAARRVDNNNDMRF	CASGLAQPQHF
	WASHC4	1	CIVRVAVTNAGKSTF	CASRYYSADTQYF
		2	CAVSGVLTGGGNKLTF	CASSEGTVSNQPQHF
OX1149	RNH1	1	CATDEAAGNKLTF	CASKRESLATGELFF
		2	CAAMYSGGGADGLTF	CASSTQGQAYEQYF
		3	CAARGGSNYKLTF	CASSTGGEQYF
		4	CATKGGNNRLAF	CASSAWTGETGYTF
		5	CAATRAGGTSYGKLTF	CAWSVLAGVSQYF
	SLC26A6	1	CAASIATDKLIF	CASSWRGQGEGYTF
		2	CVVTGGANNLFF	CASSEAGEWTQYF
		3.1	CILVEGNEKLTF	CASRLGGRTTEAFF
		3.2	CGADVQGSQGNLIF	CASRLGGRTTEAFF

Figure B.6: Summary of previously identified TCRs used during *ex vivo* high throughput screening.

References

[1] Hartmut Döhner, Daniel J. Weisdorf and Clara D. Bloomfield. 'Acute Myeloid Leukemia'. en. In: *New England Journal of Medicine* 373.12 (Sept. 2015). Ed. by Dan L. Longo, pp. 1136–1152. DOI: 10.1056/NEJMra1406184.

[2] Shai Shimony, Maximilian Stahl and Richard M. Stone. 'Acute Myeloid Leukemia: 2025 Update on Diagnosis, Risk-Stratification, and Management'. en. In: *American Journal of Hematology* 100.5 (May 2025), pp. 860–891. DOI: 10.1002/ajh.27625.

[3] Chinmay T. Jani et al. 'Burden of AML, 1990-2019: Estimates From the Global Burden of Disease Study'. en. In: *JCO Global Oncology* 9 (Sept. 2023), e2300229. DOI: 10.1200/GO.23.00229.

[4] Yeming Zhou et al. 'Global, regional, and national burden of acute myeloid leukemia, 1990–2021: a systematic analysis for the global burden of disease study 2021'. en. In: *Biomarker Research* 12.1 (Sept. 2024), p. 101. DOI: 10.1186/s40364-024-00649-y.

[5] J. M. Bennett et al. 'Proposals for the classification of the acute leukaemias. French-American-British (FAB) co-operative group'. In: *British Journal of Haematology* 33.4 (Aug. 1976), pp. 451–458. DOI: 10.1111/j.1365-2141.1976.tb03563.x.

[6] Sanam Loghavi et al. 'Fifth Edition of the World Health Classification of Tumors of the Hematopoietic and Lymphoid Tissue: Myeloid Neoplasms'. en. In: *Modern Pathology* 37.2 (Feb. 2024), p. 100397. DOI: 10.1016/j.modpat.2023.100397.

[7] Daniel A. Arber et al. 'International Consensus Classification of Myeloid Neoplasms and Acute Leukemias: integrating morphologic, clinical, and genomic data'. en. In: *Blood* 140.11 (Sept. 2022), pp. 1200–1228. DOI: 10.1182/blood.2022015850.

[8] Miguel A. Sanz et al. 'Management of acute promyelocytic leukemia: updated recommendations from an expert panel of the European LeukemiaNet'. en. In: *Blood* 133.15 (Apr. 2019), pp. 1630–1643. DOI: 10.1182/blood-2019-01-894980.

[9] Hartmut Döhner et al. 'Diagnosis and management of AML in adults: 2022 recommendations from an international expert panel on behalf of the ELN'. en. In: *Blood* 140.12 (Sept. 2022), pp. 1345–1377. DOI: 10.1182/blood.2022016867.

[10] Krzysztof Mrózek et al. 'Outcome prediction by the 2022 European LeukemiaNet genetic-risk classification for adults with acute myeloid leukemia: an Alliance study'. en. In: *Leukemia* 37.4 (Apr. 2023), pp. 788–798. DOI: 10.1038/s41375-023-01846-8.

[11] Michael Heuser et al. '2021 Update on MRD in acute myeloid leukemia: a consensus document from the European LeukemiaNet MRD Working Party'. en. In: *Blood* 138.26 (Dec. 2021), pp. 2753–2767. DOI: 10.1182/blood.2021013626.

[12] Gerrit J. Schuurhuis et al. 'Minimal/measurable residual disease in AML: a consensus document from the European LeukemiaNet MRD Working Party'. en. In: *Blood* 131.12 (Mar. 2018), pp. 1275–1291. DOI: 10.1182/blood-2017-09-801498.

[13] Adam Ivey et al. 'Assessment of Minimal Residual Disease in Standard-Risk AML'. en. In: *New England Journal of Medicine* 374.5 (Feb. 2016), pp. 422–433. DOI: 10.1056/NEJMoa1507471.

[14] J. W. Yates et al. 'Cytosine Arabinoside (NSC-63878) and Daunorubicin (NSC-83142) Therapy in Acute Nonlymphocytic Leukemia'. In: *Cancer Chemotherapy Reports* 57.4 (1973), pp. 485–488.

[15] Marlise R. Luskin et al. 'Benefit of high-dose daunorubicin in AML induction extends across cytogenetic and molecular groups'. en. In: *Blood* 127.12 (Mar. 2016), pp. 1551–1558. DOI: 10.1182/blood-2015-07-657403.

[16] Nigel Russell et al. 'Treatment intensification with FLAG-Ida may improve disease control in younger patients with secondary acute myeloid leukaemia: long-term follow up of the MRC AML15 trial'. en. In: *British Journal of Haematology* 196.6 (Mar. 2022), pp. 1344–1347. DOI: 10.1111/bjh.17974.

[17] Jeffrey E. Lancet et al. 'CPX-351 (cytarabine and daunorubicin) Liposome for Injection Versus Conventional Cytarabine Plus Daunorubicin in Older Patients With Newly Diagnosed Secondary Acute Myeloid Leukemia'. en. In: *Journal of Clinical Oncology* 36.26 (Sept. 2018), pp. 2684–2692. DOI: 10.1200/JCO.2017.77.6112.

[18] Richard M. Stone et al. 'Midostaurin plus Chemotherapy for Acute Myeloid Leukemia with a *FLT3* Mutation'. en. In: *New England Journal of Medicine* 377.5 (Aug. 2017), pp. 454–464. DOI: 10.1056/NEJMoa1614359.

[19] Harry P Erba et al. 'Quizartinib plus chemotherapy in newly diagnosed patients with FLT3-internal-tandem-duplication-positive acute myeloid leukaemia (QuANTUM-First): a randomised, double-blind, placebo-controlled, phase 3 trial'. en. In: *The Lancet* 401.10388 (May 2023), pp. 1571–1583. DOI: 10.1016/S0140-6736(23)00464-6.

[20] Robert K Hills et al. 'Addition of gemtuzumab ozogamicin to induction chemotherapy in adult patients with acute myeloid leukaemia: a meta-analysis of individual patient data from randomised controlled trials'. en. In: *The Lancet Oncology* 15.9 (Aug. 2014), pp. 986–996. DOI: 10.1016/S1470-2045(14)70281-5.

[21] Courtney D DiNardo et al. 'Safety and preliminary efficacy of venetoclax with decitabine or azacitidine in elderly patients with previously untreated acute myeloid leukaemia: a non-randomised, open-label, phase 1b study'. en. In: *The Lancet Oncology* 19.2 (Feb. 2018), pp. 216–228. DOI: 10.1016/S1470-2045(18)30010-X.

[22] Courtney D. DiNardo et al. 'Azacitidine and Venetoclax in Previously Untreated Acute Myeloid Leukemia'. en. In: *New England Journal of Medicine* 383.7 (Aug. 2020), pp. 617–629. DOI: 10.1056/NEJMoa2012971.

[23] Naseema Gangat et al. 'Venetoclax and hypomethylating agent combination therapy in newly diagnosed acute myeloid leukemia: Genotype signatures for response and survival among 301 consecutive patients'. en. In: *American Journal of Hematology* 99.2 (Feb. 2024), pp. 193–202. DOI: 10.1002/ajh.27138.

[24] Eytan M. Stein et al. 'Enasidenib in mutant IDH2 relapsed or refractory acute myeloid leukemia'. en. In: *Blood* 130.6 (Aug. 2017), pp. 722–731. DOI: 10.1182/blood-2017-04-779405.

[25] Courtney D. DiNardo et al. 'Durable Remissions with Ivosidenib in *IDH1* -Mutated Relapsed or Refractory AML'. en. In: *New England Journal of Medicine* 378.25 (June 2018), pp. 2386–2398. DOI: 10.1056/NEJMoa1716984.

[26] Gail J. Roboz et al. 'Ivosidenib induces deep durable remissions in patients with newly diagnosed IDH1-mutant acute myeloid leukemia'. en. In: *Blood* 135.7 (Feb. 2020), pp. 463–471. DOI: 10.1182/blood.2019002140.

[27] Eytan M. Stein et al. 'Ivosidenib or enasidenib combined with intensive chemotherapy in patients with newly diagnosed AML: a phase 1 study'. en. In: *Blood* 137.13 (Apr. 2021), pp. 1792–1803. DOI: 10.1182/blood.2020007233.

[28] Curtis A. Lachowiez et al. 'A Phase Ib/II Study of Ivosidenib with Venetoclax ± Azacitidine in *IDH1* -Mutated Myeloid Malignancies'. en. In: *Blood Cancer Discovery* 4.4 (July 2023), pp. 276–293. DOI: 10.1158/2643-3230.BCD-22-0205.

[29] Ghayas C. Issa et al. 'The menin inhibitor revumenib in KMT2A-rearranged or NPM1-mutant leukaemia'. en. In: *Nature* 615.7954 (Mar. 2023), pp. 920–924. DOI: 10.1038/s41586-023-05812-3.

[30] Sven Turkalj, Felix A. Radtke and Paresh Vyas. 'An Overview of Targeted Therapies in Acute Myeloid Leukemia'. en. In: *HemaSphere* 7.6 (June 2023), e914. DOI: 10.1097/HS9.0000000000000914.

[31] Bob Löwenberg. 'Sense and nonsense of high-dose cytarabine for acute myeloid leukemia'. en. In: *Blood* 121.1 (Jan. 2013), pp. 26–28. DOI: 10.1182/blood-2012-07-444851.

[32] Andrea T. Nguyen, Christopher Szeto and Stephanie Gras. 'The pockets guide to HLA class I molecules'. en. In: *Biochemical Society Transactions* 49.5 (Nov. 2021), pp. 2319–2331. DOI: 10.1042/BST20210410.

[33] Novalia Pishesha, Thibault J. Harmand and Hidde L. Ploegh. 'A guide to antigen processing and presentation'. en. In: *Nature Reviews Immunology* 22.12 (Dec. 2022), pp. 751–764. DOI: 10.1038/s41577-022-00707-2.

[34] Malte Roerden et al. 'Expression levels of HLA-DR in acute myeloid leukemia: implications for antigenicity and clinical outcome'. en. In: *Leukemia & Lymphoma* 62.8 (July 2021), pp. 1907–1919. DOI: 10.1080/10428194.2021.1885659.

[35] Janice S. Blum, Pamela A. Wearsch and Peter Cresswell. 'Pathways of Antigen Processing'. en. In: *Annual Review of Immunology* 31.1 (Mar. 2013), pp. 443–473. DOI: 10.1146/annurev-immunol-032712-095910.

[36] Paul A. Roche and Kazuyuki Furuta. 'The ins and outs of MHC class II-mediated antigen processing and presentation'. en. In: *Nature Reviews Immunology* 15.4 (Apr. 2015), pp. 203–216. DOI: 10.1038/nri3818.

[37] Carol S. K. Leung. 'Endogenous Antigen Presentation of MHC Class II Epitopes through Non-Autophagic Pathways'. en. In: *Frontiers in Immunology* 6 (Sept. 2015). DOI: 10.3389/fimmu.2015.00464.

[38] Nicholas R. J. Gascoigne et al. 'Co-Receptors and Recognition of Self at the Immunological Synapse'. en. In: *Immunological Synapse*. Ed. by Takashi Saito and Facundo D. Batista. Vol. 340. Series Title: Current Topics in Microbiology and Immunology. Berlin, Heidelberg: Springer Berlin Heidelberg, 2010, pp. 171–189. DOI: 10.1007/978-3-642-03858-7_9.

[39] Choong-Hyun Koh et al. 'CD8 T-cell subsets: heterogeneity, functions, and therapeutic potential'. en. In: *Experimental & Molecular Medicine* 55.11 (Nov. 2023), pp. 2287–2299. DOI: 10.1038/s12276-023-01105-x.

[40] Corinne Summers, Vipul S. Sheth and Marie Bleakley. 'Minor Histocompatibility Antigen-Specific T Cells'. en. In: *Frontiers in Pediatrics* 8 (June 2020), p. 284. DOI: 10.3389/fped.2020.00284.

[41] David Andreu-Sanz and Sebastian Kobold. 'Role and Potential of Different T Helper Cell Subsets in Adoptive Cell Therapy'. en. In: *Cancers* 15.6 (Mar. 2023), p. 1650. DOI: 10.3390/cancers15061650.

[42] Fenghua Qian et al. 'Interleukin-4 treatment reduces leukemia burden in acute myeloid leukemia'. en. In: *The FASEB Journal* 36.5 (May 2022). DOI: 10.1096/fj.202200251R.

[43] P Peña-Martínez et al. 'Interleukin 4 induces apoptosis of acute myeloid leukemia cells in a Stat6-dependent manner'. en. In: *Leukemia* 32.3 (Mar. 2018), pp. 588–596. DOI: 10.1038/leu.2017.261.

[44] Clint Piper and William R. Drobyski. 'Role of TH17 Cells and Interleukin 17 in Graft Versus Host Disease and Graft Versus Leukemia Reactivity'. en. In: *Immune Biology of Allogeneic Hematopoietic Stem Cell Transplantation*. Elsevier, 2019, pp. 231–249. DOI: 10.1016/B978-0-12-812630-1.00014-1.

[45] Jens Geginat et al. 'Plasticity of Human CD4 T Cell Subsets'. en. In: *Frontiers in Immunology* 5 (Dec. 2014). DOI: 10.3389/fimmu.2014.00630.

[46] Seongmin Jeong et al. '$CD4^+$ cytotoxic T cells: an emerging effector arm of anti-tumor immunity'. en. In: *BMB Reports* 56.3 (Mar. 2023), pp. 140–144. DOI: 10.5483/BMBRep.2023-0014.

[47] Tomasz Ahrends and Jannie Borst. 'The opposing roles of CD4+ T cells in anti-tumour immunity'. en. In: *Immunology* 154.4 (Aug. 2018), pp. 582–592. DOI: 10.1111/imm.12941.

[48] Anita D'Souza et al. 'Current Use and Trends in Hematopoietic Cell Transplantation in the United States'. en. In: *Biology of Blood and Marrow Transplantation* 23.9 (Sept. 2017), pp. 1417–1421. DOI: 10.1016/j.bbmt.2017.05.035.

[49] Jakob R. Passweg et al. 'Hematopoietic cell transplantation and cellular therapies in Europe 2022. CAR-T activity continues to grow; transplant activity has slowed: a report from the EBMT'. en. In: *Bone Marrow Transplantation* 59.6 (June 2024), pp. 803–812. DOI: 10.1038/s41409-024-02248-9.

[50] E. Donnall Thomas et al. 'Intravenous Infusion of Bone Marrow in Patients Receiving Radiation and Chemotherapy'. en. In: *New England Journal of Medicine* 257.11 (Sept. 1957), pp. 491–496. DOI: 10.1056/NEJM195709122571102.

[51] E. Donnall Thomas et al. 'Bone-marrow transplantation'. In: *New England Journal of Medicine* 292.17 (1975), pp. 832–843. DOI: 10.1056/NEJM197504242921706.

[52] Mary M Horowitz et al. 'Graft-Versus-Leukemia Reactions After Bone Marrow Transplantation'. en. In: *Blood* 75.3 (Feb. 1990), pp. 555–562. DOI: 10.1182/blood.V75.3.555.bloodjournal753555.

[53] Jan J. Cornelissen and Didier Blaise. 'Hematopoietic stem cell transplantation for patients with AML in first complete remission'. en. In: *Blood* 127.1 (Jan. 2016), pp. 62–70. DOI: 10.1182/blood-2015-07-604546.

[54] Jan J. Cornelissen et al. 'Results of a HOVON/SAKK donor versus no-donor analysis of myeloablative HLA-identical sibling stem cell transplantation in first remission acute myeloid leukemia in young and middle-aged adults: benefits for whom?' en. In: *Blood* 109.9 (May 2007), pp. 3658–3666. DOI: 10.1182/blood-2006-06-025627.

[55] R. F. Schlenk. 'Post-remission therapy for acute myeloid leukemia'. en. In: *Haematologica* 99.11 (Nov. 2014), pp. 1663–1670. DOI: 10.3324/haematol.2014.114611.

[56] Hong-Hu Zhu et al. 'MRD-directed risk stratification treatment may improve outcomes of t(8;21) AML in the first complete remission: results from the AML05 multicenter trial'. en. In: *Blood* 121.20 (May 2013), pp. 4056–4062. DOI: 10.1182/blood-2012-11-468348.

[57] Jad Othman et al. 'Postinduction molecular MRD identifies patients with *NPM1* AML who benefit from allogeneic transplant in first remission'. en. In: *Blood* 143.19 (May 2024), pp. 1931–1936. DOI: 10.1182/blood.2023023096.

[58] Mohamed L. Sorror et al. 'Hematopoietic cell transplantation (HCT)-specific comorbidity index: a new tool for risk assessment before allogeneic HCT'. en. In: *Blood* 106.8 (Oct. 2005), pp. 2912–2919. DOI: 10.1182/blood-2005-05-2004.

[59] Mohamed L. Sorror et al. 'Comorbidity-Age Index: A Clinical Measure of Biologic Age Before Allogeneic Hematopoietic Cell Transplantation'. en. In: *Journal of Clinical Oncology* 32.29 (Oct. 2014), pp. 3249–3256. DOI: 10.1200/JCO.2013.53.8157.

[60] AK Burnett et al. 'Curability of patients with acute myeloid leukemia who did not undergo transplantation in first remission'. In: *Journal of Clinical Oncology* 31.10 (2013). Publisher: American Society of Clinical Oncology, pp. 1293–1301. DOI: 10.1200/JCO.2012.45.6537.

[61] Francisco Barriga and Alberto Cardoso Martins Lima. 'Donor selection in allogeneic stem cell transplantation'. en. In: *Current Opinion in Hematology* 31.6 (Nov. 2024), pp. 261–269. DOI: 10.1097/MOH.0000000000000831.

[62] Michael R. Verneris et al. 'HLA Mismatch Is Associated with Worse Outcomes after Unrelated Donor Reduced-Intensity Conditioning Hematopoietic Cell Transplantation: An Analysis from the Center for International Blood and Marrow Transplant Research'. en. In: *Biology of Blood and Marrow Transplantation* 21.10 (Oct. 2015), pp. 1783–1789. DOI: 10.1016/j.bbmt.2015.05.028.

[63] Stephanie J. Lee et al. 'High-resolution donor-recipient HLA matching contributes to the success of unrelated donor marrow transplantation'. en. In: *Blood* 110.13 (Dec. 2007), pp. 4576–4583. DOI: 10.1182/blood-2007-06-097386.

[64] Katharina Fleischhauer et al. 'Effect of T-cell-epitope matching at HLA-DPB1 in recipients of unrelated-donor haemopoietic-cell transplantation: a retrospective study'. en. In: *The Lancet Oncology* 13.4 (Apr. 2012), pp. 366–374. DOI: 10.1016/S1470-2045(12)70004-9.

[65] Rohtesh S. Mehta. 'SOHO State of the Art Updates and Next Questions | Current Status and Future Directions of Donor Selection'. en. In: *Clinical Lymphoma Myeloma and Leukemia* 24.12 (Dec. 2024), pp. 821–826. DOI: 10.1016/j.clml.2024.05.011.

[66] Roni Shouval et al. 'Outcomes of allogeneic haematopoietic stem cell transplantation from HLA-matched and alternative donors: a European Society for Blood and Marrow Transplantation registry retrospective analysis'. en. In: *The Lancet Haematology* 6.11 (Nov. 2019), e573–e584. DOI: 10.1016/S2352-3026(19)30158-9.

[67] J.-M. Tiercy. 'How to select the best available related or unrelated donor of hematopoietic stem cells?' en. In: *Haematologica* 101.6 (June 2016), pp. 680–687. DOI: 10.3324/haematol.2015.141119.

[68] Loren Gragert et al. 'HLA Match Likelihoods for Hematopoietic Stem-Cell Grafts in the U.S. Registry'. en. In: *New England Journal of Medicine* 371.4 (July 2014), pp. 339–348. DOI: 10.1056/NEJMsa1311707.

[69] Leo Luznik et al. 'HLA-Haploidentical Bone Marrow Transplantation for Hematologic Malignancies Using Nonmyeloablative Conditioning and High-Dose, Posttransplantation Cyclophosphamide'. en. In: *Biology of Blood and Marrow Transplantation* 14.6 (June 2008), pp. 641–650. DOI: 10.1016/j.bbmt.2008.03.005.

[70] Frédéric Baron et al. 'Umbilical cord blood versus unrelated donor transplantation in adults with primary refractory or relapsed acute myeloid leukemia: a report from Eurocord, the Acute Leukemia Working Party and the Cord Blood Committee of the Cellular Therapy and Immunobiology Working Party of the EBMT'. en. In: *Blood Cancer Journal* 9.4 (Apr. 2019), p. 46. DOI: 10.1038/s41408-019-0204-x.

[71] Craig Kollman et al. 'The effect of donor characteristics on survival after unrelated donor transplantation for hematologic malignancy'. en. In: *Blood* 127.2 (Jan. 2016), pp. 260–267. DOI: 10.1182/blood-2015-08-663823.

[72] Michael Boeckh and W. Garrett Nichols. 'The impact of cytomegalovirus serostatus of donor and recipient before hematopoietic stem cell transplantation in the era of antiviral prophylaxis and preemptive therapy'. en. In: *Blood* 103.6 (Mar. 2004), pp. 2003–2008. DOI: 10.1182/blood-2003-10-3616.

[73] Nina Worel. 'ABO-Mismatched Allogeneic Hematopoietic Stem Cell Transplantation'. en. In: *Transfusion Medicine and Hemotherapy* 43.1 (2016), pp. 3–12. DOI: 10.1159/000441507.

[74] Erden Atilla, Pınar Ataca Atilla and Taner Demirer. 'A Review of Myeloablative vs Reduced Intensity/Non-Myeloablative Regimens in Allogeneic Hematopoietic Stem Cell Transplantations'. en. In: *Balkan Medical Journal* 34.1 (Jan. 2017), pp. 1–9. DOI: 10.4274/balkanmedj.2017.0055.

[75] Robert Ali et al. 'The Role of Anti-Thymocyte Globulin or Alemtuzumab-Based Serotherapy in the Prophylaxis and Management of Graft-Versus-Host Disease'. en. In: *Biomedicines* 5.4 (Nov. 2017), p. 67. DOI: 10.3390/biomedicines5040067.

[76] Steven M. Devine et al. 'Phase II Study of Allogeneic Transplantation for Older Patients With Acute Myeloid Leukemia in First Complete Remission Using a Reduced-Intensity Conditioning Regimen: Results From Cancer and Leukemia Group B 100103 (Alliance for Clinical Trials in Oncology)/Blood and Marrow Transplant Clinical Trial Network 0502'. en. In: *Journal of Clinical Oncology* 33.35 (Dec. 2015), pp. 4167–4175. DOI: 10.1200/JCO.2015.62.7273.

[77] Bart L. Scott et al. 'Myeloablative Versus Reduced-Intensity Hematopoietic Cell Transplantation for Acute Myeloid Leukemia and Myelodysplastic Syndromes'. en. In: *Journal of Clinical Oncology* 35.11 (Apr. 2017), pp. 1154–1161. DOI: 10.1200/JCO.2016.70.7091.

[78] Robert Zeiser and Bruce R. Blazar. 'Acute Graft-versus-Host Disease — Biologic Process, Prevention, and Therapy'. en. In: *New England Journal of Medicine* 377.22 (Nov. 2017). Ed. by Dan L. Longo, pp. 2167–2179. DOI: 10.1056/NEJMra1609337.

[79] Madan H. Jagasia et al. 'National Institutes of Health Consensus Development Project on Criteria for Clinical Trials in Chronic Graft-versus-Host Disease: I. The 2014 Diagnosis and Staging Working Group Report'. en. In: *Biology of Blood and Marrow Transplantation* 21.3 (Mar. 2015), 389–401.e1. DOI: 10.1016/j.bbmt.2014.12.001.

[80] Mary E. D. Flowers et al. 'Comparative analysis of risk factors for acute graft-versus-host disease and for chronic graft-versus-host disease according to National Institutes of Health consensus criteria'. en. In: *Blood* 117.11 (Mar. 2011), pp. 3214–3219. DOI: 10.1182/blood-2010-08-302109.

[81] Thomas F. Michniacki, Sung Won Choi and Daniel C. Peltier. 'Immune Suppression in Allogeneic Hematopoietic Stem Cell Transplantation'. en. In: *Pharmacology of Immunosuppression*. Ed. by Howard J. Eisen. Vol. 272. Series Title: Handbook of Experimental Pharmacology. Cham: Springer International Publishing, 2021, pp. 209–243. DOI: 10.1007/164_2021_544.

[82] Olaf Penack et al. 'PTCy versus ATG as graft-versus-host disease prophylaxis in mismatched unrelated stem cell transplantation'. en. In: *Blood Cancer Journal* 14.1 (Mar. 2024), p. 45. DOI: 10.1038/s41408-024-01032-8.

[83] Beatrice Drexler et al. 'Extracorporeal Photopheresis in Graft-versus-Host Disease'. en. In: *Transfusion Medicine and Hemotherapy* 47.3 (2020), pp. 214–225. DOI: 10.1159/000508169.

[84] Robert Zeiser et al. 'Ruxolitinib for Glucocorticoid-Refractory Acute Graft-versus-Host Disease'. en. In: *New England Journal of Medicine* 382.19 (May 2020), pp. 1800–1810. DOI: 10.1056/NEJMoa1917635.

[85] S L Petersen et al. 'A comparison of T-, B- and NK-cell reconstitution following conventional or nonmyeloablative conditioning and transplantation with bone marrow or peripheral blood stem cells from human leucocyte antigen identical sibling donors'. en. In: *Bone Marrow Transplantation* 32.1 (July 2003), pp. 65–72. DOI: 10.1038/sj.bmt.1704084.

[86] Benjamin R. Oshrine et al. 'Immunologic Recovery in Children after Alternative Donor Allogeneic Transplantation for Hematologic Malignancies: Comparison of Recipients of Partially T Cell–Depleted Peripheral Blood Stem Cells and Umbilical Cord Blood'. en. In: *Biology of Blood and Marrow Transplantation* 19.11 (Nov. 2013), pp. 1581–1589. DOI: 10.1016/j.bbmt.2013.08.003.

[87] Kirsten M. Williams, Frances T. Hakim and Ronald E. Gress. 'T cell immune reconstitution following lymphodepletion'. en. In: *Seminars in Immunology* 19.5 (Oct. 2007), pp. 318–330. DOI: 10.1016/j.smim.2007.10.004.

[88] Claudio Anasetti et al. 'Peripheral-Blood Stem Cells versus Bone Marrow from Unrelated Donors'. en. In: *New England Journal of Medicine* 367.16 (Oct. 2012), pp. 1487–1496. DOI: 10.1056/NEJMoa1203517.

[89] Keun Wook Bae et al. 'Factors influencing lymphocyte reconstitution after allogeneic hematopoietic stem cell transplantation in children'. en. In: *The Korean Journal of Hematology* 47.1 (2012), p. 44. DOI: 10.5045/kjh.2012.47.1.44.

[90] Nelli Bejanyan et al. 'Delayed immune reconstitution after allogeneic transplantation increases the risks of mortality and chronic GVHD'. en. In: *Blood Advances* 2.8 (Apr. 2018), pp. 909–922. DOI: 10.1182/bloodadvances.2017014464.

[91] Ioannis Politikos et al. 'Robust CD4+ T-cell recovery in adults transplanted with cord blood and no antithymocyte globulin'. en. In: *Blood Advances* 4.1 (Jan. 2020), pp. 191–202. DOI: 10.1182/bloodadvances.2019000836.

[92] Robert J. Soiffer et al. 'Prospective, Randomized, Double-Blind, Phase III Clinical Trial of Anti–T-Lymphocyte Globulin to Assess Impact on Chronic Graft-Versus-Host Disease–Free Survival in Patients Undergoing HLA-Matched Unrelated Myeloablative Hematopoietic Cell Transplantation'. en. In: *Journal of Clinical Oncology* 35.36 (Dec. 2017), pp. 4003–4011. DOI: 10.1200/JCO.2017.75.8177.

[93] E Charrier et al. 'Reconstitution of maturating and regulatory lymphocyte subsets after cord blood and BMT in children'. en. In: *Bone Marrow Transplantation* 48.3 (Mar. 2013), pp. 376–382. DOI: 10.1038/bmt.2012.176.

[94] L L Reubsaet et al. 'Stem cell source-dependent reconstitution of FOXP3+ T cells after pediatric SCT and the association with allo-reactive disease'. en. In: *Bone Marrow Transplantation* 48.4 (Apr. 2013), pp. 502–507. DOI: 10.1038/bmt.2012.174.

[95] N. Watanabe et al. 'Kinetics of pDCs, mDCs, γδT cells and regulatory T cells in association with graft versus host disease after hematopoietic stem cell transplantation: KINETICS OF IMMUNOCOMPETENT CELLS IN ASSOCIATION WITH GVHD AFTER HSCT'. en. In: *International Journal of Laboratory Hematology* 33.4 (Aug. 2011), pp. 378–390. DOI: 10.1111/j.1751-553X.2011.01300.x.

[96] John M. Magenau et al. 'Frequency of CD4+CD25hiFOXP3+ Regulatory T Cells Has Diagnostic and Prognostic Value as a Biomarker for Acute Graft-versus-Host-Disease'. en. In: *Biology of Blood and Marrow Transplantation* 16.7 (July 2010), pp. 907–914. DOI: 10.1016/j.bbmt.2010.02.026.

[97] J Peccatori et al. 'Sirolimus-based graft-versus-host disease prophylaxis promotes the in vivo expansion of regulatory T cells and permits peripheral blood stem cell transplantation from haploidentical donors'. en. In: *Leukemia* 29.2 (Feb. 2015), pp. 396–405. DOI: 10.1038/leu.2014.180.

[98] Deng-Mei Tian et al. 'Rapid Recovery of CD3+CD8+ T Cells on Day 90 Predicts Superior Survival after Unmanipulated Haploidentical Blood and Marrow Transplantation'. en. In: *PLOS ONE* 11.6 (June 2016). Ed. by Pablo Menendez, e0156777. DOI: 10.1371/journal.pone.0156777.

[99] Rick Admiraal et al. 'Viral reactivations and associated outcomes in the context of immune reconstitution after pediatric hematopoietic cell transplantation'. en. In: *Journal of Allergy and Clinical Immunology* 140.6 (Dec. 2017), 1643–1650.e9. DOI: 10.1016/j.jaci.2016.12.992.

[100] Justyna Ogonek et al. 'Possible Impact of Cytomegalovirus-Specific CD8+ T Cells on Immune Reconstitution and Conversion to Complete Donor Chimerism after Allogeneic Stem Cell Transplantation'. en. In: *Biology of Blood and Marrow Transplantation* 23.7 (July 2017), pp. 1046–1053. DOI: 10.1016/j.bbmt.2017.03.027.

[101] Yvonne Suessmuth et al. 'CMV reactivation drives posttransplant T-cell reconstitution and results in defects in the underlying TCRβ repertoire'. en. In: *Blood* 125.25 (June 2015), pp. 3835–3850. DOI: 10.1182/blood-2015-03-631853.

[102] C S Link et al. 'Abundant cytomegalovirus (CMV) reactive clonotypes in the CD8+ T cell receptor alpha repertoire following allogeneic transplantation'. en. In: *Clinical and Experimental Immunology* 184.3 (May 2016), pp. 389–402. DOI: 10.1111/cei.12770.

[103] Rupert Handgretinger and Karin Schilbach. 'The potential role of γδ T cells after allogeneic HCT for leukemia'. en. In: *Blood* 131.10 (Mar. 2018), pp. 1063–1072. DOI: 10.1182/blood-2017-08-752162.

[104] Ross Perko et al. 'Gamma Delta T Cell Reconstitution Is Associated with Fewer Infections and Improved Event-Free Survival after Hematopoietic Stem Cell Transplantation for Pediatric Leukemia'. en. In: *Biology of Blood and Marrow Transplantation* 21.1 (Jan. 2015), pp. 130–136. DOI: 10.1016/j.bbmt.2014.09.027.

[105] K. T. Godder et al. 'Long term disease-free survival in acute leukemia patients recovering with increased γδ T cells after partially mismatched related donor bone marrow transplantation'. In: *Bone Marrow Transplantation* 39.12 (June 2007), pp. 751–757. DOI: 10.1038/sj.bmt.1705650.

[106] Lia Minculescu et al. 'Improved Overall Survival, Relapse-Free-Survival, and Less Graft-vs.-Host-Disease in Patients With High Immune Reconstitution of TCR Gamma Delta Cells 2 Months After Allogeneic Stem Cell Transplantation'. en. In: *Frontiers in Immunology* 10 (Aug. 2019), p. 1997. DOI: 10.3389/fimmu.2019.01997.

[107] Vivien Beziat et al. 'Shaping of iNKT cell repertoire after unrelated cord blood transplantation'. en. In: *Clinical Immunology* 135.3 (June 2010), pp. 364–373.

[108] Aristeidis Chaidos et al. 'Graft invariant natural killer T-cell dose predicts risk of acute graft-versus-host disease in allogeneic hematopoietic stem cell transplantation'. en. In: *Blood* 119.21 (May 2012), pp. 5030–5036. DOI: 10.1182/blood-2011-11-389304.

[109] Claudia De Lalla et al. 'Invariant NKT Cell Reconstitution in Pediatric Leukemia Patients Given HLA-Haploidentical Stem Cell Transplantation Defines Distinct CD4+ and CD4- Subset Dynamics and Correlates with Remission State'. en. In: *The Journal of Immunology* 186.7 (Apr. 2011), pp. 4490–4499. DOI: 10.4049/jimmunol.1003748.

[110] Marie-Thérèse Rubio et al. 'Early posttransplantation donor-derived invariant natural killer T-cell recovery predicts the occurrence of acute graft-versus-host disease and overall survival'. en. In: *Blood* 120.10 (Sept. 2012), pp. 2144–2154. DOI: 10.1182/blood-2012-01-404673.

[111] Amanda G. Blouin and Medhat Askar. 'Chimerism analysis for clinicians: a review of the literature and worldwide practices'. en. In: *Bone Marrow Transplantation* 57.3 (Mar. 2022), pp. 347–359. DOI: 10.1038/s41409-022-01579-9.

[112] Theis Helge Terwey et al. 'Comparison of Chimerism and Minimal Residual Disease Monitoring for Relapse Prediction after Allogeneic Stem Cell Transplantation for Adult Acute Lymphoblastic Leukemia'. en. In: *Biology of Blood and Marrow Transplantation* 20.10 (Oct. 2014), pp. 1522–1529. DOI: 10.1016/j.bbmt.2014.05.026.

[113] Eva Rettinger et al. 'Preemptive immunotherapy in childhood acute myeloid leukemia for patients showing evidence of mixed chimerism after allogeneic stem cell transplantation'. en. In: *Blood* 118.20 (Nov. 2011), pp. 5681–5688. DOI: 10.1182/blood-2011-04-348805.

[114] Paul L. Weiden et al. 'Antileukemic Effect of Graft-versus-Host Disease in Human Recipients of Allogeneic-Marrow Grafts'. In: *New England Journal of Medicine* 300.19 (1979). _eprint: https://www.nejm.org/doi/pdf/10.1056/NEJM197905103001902, pp. 1068–1073. DOI: 10.1056/NEJM197905103001902.

[115] Paul L. Weiden et al. 'Antileukemic Effect of Chronic Graft-versus-Host Disease'. In: *New England Journal of Medicine* 304.25 (1981). _eprint: https://www.nejm.org/doi/pdf/10.1056/NEJM198106183042507, pp. 1529–1533. DOI: 10.1056/NEJM198106183042507.

[116] F Baron et al. 'Impact of graft-versus-host disease after reduced-intensity conditioning allogeneic stem cell transplantation for acute myeloid leukemia: a report from the Acute Leukemia Working Party of the European group for blood and marrow transplantation'. en. In: *Leukemia* 26.12 (Dec. 2012), pp. 2462–2468. DOI: 10.1038/leu.2012.135.

[117] Motohiro Kato et al. 'Impact of graft-versus-host disease on relapse and survival after allogeneic stem cell transplantation for pediatric leukemia'. en. In: *Bone Marrow Transplantation* 54.1 (Jan. 2019), pp. 68–75. DOI: 10.1038/s41409-018-0221-6.

[118] M Stern et al. 'Sensitivity of hematological malignancies to graft-versus-host effects: an EBMT megafile analysis'. en. In: *Leukemia* 28.11 (Nov. 2014), pp. 2235–2240. DOI: 10.1038/leu.2014.145.

[119] Michael Stadler et al. 'The graft-versus-leukemia effect of prophylactic donor lymphocyte infusions after allogeneic stem cell transplantation is equally effective in relapse prevention but safer compared to spontaneous graft-versus-host disease'. en. In: *Annals of Hematology* 102.9 (Sept. 2023), pp. 2529–2542. DOI: 10.1007/s00277-023-05276-5.

[120] Katie Maurer and Joseph H. Antin. 'The graft versus leukemia effect: donor lymphocyte infusions and cellular therapy'. en. In: *Frontiers in Immunology* 15 (Mar. 2024), p. 1328858. DOI: 10.3389/fimmu.2024.1328858.

[121] Ronald T Mitsuyasu et al. 'Treatment of Donor Bone Marrow with Monoclonal Anti-T-Cell Antibody and Complement for the Prevention of Graft-Versus-Host Disease'. In: *Annals of Internal Medicine* 105.1 (1986). _eprint: https://doi.org/10.7326/0003-4819-105-1-20, pp. 20–26. DOI: 10.7326/0003-4819-105-1-20.

[122] Alberto M Marmont et al. 'T-cell Depletion of HLA-Identical Transplants in Leukemia'. en. In: *Blood* 78.8 (Oct. 1991), pp. 2120–2130.

[123] R K Malladi et al. 'Alemtuzumab markedly reduces chronic GVHD without affecting overall survival in reduced-intensity conditioning sibling allo-SCT for adults with AML'. en. In: *Bone Marrow Transplantation* 43.9 (May 2009), pp. 709–715. DOI: 10.1038/bmt.2008.375.

[124] Andrea Bacigalupo et al. 'Defining the Intensity of Conditioning Regimens: Working Definitions'. en. In: *Biology of Blood and Marrow Transplantation* 15.12 (Dec. 2009), pp. 1628–1633. DOI: 10.1016/j.bbmt.2009.07.004.

[125] S. Slavin et al. 'Nonmyeloablative Stem Cell Transplantation and Cell Therapy as an Alternative to Conventional Bone Marrow Transplantation with Lethal Cytoreduction for the Treatment of Malignant and Nonmalignant Hematologic Diseases'. In: *Blood* 91.3 (Feb. 1998), pp. 756–763. DOI: 10.1182/blood.V91.3.756.

[126] S. Fadilah Abdul Wahid et al. 'Comparison of Reduced-Intensity and Myeloablative Conditioning Regimens for Allogeneic Hematopoietic Stem Cell Transplantation in Patients with Acute Myeloid Leukemia and Acute Lymphoblastic Leukemia: A Meta-Analysis'. en. In: *Stem Cells and Development* 23.21 (Nov. 2014), pp. 2535–2552. DOI: 10.1089/scd.2014.0123.

[127] Brian L. McClune et al. 'Effect of Age on Outcome of Reduced-Intensity Hematopoietic Cell Transplantation for Older Patients With Acute Myeloid Leukemia in First Complete Remission or With Myelodysplastic Syndrome'. en. In: *Journal of Clinical Oncology* 28.11 (Apr. 2010), pp. 1878–1887. DOI: 10.1200/JCO.2009.25.4821.

[128] H. J. Kolb et al. 'Donor leukocyte transfusions for treatment of recurrent chronic myelogenous leukemia in marrow transplant patients'. In: *Blood* 76.12 (Dec. 1990), pp. 2462–2465. DOI: 10.1182/blood.V76.12.2462.2462.

[129] Christoph Schmid et al. 'Donor Lymphocyte Infusion in the Treatment of First Hematological Relapse After Allogeneic Stem-Cell Transplantation in Adults With Acute Myeloid Leukemia: A Retrospective Risk Factors Analysis and Comparison With Other Strategies by the EBMT Acute Leukemia Working Party'. In: *Journal of Clinical Oncology* 25.31 (2007). _eprint: https://ascopubs.org/doi/pdf/10.1200/JCO.2007.11.6053, pp. 4938–4945. DOI: 10.1200/JCO.2007.11.6053.

[130] Z Jedlickova et al. 'Long-term results of adjuvant donor lymphocyte transfusion in AML after allogeneic stem cell transplantation'. en. In: *Bone Marrow Transplantation* 51.5 (May 2016), pp. 663–667. DOI: 10.1038/bmt.2015.234.

[131] Alexander Biederstädt and Katayoun Rezvani. 'How I treat high-risk acute myeloid leukemia using preemptive adoptive cellular immunotherapy'. en. In: *Blood* 141.1 (Jan. 2023), pp. 22–38. DOI: 10.1182/blood.2021012411.

[132] Christoph Schmid et al. 'Long-term results and GvHD after prophylactic and preemptive donor lymphocyte infusion after allogeneic stem cell transplantation for acute leukemia'. en. In: *Bone Marrow Transplantation* 57.2 (Feb. 2022), pp. 215–223. DOI: 10.1038/s41409-021-01515-3.

[133] Andrés R. Rettig et al. 'Donor lymphocyte infusions after first allogeneic hematopoietic stem-cell transplantation in adults with acute myeloid leukemia: a single-center landmark analysis'. en. In: *Annals of Hematology* 100.9 (Sept. 2021), pp. 2339–2350. DOI: 10.1007/s00277-021-04494-z.

[134] R H Collins et al. 'Donor leukocyte infusions in 140 patients with relapsed malignancy after allogeneic bone marrow transplantation.' In: *Journal of Clinical Oncology* 15.2 (1997). _eprint: https://ascopubs.org/doi/pdf/10.1200/JCO.1997.15.2.433, pp. 433–444. DOI: 10.1200/JCO.1997.15.2.433.

[135] Stephen Mackinnon et al. 'Adoptive Immunotherapy Evaluating Escalating Doses of Donor Leukocytes for Relapse of Chronic Myeloid Leukemia After Bone Marrow Transplantation: Separation of Graft-Versus-Leukemia Responses From Graft-Versus-Host Disease'. In: *Blood* 86.4 (1995), pp. 1261–1268. DOI: https://doi.org/10.1182/blood.V86.4.1261.bloodjournal8641261.

[136] Sophia Khaldoyanidi et al. 'Immune Biology of Acute Myeloid Leukemia: Implications for Immunotherapy'. en. In: *Journal of Clinical Oncology* 39.5 (Feb. 2021), pp. 419–432. DOI: 10.1200/JCO.20.00475.

[137] Luca Vago et al. 'Loss of Mismatched HLA in Leukemia after Stem-Cell Transplantation'. en. In: *New England Journal of Medicine* 361.5 (July 2009), pp. 478–488. DOI: 10.1056/NEJMoa0811036.

[138] Max Jan et al. 'Recurrent genetic HLA loss in AML relapsed after matched unrelated allogeneic hematopoietic cell transplantation'. en. In: *Blood Advances* 3.14 (July 2019), pp. 2199–2204. DOI: 10.1182/bloodadvances.2019000445.

[139] Cristina Toffalori et al. 'Genomic loss of patient-specific HLA in acute myeloid leukemia relapse after well-matched unrelated donor HSCT'. en. In: *Blood* 119.20 (May 2012), pp. 4813–4815. DOI: 10.1182/blood-2012-02-411686.

[140] Matthew J. Christopher et al. 'Immune Escape of Relapsed AML Cells after Allogeneic Transplantation'. en. In: *New England Journal of Medicine* 379.24 (Dec. 2018), pp. 2330–2341. DOI: 10.1056/NEJMoa1808777.

[141] Cristina Toffalori et al. 'Immune signature drives leukemia escape and relapse after hematopoietic cell transplantation'. en. In: *Nature Medicine* 25.4 (Apr. 2019), pp. 603–611. DOI: 10.1038/s41591-019-0400-z.

[142] Francis Mussai et al. 'Acute myeloid leukemia creates an arginase-dependent immunosuppressive microenvironment'. en. In: *Blood* 122.5 (Aug. 2013), pp. 749–758. DOI: 10.1182/blood-2013-01-480129.

[143] Valentina Folgiero et al. 'Indoleamine 2,3-dioxygenase 1 (IDO1) activity in leukemia blasts correlates with poor outcome in childhood acute myeloid leukemia'. en. In: *Oncotarget* 5.8 (Apr. 2014), pp. 2052–2064. DOI: 10.18632/oncotarget.1504.

[144] Katayoun Rezvani and A. John Barrett. 'Characterizing and optimizing immune responses to leukaemia antigens after allogeneic stem cell transplantation'. en. In: *Best Practice & Research Clinical Haematology* 21.3 (Sept. 2008), pp. 437–453. DOI: 10.1016/j.beha.2008.07.004.

[145] Amy B. Hont et al. 'The generation and application of antigen-specific T cell therapies for cancer and viral-associated disease'. en. In: *Molecular Therapy* 30.6 (June 2022), pp. 2130–2152. DOI: 10.1016/j.ymthe.2022.02.002.

[146] D. van der Harst et al. 'Recognition of minor histocompatibility antigens on lymphocytic and myeloid leukemic cells by cytotoxic T-cell clones'. In: *Blood* 83.4 (Feb. 1994), pp. 1060–1066.

[147] J H Falkenburg et al. 'Growth inhibition of clonogenic leukemic precursor cells by minor histocompatibility antigen-specific cytotoxic T lymphocytes.' en. In: *The Journal of experimental medicine* 174.1 (July 1991), pp. 27–33. DOI: 10.1084/jem.174.1.27.

[148] W. A. Erik Marijt et al. 'Hematopoiesis-restricted minor histocompatibility antigens HA-1- or HA-2-specific T cells can induce complete remissions of relapsed leukemia'. en. In: *Proceedings of the National Academy of Sciences* 100.5 (Mar. 2003), pp. 2742–2747. DOI: 10.1073/pnas.0530192100.

[149] Garry Dolton et al. 'Targeting of multiple tumor-associated antigens by individual T cell receptors during successful cancer immunotherapy'. en. In: *Cell* 186.16 (Aug. 2023), 3333–3349.e27. DOI: 10.1016/j.cell.2023.06.020.

[150] Yutaka Kawakami et al. 'Identification of human tumor antigens and its implications for diagnosis and treatment of cancer'. en. In: *Cancer Science* 95.10 (Oct. 2004), pp. 784–791. DOI: 10.1111/j.1349-7006.2004.tb02182.x.

[151] Lucia Mazzotti et al. 'T-Cell Receptor Repertoire Sequencing and Its Applications: Focus on Infectious Diseases and Cancer'. en. In: *International Journal of Molecular Sciences* 23.15 (Aug. 2022), p. 8590. DOI: 10.3390/ijms23158590.

[152] Nicoletta Cieri et al. 'Systematic identification of minor histocompatibility antigens predicts outcomes of allogeneic hematopoietic cell transplantation'. en. In: *Nature Biotechnology* 43.6 (June 2025), pp. 971–982. DOI: 10.1038/s41587-024-02348-3.

[153] Kelly S. Olsen et al. 'Shared graft-versus-leukemia minor histocompatibility antigens in DISCOVeRY-BMT'. en. In: *Blood Advances* 7.9 (May 2023), pp. 1635–1649. DOI: 10.1182/bloodadvances.2022008863.

[154] Mathias M. Schuler et al. 'SNEP: SNP-derived Epitope Prediction program for minor H antigens'. en. In: *Immunogenetics* 57.11 (Dec. 2005), pp. 816–820. DOI: 10.1007/s00251-005-0054-5.

[155] Bjoern Reynisson et al. 'Improved prediction of MHC II antigen presentation through integration and motif deconvolution of mass spectrometry MHC eluted ligand data'. In: *Journal of Proteome Research* 19.6 (Apr. 2020), pp. 2304–2315. DOI: 10.1021/acs.jproteome.9b00874.

[156] Rupa Narayan et al. 'Acute myeloid leukemia immunopeptidome reveals HLA presentation of mutated nucleophosmin'. en. In: *PLOS ONE* 14.7 (July 2019). Ed. by Marina Konopleva, e0219547. DOI: 10.1371/journal.pone.0219547.

[157] Kirti Pandey et al. 'In-depth mining of the immunopeptidome of an acute myeloid leukemia cell line using complementary ligand enrichment and data acquisition strategies'. en. In: *Molecular Immunology* 123 (July 2020). Publisher: Elsevier BV, pp. 7–17. DOI: 10.1016/j.molimm.2020.04.008.

[158] Jenny Zilberberg, Rena Feinman and Robert Korngold. 'Strategies for the Identification of T Cell–Recognized Tumor Antigens in Hematological Malignancies for Improved Graft-versus-Tumor Responses after Allogeneic Blood and Marrow Transplantation'. en. In: *Biology of Blood and Marrow Transplantation* 21.6 (June 2015), pp. 1000–1007. DOI: 10.1016/j.bbmt.2014.11.001.

[159] Kyra J Fuchs et al. 'DNA barcoded peptide-MHC multimers to measure and monitor minor histocompatibility antigen-specific T cells after allogeneic stem cell transplantation'. en. In: *Journal for ImmunoTherapy of Cancer* 12.12 (Dec. 2024), e009564. DOI: 10.1136/jitc-2024-009564.

[160] Amalie Kai Bentzen et al. 'Large-scale detection of antigen-specific T cells using peptide-MHC-I multimers labeled with DNA barcodes'. en. In: *Nature Biotechnology* 34.10 (Oct. 2016), pp. 1037–1045. DOI: 10.1038/nbt.3662.

[161] Jochen Greiner and Michael Schmitt. 'Leukemia-associated antigens as target structures for a specific immunotherapy in chronic myeloid leukemia'. en. In: *European Journal of Haematology* 80.6 (June 2008), pp. 461–468. DOI: 10.1111/j.1600-0609.2008.01053.x.

[162] Lothar Bergmann et al. 'High Levels of Wilms' Tumor Gene (wt1) mRNA in Acute Myeloid Leukemias Are Associated With a Worse Long-Term Outcome'. en. In: *Blood* 90.3 (Aug. 1997), pp. 1217–1225. DOI: 10.1182/blood.V90.3.1217.

[163] Sara Galimberti et al. '*WT1* expression levels at diagnosis could predict long-term time-to-progression in adult patients affected by acute myeloid leukaemia and myelodysplastic syndromes'. en. In: *British Journal of Haematology* 149.3 (May 2010), pp. 451–454. DOI: 10.1111/j.1365-2141.2009.08063.x.

[164] Katayoun Rezvani et al. 'Leukemia-associated antigen-specific T-cell responses following combined PR1 and WT1 peptide vaccination in patients with myeloid malignancies'. en. In: *Blood* 111.1 (Jan. 2008), pp. 236–242. DOI: 10.1182/blood-2007-08-108241.

[165] Aude G. Chapuis et al. 'Transferred WT1-Reactive $CD8^+$ T Cells Can Mediate Antileukemic Activity and Persist in Post-Transplant Patients'. en. In: *Science Translational Medicine* 5.174 (Feb. 2013). DOI: 10.1126/scitranslmed.3004916.

[166] Aude G. Chapuis et al. 'T cell receptor gene therapy targeting WT1 prevents acute myeloid leukemia relapse post-transplant'. en. In: *Nature Medicine* 25.7 (July 2019), pp. 1064–1072. DOI: 10.1038/s41591-019-0472-9.

[167] Gheath Alatrash, Jeffrey J. Molldrem and Muzaffar H. Qazilbas. 'Targeting PR1 in myeloid leukemia'. en. In: *Oncotarget* 9.4 (Jan. 2018), pp. 4280–4281. DOI: 10.18632/oncotarget.23403.

[168] A Sergeeva et al. 'Activity of 8F4, a T-cell receptor-like anti-PR1/HLA-A2 antibody, against primary human AML in vivo'. en. In: *Leukemia* 30.7 (July 2016), pp. 1475–1484. DOI: 10.1038/leu.2016.57.

[169] Emily K. Curran, James Godfrey and Justin Kline. 'Mechanisms of Immune Tolerance in Leukemia and Lymphoma'. en. In: *Trends in Immunology* 38.7 (July 2017), pp. 513–525. DOI: 10.1016/j.it.2017.04.004.

[170] Elli Papaemmanuil et al. 'Genomic Classification and Prognosis in Acute Myeloid Leukemia'. en. In: *New England Journal of Medicine* 374.23 (June 2016), pp. 2209–2221. DOI: 10.1056/NEJMoa1516192.

[171] Fabio Forghieri et al. 'Neoantigen-Specific T-Cell Immune Responses: The Paradigm of NPM1-Mutated Acute Myeloid Leukemia'. en. In: *International Journal of Molecular Sciences* 22.17 (Aug. 2021), p. 9159. DOI: 10.3390/ijms22179159.

[172] A Liso et al. 'Nucleophosmin leukaemic mutants contain C-terminus peptides that bind HLA class I molecules'. en. In: *Leukemia* 22.2 (Feb. 2008), pp. 424–426. DOI: 10.1038/sj.leu.2404887.

[173] Fabio Forghieri et al. 'Characterization and dynamics of specific T cells against nucleophosmin-1 (NPM1)-mutated peptides in patients with NPM1-mutated acute myeloid leukemia'. en. In: *Oncotarget* 10.8 (Jan. 2019), pp. 869–882. DOI: 10.18632/oncotarget.26617.

[174] Melinda A. Biernacki et al. 'CBFB-MYH11 fusion neoantigen enables T cell recognition and killing of acute myeloid leukemia'. en. In: *Journal of Clinical Investigation* 130.10 (Aug. 2020), pp. 5127–5141. DOI: 10.1172/JCI137723.

[175] Peter D. Katsikis, Ken J. Ishii and Christopher Schliehe. 'Challenges in developing personalized neoantigen cancer vaccines'. en. In: *Nature Reviews Immunology* 24.3 (Mar. 2024), pp. 213–227. DOI: 10.1038/s41577-023-00937-y.

[176] André Kahles et al. 'Comprehensive Analysis of Alternative Splicing Across Tumors from 8,705 Patients'. en. In: *Cancer Cell* 34.2 (Aug. 2018), 211–224.e6. DOI: 10.1016/j.ccell.2018.07.001.

[177] Mark Cobbold et al. 'MHC Class I–Associated Phosphopeptides Are the Targets of Memory-like Immunity in Leukemia'. en. In: *Science Translational Medicine* 5.203 (Sept. 2013). DOI: 10.1126/scitranslmed.3006061.

[178] Mohamed Chour et al. 'Endogenous retroelements in hematological malignancies: From epigenetic dysregulation to therapeutic targeting'. en. In: *American Journal of Hematology* 100.1 (Jan. 2025), pp. 116–130. DOI: 10.1002/ajh.27501.

[179] Yangyang Cai et al. 'MHC-I-presented non-canonical antigens expand the cancer immunotherapy targets in acute myeloid leukemia'. en. In: *Scientific Data* 11.1 (Aug. 2024), p. 831. DOI: 10.1038/s41597-024-03660-y.

[180] L. A. Sherman and S. Chattopadhyay. 'The Molecular Basis of Allorecognition'. In: *Annual Review of Immunology* 11 (Apr. 1993), pp. 385–402. DOI: 10.1146/annurev.iy.11.040193.002125.

[181] Jacqueline H. Y. Siu et al. 'T cell Allorecognition Pathways in Solid Organ Transplantation'. en. In: *Frontiers in Immunology* 9 (Nov. 2018), p. 2548. DOI: 10.3389/fimmu.2018.02548.

[182] A Bacigalupo et al. 'Unmanipulated haploidentical bone marrow transplantation and post-transplant cyclophosphamide for hematologic malignanices following a myeloablative conditioning: an update'. en. In: *Bone Marrow Transplantation* 50.S2 (June 2015), S37–S39. DOI: 10.1038/bmt.2015.93.

[183] Nelson J Chao. 'Minors come of age: minor histocompatibility antigens and graft-versus-host disease'. en. In: *Biology of Blood and Marrow Transplantation* 10.4 (Apr. 2004), pp. 215–223. DOI: 10.1016/j.bbmt.2003.10.003.

[184] H Torikai et al. 'The HLA-A*0201-restricted minor histocompatibility antigen HA-1H peptide can also be presented by another HLA-A2 subtype, A*0206'. en. In: *Bone Marrow Transplantation* 40.2 (July 2007), pp. 165–174. DOI: 10.1038/sj.bmt.1705689.

[185] Tuna Mutis et al. 'Efficient induction of minor histocompatibility antigen HA-1-specific cytotoxic T-cells using dendritic cells retrovirally transduced with HA-1-coding cDNA'. en. In: *Biology of Blood and Marrow Transplantation* 8.8 (Aug. 2002), pp. 412–419. DOI: 10.1053/bbmt.2002.v8.pm12234166.

[186] P. Brossart et al. 'Induction of minor histocompatibility antigen HA-1–specific cytotoxic T cells for the treatment of leukemia after allogeneic stem cell transplantation'. In: *Blood* 94.12 (Dec. 1999), pp. 4374–4376. DOI: 10.1182/blood.V94.12.4374.4374.

[187] Eric Spierings et al. 'Multicenter Analyses Demonstrate Significant Clinical Effects of Minor Histocompatibility Antigens on GvHD and GvL after HLA-Matched Related and Unrelated Hematopoietic Stem Cell Transplantation'. en. In: *Biology of Blood and Marrow Transplantation* 19.8 (Aug. 2013), pp. 1244–1253. DOI: 10.1016/j.bbmt.2013.06.001.

[188] Elizabeth F. Krakow et al. 'HA-1–targeted T-cell receptor T-cell therapy for recurrent leukemia after hematopoietic stem cell transplantation'. en. In: *Blood* 144.10 (Sept. 2024), pp. 1069–1082. DOI: 10.1182/blood.2024024105.

[189] Peter Van Balen et al. 'HA-1H T-Cell Receptor Gene Transfer to Redirect Virus-Specific T Cells for Treatment of Hematological Malignancies After Allogeneic Stem Cell Transplantation: A Phase 1 Clinical Study'. en. In: *Frontiers in Immunology* 11 (Aug. 2020), p. 1804. DOI: 10.3389/fimmu.2020.01804.

[190] Anita N. Kremer et al. 'Discovery and Differential Processing of HLA Class II-Restricted Minor Histocompatibility Antigen LB-PIP4K2A-1S and Its Allelic Variant by Asparagine Endopeptidase'. en. In: *Frontiers in Immunology* 11 (Mar. 2020), p. 381. DOI: 10.3389/fimmu.2020.00381.

[191] Jacques Neefjes et al. 'Towards a systems understanding of MHC class I and MHC class II antigen presentation'. en. In: *Nature Reviews Immunology* 11.12 (Dec. 2011), pp. 823–836. DOI: 10.1038/nri3084.

[192] Peter Van Balen et al. 'CD4 Donor Lymphocyte Infusion Can Cause Conversion of Chimerism Without GVHD by Inducing Immune Responses Targeting Minor Histocompatibility Antigens in HLA Class II'. en. In: *Frontiers in Immunology* 9 (Dec. 2018). Publisher: Frontiers Media SA. DOI: 10.3389/fimmu.2018.03016.

[193] Melinda A. Biernacki, Vipul S. Sheth and Marie Bleakley. 'T cell optimization for graft-versus-leukemia responses'. en. In: *JCI Insight* 5.9 (May 2020), e134939. DOI: 10.1172/jci.insight.134939.

[194] Sebastian Boegel et al. 'HLA and proteasome expression body map'. en. In: *BMC Medical Genomics* 11.1 (Dec. 2018). Publisher: Springer Science and Business Media LLC. DOI: 10.1186/s12920-018-0354-x.

[195] Malene Erup Larsen et al. 'Degree of Predicted Minor Histocompatibility Antigen Mismatch Correlates with Poorer Clinical Outcomes in Nonmyeloablative Allogeneic Hematopoietic Cell Transplantation'. en. In: *Biology of Blood and Marrow Transplantation* 16.10 (Oct. 2010), pp. 1370–1381. DOI: 10.1016/j.bbmt.2010.03.022.

[196] Willemijn Hobo et al. 'Association of Disparities in Known Minor Histocompatibility Antigens with Relapse-Free Survival and Graft-versus-Host Disease after Allogeneic Stem Cell Transplantation'. en. In: *Biology of Blood and Marrow Transplantation* 19.2 (Feb. 2013), pp. 274–282. DOI: 10.1016/j.bbmt.2012.09.008.

[197] Robert Zeiser et al. 'Biology-Driven Approaches to Prevent and Treat Relapse of Myeloid Neoplasia after Allogeneic Hematopoietic Stem Cell Transplantation'. en. In: *Biology of Blood and Marrow Transplantation* 25.4 (Apr. 2019), e128–e140. DOI: 10.1016/j.bbmt.2019.01.016.

[198] Connor Sweeney. 'Harnessing the Graft-versus-Leukaemia Effect in Acute Myeloid Leukaemia'. DPhil Thesis. Oxford, UK: University of Oxford, 2021.

[199] Gerda Mickute. 'Description of a Novel MHC Class II Restricted Allogeneic TCR T Cell Therapy for Acute Myeloid Leukaemia'. DPhil Thesis. Oxford, UK: University of Oxford, 2023.

[200] Edita Karosiene et al. 'NetMHCIIpan-3.0, a common pan-specific MHC class II prediction method including all three human MHC class II isotypes, HLA-DR, HLA-DP and HLA-DQ'. en. In: *Immunogenetics* 65.10 (Oct. 2013), pp. 711–724. DOI: 10.1007/s00251-013-0720-y.

[201] Vanessa Jurtz et al. 'NetMHCpan-4.0: Improved Peptide-MHC Class I Interaction Predictions Integrating Eluted Ligand and Peptide Binding Affinity Data'. In: *The Journal of Immunology* 199.9 (Nov. 2017), pp. 3360–3368. DOI: 10.4049/jimmunol.1700893.

[202] Carla Cendón et al. 'Resident memory CD4$^+$ T lymphocytes mobilize from bone marrow to contribute to a systemic secondary immune reaction'. en. In: *European Journal of Immunology* 52.5 (May 2022), pp. 737–752. DOI: 10.1002/eji.202149726.

[203] Melania Carlisi et al. 'Evaluation of Bone Marrow CD8+ tissue-Resident Memory T Cells in Multiple Myeloma'. In: *Blood* 134.Supplement_1 (Nov. 2019), pp. 4389–4389. DOI: 10.1182/blood-2019-131349.

[204] A John Barrett and Minoo Battiwalla. 'Relapse after allogeneic stem cell transplantation'. en. In: *Expert Review of Hematology* 3.4 (Aug. 2010), pp. 429–441. DOI: 10.1586/ehm.10.32.

[205] The Human Protein Atlas Project. *The Human Protein Atlas*. 2024. URL: https://www.proteinatlas.org.

[206] Mathias Uhlén et al. 'Tissue-based map of the human proteome'. In: *Science* 347.6220 (2015). Publisher: American Association for the Advancement of Science, p. 1260419. DOI: 10.1126/science.1260419.

[207] Max Karlsson et al. 'A single-cell type transcriptomics map of human tissues'. In: *Science Advances* 7.31 (2021), eabh2169. DOI: 10.1126/sciadv.abh2169.

[208] Frederik O Bagger et al. 'BloodSpot: a database of gene expression profiles and transcriptional programs for healthy and malignant haematopoiesis'. In: *Nucleic Acids Research* 44.D1 (2016). Publisher: Oxford University Press, pp. D917–D924. DOI: 10.1093/nar/gkv1101.

[209] FOB Project Team. *FOB: Functional Omics in Blood — HemaExplorer v1 Dataset Viewer*. 2024. URL: https://www.fobinf.com/?gene=METTL22&dataset=nl_human_data_HemaExp_v_1.

[210] Jeffrey W Tyner et al. 'Functional genomic landscape of acute myeloid leukaemia'. In: *Nature* 562.7728 (2018), pp. 526–531. DOI: 10.1038/s41586-018-0603-z.

[211] National Cancer Institute. *TARGET Acute Myeloid Leukemia (TARGET-AML)*. 2024. URL: https://ocg.cancer.gov/programs/target/projects/acute-myeloid-leukemia.

[212] The Cancer Genome Atlas Research Network. 'Genomic and epigenomic landscapes of adult de novo acute myeloid leukemia'. In: *New England Journal of Medicine* 368.22 (2013), pp. 2059–2074. DOI: 10.1056/NEJMoa1301689.

[213] Torsten Haferlach et al. 'Clinical utility of microarray-based gene expression profiling in the diagnosis and subclassification of leukemia: report from the International Microarray Innovations in Leukemia Study Group'. In: *Leukemia* 24.3 (2010), pp. 706–715. DOI: 10.1038/leu.2010.6.

[214] Frederik O Bagger et al. 'HemaExplorer: a database of mRNA expression profiles in normal and malignant haematopoiesis'. In: *Nucleic Acids Research* 41.D1 (2013). Publisher: Oxford University Press, pp. D1034–D1039. DOI: 10.1093/nar/gks1074.

[215] Clara Domínguez Conde et al. 'CellTypist: automated cell type annotation for scRNA-seq datasets'. In: *Nature Methods* 19.9 (2022), pp. 1104–1112. DOI: 10.1038/s41592-022-01521-8.

[216] Mikhail Shugay et al. 'VDJdb: a curated database of T-cell receptor sequences with known antigen specificity'. In: *Nucleic Acids Research* 46.D1 (2018), pp. D419–D427. DOI: 10.1093/nar/gkx760.

[217] ImmunoMind Team. *immunarch: An R Package for Painless Bioinformatics Analysis of T-Cell and B-Cell Immune Repertoires*. Aug. 2019. DOI: 10.5281/zenodo.3367200. URL: https://doi.org/10.5281/zenodo.3367200.

[218] Julien Racle et al. 'Machine learning predictions of MHC-II specificities reveal alternative binding mode of class II epitopes'. In: *Immunity* 56.6 (2023), pp. 1359–1375. DOI: 10.1016/j.immuni.2023.03.009.

[219] Julien Racle et al. 'Robust prediction of HLA class II epitopes by deep motif deconvolution of immunopeptidomes'. In: *Nature Biotechnology* 37 (2019), pp. 1283–1286. DOI: 10.1038/s41587-019-0289-6.

[220] Arthur Liberzon et al. 'Molecular signatures database (MSigDB) 3.0'. In: *Bioinformatics* 27.12 (2011). Publisher: Oxford University Press, pp. 1739–1740. DOI: 10.1093/bioinformatics/btr260.

[221] Marc Gillespie et al. 'The Reactome pathway knowledgebase 2022'. In: *Nucleic Acids Research* 50.D1 (2022). Publisher: Oxford University Press, pp. D687–D692. DOI: 10.1093/nar/gkab1028.

[222] Frank J. Lowery et al. 'Molecular signatures of antitumor neoantigen-reactive T cells from metastatic human cancers'. en. In: *Science* 375.6583 (Feb. 2022), pp. 877–884. DOI: 10.1126/science.abl5447.

[223] Yuhan Hao et al. 'Integrated analysis of multimodal single-cell data'. In: *Cell* 184.13 (July 2021), 3573–3587.e29. DOI: 10.1016/j.cell.2021.04.048.

[224] Caleb M. Radens et al. 'Meta-analysis of transcriptomic variation in T-cell populations reveals both variable and consistent signatures of gene expression and splicing'. en. In: *RNA* 26.10 (Oct. 2020), pp. 1320–1333. DOI: 10.1261/rna.075929.120.

[225] Eddie Cano-Gamez et al. 'Single-cell transcriptomics identifies an effectorness gradient shaping the response of CD4+ T cells to cytokines'. en. In: *Nature Communications* 11.1 (Apr. 2020), p. 1801. DOI: 10.1038/s41467-020-15543-y.

[226] Enrico Velardi, Jennifer J. Tsai and Marcel R. M. Van Den Brink. 'T cell regeneration after immunological injury'. en. In: *Nature Reviews Immunology* 21.5 (May 2021), pp. 277–291. DOI: 10.1038/s41577-020-00457-z.

[227] Linde Dekker et al. 'Reconstitution of T Cell Subsets Following Allogeneic Hematopoietic Cell Transplantation'. en. In: *Cancers* 12.7 (July 2020), p. 1974. DOI: 10.3390/cancers12071974.

[228] Marcel R. M. van den Brink, Enrico Velardi and Miguel-Angel Perales. 'Immune reconstitution following stem cell transplantation'. In: *Nature Reviews Clinical Oncology* 12.10 (2015). Publisher: Nature Publishing Group, pp. 563–575. DOI: 10.1038/nrclinonc.2015.123.

[229] Nicoletta Cieri et al. 'IL-7 and IL-15 instruct the generation of human memory stem T cells from naive precursors'. en. In: *Blood* 121.4 (Jan. 2013), pp. 573–584. DOI: 10.1182/blood-2012-05-431718.

[230] Stefanie Herda et al. 'Long-term in vitro expansion ensures increased yield of central memory T cells as perspective for manufacturing challenges'. en. In: *International Journal of Cancer* 148.12 (June 2021), pp. 3097–3110. DOI: 10.1002/ijc.33523.

[231] Manuela Battaglia et al. 'Coexistence of Two Functioning T-Cell Repertoires in Healthy Ex-Thalassemics Bearing a Persistent Mixed Chimerism Years After Bone Marrow Transplantation'. en. In: *Blood* 94.10 (Nov. 1999), pp. 3432–3438. DOI: 10.1182/blood.V94.10.3432.422k17_3432_3438.

[232] Dan Koning et al. 'In vitro expansion of antigen-specific CD8+ T cells distorts the T-cell repertoire'. en. In: *Journal of Immunological Methods* 405 (Mar. 2014), pp. 199–203. DOI: 10.1016/j.jim.2014.01.013.

[233] Elisa Rosati et al. 'Overview of methodologies for T-cell receptor repertoire analysis'. en. In: *BMC Biotechnology* 17.1 (Dec. 2017), p. 61. DOI: 10.1186/s12896-017-0379-9.

[234] Victor Greiff et al. 'Bioinformatic and Statistical Analysis of Adaptive Immune Repertoires'. en. In: *Trends in Immunology* 36.11 (Nov. 2015), pp. 738–749. DOI: 10.1016/j.it.2015.09.006.

[235] Jeffrey R Currier et al. 'A panel of MHC class I restricted viral peptides for use as a quality control for vaccine trial ELISPOT assays'. en. In: *Journal of Immunological Methods* 260.1-2 (Feb. 2002), pp. 157–172. DOI: 10.1016/S0022-1759(01)00535-X.

[236] Zuleika Calderin Sollet et al. 'CMV serostatus and T-cell repertoire diversity 5 years after allogeneic hematopoietic stem cell transplantation'. en. In: *Leukemia* 37.4 (Apr. 2023), pp. 948–951. DOI: 10.1038/s41375-023-01836-w.

[237] Douglas R. Green, Nathalie Droin and Michael Pinkoski. 'Activation-induced cell death in T cells'. en. In: *Immunological Reviews* 193.1 (June 2003), pp. 70–81. DOI: 10.1034/j.1600-065X.2003.00051.x.

[238] E. John Wherry and Mahiko Kurachi. 'T Cell Exhaustion'. In: *Annual Review of Immunology* 42 (Apr. 2024). DOI: 10.1146/annurev-immunol-090222-110914.

[239] Nasser Gholijani, Gholamreza Daryabor and Fatemeh Rezaei Kahmini. 'T cell-Intrinsic Peripheral Tolerance: A Checkpoint Target to Treat Autoimmunity'. en. In: *Journal of Cellular Immunology* 6.2 (2024), pp. 87–97. DOI: 10.33696/immunology.6.194.

[240] A Oras et al. 'Comprehensive flow cytometric reference intervals of leukocyte subsets from six study centers across Europe'. en. In: *Clinical and Experimental Immunology* 202.3 (Nov. 2020), pp. 363–378. DOI: 10.1111/cei.13491.

[241] Sven Koch et al. 'Multiparameter flow cytometric analysis of CD4 and CD8 T cell subsets in young and old people'. en. In: *Immunity & Ageing* 5.1 (Dec. 2008), p. 6. DOI: 10.1186/1742-4933-5-6.

[242] Ana C. Alho et al. 'Unbalanced recovery of regulatory and effector T cells after allogeneic stem cell transplantation contributes to chronic GVHD'. en. In: *Blood* 127.5 (Feb. 2016), pp. 646–657. DOI: 10.1182/blood-2015-10-672345.

[243] Francesca Di Rosa and Thomas Gebhardt. 'Bone Marrow T Cells and the Integrated Functions of Recirculating and Tissue-Resident Memory T Cells'. en. In: *Frontiers in Immunology* 7 (Feb. 2016). DOI: 10.3389/fimmu.2016.00051.

[244] Ruka Setoguchi, Yui Matsui and Kousuke Mouri. 'mTOR signaling promotes a robust and continuous production of IFN-γ by human memory $CD8^+$ T cells and their proliferation'. en. In: *European Journal of Immunology* 45.3 (Mar. 2015), pp. 893–902. DOI: 10.1002/eji.201445086.

[245] William E. Paul and Jinfang Zhu. 'How are TH2-type immune responses initiated and amplified?' en. In: *Nature Reviews Immunology* 10.4 (Apr. 2010), pp. 225–235. DOI: 10.1038/nri2735.

[246] Jinfang Zhu, Hidehiro Yamane and William E. Paul. 'Differentiation of Effector CD4 T Cell Populations*'. In: *Annual Review of Immunology* 28.Volume 28, 2010 (2010). Publisher: Annual Reviews Type: Journal Article, pp. 445–489. DOI: https://doi.org/10.1146/annurev-immunol-030409-101212.

[247] Irina G Luzina et al. 'Regulation of inflammation by interleukin-4: a review of "alternatives"'. en. In: *Journal of Leukocyte Biology* 92.4 (Oct. 2012), pp. 753–764. DOI: 10.1189/jlb.0412214.

[248] Cornelis A. M. van Bergen et al. 'Selective graft-versus-leukemia depends on magnitude and diversity of the alloreactive T cell response'. In: *The Journal of Clinical Investigation* 127.2 (Feb. 2017). Publisher: The American Society for Clinical Investigation, pp. 517–529. DOI: 10.1172/JCI86175.

[249] Kelly Broen et al. 'Concurrent Detection of Circulating Minor Histocompatibility Antigen-Specific CD8+ T Cells in SCT Recipients by Combinatorial Encoding MHC Multimers'. en. In: *PLoS ONE* 6.6 (June 2011). Ed. by Naglaa H. Shoukry, e21266. DOI: 10.1371/journal.pone.0021266.

[250] Jeroen W J Van Heijst et al. 'Quantitative assessment of T cell repertoire recovery after hematopoietic stem cell transplantation'. en. In: *Nature Medicine* 19.3 (Mar. 2013), pp. 372–377. DOI: 10.1038/nm.3100.

[251] Christopher G. Kanakry et al. 'Early lymphocyte recovery after intensive timed sequential chemotherapy for acute myelogenous leukemia: peripheral oligoclonal expansion of regulatory T cells'. en. In: *Blood* 117.2 (Jan. 2011), pp. 608–617. DOI: 10.1182/blood-2010-04-277939.

[252] Inna V. Grishkan et al. 'Helper T cells down-regulate CD4 expression upon chronic stimulation giving rise to double-negative T cells'. en. In: *Cellular Immunology* 284.1-2 (July 2013). Publisher: Elsevier BV, pp. 68–74. DOI: 10.1016/j.cellimm.2013.06.011.

[253] Peng Qiu. 'Embracing the dropouts in single-cell RNA-seq analysis'. en. In: *Nature Communications* 11.1 (Mar. 2020). Publisher: Springer Science and Business Media LLC. DOI: 10.1038/s41467-020-14976-9.

[254] Anna Śledzińska et al. 'Regulatory T Cells Restrain Interleukin-2- and Blimp-1-Dependent Acquisition of Cytotoxic Function by CD4+ T Cells'. en. In: *Immunity* 52.1 (Jan. 2020). Publisher: Elsevier BV, 151–166.e6. DOI: 10.1016/j.immuni.2019.12.007.

[255] Bernard Khor and Barry P Sleckman. 'Allelic exclusion at the TCRβ locus'. en. In: *Current Opinion in Immunology* 14.2 (Apr. 2002). Publisher: Elsevier BV, pp. 230–234. DOI: 10.1016/s0952-7915(02)00326-6.

[256] Nicholas R J Gascoigne and S Munir Alam. 'Allelic exclusion of the T cell receptor a-chain: developmental regulation of a post-translational event'. en. In: *Seminars in Immunology* 11.5 (Oct. 1999), pp. 337–347. DOI: 10.1006/smim.1999.0190.

[257] Pleun Hombrink et al. 'High-Throughput Identification of Potential Minor Histocompatibility Antigens by MHC Tetramer-Based Screening: Feasibility and Limitations'. en. In: *PLoS ONE* 6.8 (Aug. 2011). Ed. by Jean Kanellopoulos, e22523. DOI: 10.1371/journal.pone.0022523.

[258] Paul Shafer, Lauren M. Kelly and Valentina Hoyos. 'Cancer Therapy With TCR-Engineered T Cells: Current Strategies, Challenges, and Prospects'. en. In: *Frontiers in Immunology* 13 (Mar. 2022). Publisher: Frontiers Media SA. DOI: 10.3389/fimmu.2022.835762.

[259] Denise M. McKinney et al. 'A strategy to determine HLA class II restriction broadly covering the DR, DP, and DQ allelic variants most commonly expressed in the general population'. en. In: *Immunogenetics* 65.5 (May 2013). Publisher: Springer Science and Business Media LLC, pp. 357–370. DOI: 10.1007/s00251-013-0684-y.

[260] Paola Panina-Bordignon et al. 'Universally immunogenic T cell epitopes: promiscuous binding to human MHC class II and promiscuous recognition by T cells'. en. In: *European Journal of Immunology* 19.12 (Dec. 1989). Publisher: Wiley, pp. 2237–2242. DOI: 10.1002/eji.1830191209.

[261] Samantha Reiss et al. 'Comparative analysis of activation induced marker (AIM) assays for sensitive identification of antigen-specific CD4 T cells'. en. In: *PLOS ONE* 12.10 (Oct. 2017). Ed. by Lishomwa C. Ndhlovu. Publisher: Public Library of Science (PLoS), e0186998. DOI: 10.1371/journal.pone.0186998.

[262] Chad Poloni et al. 'T-cell activation–induced marker assays in health and disease'. en. In: *Immunology & Cell Biology* 101.6 (July 2023), pp. 491–503. DOI: 10.1111/imcb.12636.

[263] Zhen Qin and Tao Xu. 'Deciphering the deterministic role of TCR signaling in T cell fate determination'. en. In: *Frontiers in Immunology* 16 (May 2025), p. 1562248. DOI: 10.3389/fimmu.2025.1562248.

[264] Steven A Rosenberg et al. 'Treatment of patients with metastatic melanoma with autologous tumor-infiltrating lymphocytes and interleukin-2'. In: *Journal of the National Cancer Institute* 80.9 (1988). Publisher: Oxford University Press, pp. 604–610.

[265] Cansu Cimen Bozkus et al. 'A T-cell-based immunogenicity protocol for evaluating human antigen-specific responses'. en. In: *STAR Protocols* 2.3 (Sept. 2021). Publisher: Elsevier BV, p. 100758. DOI: 10.1016/j.xpro.2021.100758.

[266] Rebekka Geiger et al. 'Human naive and memory CD4+ T cell repertoires specific for naturally processed antigens analyzed using libraries of amplified T cells'. en. In: *Journal of Experimental Medicine* 206.7 (July 2009), pp. 1525–1534. DOI: 10.1084/jem.20090504.

[267] John G. Tooley, James P. Catlin and Christine E. Schaner Tooley. 'METTLing in Stem Cell and Cancer Biology'. en. In: *Stem Cell Reviews and Reports* 19.1 (Jan. 2023). Publisher: Springer Science and Business Media LLC, pp. 76–91. DOI: 10.1007/s12015-022-10444-7.

[268] Philippe Cloutier et al. 'Methylation of the DNA/RNA-binding protein Kin17 by METTL22 affects its association with chromatin'. en. In: *Journal of Proteomics* 100 (Apr. 2014). Publisher: Elsevier BV, pp. 115–124. DOI: 10.1016/j.jprot.2013.10.008.

[269] Tianxu Han et al. 'Identification of novel genes and networks governing hematopoietic stem cell development'. en. In: *EMBO reports* 17.12 (Dec. 2016). Publisher: Springer Science and Business Media LLC, pp. 1814–1828. DOI: 10.15252/embr.201642395.

[270] Sergio A. Quezada et al. 'Tumor-reactive CD4+ T cells develop cytotoxic activity and eradicate large established melanoma after transfer into lymphopenic hosts'. en. In: *Journal of Experimental Medicine* 207.3 (Mar. 2010). Publisher: Rockefeller University Press, pp. 637–650. DOI: 10.1084/jem.20091918.

[271] David Y. Oh and Lawrence Fong. 'Cytotoxic CD4+ T cells in cancer: Expanding the immune effector toolbox'. en. In: *Immunity* 54.12 (Dec. 2021). Publisher: Elsevier BV, pp. 2701–2711. DOI: 10.1016/j.immuni.2021.11.015.

[272] Kaitlin A. Read et al. 'IL-2, IL-7, and IL-15: Multistage regulators of CD4+ T helper cell differentiation'. en. In: *Experimental Hematology* 44.9 (Sept. 2016). Publisher: Elsevier BV, pp. 799–808. DOI: 10.1016/j.exphem.2016.06.003.

[273] Yi Xie et al. 'Comparative Analysis of Single-Cell RNA Sequencing Methods with and without Sample Multiplexing'. en. In: *International Journal of Molecular Sciences* 25.7 (Mar. 2024), p. 3828. DOI: 10.3390/ijms25073828.

[274] Xiao-Hua Luo et al. 'Different recovery patterns of CMV-specific and WT1-specific T cells in patients with acute myeloid leukemia undergoing allogeneic hematopoietic cell transplantation: Impact of CMV infection and leukemia relapse'. en. In: *Frontiers in Immunology* 13 (Feb. 2023), p. 1027593. DOI: 10.3389/fimmu.2022.1027593.

[275] Heike Uhlemann et al. 'Shape of the art: TCR-repertoire after allogeneic hematopoietic cell transplantation'. en. In: *Best Practice & Research Clinical Haematology* 37.2 (June 2024), p. 101558. DOI: 10.1016/j.beha.2024.101558.

[276] Huang Huang et al. 'Analyzing the Mycobacterium tuberculosis immune response by T-cell receptor clustering with GLIPH2 and genome-wide antigen screening'. en. In: *Nature Biotechnology* 38.10 (Oct. 2020), pp. 1194–1202. DOI: 10.1038/s41587-020-0505-4.

[277] John-William Sidhom et al. 'DeepTCR is a deep learning framework for revealing sequence concepts within T-cell repertoires'. en. In: *Nature Communications* 12.1 (Mar. 2021), p. 1605. DOI: 10.1038/s41467-021-21879-w.

[278] Alessandro Montemurro et al. 'NetTCR-2.0 enables accurate prediction of TCR-peptide binding by using paired TCRα and β sequence data'. en. In: *Communications Biology* 4.1 (Sept. 2021), p. 1060. DOI: 10.1038/s42003-021-02610-3.

[279] Ke-Yue Ma et al. 'High-throughput and high-dimensional single-cell analysis of antigen-specific CD8+ T cells'. en. In: *Nature Immunology* 22.12 (Dec. 2021), pp. 1590–1598. DOI: 10.1038/s41590-021-01073-2.

[280] Andrew K. Sewell. 'Why must T cells be cross-reactive?' en. In: *Nature Reviews Immunology* 12.9 (Sept. 2012), pp. 669–677. DOI: 10.1038/nri3279.

[281] Gabrielle A. Rizzuto et al. 'Self-antigen–specific CD8+ T cell precursor frequency determines the quality of the antitumor immune response'. en. In: *Journal of Experimental Medicine* 206.4 (Apr. 2009), pp. 849–866. DOI: 10.1084/jem.20081382.

[282] Sara E. Hamilton and Stephen C. Jameson. 'CD8 T cell memory: it takes all kinds'. en. In: *Frontiers in Immunology* 3 (2012). DOI: 10.3389/fimmu.2012.00353.

[283] Ryuhjin Ahn, Yufei Cui and Forest M. White. 'Antigen discovery for the development of cancer immunotherapy'. en. In: *Seminars in Immunology* 66 (Mar. 2023), p. 101733. DOI: 10.1016/j.smim.2023.101733.

[284] Eric Spierings. 'Minor histocompatibility antigens: past, present, and future'. en. In: *Tissue Antigens* 84.4 (Oct. 2014), pp. 374–360. DOI: 10.1111/tan.12445.

[285] Y Jiang, Y Li and B Zhu. 'T-cell exhaustion in the tumor microenvironment'. en. In: *Cell Death & Disease* 6.6 (June 2015), e1792–e1792. DOI: 10.1038/cddis.2015.162.

[286] Weiqin Jiang et al. 'Exhausted CD8+T Cells in the Tumor Immune Microenvironment: New Pathways to Therapy'. en. In: *Frontiers in Immunology* 11 (Feb. 2021), p. 622509. DOI: 10.3389/fimmu.2020.622509.

[287] Wei Meng, Robert D. Schreiber and Cheryl F. Lichti. 'Recent advances in immunopeptidomic-based tumor neoantigen discovery'. en. In: *Advances in Immunology*. Vol. 160. Elsevier, 2023, pp. 1–36. DOI: 10.1016/bs.ai.2023.10.001.

[288] Jacopo Chiaro et al. 'Proteogenomic approach to immunopeptidomics of ovarian tumors identifies shared peptide vaccine candidates'. en. In: *npj Vaccines* 10.1 (Aug. 2025), p. 195. DOI: 10.1038/s41541-025-01234-6.

[289] Elena Montauti, David Y. Oh and Lawrence Fong. 'CD4+ T cells in antitumor immunity'. en. In: *Trends in Cancer* 10.10 (Oct. 2024), pp. 969–985. DOI: 10.1016/j.trecan.2024.07.009.

[290] Jannie Borst et al. 'CD4+ T cell help in cancer immunology and immunotherapy'. en. In: *Nature Reviews Immunology* 18.10 (Oct. 2018), pp. 635–647. DOI: 10.1038/s41577-018-0044-0.

[291] Georgios Petros Barakos and Eleftheria Hatzimichael. 'Microenvironmental Features Driving Immune Evasion in Myelodysplastic Syndromes and Acute Myeloid Leukemia'. en. In: *Diseases* 10.2 (June 2022), p. 33. DOI: 10.3390/diseases10020033.